

1990

Metamorphic Petrology And Gold Mineralization Of The White River Gold Prospect, Hemlo Area, Ontario

Yuanming Pan

Follow this and additional works at: <https://ir.lib.uwo.ca/digitizedtheses>

Recommended Citation

Pan, Yuanming, "Metamorphic Petrology And Gold Mineralization Of The White River Gold Prospect, Hemlo Area, Ontario" (1990). *Digitized Theses*. 1896.
<https://ir.lib.uwo.ca/digitizedtheses/1896>

This Dissertation is brought to you for free and open access by the Digitized Special Collections at Scholarship@Western. It has been accepted for inclusion in Digitized Theses by an authorized administrator of Scholarship@Western. For more information, please contact tadam@uwo.ca, wlsadmin@uwo.ca.



National Library
of Canada

Bibliothèque nationale
du Canada

Canadian Theses Service

Service des thèses canadiennes

Ottawa, Canada
K1A 0N4

NOTICE

The quality of this microform is heavily dependent upon the quality of the original thesis submitted for microfilming. Every effort has been made to ensure the highest quality of reproduction possible.

If pages are missing, contact the university which granted the degree.

Some pages may have indistinct print especially if the original pages were typed with a poor typewriter ribbon or if the university sent us an inferior photocopy.

Reproduction in full or in part of this microform is governed by the Canadian Copyright Act, R.S.C. 1970, c. C-30, and subsequent amendments.

AVIS

La qualité de cette microforme dépend grandement de la qualité de la thèse soumise au microfilmage. Nous avons tout fait pour assurer une qualité supérieure de reproduction.

S'il manque des pages, veuillez communiquer avec l'université qui a conféré le grade.

La qualité d'impression de certaines pages peut laisser à désirer, surtout si les pages originales ont été dactylographiées à l'aide d'un ruban usé ou si l'université nous a fait parvenir une photocopie de qualité inférieure.

La reproduction, même partielle, de cette microforme est soumise à la Loi canadienne sur le droit d'auteur, SRC 1970, c. C-30, et ses amendements subséquents.

**METAMORPHIC PETROLOGY AND GOLD MINERALIZATION
OF THE WHITE RIVER GOLD PROSPECT, HEMLO AREA, ONTARIO**

by

Yuanming Pan

Department of Geology

**Submitted in partial fulfilment
of the requirement for the degree of
Doctor of Philosophy**

**Faculty of Graduate Studies
The University of Western Ontario
London, Ontario
February 1990**

© Yuanming Pan 1990



National Library
of Canada

Bibliothèque nationale
du Canada

Canadian Theses Service Service des thèses canadiennes

Ottawa, Canada
K1A 0N4

The author has granted an irrevocable non-exclusive licence allowing the National Library of Canada to reproduce, loan, distribute or sell copies of his/her thesis by any means and in any form or format, making this thesis available to interested persons.

The author retains ownership of the copyright in his/her thesis. Neither the thesis nor substantial extracts from it may be printed or otherwise reproduced without his/her permission.

L'auteur a accordé une licence irrévocable et non exclusive permettant à la Bibliothèque nationale du Canada de reproduire, prêter, distribuer ou vendre des copies de sa thèse de quelque manière et sous quelque forme que ce soit pour mettre des exemplaires de cette thèse à la disposition des personnes intéressées.

L'auteur conserve la propriété du droit d'auteur qui protège sa thèse. Ni la thèse ni des extraits substantiels de celle-ci ne doivent être imprimés ou autrement reproduits sans son autorisation.

ISBN 0-315-55272-7

Canada

ABSTRACT

The White River exploration property of LAC Minerals Ltd. is located about 5 km east of the Hemlo gold deposit in the Hemlo-Heron Bay greenstone belt of the Superior Province of the Canadian Shield, and is composed mainly of metamorphosed, metasomatized, and intensively deformed volcano-sedimentary rocks of late Archean age. The supracrustal rocks are bounded by a crystalline basement (Pukaskwa Gneissic Complex) to the south and a granodioritic intrusion (Cedar Lake Pluton) to the north. The clastic metasedimentary rocks were mainly derived from intermediate volcanic sources, admixed with minor ultramafic and mafic volcanic materials and continental weathering products, and deposited as turbidites in a large volcanoclastic-sedimentary basin.

All supracrustal rocks in the study area have been subjected to multi-phase deformation and metamorphism. An earlier Barrovian-type metamorphism (6-6.5 kbar and 455-520°C) occurred probably in response to tectonically-induced crustal thickening. The present geometry of the Archean terrain largely resulted from a progressive, dextral, brittle-ductile shear deformation, which was broadly contemporaneous with a peak thermal metamorphism. The peak andalusite-sillimanite series metamorphism was generally low in grade at greenschist-amphibolite transitional facies (3.2 kbar and 475-500°C) and climaxed at middle amphibolite facies (4.2-4.5 kbar and 580±20°C) in two narrow zones in close association with maximum shear deformation. The peak metamorphism was probably associated with heat from magmatism in the lower crust, and the metamorphic zones of medium grade and maximum shear deformation are related to "thermal-domains". The

supracrustal rocks have been affected also by a pervasive low- to very-low-grade (1.2-1.7 kbar and $360\pm 20^{\circ}\text{C}$) calc-silicate alteration at about 2632-45 Ma.

Three prominent ore-mineral-calc-silicate occurrences (Cr-rich, Fe-rich and REE-enriched) are located within major structural failures and their salient mineralogical and geochemical characteristics and metallogenic associations strongly correlate with host lithologies. All three calc-silicate occurrences belong to a protracted phase of skarn development, which began during the peak regional metamorphism, continued with a pervasive epidote-prehnite alteration, and concluded with sulfidation, carbonization and gold deposition.

Gold mineralization is associated with REE-enriched skarn (with REE-bearing clinozoisite and F-, Cl-bearing allanite), and is located within a Local Shear Zone. This auriferous skarn is clearly differentiated from typical Archean lode gold deposits by fluid inclusions of moderate salinity (about 4.5 wt. % NaCl equivalent), and from Phanerozoic counterparts by its structural setting in a brittle-ductile shear zone and carbonate-free host rocks. Although the dilatant Local Shear Zone most likely acted as a fluid conduit during skarn formation, the precise localization of gold deposition was controlled by a pre-existing pyritic zone. There are remarkable similarities and some discrepancies between this auriferous skarn and the Hemlo gold deposit.

ACKNOWLEDGEMENTS

The writer would like to express his appreciation to a number of individuals and organizations for helping to make possible this study. First and foremost, credit goes to Dr. Michael E. Fleet for his valuable ideas and challenging discussions. This study could not have been completed without his guidance. Special thanks are extended to LAC Minerals Ltd. for provision of drill-core material, access to the White River property and mapping information, particularly to Mr. R.A. Campbell and Dr. W.E. Stone for their contribution to the field work. Thanks are also given to Mr. J.A. Forth for preparation of polished thin sections, to Mr. R.L. Barnett and Mr. D.M. Kingston for assistance with microprobe analyses and fluid inclusion techniques, and to Ms. Y. Cheng for assistance with X-ray diffraction techniques. I am also very grateful to Drs. D.M. Burt, W.R. Church, C.V. Guidotti, R.W. Hodder, N.D. MacRae, F.F. Martin, S.M. McLennan, L.D. Meinert, W.H. Nesbitt, W.E. Stone, and G.M. Young, Mr. R.L. Barnett and fellow graduate students for many constructive suggestions.

Funding for this study was provided by an Ontario Geological Survey Geosciences Research Grant No. 305 to Dr. M.E. Fleet. Additional financial support was from a National Scholarship for Geosciences from the State Education Commission of P.R. China and a Graduate Scholarship, a Graduate Research Award, and a Teaching Assistantship from the University of Western Ontario awarded to the writer.

GLOSSARY OF ABBREVIATIONS

al:	albite	act:	actinolite
al:	allanite	alm:	almandine
als:	Al ₂ SiO ₅ -minerals	an:	anorthite
and:	andalusite	andr:	andradite
ap:	apatite	ay:	anthophyllite
bar:	barroisite	biot:	biotite
cc:	calcite	chl:	chlorite
cn:	celsian	cum:	cummingtonite
czo:	clinozoisite	di:	diopside
ed:	ederite	ep:	epidote
ged:	gairdrite	gl:	glaucophane
gnt:	garnet	gr:	grossular
hd:	hedenbergite	hn:	hornblende
kfp:	K-feldspar	ky:	kyanite
ml:	millerite	mus:	muscovite
mt:	magnetite	mz:	monazite
or:	orthoclase	pg:	pargasite
pl:	plagioclase	pm:	pumpellyite
pr:	prehnite	ps:	pistacite
py:	pumpellyite	pyr:	pyrope
pyp:	pyrophyllite	qtz:	quartz
rt:	rutile	sg:	siegenite
sill:	sillimanite	sp:	sphalerite
sps:	spessartine	tr:	tremolite
tsch:	tschermakite	uv:	uvavovite

a:	activity	γ:	activity coefficient
K:	reaction coefficient	σ:	standard deviation
P:	pressure	T:	temperature

AZ:	Anomalous Zone
BIF:	banded iron formation
CAR:	cordierite-anthophyllite rocks
CFZ:	Cadi Fracture Zone
CIA:	chemical indices of alteration
CLP:	Cedar Lake Pluton
HFZ:	Heilo Fault Zone
HSZ:	Hemlo Shear Zone
LSZ:	Local Shear Zone
LTZ:	Lower Tectonic zone
PGC:	Pukaskwa Gneissic Complex
REE:	rare earth element
UTZ:	Upper Tectonic Zone
X(CO ₂):	mole per cent of CO ₂ in a H ₂ O-CO ₂ fluid

TABLE OF CONTENTS

	Page
CERTIFICATE OF EXAMINATION	ii
ABSTRACT	iii
ACKNOWLEDGEMENTS	v
GLOSSARY OF ABBREVIATIONS	vi
TABLE OF CONTENTS	vii
LIST OF FIGURES	xi
LIST OF PHOTOGRAPHIC PLATES	xii
LIST OF TABLES	xiii
LIST OF APPENDICES	xiii
CHAPTER 1 INTRODUCTION	1
1.1 General Statement and Purpose of Study	1
1.2 Location and Access	4
1.3 Previous Study	5
1.4 Methodology	6
CHAPTER 2 GENERAL GEOLOGY	9
2.1 Regional Geology	9
2.1-1 Introduction	9
2.1-2 Stratigraphy	9
2.1-3 Structures	13
2.2 Geology of the White River Property	15
2.2-1 Introduction	15
2.2-2 Stratigraphy	16
2.2-3 Intrusive rocks	29
2.2-4 Regional and local structures	31
CHAPTER 3 GEOCHEMISTRY OF METASEDIMENTARY ROCKS	33
3.1 Introduction	33
3.2 Metasedimentary Rocks	33
3.2-1 Playter Harbour Group	34
3.2-2 Heron Bay Group	35
3.2-2a Middle metasedimentary sequence	35
3.2-2b Upper metasedimentary sequence	36
3.3 Geochemical Characteristics of Metasediments	36
3.3-1 Clastic metasediments	37
3.3-1a Major element oxides	37
3.3-1b Ferromagnesian trace elements (transition metals)	40
3.3-1c Rare-earth-element (REE)	40
3.3-1d Other trace elements	43
3.3-2 Chemical metasediments (BIF)	48
3.3-3 Cordierite-anthophyllite rocks (CAR)	48
3.4 Genesis of Cordierite-anthophyllite Rocks	49

3.5	Chemical Signature of Sedimentary and Weathering Processes	51
3.6	Provenance and Tectonic Setting	57
CHAPTER 4 MINERAL CHEMISTRY		59
4.1	Introduction	59
4.2	Feldspar	59
	4.2-1 Plagioclase	59
	4.2-2 K-feldspar	60
4.3	Amphibole	63
	4.3-1 Introduction	63
	4.3-2 Mg-Fe-Mn amphibole	64
	4.3-2a Orthoamphibole	64
	4.3-2b Cummingtonite	65
	4.3-3 Calcic amphibole	66
	4.3-3a Calcic amphibole in ultramafic volcanic rocks	67
	4.3-3b Calcic amphibole in mafic metavolcanic rocks	67
	4.3-3c Calcic amphibole in other lithologies	74
4.4	Garnet Group Minerals	77
	4.4-1 Introduction	77
	4.4-2 Pyrospite	77
	4.4-3 Ugrandite	80
4.5	Mica Group Minerals	85
	4.5-1 Introduction	85
	4.5-2 Dioctahedral micas	85
	4.5-2a Muscovite	86
	4.5-2b Margarite	87
	4.5-3 Trioctahedral micas	88
	4.5-3a Phlogopite	88
	4.5-3b Biotite	88
4.6	Chlorite	90
4.7	Epidote Group Minerals	91
	4.7-1 Introduction	91
	4.7-2 Clinozoisite and epidote	92
	4.7-3 Halogen-bearing allanite and REE-bearing clinozoisite	93
4.8	Clinopyroxene	99
4.9	Prehnite and Pumpellyite	100
	4.9-1 Prehnite	100
	4.9-2 Pumpellyite	101
4.10	Other Minerals	101
	4.10-1 Al ₂ SiO ₅ minerals	101
	4.10-2 Staurolite and cordierite	102
	4.10-3 Carbonate minerals	103
	4.10-4 Tourmaline	104
	4.10-5 Apatite	105
	4.10-6 Monazite	105
	4.10-7 Oxide minerals	106
	4.10-8 Sulfide minerals	106

CHAPTER 5 METAMORPHIC PETROLOGY	109
5.1 Introduction	109
5.2 Metamorphic Zones	109
5.3 Textural Relationships and Polymetamorphism	119
5.3-1 Metapelitic rocks	119
5.3-2 Mafic metavolcanic rocks	121
5.3-3 Calc-silicates	123
5.4 Metamorphic Conditions	123
5.4-1 Stability of Al_2SiO_5 minerals	124
5.4-2 Garnet-biotite geothermometer	125
5.4-3 Garnet-hornblende geothermometer	129
5.4-4 Garnet-plagioclase- Al_2SiO_5 -quartz geobarometer	130
5.4-5 The orthoamphibole solvus	133
5.5 P-T-t Trajectory and Discussion	133
5.5-1 P-T-t trajectory	133
5.5-2 The timing and cause for the earlier metamorphism	136
5.5-3 The timing and cause for the peak metamorphism	137
 CHAPTER 6 GOLD MINERALIZATION IN LOCAL SHEAR ZONE	 144
6.1 Introduction	144
6.2 The Anomalous Zone and the Local Shear Zone	144
6.2-1 Geological setting	144
6.2-2 Local brittle-ductile shear zone	146
6.2-3 Lithology and mineralogy	149
6.3 Hydrothermal Alterations	151
6.3-1 Hydrothermal alterations	151
6.3-2 Genetic relationships	153
6.4 Gold Mineralization	156
6.5 Geochemical Characteristics	158
6.6 Summary	165
 CHAPTER 7 SKARN DEVELOPMENT	 167
7.1 Introduction	167
7.2 Calc-silicate Occurrences	167
7.2-1 Cr-rich calc-silicates	169
7.2-2 Fe-rich calc-silicates	172
7.2-3 REE-enriched calc-silicates	173
7.2-4 Other calc-silicates	174
7.3 Geochemistry of calc-silicates	175
7.4 Skarns	179
7.4-1 Terminology and classification	179
7.4-2 Regional metamorphism	181
7.4-3 Retrograde alteration	182
7.4-4 Late calc-silicate alteration	183
7.4-5 Discussion	184
7.5 Conditions of Skarn Formation	186

7.5-1 The earlier skarns	186
7.5-1a Geothermometers and geobarometers	186
7.5-1b P-T-X calculations	187
7.5-2 Late calc-silicate alteration	191
7.5-2a P-T-X grids	191
7.5-2b Fluid inclusion study	194
7.6 A Genetic Model for Gold Mineralization in Local Shear Zone	195
7.6-1 An auriferous skarn deposit	195
7.6-2 Sources, transportation and deposition of gold	196
7.6-3 Comparison with other auriferous skarns	202
7.7 Genetic Significance for the Hemlo Gold Deposit and Metallogenesis in the Hemlo-Heron Bay Greenstone Belt	203
 CHAPTER 8 CONCLUSIONS	 207
 APPENDIX I WHOLE-ROCK COMPOSITIONS	 212
 APPENDIX II MINERAL COMPOSITIONS	 223
 REFERENCES	 238
 VITA	 256

LIST OF FIGURES

Figure 1.1 Location map	2
Figure 2.1 Geological map of the Hemlo area	10
Figure 2.2 Geological map of the White River property	17
Figure 2.3 Stratigraphic cross-section	18
Figure 2.4 Geological map of the Playter Harbour Group	22
Figure 3.1 Plot of TiO_2 versus Al_2O_3	39
Figure 3.2 Plots of TiO_2 and $Fe_2O_3^*$ versus MgO	41
Figure 3.3 Plot of Sc versus Co	42
Figure 3.4 Chondrite-normalized REE patterns	44
Figure 3.5 Range of REE abundances	45
Figure 3.6 Plot of Th versus La	47
Figure 3.7 Plot of Ni versus MgO	53
Figure 3.8 Ternary plot of Al_2O_3 - K_2O -($CaO^* + Na_2O$)	55
Figure 3.9 Plots of $Th-Co-Zr/10$ and $Th-Sc-Zr/10$	57
Figure 4.1 Plot of ^{IV}Al versus ($^{IV}Al + Fe^{3+} + Ti$)	70
Figure 4.2 Plot of ^{IV}Al versus ($Fe^{2+} + Fe^{3+}$) for metavolcanic rocks	72
Figure 4.3 Plot of ^{IV}Al versus ($Fe^{2+} + Fe^{3+}$) for metasediments	75
Figure 4.4 Sketch of a broken garnet porphyroblast	79
Figure 4.5 Ugrandite composition	82
Figure 4.6 Comparison of ugrandite composition	84
Figure 4.7 Clinozoisite-allanite compositions	97
Figure 4.8 Chondrite-normalized REE patterns of REE-rich minerals	98
Figure 4.9 Sulfide compositions	107
Figure 5.1 Schematic cross-section showing metamorphic zones	110
Figure 5.2 P-T-t diagram	134
Figure 6.1 Schematic cross-section showing the Local Shear Zone	145
Figure 6.2 Comparison of REE abundances	164
Figure 7.1 Schematic cross-section showing calc-silicate occurrences	168
Figure 7.2 Jenson Cation Plot	176
Figure 7.3 REE abundances of calc-silicates	178
Figure 7.4 P-T-X diagram for Cr-rich calc-silicates	189
Figure 7.5 P-T-X diagram for Fe-rich calc-silicates	190
Figure 7.6 P-T diagram for late calc-silicate alteration	193
Figure 7.7 Fluid inclusion data	199

LIST OF PHOTOGRAPHIC PLATES

Plate I	24
a: Cr-rich calc-silicates of the Cadi Fracture Zone	
b: Relict mafic fragment in Cr-rich calc-silicates	
c: Strongly deformed pillows	
d: Hemlo Fault Zone (HFZ)	
e: Almandine-rich metasedimentary rocks	
f: Banded iron formation (BIF)	
g: Mafic boudinages in unit 8 metapelites	
h: Late local fractures	
Plate II	62
a: Three-feldspar assemblage	
b: Plagioclase and microcline overgrowth	
c: Zonation in calcic amphibole	
d: Zoned garnet porphyroblast	
e: Fibrous uvarovite after chromite	
f: Twinning and zonation in Cr-rich garnet	
g: Margarite after andalusite porphyroblasts	
h: Lamellar intergrowth of prehnite and biotite	
Plate II (cont.)	95
i: REE-rich mineral aggregate	
j: REE-rich mineral aggregate along a foliation plane	
k: Allanite associated with pyrrhotite	
l: Zoned allanite	
Plate III	114
a: Cordierite-anthophyllite rocks	
b: Sillimanite aggregate parallel to the main foliation	
c: Sillimanite after plagioclase	
d: Kyanite porphyroblast	
e: Sericite after kyanite	
f: Staurolite porphyroblast	
Plate IV	148
a: Sericitic and pyritic zones in the Local Shear Zone	
b: Pyrite in muscovite schist	
c: Sulfide and calc-silicate vein	
d: Prehnite vein	
e: Calcite in a feldspar-rich rock	
f: Native gold along pyrite-grain fractures	
g: Native gold along a pyrite grain margin	
h: Native gold associated with silicate minerals	

- a: Cr-rich calc-silicates of the Cadi Fracture Zone
- b: Calcic amphibole after clinopyroxene in Fe-rich calc-silicates
- c: Pyrite in-filling along garnet fractures in Fe-rich calc-silicates
- d: Pervasive prehnite alteration in mafic metavolcanic rocks
- e: Epidote after pyrite
- f: Exsolution lamellar Fe-rich siegenite and cobaltian pentlandite

LIST OF TABLES

Table 5.1 Summary of metamorphic P and T conditions	126
Table 6.1 Chemical compositions of native gold	157

LIST OF APPENDICES

APPENDIX I	WHOLE-ROCK COMPOSITIONS	212
1	Analytical data of clastic metasedimentary rocks	212
2	Analytical data of CAR and BIF	214
3	Analytical data of samples from LSZ	215
4	Analytical data of calc-silicates	217
5	Analytical data of (meta-)volcanic rocks	219
APPENDIX II	MINERAL COMPOSITIONS	223
1	Feldspar Compositions	223
1a.	Plagioclase	223
1b.	K-feldspar	224
2	Amphibole Compositions	225
2a.	Mg-Fe-Mn amphibole	225
2b.	Calcic amphibole in metavolcanic rocks	225
2c.	Calcic amphibole in metasedimentary rocks	226
2d.	Calcic amphibole in calc-silicates	227
3	Garnet Compositions	228
3a.	Pyalspite	228
3b.	Ugrandite	229
4	Mica Compositions	230
4a.	Diocahedral micas	230
4b.	Triocahedral micas	230
5	Chlorite Compositions	232

6	Epidote-Group Mineral Compositions	233
6a.	Epidote-group minerals in Cr- and Fe-rich calc-silicates	233
6b.	Epidote-group minerals in other lithologies	233
6c.	Epidote-group minerals in the Local Shear Zone	234
7	Clinopyroxene Composition	235
8	Prehnite and Pumpellyite Compositions	235
9	Other Mineral Compositions	236
10	Oxide Mineral Compositions	237
11	Sulfide Mineral Compositions	237

The author of this thesis has granted The University of Western Ontario a non-exclusive license to reproduce and distribute copies of this thesis to users of Western Libraries. Copyright remains with the author.

Electronic theses and dissertations available in The University of Western Ontario's institutional repository (Scholarship@Western) are solely for the purpose of private study and research. They may not be copied or reproduced, except as permitted by copyright laws, without written authority of the copyright owner. Any commercial use or publication is strictly prohibited.

The original copyright license attesting to these terms and signed by the author of this thesis may be found in the original print version of the thesis, held by Western Libraries.

The thesis approval page signed by the examining committee may also be found in the original print version of the thesis held in Western Libraries.

Please contact Western Libraries for further information:

E-mail: libadmin@uwo.ca

Telephone: (519) 661-2111 Ext. 84796

Web site: <http://www.lib.uwo.ca/>

CHAPTER 1 INTRODUCTION

1.1 General Statement and Purpose of Study

The Hemlo gold deposit, which contains at least 70 million tonnes of gold ore with an average grade of 7.6 grams Au per tonne (Tintor, 1986), was discovered in 1982 and is the largest gold reserve in Canada. It is located near the northeast shore of Lake Superior, 35 km east of Marathon adjacent to the Trans-Canada Highway 17, at latitude 48°40"N and longitude 86°00"W (Fig. 1.1), and is situated in the Hemlo-Heron Bay greenstone belt, which is part of the larger east-trending Schreiber-White River Belt of the Wawa Subprovince of the Archean Superior Province of the Canadian Shield.

Since the discovery of the Hemlo gold deposit in 1982, various genetic models covering a broad spectrum of geological processes have been proposed for its origin. These opinions are summarized: (1) syngenetic/exhalative (Quartermain, 1985; Cameron & Hattori, 1985; Valliant & Bradbrook, 1986; Ccrrfu & Muir, 1989b), (2) hot spring or epithermal replacement (Goldie, 1985), (3) hypabyssal porphyry-related (Kuhns et al., 1986; Kuhns, 1986), and structurally-focused metamorphic/metasomatic (Hugon, 1984; 1986; Phillips, 1985; Burk et al., 1986; Walford et al., 1986). Corresponding opinions on the timing of the gold mineralization relative to the time of peak metamorphism are therefore: pre-peak (Quartermain, 1985; Cameron & Hattori, 1985; Valliant & Bradbrook, 1986; Kuhns et al., 1986; Kuhns, 1986); close to peak or immediate post-peak (Phillips, 1985; Burk et al., 1986); and post-peak (Walford et al., 1986; Hugon, 1984; 1986).

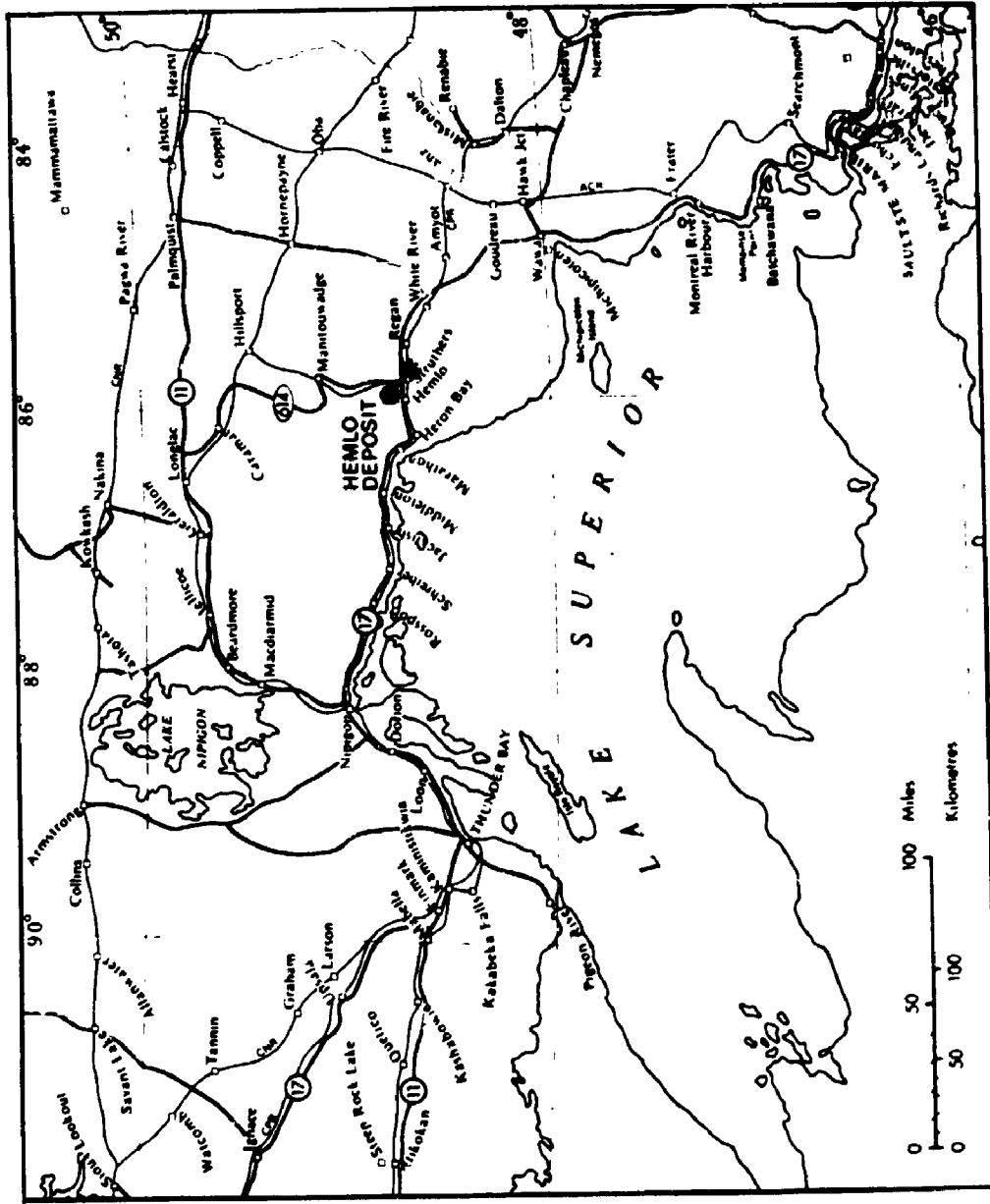


Fig. 1. Location map of the Lake Superior area, North America. Circle indicates the Hemlo gold deposit; star indicates the White River exploration property.

However, it is recognized that many of these conclusions are preliminary, since it has not yet been established to what extent post-peak metamorphism and retrograde processes have obscured the rock record regarding the emplacement of gold. The Hemlo gold deposit differs distinctly from most other Archean gold deposits by its setting in a medium grade metamorphic terrain, association with anomalies of geochemically incompatible (As-Hg-Mo) elements, and lack of extensive carbonate alteration. It appears to be an unusual (probably unique) deposit type of particular genetic significance.

The White River exploration property of LAC Minerals Limited is about 5 km eastward along strike from the Hemlo gold deposit (Fig. 1.1). After discovery of the Hemlo gold deposit in the Hemlo-Heron Bay greenstone belt, it was one of the more important gold prospects. The overall stratigraphy, representation of characteristic rock units, and nature of the gold mineralization are very similar to those at the Hemlo deposit, but with less deformation and pervasive alteration. Therefore, the White River property is ideal for a systematic study of the petrography, mineral chemistry, geochemistry and metamorphic petrology of the Hemlo-Heron Bay greenstone belt rocks. It was hoped that this study might contribute to our understanding of the gold mineralization at the Hemlo deposit.

The original aims of this study were to document geochemical characteristics of the principal lithologies and the variation in metamorphic grade and P-T conditions in the Hemlo-Heron Bay greenstone belt at the White River property. It was also anticipated to further understanding of the relative roles of hydrothermal and metamorphic processes in either forming or modifying Hemlo-type gold deposits. The discovery of three prominent calc-silicate occurrences and abundant

calc-silicate veins and veinlets at the study area gave rise to another major objective of this thesis research: to examine the salient mineralogical and geochemical characteristics and genetic relationships of the calc-silicate occurrences and their relationships with the gold mineralization at the study area and within the entire Hemlo-Heron Bay greenstone belt.

1.2 Location and Access

The White River exploration property of LAC Minerals Limited is 40 km east of the town of Marathon, and 5 km east of the Hemlo gold deposit, in the Thunder Bay mining district of northwestern Ontario (Fig. 1.1). The study area is a central portion of the White River exploration property of LAC Minerals Ltd., with the township limit of Struthers to the west and Rust Lake to the east.

Access to the study area, as well as the entire property, is made via a logging trail (the Campbell Express) from Highway 17 (Trans-Canada Highway), and the Cedar Lake from the exploration camp of LAC Minerals Ltd. The entire study area is largely covered by a virgin forest and very few natural outcrops are available for examination. Field study for this thesis research was largely carried out on over a dozen stripped outcrops and trenches, which were prepared by exploration staff of LAC Minerals Ltd. and can be reached through linecuts from the trail.

1.3 Previous Study

In the Hemlo area, sporadic exploration for precious metals, Au in particular, can be dated back to the middle of the last century (Patterson, 1983). Work leading to the actual discovery of the Hemlo deposit followed from the field mapping of Thomson (1931), who recognized the area's potential, and Au was found on the present Page-Williams mine site by a prospector named Moses Fisher (Patterson, 1983). Systematic study in the Hemlo-Heron Bay greenstone belt was not started until about 10 years ago (end of 1970's), when the Ontario Geological Survey began to map and carry out a stratigraphic-tectonic study for the entire greenstone belt from the Lake Superior shoreline near Heron Bay, to the west (Muir, 1978; 1982a; 1982b), to the White River area, to the east (Siragusa, 1983).

Since the discovery of the very large gold deposit at Hemlo in 1982, numerous studies have been carried out by various institutions and investigators. Metallogenic aspects of the regional geology of the Hemlo gold deposit have been reviewed by Robinson & McMillan (1985). The geology of the Hemlo area has been reviewed by Muir (1985) and Patterson (1985). Recent detailed studies on geological, geochemical and geochronologic aspects include Cameron & Hattori (1985), Harris (1986; 1989), Burk et al. (1986), Kuhns et al. (1986), Kuhns (1986, 1989), Valliant & Bradbrook, (1986), Walford et al. (1986), and Corfu & Muir (1989a, 1989b); many of these were presented in the Gold'86 symposium at Toronto. Also, many thesis projects on geological, geochemical and metallogenic aspects of the Hemlo gold deposit have been carried out recently or are currently in progress at a number of North American universities (Schnieders & Smyk, 1988).

1.4 Methodology

The author made four field trips to the Hemlo area during the course of the thesis study. Approximately 2 months were spent visiting prepared outcrops and underground tours of the Williams mine, mapping surface outcrops, logging drill core, and collecting surface samples from the study area.

Two hundred rock samples were collected from diamond drill-holes and outcrops from the White River property. Whole-rock analyses for 154 samples for major and trace element compositions were carried out by a combination of X-ray fluorescence spectrometry (XRF), directly-coupled plasma spectrometry (DCP) and instrumental neutron activation analysis (INAA) methods at Neutron Activation Services Limited of Hamilton, Ontario. Polished thin sections for all rock samples were also prepared for petrographic study.

Mineral compositions were analyzed in detail with two electron microprobes in the Department of Geology, University of Western Ontario. Amphibole and feldspar compositions were made with a MAC-400 electron-microprobe fitted with the KRISSEL automation system and the data were reduced on line with the MAGIC data reduction program. Compositions for all other minerals were obtained by using a JEOL JXA-8600 superprobe with Tracor-Northern 5500 automation and matrix corrections were made using the Tracor-Northern ZAF program. Operating conditions were identical for both electron microprobes: 15 kV, 10 nA, and beam diameters of 2 to 5 μm , using the following mineral and synthetic glass standards: Si, Mg, Ca: diopside; Al, Ti: kaersutite; Cr: chromite; Fe: orthopyroxene; Mn: rhodonite; Ba: Na: albite; K: orthoclase. Precision of the analytical method was

indicated by replicate determinations of the standards (kaersutite for amphibole and micas and anorthite for plagioclase, for example) as calibration monitors.

The 22-element analyses (Appendix II: Table 6c) required for REE-rich minerals were made in three separate schedules because the Tracor-Northern ZAF program accommodates a maximum of only 13 elements per analysis. Twenty elements were determined in two schedules with Ca, La, Ce and Nd common to each schedule. Europium and gadolinium were determined separately in a schedule which included Si, Al, Ca, Fe, La, Ce, Na and P. Electron microprobe analysis of rare earth elements (REE) in minerals is not straightforward due to X-ray line interference (peak overlap; e.g., Exley 1980, Roeder 1985). This interference can be either avoided, by selecting X-ray lines showing minimum interference (Exley 1980), or corrected for, using empirically-determined peak-overlap correction factors (Åmli & Griffin 1975). Roeder (1985) analyzed a selection of REE-minerals by electron microprobe and found that both methods were satisfactory compared with independent chemical analyses. Possible line interferences and correction factors for wavelength-dispersion spectra are given in Table 2 of Roeder (1985). For the REE composition of the present study, the $L\alpha_1$ line of Gd would experience significant interference from Ce $L\gamma_1$. Also, the Eu $L\alpha_1$ line would experience minor interference from Nd $L\beta_1$. I avoided these problems by using the $L\beta_1$ line for both Gd and Eu; the remaining REE (Appendix II: Table 6c) were analyzed with $L\alpha_1$ lines.

X-ray powder diffraction methods were used for mineral identification and recognition of mineral polymorphs of mineral groups, such as mica and alkali feldspar. Powder patterns of minerals of sufficient quantity were obtained with a Rigaku powder diffractometer with Cu $K\alpha$ radiation and quartz as internal standard.

8

X-ray diffraction patterns for mineral grain(s) removed from thin sections were obtained with a 57.3 mm Gandolfi camera with Cr K α radiation. Grains of minerals (or mineral aggregates) were removed from thick thin sections (60 μ m) and examined by X-ray single crystal precession method (Mo K α radiation).

Double-polished 60 μ m-thick chips for the microthermometric examination of fluid inclusions were prepared by the method described by Holland et al. (1978). Homogenization and freezing temperatures were measured on a Linkam TH 600 programmable heating-cooling stage, mounted on a Leitz Orthoplan binocular microscope fitted with a long working distance UTK 50/0.63 objective lens and a long focal length condenser lens assembly. Calibration of the heating-freezing stage was carried out according to the procedures of Macdonald & Spooner (1981).

A GPP (Geist et al., 1985) program was adopted to perform statistical calculations and graphics for the whole-rock geochemical data on a TRON personal computer (IBM compatible, operating with DOS 3.1). Mineral formulae were calculated on the basis of number of oxygen atoms (or equivalent) in individual mineral species or mineral groups on the Cyber computing system at the University of Western Ontario. The Fe²⁺/Fe³⁺ proportion was estimated mainly by charge-balance calculations according to ideal stoichiometries, except for that in calcic amphibole for which the "mid point" of the Papike et al.'s (1974) procedure was used. Details for the computation of P-T-X conditions for all principal assemblages (including calc-silicates) will be given in the text.

CHAPTER 2 GENERAL GEOLOGY

2.1 Regional Geology

2.1-1 Introduction

The White River exploration property of LAC Minerals Limited is part of the Archean Hemlo-Heron Bay greenstone belt, which is part of the larger east-trending Schreiber-White River Belt of the Wawa Subprovince of the Superior Province of the Canadian Shield (Thomson, 1931; Muir, 1982a; 1982b; Siragusa, 1983). In the Hemlo-Heron Bay area, sections of the metavolcanics and metasediments of the Archean greenstone belt are surrounded by two granitic bodies (the Gowan Lake Pluton to the north and the Pukaskwa Gneissic Complex to the south), and one alkalic intrusive body (Coldwell Alkalic Complex) to the West (Fig. 2.1). Late Archean granitoid intrusions including the Cedar Lake Pluton, Cedar Creek Stock and Heron Bay Pluton intrude the supracrustal rocks near the axis of an interpreted synform (Patterson, 1984). Dykes of various composition intrude both supracrustal rocks and granitoid bodies.

2.1-1 Stratigraphy

Muir (1982a) has divided the supracrustal rocks into two major stratigraphic sequences near the town of Heron Bay; the Playter Harbour Group to the south, and the Heron Bay Group to the north (Fig. 2.1).

The Playter Harbour Group consists largely of high-iron tholeiitic and pillowed metabasaltic flows in both variolitic and non-variolitic forms (Muir, 1982a). A number of relatively thin, intercalated, discontinuous units of intermediate to

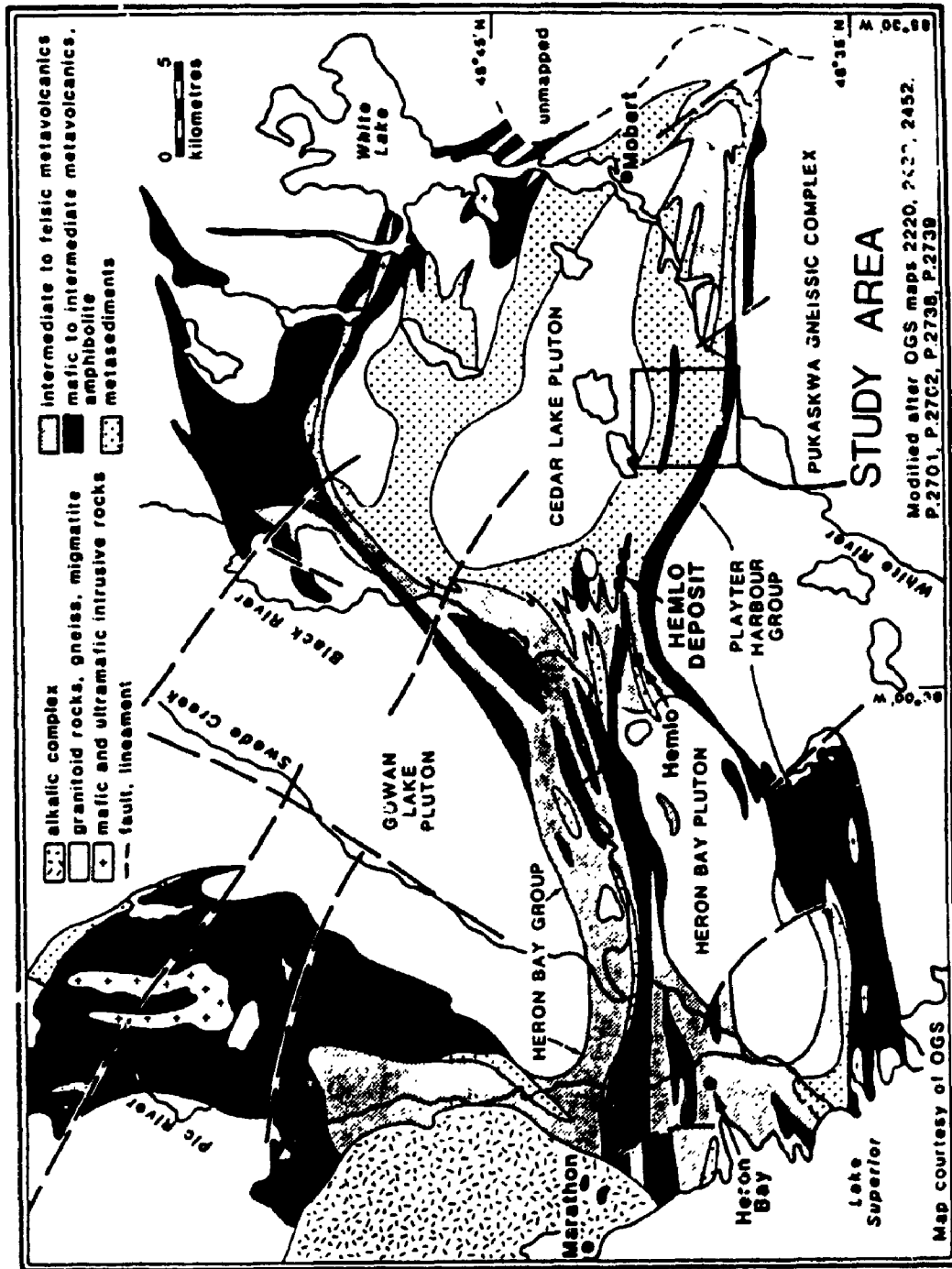


Fig. 2.1. Geological map of the Hemlo area, locating the study area (map compiled by T.L. Muir and reproduced from McMillan & Robinson, 1985).

felsic tuff and lapilli-tuff as well as siltstone were found along the Lake Superior shoreline (Muir, 1982a). These units were rarely found inland. Minor amounts of poorly banded chert, amphibolite, and magnetite ironstone also occur in the west. Isolated lens-shape bodies (sills ?) of pyroxenite and lherzonite are found within the mafic flows in the Heron Bay area, and throughout this group to the east. There are several very thin units of altered graphitic mudstone which contain various amounts and combinations of pyrrhotite, chalcopyrite, and pyrite in the Heron Bay area.

The bulk of the Heron Bay Group is comprised of dacitic and rhyolitic calc-alkalic pyroclastic breccia, tuff-breccia, lapilli-tuff, and tuff; rocks of rhyolitic composition are minor and restricted to the vicinity of Heron Bay (Muir, 1982a). The remainder of the group consists of calc-alkalic basalts as pyroclastic rocks, pillow breccia, and some flows.

The Pukaskwa Gneissic Complex to the south mainly consists of lineated and foliated to weakly gneissic biotite-hornblende trondhjemite and granodiorite (plagioclase-porphyratic and nonporphyritic) with altered small bodies and dikes of massive pegmatite and aplite (Muir, 1982a). Locally within the older granitic rocks there are small areas with well-developed gneisses, or amphibolite inclusions, or bodies which may represent recrystallized and moderately assimilated remnants of intermediate to felsic metavolcanics and metasediments. Within about 1 km of the supracrustal rocks, the trondhjemitic and granodioritic rocks show a weak to moderately developed mylonitic texture with a trend that parallels the contact (to the Playter Harbour Group supracrustal rocks).

The north-central part of the area is underlain by the Gowan Lake Pluton, which consists of lineated and microcline-porphyratic varieties of biotite-hornblende

quartz monzonite (Muir, 1982b). The northwest corner of the area is underlain by part of the Coldwell Alkalic Complex, which consists of olivine gabbro, biotite gabbro, pyroxene monzonite, and pegmatitic hornblende quartz syenite.

An extensive number of relatively late alkalic and subalkalic dikes are present along the Lake Superior shoreline area; they decrease in abundance along the southern parts of the shoreline and rapidly become scarce inland. These dikes, which are probably associated with the Coldwell Alkalic Complex, strike, on average, south-southeast and may be a result of crustal extension as part of the Lake Superior Rift Structure (Muir, 1982b). A few dikes were found west of the Hemlo deposit. Most dikes post-date the subalkalic ("normal") diabase dikes (which have at least two ages; quartz-bearing predates olivine-bearing), porphyritic diabase, lamprophyres, porphyritic syenite, carbonatite, and diatreme-like intrusion breccia. Some of these types of dikes have a number of subtypes; overall age relationships are complex.

Radiometric studies on the ages of various types of rocks in the region have been carried out by Corfu & Muir (1989a; 1989b). Their U-Pb zircon data indicated the occurrence of three main generations of granitoid plutons. A 2719 Ma-old granodiorite near the margin of the Pukaskwa Gneissic Complex is the oldest intrusive rock dated. The most widespread phase of plutonism formed at 2688-2684 Ma (the Cedar Lake Pluton, Cedar Creek Stock, the Heron Bay Pluton and granodioritic phases within the Pukaskwa Gneissic Complex). The youngest intrusion is the Gowan Lake Pluton dated at about 2678 Ma. The Coldwell Alkalic Complex to the west at Marathon has been the object of several geochronologic studies. The most precise ages of 1108 ± 1 Ma for earlier gabbroic and syenitic phases and 1099

Ma for late granitoid phases were reported by Heaman & Machado (1987).

2.1-3 Structures

The large scale structure of the Hemlo-Heron Bay greenstone belt has been described as a broad synform, with the later granitic-granodioritic intrusions (Heron Bay Pluton and Cedar Lake Pluton) along its east-trending fold axis (Patterson, 1984). Opposing dips to the foliations are common on the north and the south sides of the belt, and a distinct fold nose has also been observed near the town of the White River (Milne, 1968; Patterson, 1984). Brittle deformation (faulting and shearing) commonly occur along the contact of brittle and ductile rocks parallel to bedding. Hugon (1984) was the first to report dextral shear within the Hemlo area. Hugon (1984, 1986) concluded that the present geometry of the supracrustal rocks of the Hemlo-Heron Bay greenstone belt resulted from a single, progressive and protracted, dextral deformation event. Other investigators (Kuhns et al., 1986; Muir, 1986; Muir & Elliott, 1987; Muir, 1988) agreed that progressive deformation is probably responsible for some of the observed structures but emphasized that multiple generations of structures with differences in style, rate and physicochemical conditions prevailed during the development of the Hemlo-Heron Bay greenstone belt.

Kuhns et al. (1986) showed that at least four generations of distinct structural events may be recognized in the Hemlo area. They are: (1) pre-peak metamorphic F_1 folds, (2) post-peak metamorphic F_2 folds (the major megascopic structures in this greenstone belt), (3) ductile-brittle T_1 faulting, and (4) brittle T_2 faulting.

Pre-peak metamorphic folding (F_1) is recognized by the presence of isoclinal folds through which a penetrative metamorphic fabric (axial plane foliation or schistosity) has developed. This fabric is characterized by the alignment of metamorphic minerals such as muscovite, biotite and garnet. The amplitude of F_1 is uncertain, since these folds are difficult to recognize unless hinge zones are observed. Post-peak metamorphic folding F_2 is recognized by the presence of isoclinal folding of the metamorphic fabric and refolding of F_1 generation structures. Isoclinal F_2 generation folds have amplitudes which vary from centimetre to metre scale, up to kilometre scale. Flattening associated with F_2 deformation caused boudinage deformation of the banded schists and resulted in significant elongation of primary volcanic fragments and sedimentary clasts; axial ratios of up to 20:1 are observed in some fragments and clasts.

Following F_2 folding, at least two generations of faulting developed parallel or at low-angles to the metamorphic fabric. The earlier of the two tectonic zones (T_1) is referred to as the Lower Tectonic Zone [LTZ, termed as the Lake Superior Shear Zone by Bartley & Page (1957) and the Hemlo Shear Zone by Hugon (1984, 1986)] and is spatially coincident with much of the Hemlo ore zone. A recrystallized and annealed matrix, and development of a weakly to moderately oriented mylonitic fabric are characteristic of the structure. A later tectonic (T_2) is recognized in the upper metasedimentary schists and is referred to as the Upper Tectonic Zone (UTZ). This zone exhibits multiple, well-developed fault breccia and gouge zones, which are developed parallel to the metamorphic fabric. Faulting of the metamorphic rocks occurs over a stratigraphic interval of 30 to 60 m. The UTZ is clearly distinct from, and is interpreted to be younger than, the LTZ by the

absence of a recrystallized matrix and oriented fabrics.

Muir & Elliott (1987) also identified at least four generations of structures produced by at least two deformation events: (1) an early phase resulting in F_1 folds and low-angle normal or thrust faults; (2) a major second phase producing tight to isoclinal F_2 folds and a penetrative axial plane schistosity and differentiated layering (S_2), possibly associated with sinistral shearing and mylonitization; (3) dextral shear which locally resulted in mylonites and small- to medium-scale F_3 folds with axial plane schistosity and crenulation cleavage (S_3); and (4) kink folds and brittle faults.

In addition to the Hemlo Shear Zone (Hugon 1984, 1986), two other structures, which are also of regional significance and are mentioned frequently late in the present study, are described here: (1) a dextral low-angle reverse fault, which is characterized by a distinct unit (up to 3 m thick) of actinolite-chlorite schists and is traceable on the surface for more than 11 km, is present in the lower contact to the south of the HSZ in the central portion of the greenstone belt and is referred to as the Hemlo Fault Zone (HFZ), and (2) a fracture zone [referred to as the Cadi Fracture Zone (CFZ) by field geologists of the LAC Minerals Ltd., and characterized by a magnetic anomaly from the surrounding rocks] occurs at or near the boundaries between clastic metasediments and basic metavolcanic rocks in the southern portion of the belt (Holding, 1987).

2.2 Geology of the White River Property

2.2-1 Introduction

The White River property of LAC Minerals Ltd. is located about 5 km east along strike from the Hemlo gold deposit (Fig. 2.1). The supracrustal rocks, which

strike approximately 75° (ENE) and dip 60° north in the western part of the property and gradually change to a strike of 85° and a dip of 45° north in the central and eastern parts, belong to the southern limb of the interpreted synform, with the Cedar Lake Pluton lying along the fold axis (Patterson, 1984). However, a number of differences in respect to those to the west in the area of the Hemlo gold deposit and near the town of Heron Bay have been recognized at the property. One of these is a prominent transition from dominant calc-alkalic volcanic rocks to the west near the town of Heron Bay to dominant clastic sediments-dominant to the east, which occurs where the Hemlo gold deposit is situated. Therefore, the study area to the east of the Hemlo gold deposit is largely a volcanoclastic-sedimentary basin (Fig. 2.1).

2.2-2 Stratigraphy

At the White River property, the stratigraphically lower high-iron tholeiitic basalts and associated molybdenite and Cu-Zn sulphide occurrences (Siragusa, 1983; Valliant and Bradbrook, 1986; Holding, 1987) to the south and marginal to the Pukaskwa Gneissic Complex are similar in both lithology and metal occurrences to the Playter Harbour Group (Muir, 1982a). The stratigraphically upper sequences of calc-alkaline intermediate to felsic volcanic rocks and clastic sedimentary rocks in association with gold occurrences are similar to the Heron Bay Group. Therefore, Muir's (1982a) divisions for the supracrustal rocks at Heron Bay are applicable to the study area. The supracrustal rocks of the White River property have also been further subdivided into nine lithostratigraphic units (Figs. 2.2, 2.3) on the basis of stratigraphic, lithologic, compositional and textural criteria, arranged in north to

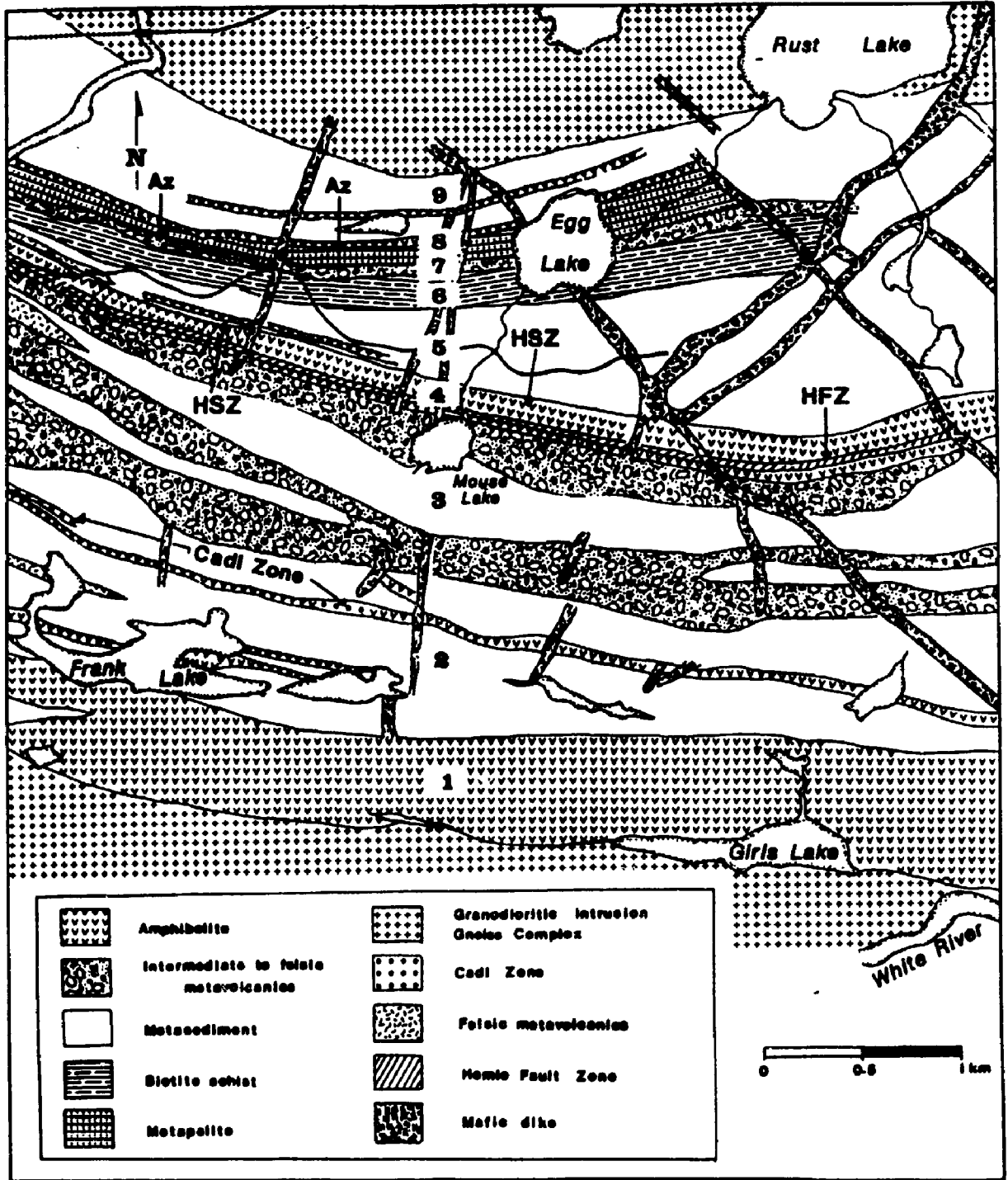
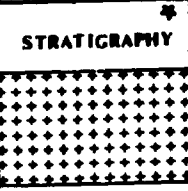
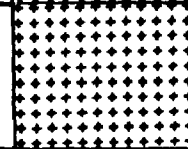


Fig. 2.2. Geology of the White River property (after LAC Minerals Ltd.).

Fig. 2.3. Stratigraphic section of the Hemlo-Heron Bay greenstone belt at the White River property, showing compositional variations in plagioclase and calcic amphibole. * For stratigraphic legend, see Figure 2.2.

GROUP	UNIT	STRATIGRAPHY	THICKNESS (m)	DESCRIPTION	An-CONTENT OF PLAGIOCLASE	AMPHIBOLE	
CEDAR LAKE PLUTON				granodiorite	(8-10) (zoned pl.n.)		
			150	metagreywacke	26		
H E R O N B A Y	9		10	amphibolite	18	Act - Hb — Hb	
			100	metagreywacke	27		
			10	amphibolite	19	Act - Hb — Hb	
			50	metapelite	29		
	8		6	Muscovite schist	26	Act - Hb — Hb	
			70	intermediate metavolcanics	17	Act — Act - Hb	
	7		80	quartz-biotite schists	42	Ay	
			5	banded iron formation	30	(Mg, Fe) Ay + Hb + Ged + Cum	
	6			150	biotite greywacke	22	
				5	lean iron formation	29	Hb + Cum
	5			5	quartz-feldspar porphyry	13	
				60	amphibolite	39	Hb
	4			4	actinolite - chlorite schist	38 + 36	Act — Act - Hb
				120	intermediate - felsic metavolcanics	17 (12)	Act - Hb
			120	metasediments	30	Hb	
			250	intermediate-felsic metavolcanics	20	Act - Hb — Hb	
2			150	metagreywacke	19		
			20	amphibolite	19	Act - Hb — Hb	
			25	calc-silicates	1	Act	
			30	amphibolite	18	Act - Hb — Hb	
					quartz porphyry		
				50	metagreywacke	23	
				20	amphibolite	1	Act - Hb — Hb
				200	metagreywacke		
1			300	amphibolite	35	Hb	
			60	variolitic flows		Hb	
			450	amphibolite	38	Hb	
PUKASKWA GNEISS COMPLEX				granitic gneiss			

south (top to bottom) sequence as:

9. metagreywackes with mafic metavolcanic rocks
8. metapelites
7. upper intermediate to felsic metavolcanic rocks
6. quartz-biotite schists
5. biotite-rich metagreywackes
4. middle mafic metavolcanic rocks
3. lower intermediate to felsic metavolcanic rocks
2. lower metasedimentary rocks
1. lower mafic metavolcanic rocks

Units 1 and 2 correspond to the Playter Harbour Group and units 3 to 9 to the Heron Bay Group.

Unit 1: this lowest unit of mafic metavolcanic rocks structurally overlies the Pukaskwa Gneissic Complex. It consists largely of massive and variolitic varieties of high-iron tholeiitic flows and pillowed basalt flows with a thickness of up to 300 m, which have been metamorphosed to strongly foliated, dark green amphibolite (green to brown hornblende + plagioclase + microcline + biotite). The amphibolite of this unit is distinguished from the amphibolites of the Heron Bay Group by the abundance of medium to very large, zoned plagioclase phenocrysts (2 to 5 mm in diameter). Clastic metasediments are also present as intercalated thin layers (up to a few meters thick) within the mafic metavolcanic rocks. They are mainly composed of quartz, plagioclase, K-feldspar, biotite, garnet, sillimanite, epidote, clinozoisite, and chlorite.

Unit 2: overlying the lower mafic metavolcanic rocks of unit 1 is a very thick (400-700 m) metasedimentary unit (referred to as the lower metasedimentary sequence hereafter). This unit consists of strongly foliated, fine- to medium grained, grey-white, quartz-feldspar mica schists (quartz + plagioclase + microcline + biotite + chlorite + actinolitic hornblende + epidote). Locally, almandine-rich garnet poikiloblasts are present. These clastic metasediments are mineralogically characterized by the presence of calcic amphibole and have blastic-psammitic texture in the eastern part of the study area near the Dunc Lake Fault, they have relics of quartz and feldspar clasts in a weakly foliated or unfoliated, fine-grained matrix. Recrystallization at the margins or grain boundaries of the quartz-clastic relics is well-developed. A laterally extensive band of felsic metavolcanic rocks is present in the lower portion of the unit. This band of felsic metavolcanic rocks is characterized by a well-developed foliation and the abundance of quartz and feldspar fragments which align parallel to the foliation. Small quartz veins (pyrite-bearing) are locally present in this band of felsic metavolcanic rocks. A band (30 m thick) of dark green amphibolite can be traced subparallel to the foliation in the upper portion: a few wedge-shaped fragments of Cr-rich calc-silicates [diopside-hedenbergite + epidote (including Cr-rich epidote) + (end-member) albite + microcline + uvarovite + grandite + actinolite + chlorite + prehnite + pumpellyite, with minor pentlandite + molybdenite + pyrrhotite] occur within or adjacent to the amphibolite band (this is referred to as the "Cadi Fracture Zone (CFZ)" by field geologists of LAC Minerals Ltd.) (Fig. 2.4). Locally, gradational contacts between the Cr-rich calc-silicates and the underlying mafic metavolcanic rocks are observed (Plate Ia). Within the CFZ, abundant relic mafic fragments, which have been metamorphosed to actinolite-

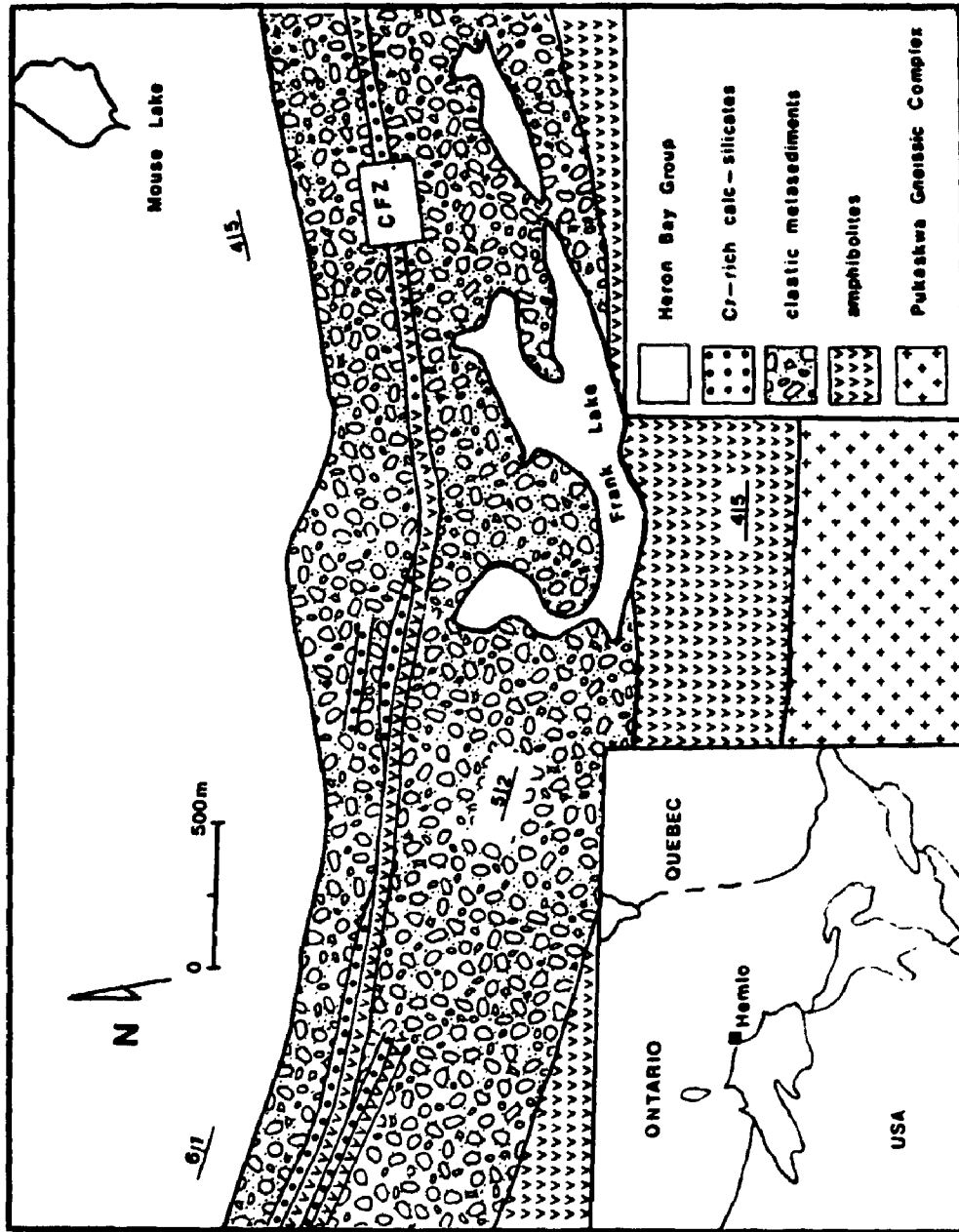
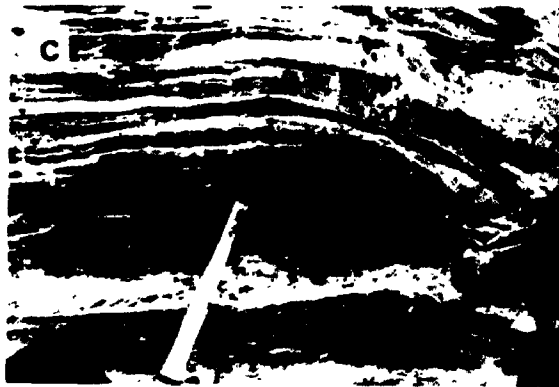


Fig. 2.4. Geological map of the Player Harbour Group and the Cadi Fracture Zone (CFZ is the Cadi Fracture Zone).

PLATE I

- A:** Gradational boundary between Cr-rich calc-silicates and underlying mafic metavolcanic rocks in the Cadi Fracture Zone; note the white cross-cutting vein to the right is an albite vein.
- B:** This photograph shows relict mafic fragments in Cr-rich calc-silicates from the Cadi Fracture Zone, the large crystal to the left is green Cr-bearing garnet.
- C:** Strongly deformed pillows from unit 4; arrows indicate the garnet-bearing (Fe-rich) pillow margin.
- D:** Hemlo Fault Zone as represented by a thin layer of actinolite-chlorite schists.
- E:** Almandine garnet-rich metasedimentary rocks from unit 6.
- F:** The regional banded iron formation (BIF) in unit 6.
- G:** This photograph illustrates the high intensity of deformation close to the Local Shear Zone, as indicated by the development of mafic boudinages in hanging-wall metapelites.
- H:** This photograph was taken from unit 8 metapelites and illustrates the development of late local fractures, which occur nearly perpendicular to the main foliation.



chlorite schist, are well-preserved (Plate Ib). A lens of ultramafic metavolcanic rocks is also present parallel to the plane of foliation in metasedimentary rocks, between two fragments of the Cr-rich calc-silicates.

Unit 3: unit 3 is composed of a sequence with variable thickness (550-750 m) of intermediate to felsic metavolcanic rocks separated by a thick band (200 m) of metasedimentary rocks. These intermediate to felsic metavolcanic rocks are massive, locally weakly-foliated, fine-grained, grey-white rocks containing muscovite, actinolitic hornblende, biotite, quartz, plagioclase, microcline, epidote, and minor zircon, tourmaline, magnetite, pyrite, titanite and apatite. Most rocks of this unit, particularly in the upper portion, contain quartz and plagioclase phenocrysts (average 2 mm diameter): the latter are well zoned and extensively replaced by sericite.

Two layers of very strongly foliated biotite schists are present within unit 3 and contain abundant biotite porphyroblasts and a few almandine-rich garnet poikiloblasts.

Unit 4: the middle sequence of mafic metavolcanic rocks attains a maximum thickness of 140 m and structurally overlies the lower intermediate to felsic metavolcanic rocks of unit 3. Unit 4 is composed of strongly foliated, dark green amphibolite (brown hornblende + biotite + plagioclase + microcline + almandine-rich garnet + quartz) with pillow structures locally present (Plate Ic). These pillows are extensively deformed, particularly near the Hemlo Fault Zone (HFZ), to ellipsoidal shapes with a long axis ranging from 40 to 60 cm and a short axis of about 15 cm. The core of each individual pillow has been metamorphosed to common amphibolite, the outer zone (surface) has invariably been metamorphosed to a distinct thin layer which is characterized by the abundance of large (5 to 6 mm

diameter) almandine-rich garnet porphyroblasts (Plate Ic). A thin (1-3 m) layer of actinolite-chlorite schist can be traced along the lower portion (Plate Id). This schist has been interpreted to represent the Hemlo Fault Zone (HFZ) and is thought to be a regional structure (Patterson, 1984). Carbonate (calcite) veins are well developed in this mafic unit, particularly in the lower portion adjacent to the actinolite-chlorite schist (i.e. HFZ; Plate Id). Veins or veinlets of (prehnite + epidote + calcite + K-feldspar + actinolite + albite) are also extensively developed within the mafic metavolcanic rocks of unit 4.

The middle metasedimentary sequence of supracrustal rocks is approximately 250 m thick in the western part of the study area and up to 800 m thick at the east, and has been subdivided into units 5 and 6.

Unit 5 is characterized by a group of foliated, medium- to fine-grained, biotite-rich metagreywackes. A few fragments of lean iron formation, consisting of hornblende + almandine-rich garnet + plagioclase + quartz + magnetite, are locally present in the lower and middle portion of the unit at the central and eastern part of the study area. A band (10 m thick) of very strongly foliated, coarse-grained, sillimanite-bearing biotite schist is present in the lower portion of this unit near the contact with the mafic metavolcanic rocks of unit 4 at the central and eastern part of the study area.

Unit 6: this unit is typified by a group of very strongly foliated, medium- to coarse-grained, yellowish- or brownish-grey quartz-biotite schists. Thin layers (10 cm to 5 m thick) of aluminous rocks with abundant almandine garnet porphyroblasts are also common in this unit (Plate Ie). Staurolite-bearing quartz-biotite schists generally contain almandine-rich garnet and abundant tourmaline, and staurolite and garnet,

which make up about 10 % of the rock, are commonly poikiloblastic and exhibit the "augen" texture. Sillimanite-quartz-biotite schists commonly containing garnet and staurolite poikiloblasts occur as thin bands (2-3 m thick) in the upper portion of this unit. These bands are characterized by fibrous sillimanite aggregates aligned on the foliation plane. Poikiloblastic cordierite and medium-grained kyanite (partly replaced by muscovite and chlorite) are locally developed, and the alignment of kyanite grains is generally discordant to the penetrative foliation.

There is a regional banded iron formation (BIF) (up to 5 m thick) in the lower portion of this unit. Thin magnetite-dominated layers are interbanded with brown hornblende and quartz-rich layers (Plate If). Coexisting hornblende and cummingtonite are present at the contacts with thin layers of (Mg, Fe)-rich rocks (cordierite-anthophyllite rocks). Very locally, poikiloblastic almandine-rich garnet is replaced by dark-green hornblende and chlorite.

Cordierite-anthophyllite (minor gedrite or cummingtonite as well) rocks are also locally present as thin layers in unit 6 and occur invariably in either close association or direct contact with the regional BIF. Elongated anthophyllite (or gedrite) occurs parallel to the foliation and is partially replaced by chlorite. Cordierite is generally present as large porphyroblasts (up to 2 mm in diameter). Locally, cummingtonite-bearing quartz-mica schists, rather than cordierite-anthophyllite rocks, are present in close association with BIF.

Unit 7: the upper intermediate to felsic metavolcanic unit is up to 100 m thick and is in sharp contact with the quartz-biotite schist of unit 6. It is distinguished from the metasedimentary rocks by a massive, or locally weakly-foliated, fine- to medium-grained texture. It is composed of quartz, plagioclase,

microcline, actinolitic hornblende, epidote, minor pyrite, magnetite, titanite, apatite, tourmaline, and disseminated and veined calcite.

Unit 8: the metapelite of unit 8 is approximately 30 m thick, and is in gradational contact with the unit 7 intermediate to felsic metavolcanic rocks. It is strongly foliated, containing medium- to coarse-grained quartz-biotite, untwinned plagioclase, chlorite, titanite, apatite, tourmaline, and disseminated calcite. Strong deformation in metapelites of unit 8 is indicated by occurrences of mafic boudinages close to lithologic contacts with intermediate to felsic metavolcanic rocks of unit 7 (Plate Ig).

At the boundary between unit 7 (upper intermediate to felsic metavolcanic rocks) and unit 8 (metapelite), a thin layer (up to 25 m thick) of medium- to coarse-grained muscovite schist contains a zone of anomalous gold values ranging from 37 ppb to 27 ppm (Figs. 2.2, 2.3). This thin layer of muscovite schist occurs roughly parallel to the margin of the Cedar Lake Pluton and dips to the north. Mineralogically, this muscovite schist zone is mainly composed of white micas, biotite, plagioclase, microcline, quartz, epidote, clinozoisite, prehnite, margarite, sericite, titanite, apatite and tourmaline with variable amount of pyrite, pyrrhotite, and chalcopyrite. A sharp contact between the muscovite schist and the underlying intermediate to felsic metavolcanic rocks of unit 7 is obvious on stripped outcrops near the Gold Lake, whereas the contact between the muscovite schist and the metapelite of unit 8 is gradational.

Unit 9: the metagreywacke varies from 350 to 600 thick. It is characterized by highly-foliated, yellowish-grey, fine- to very fine-grained quartz-feldspar schists, which consist mainly of quartz, plagioclase, biotite, chlorite, sericite, muscovite, and

locally almandine-rich garnet porphyroblasts, particularly in the metagreywacke adjacent to the contact with the Cedar Lake Pluton, and minor titanite, magnetite and apatite.

Unit 9 contains two laterally extensive bands of mafic metavolcanic rocks, 10 m thick, and in sharp contact with the enclosing metasedimentary rocks. They are strongly-foliated, fine- to medium-grained, dark-green amphibolites (actinolitic hornblende + biotite + plagioclase + microcline), with local abundance of tourmaline grains. Prehnite, epidote, and calcite are present locally as microveins and groundmass in these mafic metavolcanic bands.

2.2-3 Intrusive Rocks.

Earlier (Archean, Muir, 1982a) dykes are common but minor in volume. They range from ultramafic to felsic in composition (peridotite and quartz-feldspar porphyry, etc.) and generally occur parallel to the main foliation. They are invariably altered to some degree. Large plagioclase and K-feldspar phenocrysts generally are partly altered to sericite and chlorite.

The Cedar Lake Pluton is a large irregular granodioritic body, which occurs in the centre and probably along the fold axis (Patterson, 1984) of the Hemlo Heron Bay greenstone belt, and is the northern limit of the study area. It extends nearly parallel to the main foliation. The margin of the Cedar Lake Pluton also dips to the north but at a higher angle than the supracrustal rocks. Mineralogically, the Cedar Lake Pluton is mainly composed of quartz, plagioclase, K-feldspar, hornblende, biotite, epidote and chlorite with titanite, zircon, apatite, oxide minerals, such as ilmenite and magnetite, and pyrite as accessory minerals.

Later (Proterozoic; Muir, 1982a) intrusive rocks are mainly diabase dikes. They are much more abundant than their earlier counterparts and intersect all supracrustal rocks nearly perpendicularly and trend NNE. They are commonly fresh in nature and show no visible features of alteration. To the northeast of the study area, diabase dikes even extend into the Cedar Lake Pluton, clearly indicating their later age.

At the study area, K-feldspar-rich pegmatitic veins are very common in the Playter Harbour Group to the south. Almost all diamond-drill holes from the southern part of the study area intersect a few meters (up to 15 m) of pink, coarse-grained K-feldspar-rich pegmatite. The pegmatite is mainly composed of coarse-grained K-feldspar and quartz with minor biotite and muscovite. Chlorite, molybdenite and sphalerite are also common in fractures of the pegmatitic veins. All pegmatitic veins examined by the present study are generally fresh-looking without evidence of metamorphism and alteration, and the veins are clearly discordant with the main foliation of the supracrustal rocks. Therefore, the emplacement of these pegmatitic veins was definitely later than the formation of the supracrustal rocks, although an absolute age is not available. Their genetic relationship with the major later granodioritic intrusive bodies (Cedar Lake Pluton, Heron Bay Pluton and Cedar Creek Stock) are unclear, but unaltered pink two-mica-bearing K-feldspar-quartz pegmatitic veins are also locally abundant in the greywackes of the unit 9 near the Cedar Lake Pluton.

2.2-4 Regional and Local Structures

It has been stated earlier that the White River property is part of the Hemlo-

Heron Bay greenstone belt. Therefore, many of the regional geological characteristics are also observed at the study area. The nature and complexity of deformation are typical of that within the greenstone belt, and the major regional structures, including Hemlo Shear Zone, Hemlo Fault Zone and Cadi Fracture Zone, also extend into the study area. Some structures which appear to have local significance are dealt with in the following sections.

The supracrustal rocks of the White River property form the southern limb of the interpreted synform and dip at various angles (mainly 45-60°) to the north. The White River property, lying to the east of the Hemlo gold deposit, is a part of the large volcanoclastic sedimentary basin and the most common lithology in the study area is, therefore, deformed and recrystallized clastic metasedimentary rocks. All clastic metasedimentary rocks are generally fine- to medium- grained, and conglomerates, which are present in the area of the Hemlo gold deposit to the west, are typically absent in the study area.

All supracrustal rocks, particularly those at or near lithological boundaries between brittle and ductile (metavolcanic and metasedimentary rocks, respectively) have been subjected to extensive shear deformation (Kuhns et al., 1986; Muir and Elliott, 1987). The Hemlo Shear Zone, which extends from the Hemlo gold deposit area, occurs at or near the boundaries between units 4 and 5 throughout the study area. Numerous thin layers of relatively high strain are also observed but are generally of limited lateral extent. One notable exception is in the thin layer of muscovite schist at or near the boundaries between units 7 and 8, and hosting the zone of anomalous gold values. This is referred to as the Local Shear Zone (LSZ) in order to distinguish it from the regional Hemlo Shear Zone (HSZ). The

characteristics of the LSZ will be further described in Chapter 6.

Three major fracture zones are present in the study area. The Cadi Fracture Zone (CFZ), which is represented by Cr-rich calc-silicates and extends westwards to the Hemlo area, is particularly well-developed at or near the boundaries between basic volcanic flows and clastic metasediments in lithological unit 2 of the Playter Harbour Group. The Hemlo Fault Zone (HFZ), which is represented by thin layers (up to 3 m thick) actinolite-chlorite schists, is situated in the lower portion of the mafic metavolcanic unit 4 of the Heron Bay Group. The Dunc Lake Fault, which forms the eastern boundary of the study area and crosscuts all supracrustal rocks and the Cedar Lake Pluton and even intersects the later north-south trending diabase dykes, apparently did not significantly effect the supracrustal rocks and is not considered further.

Local fractures and faults, which laterally extend only a meter or a few meters, are abundant in the northern part of the study area, and appear to radiate from the Cedar Lake Pluton (nearly perpendicular to the main foliation, Plate 1h).

CHAPTER 3 GEOCHEMISTRY OF METASEDIMENTARY ROCKS

3.1 Introduction

A knowledge of tectonic setting is essential for studies metamorphic petrology and metallogeny in a metamorphic terrain, because variations in metamorphism and metallogeny were largely controlled by systematic variations in structure, sedimentation environment, magmatic activity, and chemical composition related to tectonic setting. However, the tectonic environments of Archean terrains are poorly understood due to their long and complex history, and extensive deformation, uplifting and erosion of their supracrustal rocks. In the past two decades, studies of the geochemical characteristics of volcanic and sedimentary rocks have lead to documentation of their geochemical characteristics and made possible comparisons with modern tectonic environments.

The geochemical characteristics of the host rocks of the gold mineralization (muscovite schists) and calc-silicates (metavolcanic rocks) will be discussed in Chapters 6 and 7, respectively. The major objective here is to document the geochemical characteristics of the metasedimentary rocks, the most abundant lithology in the study area, and to attempt to determine the provenances and tectonic environment of the pre-existing sediments.

3.2 Metasedimentary Rocks

A prominent lithological transition from calc-alkalic volcanic-dominant to the

west passing into a large volcanoclastic-sedimentary basin to the east coincides with the location of the Hemlo gold deposit (Patterson, 1984; Valliant & Bradbrook, 1986). The White River property, to the east of the Hemlo gold deposit, is, therefore, part of the large sedimentary basin and is mainly composed of clastic metasedimentary rocks (Figs. 2.1, 2.2). Metasedimentary rocks of predominantly intermediate composition are commonly well-bedded and laminated. Primary textures, such as graded-bedding and cross-bedding, which have been recognized in the Heron Bay Group sedimentary rocks at the Hemlo gold deposit (Muir, 1988, pers. comm.), are rarely observed in the study area due to extensive deformation and the lack of field exposure. However, blasto-psammitic texture with quartz and K-feldspar relics in a mafic matrix occur in a few weakly-foliated to unfoliated domains. Textural and mineralogical descriptions for metasedimentary rocks in individual lithological units have been given in Chapter 2. These are summarized in the following sections.

3.2-1 Playter Harbour Group

The Playter Harbour Group is mainly composed of high-iron tholeiitic basaltic flows to the western limit of the greenstone belt near Heron Bay (Muir, 1982a). In the study area, a thick unit (unit 2) of clastic metasediments (the lower metasedimentary sequence) occurs to the north of the lowest mafic metavolcanic unit (lithological unit 1). The lower metasedimentary sequence is characterized by dark-grey colour and fine-grained textures, locally with abundant rock fragments consisting mainly of quartz and feldspar. Mineralogically, it differs from clastic metasediments of the Heron Bay Group at the White River property by the presence

of calcic amphibole and low abundance of biotite and muscovite. Other minerals present are quartz, feldspar (mainly plagioclase and minor K-feldspar), epidote, chlorite, and minor to trace amounts of titanite, apatite and opaque minerals (mainly sulfides).

3.2-2 Heron Bay Group

In contrast to the Playter Harbour Group to the south, clastic metasediments are the predominant lithology in the Heron Bay Group. Clastic metasediments are present in all lithologic units with the exception of unit 7. They occur as intercalated layers in metavolcanic rocks of units 3 and 4 and as two thick metasedimentary sequences referred to as the middle sequence (units 5 and 6) and the upper sequence (units 8 and 9). Only a few samples from units 3 and 4 were included in this study. Most of the data for the Heron Bay Group refer to the middle and upper metasedimentary sequences.

3.2-2a Middle metasedimentary sequence

The middle metasedimentary sequence includes two lithological units: biotite-rich greywackes of unit 5 and metapelites of unit 6. The middle metasedimentary sequence (particularly metapelites of unit 6) differs from its lower and upper counterparts by its coarse-grained texture. Mineralogically, it is characterized by high abundances of two micas (biotite and muscovite) and the local presence of aluminum-rich porphyroblasts including kyanite, sillimanite, garnet and staurolite.

Chemical sediments are characteristically present in the middle metasedimentary sequence (in both units 5 and 6) and are invariably oxide-silicate

facies banded iron formations (BIF). They occur generally as thin layers or discontinuous lenses intercalated with clastic metasediments and are best developed in a regional BIF (up to 5 m thick) in the upper portion of unit 6, which is laterally-extensive throughout the study area.

In addition to aluminous schists, a few rocks with mineral assemblages consisting mainly of Fe-Mg-Mn amphiboles (mainly anthophyllite with minor gedrite and cummingtonite) and cordierite are particularly distinctive and are referred to as cordierite-anthophyllite rocks (CAR). The separation of the CAR from aluminous metasediments is particularly evident on geochemical grounds. The CAR are generally spatially related to BIF.

3.2-2b Upper metasedimentary sequence

The upper metasedimentary sequences also includes two lithological units: i.e. metapelites of unit 8 and metagreywackes of unit 9. The unit 8 metapelites are generally medium-grained and are composed of abundant biotite and, locally, minor porphyroblasts of andalusite and garnet. The unit 9 metagreywackes are characteristically fine-grained in texture and the abundance of mica is generally low. Rock fragments also are locally present in the metagreywackes of unit 9 but are considerably less abundant than those in the lower metasedimentary sequence.

3.3 Geochemical Characteristics of Metasediments

Geochemical data, including 13 major element oxides and 25 trace elements, are given in Appendix I. In this section, description and discussion are arranged

according to the lithologic groups (i.e. clastic metasediments, chemical metasediments and CAR) rather than lithostratigraphic sequences (lower, middle and upper sequences), in order to generalize the geochemical characteristics of each lithology and to determine systematic variations of a given lithology with stratigraphic position.

3.3-1 Clastic Metasediments

3.3-1a Major element oxides

The clastic metasediments are generally intermediate to felsic in major element composition and, as a whole, have a very complicated geochemistry. The abundances of the individual major element oxides are highly variable in different rock types, particularly SiO_2 (58-73 wt. %) and Al_2O_3 (12-22 wt. %) show large-scale variations. The greywackes are generally lower in Al_2O_3 and K_2O but higher in Na_2O and CaO relative to metapelites. There also are apparent correlations between major element oxides and the observed mineralogy. For example, clastic metasediments of the lower metasedimentary sequence are characterized by high CaO content (4 to 5.5 wt. %) and low K_2O (1.5 to 2.2 wt. %), corresponding to the presence of calcic amphibole and low abundance in mica. Similarly, Al_2SiO_5 minerals (andalusite, sillimanite, kyanite) and other aluminum silicate minerals, such as garnet and staurolite, are confined to very aluminous rocks. From inspection of all geochemical and petrographic data, the minimum whole-rock Al_2O_3 content associated with the presence of Al_2SiO_5 minerals and aluminum-rich minerals appears to be above 17 wt. %. However, it is necessary to point out here that Al_2SiO_5 -minerals and aluminum-rich minerals do not necessarily occur in all high-

aluminum rocks. In fact, a large amount of the Al content is generally distributed between feldspar and/or mica minerals in all clastic metasediments.

Although the $\text{Al}_2\text{O}_3/\text{Na}_2\text{O}$ weight ratio (the maturity index) of metapelites is slightly higher than that of greywackes, the average values at about 3.4 (2.8-4.0) of unit 2, 4.2 (3.9-5.0) of unit 5, 7.1 (4.4-12.1) of unit 6, 5.2 (3.6-7.9) of unit 8, and 3.5 (3.3-3.8) of unit 9 are typical of that for immature sediments, which supports the textural evidence (the presence of rock fragments) that the maturities of the clastic metasediments from the study area are generally low. Although large variation in Na_2O and K_2O contents is present between all samples analyzed, the weight ratio of $\text{K}_2\text{O}/\text{Na}_2\text{O}$ of clastic metasediments from the study area is typically lower than 1 and mostly lower than 0.7, which is comparable to that of most clastic metasediments formed about 2.5 Ga (cf. Engel et al., 1974).

The values of the $\text{Al}_2\text{O}_3/\text{TiO}_2$ weight ratio in the lower metasedimentary sequence show a wide range of variation from 27 to 45 with an average value of 33 ($\sigma=2.5$, $n=9$). In the middle metasedimentary sequence, although Al_2O_3 and TiO_2 both show a wide range of variation individually, their weight ratio is very constant at about 26 ($\sigma=0.6$, $n=18$); Al_2O_3 and TiO_2 show a good positive correlation (Fig. 3.1). In the upper metasedimentary sequence, the $\text{Al}_2\text{O}_3/\text{TiO}_2$ weight ratio falls into two groups corresponding to lithology (Fig. 3.1): (1) about 27 ($\sigma=1.6$, $n=8$) in metapelites of unit 8 (close to that of the middle metasedimentary sequence), and (2) showing a considerable range of variation with an average of about 36 ($\sigma=3.6$, $n=6$) in metagreywackes of unit 9, which is similar to the lower metasedimentary sequence.

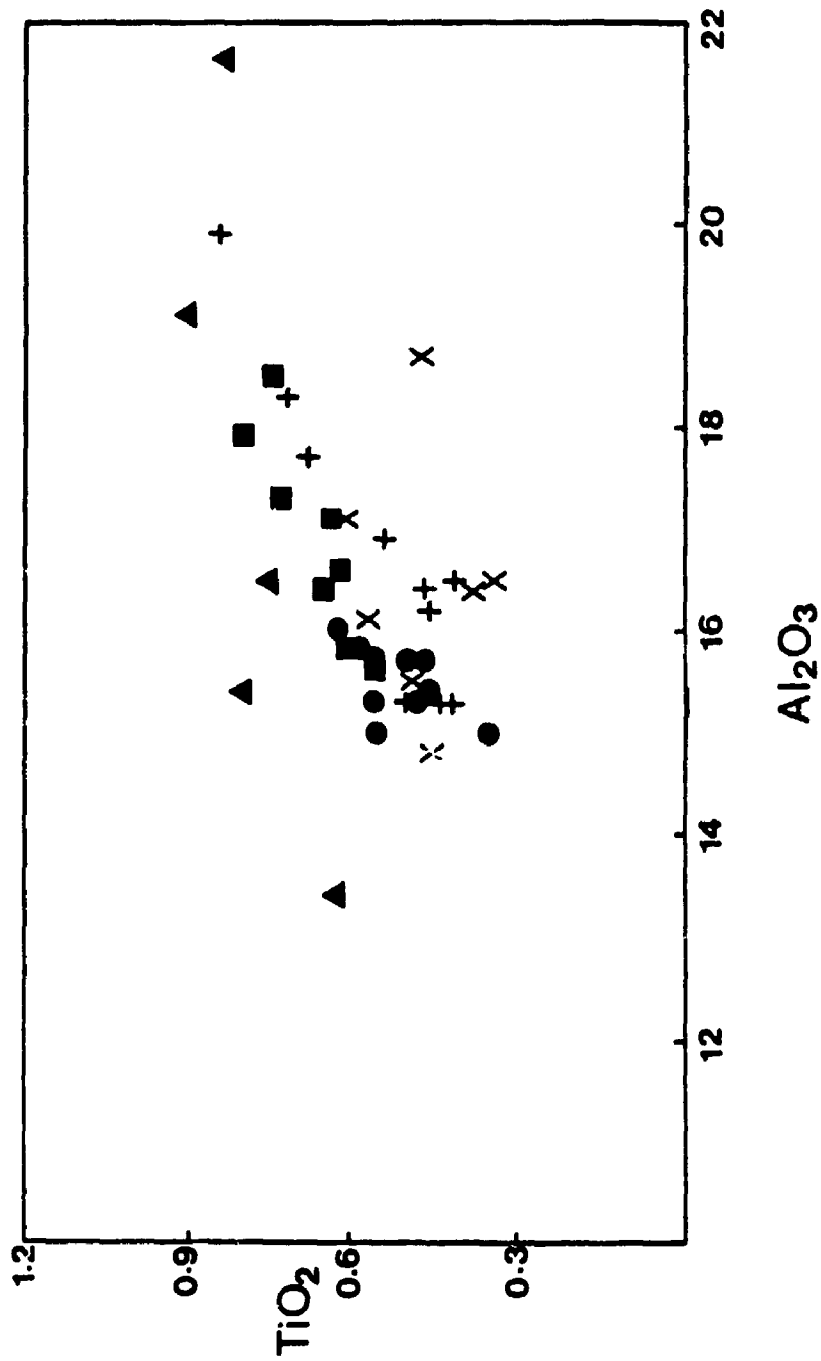


Fig. 3.1. Al_2O_3 - TiO_2 plot for all clastic metasedimentary rocks from the White River property: circles represent unit 1; squares represent units 5 and 6; triangles represent cordierite-anthophyllite rocks of units 5 and 6, crosses represent units 8; and X represents unit 9.

Ferromagnesian oxides, including TiO_2 , Fe_2O_3^* (total iron), MgO and MnO , show fairly good positive correlation with SiO_2 . Figure 3.2 shows plots of Fe_2O_3^* and MnO versus MgO for all clastic metasediments. On this diagram, it is apparent that Fe_2O_3^* and MnO all exhibit good positive correlation with MgO (Fig. 3.2).

3.3-1b Ferromagnesian trace elements (transition metals)

Like most Archean metasedimentary rocks (metagreywackes in particular), clastic metasediments from the study area are characterized by high concentrations of transition metals, including V, Sc, Cr, Co and Ni, particularly Cr (13-410 ppm) and Ni (33-120 ppm). Many investigators (Danchin, 1967; Taylor, 1977; Argst & Donnelly, 1986 and many more) attributed high contents of Cr and Ni to ultramafic or mafic sources and suggested that the earlier crust was more mafic and ultramafic in nature. Some others (McLennan et al., 1983; McLennan & Taylor, 1984) also observed high concentrations of Cr and Ni but argued that secondary enrichment must have played an important role in their enrichment. The most interesting feature of the distributions of these ferromagnesian elements in the present study area is that they have definite positive correlations with Fe_2O_3^* and MgO and negative correlations with SiO_2 . Also, Sc and Co, which have long been viewed as the most immobile ferromagnesian elements (for review see McLennan & Taylor, 1984), are positively correlated (Fig. 3.3).

3.3-1c Rare-earth-element (REE)

Although large variations are characteristically observed in both major and trace element contents of the clastic metasediments from the study area, REE

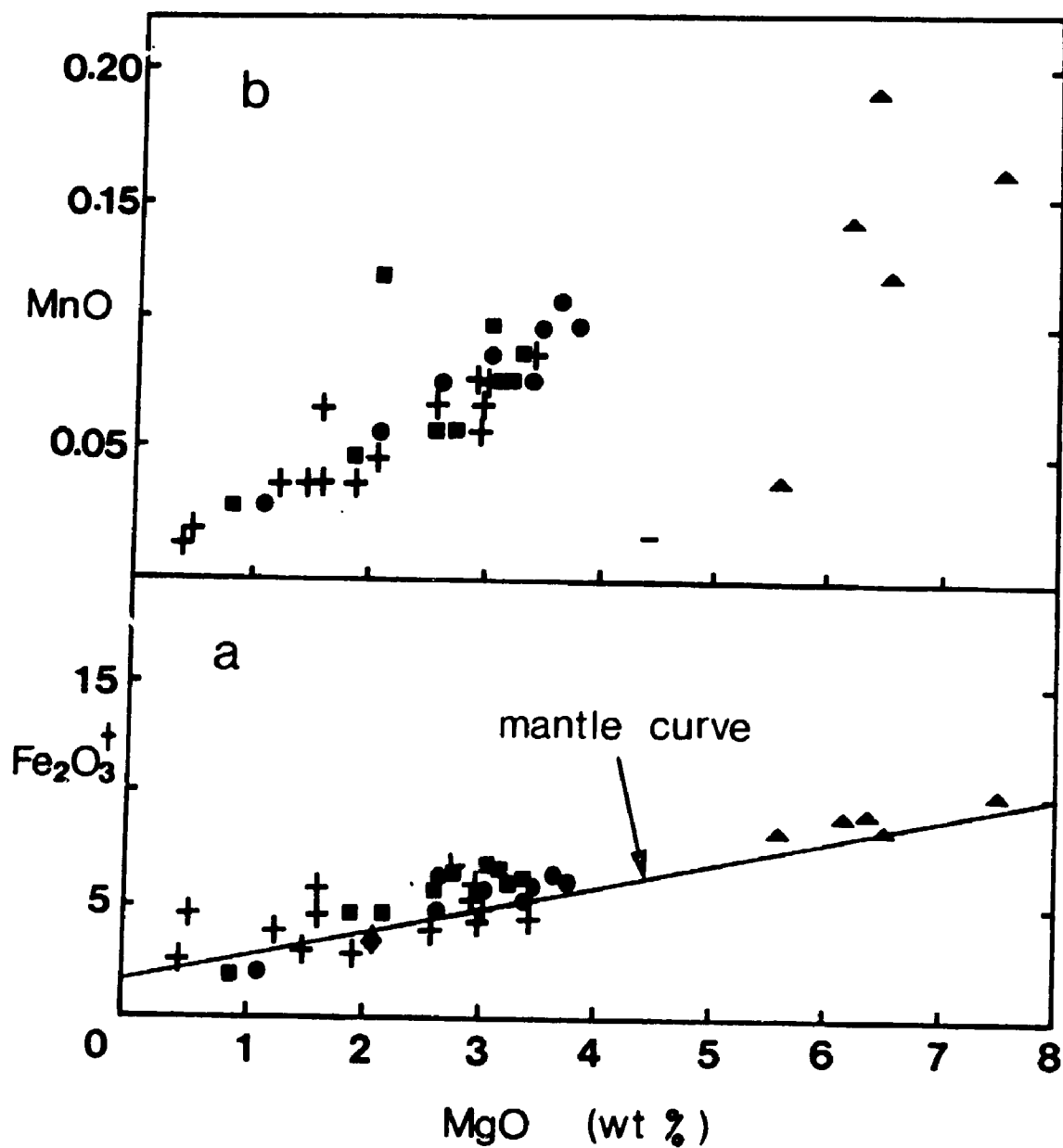


Fig. 3.2. Plots of Fe₂O₃* and MnO versus MgO for all clastic metasedimentary rocks from the White River property: symbols as Fig. 3.1, except that crosses are for all upper metasedimentary rocks (units 8 and 9).

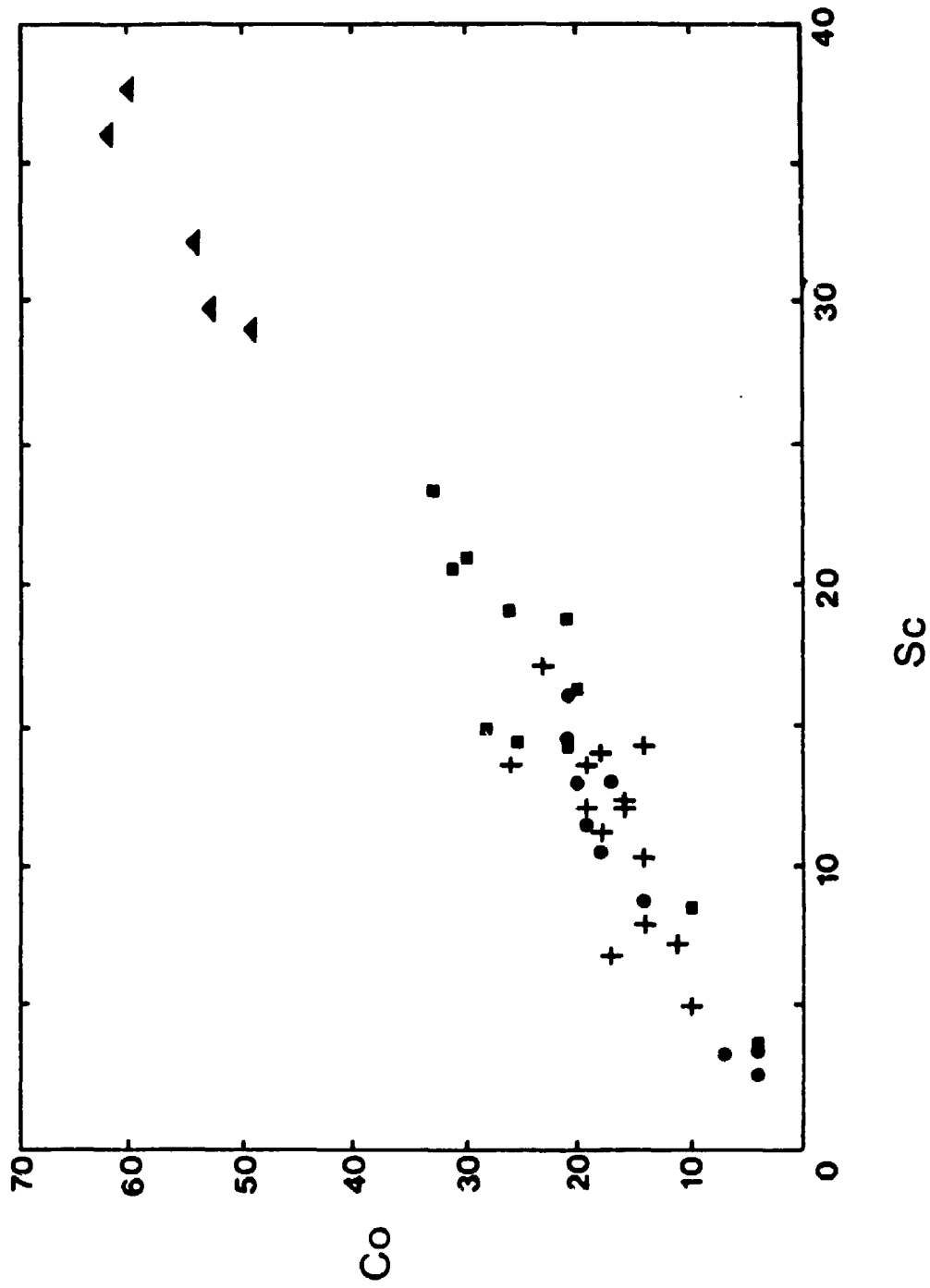


Fig. 3.3. A plot of Sc-Co for all clastic metasedimentary rocks from the White River property: symbols as Fig. 3.1, except that crosses are for both units 8 and 9.

contents are fairly similar for all samples and nearly constant for samples from a given lithology. The absolute abundances for eight REE are given in Appendix I and representative chondrite-normalized patterns are illustrated in Figure 3.4a. The range of REE abundance and patterns for the clastic metasediments from the White River property, which show overall light REE (LREE) enrichment and an absence of an Eu anomaly, resemble the average compositions of Post-Archean Australian sediments (PAAS) but not of Australian Archean sediments (AAS) (Fig. 3.5).

There is no obvious correlation between individual REE abundance and major element oxides in the clastic metasediments. However, the La_N/Yb_N ratio [the fractionation index between LREE and heavy REE (HREE)], in these rocks strongly correlates with major element compositions and exhibits a good negative correlation with $Fe_2O_3^*$. The maximum value of La_N/Yb_N (75) is associated with a low $Fe_2O_3^*$ content and indicates a high fractionation of LREE and HREE, similar to that in intermediate to felsic metavolcanic rocks.

3.3-1d Other trace elements

The concentration of Rb (large monovalent cation) is highly variable (<10-180 ppm) and shows a good positive correlation with the content of SiO_2 , whereas that of Sr (a "small" divalent cation) is also highly variable and elevated (160-1800 ppm) but shows a negative correlation with SiO_2 . However, the ratio of the "large" cations ($K/Rb = 150-400$) and the "small" cations ($Na/Sr = 20-200$) show a very large scatter, in contrast to their incompatible nature and similar behaviour during sedimentary processes. Naqvi et al. (1988) have attributed this to the incomplete mixing and rapidity of sedimentary processes.

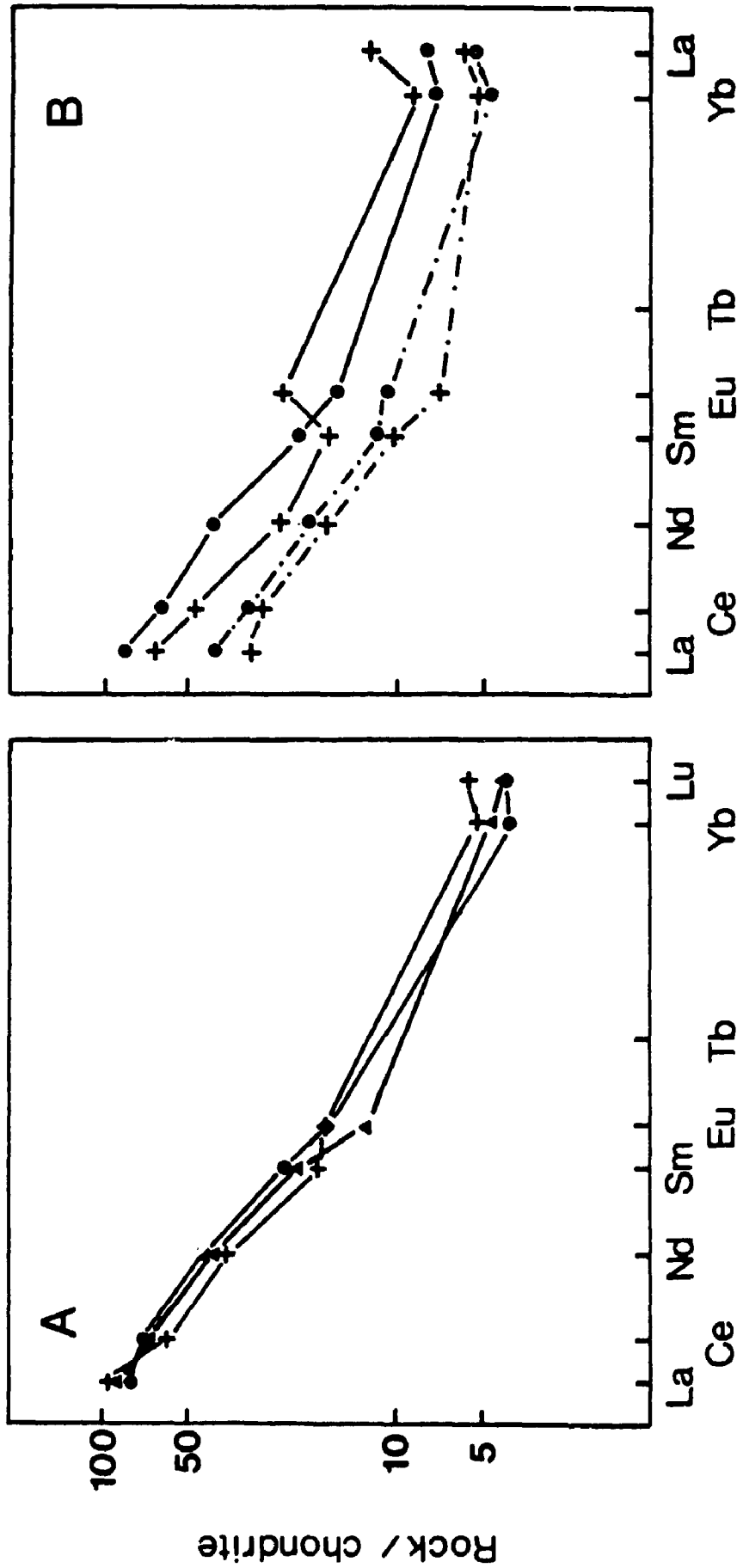


Fig. 3.4. Chondrite-normalized rare earth element (REE) patterns of metasedimentary rocks of the

White River property: A): circle is an average of the lower metasedimentary sequence

(unit 2); triangle is an average of middle metasedimentary sequence; and cross is an

average of upper metasedimentary sequence; B): crosses are cordierite-anthophyllite rocks

of unit 6; circles are banded iron formation (BIF).

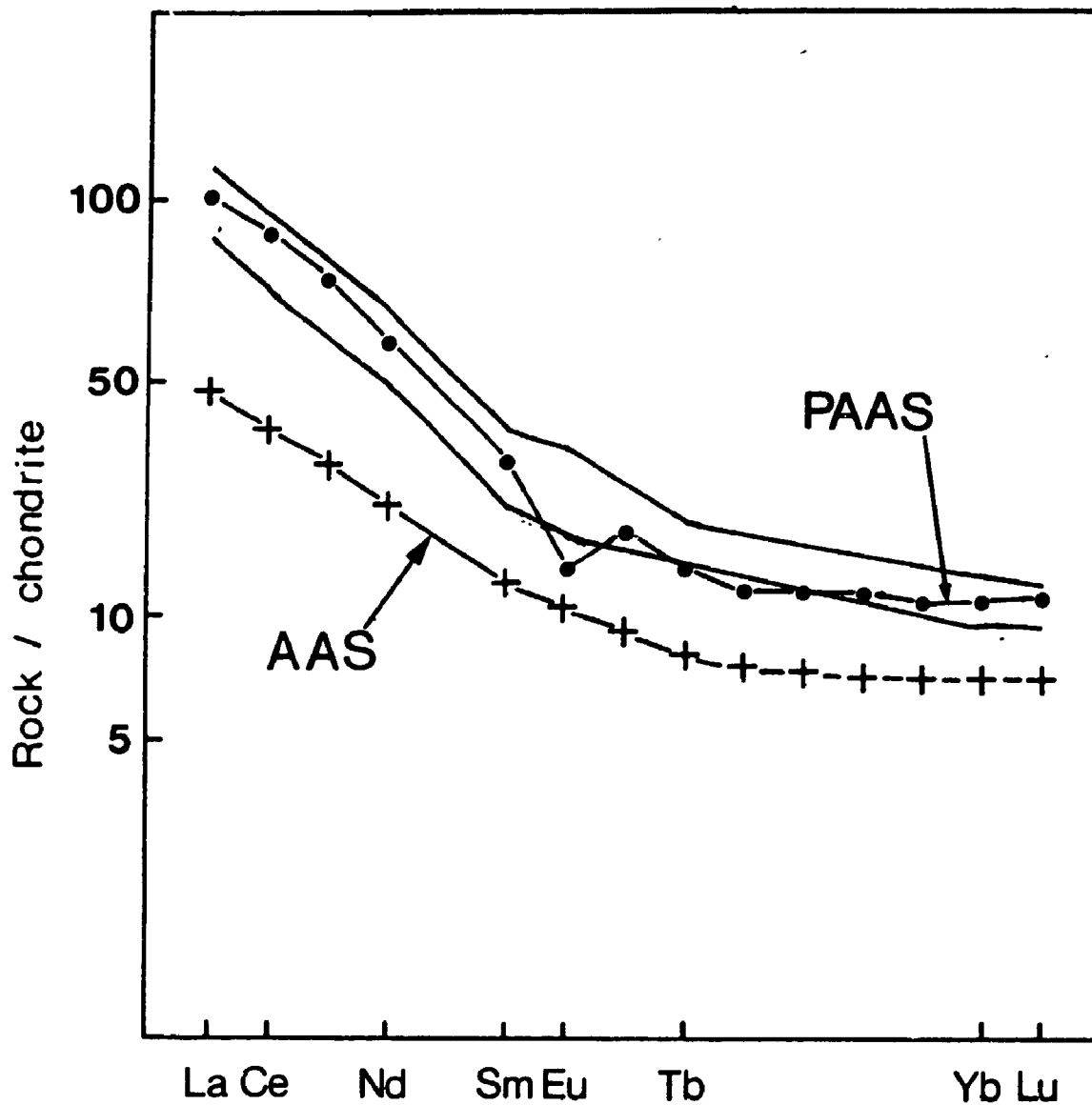


Fig. 3.5. Range of REE abundances in clastic metasedimentary rocks of the White River property, and comparisons with the average compositions of Australia Archean sediments (AAS; cf. McLennan & Taylor, 1980) and Post-Archean Australia sediments (PAAS, cf. Nance & Taylor, 1976).

The contents of B (20-310 ppm) and Ba (70-1100 ppm) are also fairly elevated and extremely variable in the clastic metasediments from the study area. These two elements strongly correlate with mineralogy. B is generally low (<50 ppm) in the Playter Harbour Group and increases northward towards to the Cedar Lake Pluton. This is consistent with the distribution of tourmaline (mainly in veins) which correlates with proximity to the Cedar lake Pluton and not host lithology. Ba does not show a systematic variation with stratigraphy but correlates with the abundance of K-feldspar, which is the main carrier of Ba.

Although the abundances of Th and U are highly variable (0.8-6.3 ppm and <0.5-2.7 ppm, respectively), the Th/U ratios are quite constant for all samples, especially for those from a given lithologic unit, but the average of Th/U ratio of about 3.6 ($\sigma=0.2$, $n=29$) in all samples from the study area is considerably lower than that of post-Archean shales (Th/U = 4.5-5.5; McLennan & Taylor, 1980) but is similar to that of Archean shales and is indistinguishable from that of typical igneous rocks (McLennan & Taylor, 1984).

The geochemical coherence between Th and LREE in sedimentary rocks has been documented by McLennan et al. (1980). This correlation also is observed in clastic metasediments from the study area (Fig. 3.6). However, the La/Th ratio (6-7, with a few values up to 9) is considerably higher than the average estimate (3.5 ± 0.3) for Archean sedimentary rocks (McLennan & Taylor, 1984). It is necessary to point out that the La/Th ratio of the Playter Harbour Group metagreywackes is slightly higher than that of the Heron Bay Group, which, in turn, is slightly higher than that of the metapelites.

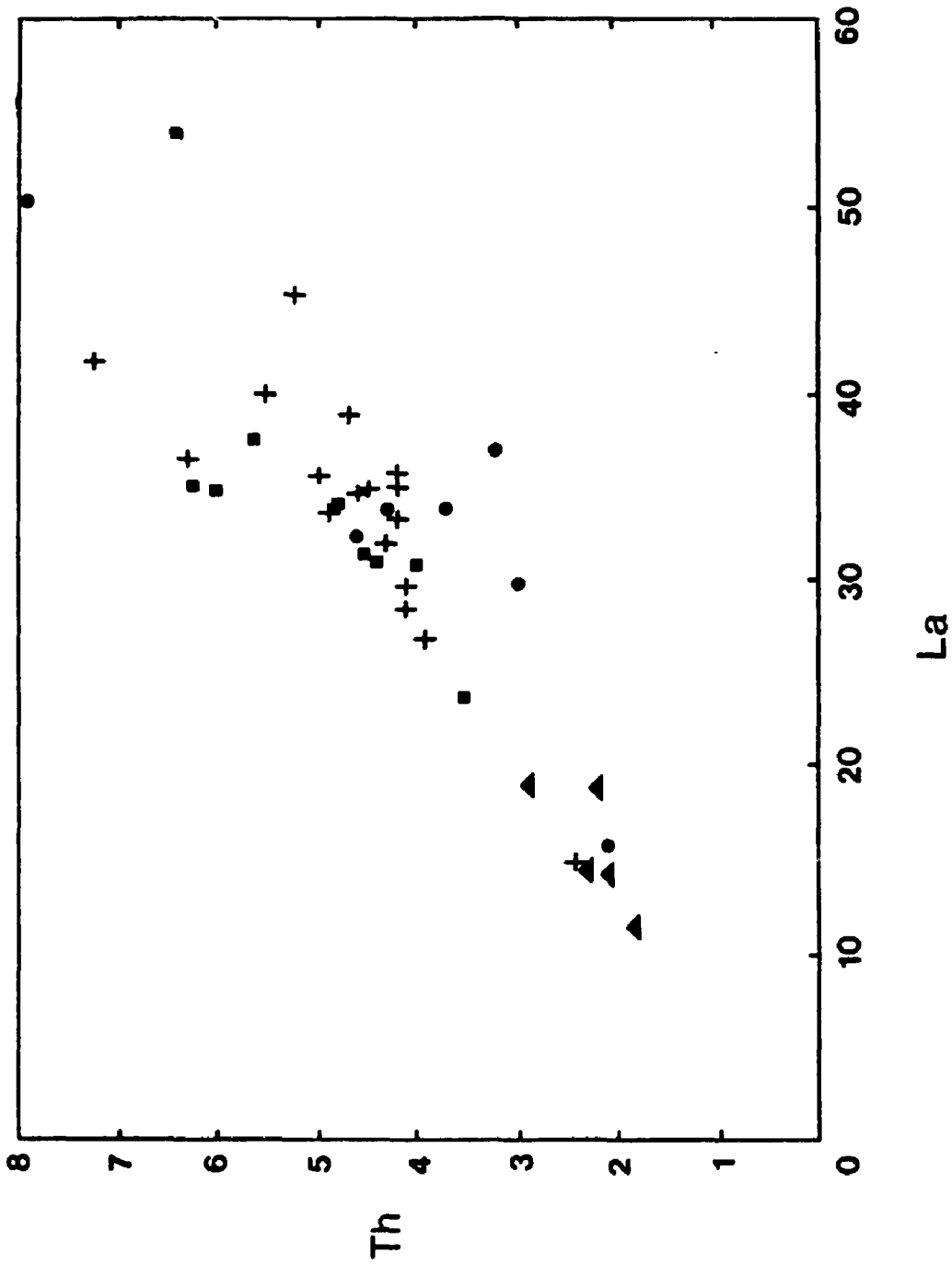


Fig. 3.6. La-Th plot for all clastic metasedimentary rocks from the White River property: symbols as Fig. 3.1; except that crosses are for both units 8 and 9.

3.3-2 Chemical Metasediments (BIF)

In the study area, banded iron formation satisfies the criteria ($\text{Fe}_2\text{O}_3^* > 15$ wt. %) as defined by James (1954). It is characterized by high contents of aluminum and silica (up to 11.8 and 63.1 wt. %, respectively), which correspond to the presence of abundant high-Al calcic amphibole and, locally, almandine garnet as well. The $\text{Al}_2\text{O}_3/\text{TiO}_2$ weight ratio is rather uniform at about 28.6 ($\sigma=0.3$, $n=6$) similar to that of the clastic metasedimentary host rocks. The $\text{K}_2\text{O}/\text{Na}_2\text{O}$ weight ratio, however, shows a considerable range of variation with values greater than 1. There is no coherent correlation between Fe_2O_3^* and MgO nor among ferromagnesian trace elements and MgO. It is noticeable that ferromagnesian trace element abundances, Ni (32-95 ppm) and Cr (160-380 ppm) for example, are well within the range for the clastic metasediments despite significantly higher Fe_2O_3^* contents in the former. The chondrite-normalized REE patterns (Fig. 3.4b) exhibit a strong fractionation between LREE and HREE as indicated by La_N/Yb_N ratios up to 15. This, along with the absence of a positive europium anomaly, differs from other Precambrian counterparts but is similar to that of post-Cambrian ironstones (cf. Fryer, 1977).

3.3-3 Cordierite-Anthophyllite Rocks (CAR)

In the study area, cordierite-anthophyllite rocks (CAR) are distinguished from clastic metasedimentary rocks by their low contents of SiO_2 and high concentrations of Mg and Fe (5.59-6.51 wt. % MgO and 8.40-9.32 wt. % Fe_2O_3^*), and from BIF by lower contents of Fe_2O_3^* (<10 wt. %). The $(\text{Fe}_2\text{O}_3^* + \text{MgO})/\text{Al}_2\text{O}_3$ weight ratio is characteristically greater for whole-rock than for cordierite (cf., Reinhardt, 1987). Although values of $\text{Al}_2\text{O}_3/\text{Na}_2\text{O}$ (4.22-6.88) and $\text{K}_2\text{O}/\text{Na}_2\text{O}$ (0.40-0.91) are similar to

or slightly higher than corresponding values in metagreywackes, the $\text{Al}_2\text{O}_3/\text{TiO}_2$ weight ratio is fairly constant at an average of 21 ($\sigma=0.6$, $n=5$) close to the chondritic and komatiitic values (Sun & Nesbitt, 1978; Condie, 1981). The abundances of transition metals, especially Cr (480-770 ppm) and Ni (300-500 ppm) are significantly higher than in clastic metasediments but are similar to those of komatiitic basalt and komatiite. The chondrite-normalized REE patterns of CAR are also characteristically flat ($\text{La}_N/\text{Yb}_N < 10$) and are accompanied by a positive europium anomaly (Fig. 3.4b). The less mobile incompatible elements, such as Ta, Hf and Th, in CAR also are generally lower in abundances than clastic metasediments.

3.4 Genesis of Cordierite-Anthophyllite Rocks

Before continuing with discussion of the observed geochemical features of the metasediments from the White River property, I shall appraise the genesis of CAR based on available geological, mineralogical and geochemical characteristics outlined in previous sections. This will facilitate later discussion of the geochemical characteristics of clastic metasediments.

Cordierite-anthophyllite rocks (CAR) have attracted much attention since the beginning of this century, because of their most common occurrence in association with volcanogenic massive sulfide deposits and their unusual whole-rock composition which is without equivalents amongst common igneous and sedimentary rocks. The various genetic models proposed for their origin have been tabulated by Reinhardt (1987: Table 1) and are summarized here: (1) synmetamorphic-

metasomatic (Eskola, 1914; Kuroda, 1959; Floyd, 1965; Andres-Jones, 1966; Nilsen, 1971; Irving & Ashley, 1976; Pollard, 1981), (2) metamorphism of Al-contaminated ultrabasic rocks (Pride, 1940), (3) metamorphism of synkinemetamorphically altered rocks (Tuominen & Mikkola, 1950); (4) metamorphism of weathering products (Tilley & Flett, 1929, and later refuted by Tilley, 1935; 1937; Gable & Sims, 1950), (5) residuum of partial melts (Grant, 1968; Lal & Moorehouse, 1969), (6) isochemical metamorphism of hydrothermally altered rocks (Vallance, 1967; De Rosen-Spence, 1969; Froese, 1969; Morton, 1972; James et al., 1978; Schermerhorn, 1978; Hudson & Harte, 1985); and (7) isochemical metamorphism of sediments (Reinhardt, 1987).

The geochemical data [i.e. the $\text{Al}_2\text{O}_3/\text{TiO}_2$ weight ratio close to the chondritic value, extremely high Cr and Ni abundances, a good positive correlation between Ni and MgO, low concentrations of the less mobile incompatible elements (Hf, Ta and Th), low total REE abundance and flat chondrite-normalized REE patterns] collectively favour an ultramafic precursor. Considering geological setting and textural evidence, the cordierite-anthophyllite rocks from the study area are present exclusively in the middle metasedimentary sequence and occur in spatial association with BIF and metapelites. A origin through volcanogenic-hydrothermal alteration cannot be excluded due to the irregularities in morphologies of some CAR occurrences. Thin layers or lenses of high-iron tholeiitic basaltic and komatiitic basaltic flows are not uncommon in all three metasedimentary sequences at the White River property and elsewhere in the Hemlo-Heron Bay greenstone belt. However, these mafic volcanic rocks within the thick metasedimentary sequences were generally metamorphosed isochemically to amphibolites without convincing

evidence either of extensive hydrothermal alteration prior to the regional metamorphism or partial melting during the metamorphic processes. Furthermore, the characteristic geometrical features of alteration pipes (i.e. vertical extension and vaguely conical shape with irregular outlines cutting across footwall strata, cf. Hall, 1982) are generally absent in CAR occurrences. In the study area, the exclusive stratification and lithological association of CAR within a metasedimentary sequence, therefore, favour a sedimentary origin.

Reinhardt's (1987) model of isochemical metamorphism of sediments rests on both field observations and chemical composition of Proterozoic CAR (highly magnesian metamorphic rocks) from Queensland, Australia and on similarities with evaporitic clays and shales. Highly magnesian and extremely (Cr, Ni)-rich (meta-)sedimentary rocks are not uncommon in Archean terrains: e.g. shales from the Fig Tree formation, South Africa and Pilbara, Australia (Danchin, 1967; McLennan & Taylor, 1984). The hosting middle metasedimentary sequence is largely composed of "normal" pelites (shales, mudstones and siltstones, cf. Muir, 1982b). Therefore, the cordierite-anthophyllite rocks from the study area were probably a metamorphic equivalent of (Mg, Fe, Cr and Ni)-rich sediments, which, in turn, may have been derived from a komatiitic source.

3.5 Chemical Signature of Sedimentary and Continental Weathering Processes

One of the most important features of the clastic metasediments from the White River property is their striking similarity in chemical composition to the intercalated and associated intermediate to felsic metavolcanic rocks, as indicated by

the $\text{Al}_2\text{O}_3/\text{Na}_2\text{O}$ weight ratio, good correlations between ferromagnesian trace elements and MgO, the Th/U ratio and the REE composition. This, of course, supports the textural evidence that the clastic metasediments in the Hemlo-Heron Bay greenstone belt at the White River property are generally very immature. This probably resulted from a combination of incomplete mixing and rapid deposition as turbidite deposits. Other limited field evidences [the presence of cross-bedding and conglomerates in greywackes stratigraphically above the Hemlo deposit, the common occurrences of thin quartz-feldspar-rich layers interlayered with thin biotite-muscovite-rich layers in the study area (Bouma A & B sequences ? cf. Bouma, 1962)] collectively favour a turbiditic origin for the clastic metasediments in the Hemlo-Heron Bay greenstone belt.

Although many ferromagnesian trace elements exhibit good correlations with Fe_2O_3^* and MgO contents (similarly to those in volcanic rocks), their elevated abundances at given Fe_2O_3^* and MgO contents distinguish them from intermediate to felsic metavolcanic rocks. Figure 3.7 is a plot of Ni versus MgO for all whole-rock analyses for supracrustal rocks from the study area. Although there is extensive overlap at $\text{MgO} < 3$ wt. %, the average of Ni abundance in clastic metasediments is slightly higher than that in volcanic rocks at a given MgO content. Above an MgO content of 3 wt. %, two distinct trends are apparent with Ni more enriched in clastic metasediments than in metavolcanic rocks. CAR also are plotted in the Figure 3.7. It is interesting to note that there is a good positive correlation between Ni and MgO in these (Mg, Fe)-rich rocks and, in particular, the Ni-MgO trend appears to coincide with that for the sediments, which further supports a sedimentary origin for the CAR.

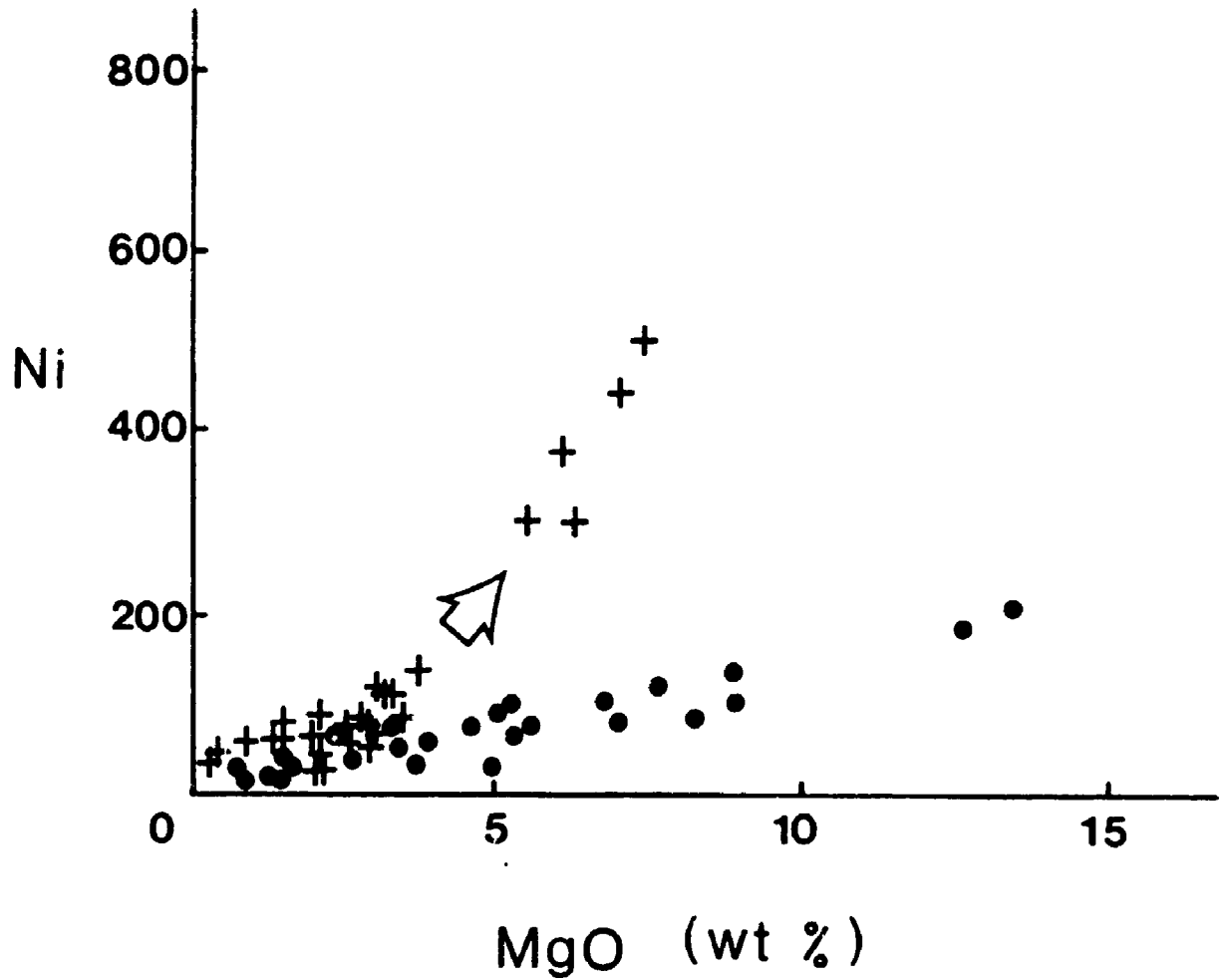


Fig. 3.7. A plot of Ni versus MgO for all supracrustal rocks (except banded iron formation and ultramafic metavolcanic rocks) of the White River property: crosses represent metasedimentary rocks and circles represent metavolcanic rocks.

The relative abundance of weathering products in sediments can be quantified by using a chemical index of alteration (CIA) (Nesbitt & Young, 1982). This permits evaluation of the chemical signature of weathering processes, which can be calculated from the following oxide concentrations expressed in moles:

$$\text{CIA} = [\text{Al}_2\text{O}_3 / (\text{Al}_2\text{O}_3 + \text{CaO}^* + \text{Na}_2\text{O} + \text{K}_2\text{O})] * 100,$$

where CaO* represents Ca associated with silicate phases only. Detailed microscopic observation reveals that the Ca content in sediments from the study area is mainly associated with plagioclase and calcic amphiboles, whereas carbonates and apatite are minor or rare in modal abundances. Therefore, little error is introduced in using the CaO content for CaO*.

The CIA values and a ternary plot of Al_2O_3 - K_2O -($\text{CaO}^* + \text{Na}_2\text{O}$) (Fig. 3.8) for rocks of the study area reveal a well-defined weathering trend for the clastic sedimentary rocks. It is apparent that metagreywackes have low CIA values slightly above and overlapping the volcanic field, whereas metapelites have values greater than the greywackes. The range of CIA-values for the clastic sediments (CIA = 54-69) and the average value of 62 are lower than data for the average shale (CIA = 72-75) and deep-sea mud (CIA = 69). This corroborates textural and the trace element evidence that these clastic sediments from the study area are generally immature and contain significant amounts of volcanic materials. The expected higher CIA values of metapelites relative to metagreywacke indicate either a higher proportion of secondary weathering products or in-situ alteration before diagenesis and lithification.

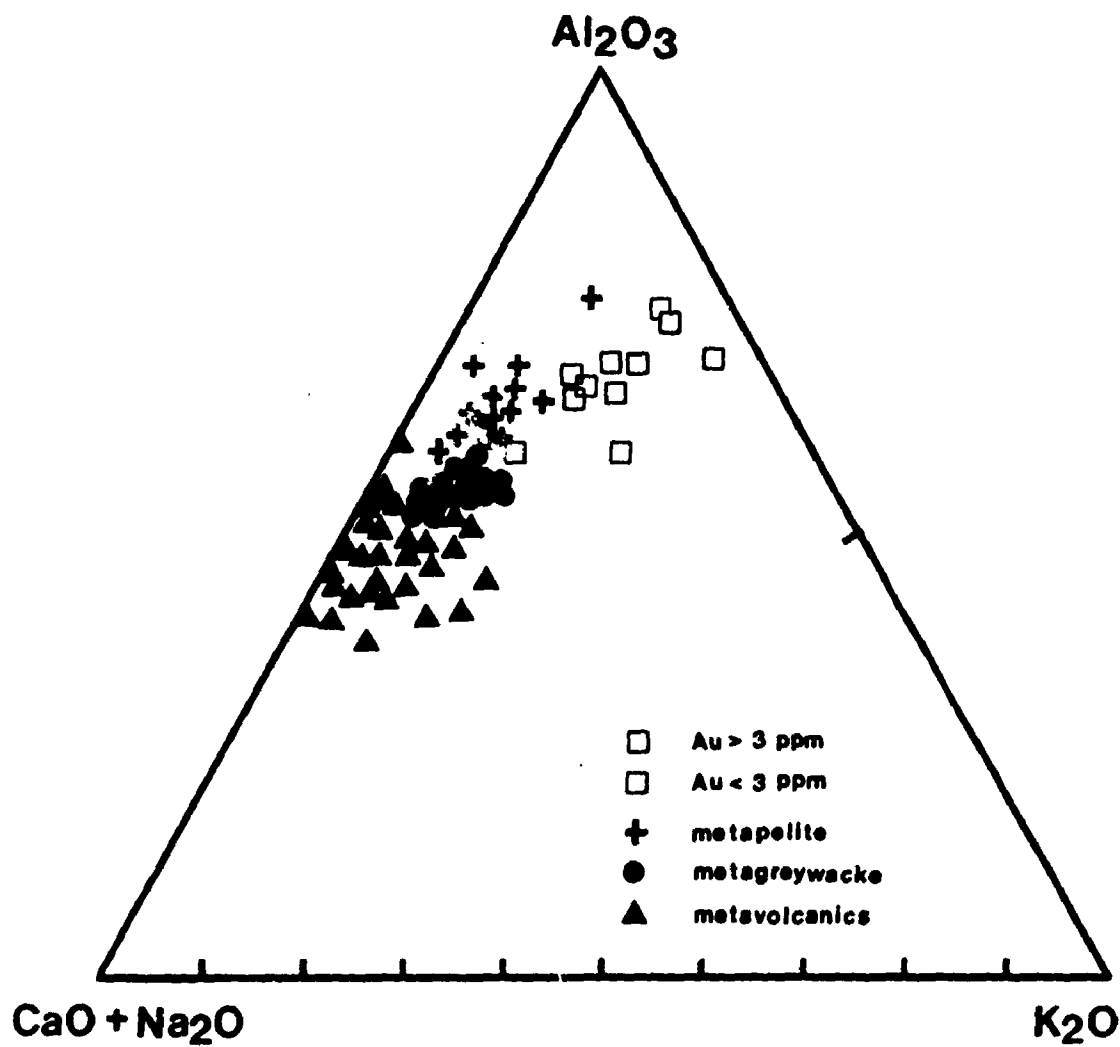


Fig. 3.8. Al_2O_3 -($\text{CaO} + \text{Na}_2\text{O}$)- K_2O ternary plot for all lithologies of the White River property. Note the potassium enrichment in rocks from the Anomalous Zone and the weathering trend from metavolcanic rocks, metagreywackes to metapelites.

3.6 Provenance and Tectonic Setting

Recently, petrographical and geochemical characteristics of sediments deposited in different plate-tectonic environments have been determined. The basic concept is that away from the continent in an ocean basin, the distribution of continental debris is reduced. Deposition in an ocean-island arc, continental-island arc, active continental margin or passive continental margin would be reflected in the mineralogical composition of the sediments. This concept has been used for the Palaeozoic oceanic sediments of Australia and for some other localities, and chemical parameters from known geological settings have been identified for the discrimination of greywackes deposited in several tectonic settings (e.g. Bhatia, 1983; Bhatia & Crook, 1986). These authors have found that the $(\text{Fe}_2\text{O}_3 + \text{MgO})$ content along with the constituents that have a continental source, like $\text{K}_2\text{O}/\text{Na}_2\text{O}$ or $\text{Al}_2\text{O}_3/\text{SiO}_2$ ratios, are very useful for characterizing the various tectonic settings of sedimentation. Trace elements, such as La, Sc, V, Ti, Zr and Th are also found to be useful. However, this concept is not entirely applicable to Archean sediments, as K_2O was not as abundant in Archean continental crust compared to continental crust in Proterozoic and Phanerozoic time. Instead, Na_2O was predominant over K_2O in Archean continental crust (e.g. tonalitic gneisses). Also, during the late Archean, the BIF supplied considerable debris to sediments, which was recycled into greywackes of about 2.6 Ga. Therefore, both the $\text{K}_2\text{O}/\text{Na}_2\text{O}$ ratio and the $(\text{Fe}_2\text{O}_3 + \text{MgO})$ content are to some extent misleading for discrimination purposes in the Archean (Naqvi et al., 1988). In the clastic metasediments from the study area, Na_2O is predominant and the relatively low K_2O abundance is indicated by a $\text{K}_2\text{O}/\text{Na}_2\text{O}$ weight ratio < 1 .

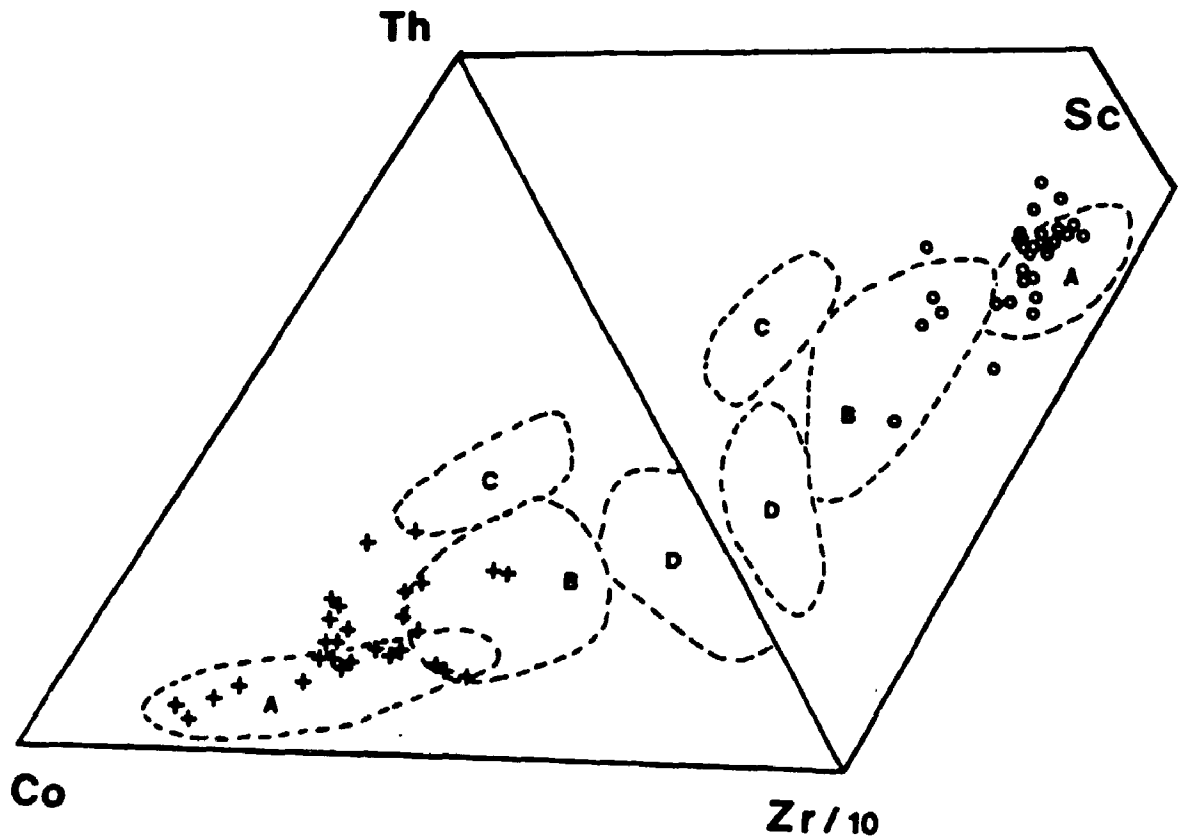


Fig. 3.9. Th-Co-Zr/10 and Th-Sc-Zr/10 triangular plots of the clastic metasedimentary rocks from the White River property for discrimination of tectonic setting. Fields are indicated by dashed lines: A, ocean island arc; B, continental island arc; C, active continental margins; D, passive continental margins (after Bhatia & Crook, 1986).

Although a number of small BIF occurrences are, indeed, present in the study area and elsewhere in the Hemlo-Heron Bay greenstone belt, the good positive correlation between Fe_2O_3^* and MgO (close to the Fe_2O_3 -MgO mantle distribution; Fig. 3.2a) for the clastic metasediments indicates that no significant part of the Fe_2O_3^* content was contributed by BIF.

Sc, V, and Co are well known to be derived from simatic sources, while Th and Zr are from sialic sources. Proportions of these elements are used to distinguish various tectonic settings (Bhatia & Crook, 1986; Naqvi et al., 1988). Figure 3.9 shows triangular plots of Th-Co-Zr/10 and Th-Sc-Zr/10. Like most Archean samples, the clastic sediments from the study area exhibit a wide spread for these geochemical discriminants, but essentially plot within or around the continental island arc or ocean island arc fields. Distinct from most Archean sediments, these clastic sedimentary rocks from the study area are intermediate to felsic in composition with enrichments of highly charged elements such as Th and Zr. The data points in these plots show a shift towards the Th-Zr join. All geochemical discriminants indicate that these clastic sediments were mainly derived from predominantly intermediate volcanic rocks admixed with minor amounts of mafic and ultramafic materials and variable proportions of continental weathering products.

CHAPTER 4 MINERAL CHEMISTRY

4.1 Introduction

At the White River property, the following minerals have been observed in the supracrustal rocks: quartz, feldspars, amphiboles, garnets, micas, chlorite, epidote, clinopyroxene, sillimanite, andalusite, kyanite, staurolite, cordierite, prehnite, pumpellyite, titanite, tourmaline, apatite, calcite, monazite, and some oxide minerals and sulfide minerals. To elucidate the details of complex polymetamorphism in this Archean greenstone belt and to follow the metamorphic reactions in various types of lithologies, chemical analyses of all major mineral phases were carried out by electron microprobe. Most attention was focused on the compositional variations within the rock-forming mineral groups.

4.2 Feldspar

4.2-1 Plagioclase

Petrologists have long been aware of the increase in anorthite content in plagioclase from metamorphic rocks accompanying an increase in metamorphic grade (Goldsmith, 1982, and references herein). Over most of the study area, plagioclase is oligoclase, in units 1, 4, 5, and 6, it is andesine, except for bytownite (An_{40}) in intercalated metasedimentary rocks of lithological unit 1 (Fig. 2.3, Appendix II: Table 1a). Albite is also a frequent constituent in the study area but is generally either confined to veins and veinlets or locally present as a turbid (cloudy) fine-grained replacement of original plagioclase grains. Therefore, albite appears to

be a later alteration product.

In the lowest mafic volcanic rocks of unit 1, plagioclase is one of the predominant constituents, next only to calcic amphibole, and generally occurs as large porphyroblasts (up to 2 mm in diameter) exhibiting a zonation with an oligoclase core and an andesine margin. Plagioclase is also present as a major phase in all other metamorphosed mafic volcanic rocks, but differs distinctly from its counterpart of unit 1 by the lack of chemical zonation.

Interestingly, the actinolitic hornblende-chlorite schists of unit 4 (ultramafic layer) contain an unusual feldspar assemblage [andesine (An_{38}) + bytownite (An_{66}) + K-feldspar] (Plate IIa). This assemblage is similar to that described by Spear (1977) and Grove et al. (1983), who attributed it to equilibrium phase relationships within the $NaAlSi_3O_8$ and $CaAl_2Si_2O_8$ binary series [i.e. albite and andesine coexisting at a low temperature (greenschist facies) and andesine and bytownite at a higher temperature (amphibolite facies)].

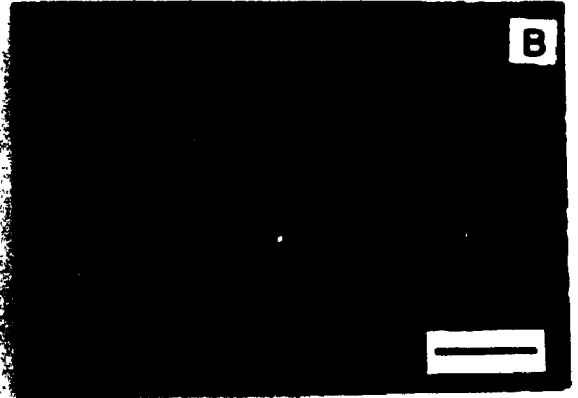
Plagioclase from metasedimentary rocks of units 5 and 6 is generally andesine and compositionally homogeneous. Zoned grains with an oligoclase core and an andesine margin are also locally common (Appendix II: Table 1a); the oligoclase core commonly being partly replaced by very fine-grained sericite. Plagioclase from other metasedimentary rocks (units 2, 8 and 9) is oligoclase and generally homogeneous, with the exception of that in the local shear zone of unit 8, which has a "cloudy" albitic rim.

4.2-2 K-feldspar

K-feldspar is relatively less abundant compared to plagioclase, but it is still

PLATE II

- A: Photomicrograph of three-feldspar assemblage (clear andesine and turbid bytownite; K-feldspar is 0.5 mm outside the field of view) in amphibolites near the Hemlo Fault Zone; scale bar is 0.5 mm.
- B: Photomicrograph of plagioclase and microcline overgrowth in intermediate to felsic metavolcanic rocks of unit 3; scale bar is 0.5 mm.
- C: Photomicrograph of zonation in calcic amphibole (a colourless core and a green margin with a sharp boundary) in amphibolites of unit 9; scale bar is 0.5 mm.
- D: Photomicrograph of a zoned garnet porphyroblast (an inclusion-rich core and an inclusion-poor margin): note that the inclusion trail in the margin is concordant with the schistosity (as defined by alignment of biotite and cummingtonite), whereas the inclusion trail in the core is not; scale bar is 0.5 mm.
- E: Fibrous uvarovite after chlorite in Cr-rich calc-silicates of the Cadi Fracture Zone; scale bar is 0.5 mm.
- F: Photomicrograph illustrating twinning and compositional zonation in Cr-rich garnet; scale bar is 0.5 mm.
- G: Photomicrograph of margarite replacing andalusite along fractures from the Local Shear Zone; note that the elongation and c-axis of andalusite porphyroblasts are parallel to the rock schistosity (as defined by biotite); scale bar is 0.5 mm.
- H: Photomicrograph illustrating lamellar intergrowth of prehnite (white) and biotite in amphibolites of unit 4; scale bar is 0.5 mm.



very common and is present in most rock-types of the study area. It occurs as one of the major phases in sillimanite- and/or kyanite-bearing quartz biotite schists of units 5 and 6 and intermediate to felsic metavolcanic rocks of units 3 and 7 (Plate IIb). One of the most interesting features in chemical composition of K-feldspar from the study area is that barium is commonly present as a minor constituent, particularly K-feldspar from intermediate to felsic metavolcanic rocks (up to 4.1 wt. % BaO corresponding to 8.4 mol. % celsian content). K-feldspar is also present in cross-cutting veins but is generally barium free, with the exception of vein K-feldspar in the Cadi Fracture Zone Cr-rich calc-silicates of the Playter Harbour Group (about 2 wt. % BaO). However, barium is generally at or below detection limit in K-feldspar from most metasedimentary rocks (Appendix II: Table 1b).

An X-ray powder diffraction of K-feldspar with well-developed cross hatch-twinning from cross-cutting veins gives the following diagnostic diffraction angles for Cu-K α radiation (quartz as internal standard): $2\theta(060) = 41.77^\circ$, $2\theta(204) = 50.55^\circ$, $2\theta(131) = 29.35^\circ$ and $2\theta(\bar{1}\bar{3}1) = 30.18^\circ$. Thus, it plots near "maximum microcline" on Wright's (1968) diagram, and its triclinic obliquity $12.5[d(131)-d(\bar{1}\bar{3}1)]$ (cf. Goldsmith & Laves (1954) is 0.94.

4.3 Amphibole

4.3-1 Introduction

Amphibole-group minerals are ubiquitous at the study area (Fig. 2.3). They occur in mafic and ultramafic metavolcanic rocks, in which they make up to 90 vol. % of the rock. They are also present in intermediate to felsic metavolcanic rocks and some of the (Mg-Fe)-rich metasedimentary rocks and BIF at the study area. All

amphiboles from the study area fall into two subgroups: (1) Mg-Fe-Mn amphibole, and (2) calcic amphibole, according to the classification and nomenclature of Leake (1978).

4.3-2 Mg-Fe-Mn Amphibole

Mg-Fe-Mn amphiboles, including cummingtonite, anthophyllite, and minor gedrite, are of restricted occurrences. Among these three Mg-Fe-Mn amphiboles, cummingtonite is the most common species and occurs in thin layers of (Mg, Fe)-rich metasedimentary rocks and BIF of units 5 and 6 and in mafic metavolcanic rocks of unit 4. Orthoamphiboles (anthophyllite and gedrite) are confined to thin layers of (Mg, Fe)-rich metasedimentary rocks and some BIF of units 5 and 6.

4.3-2a Orthoamphibole

Orthoamphiboles (anthophyllite and gedrite) are optically distinguished from other amphibole by their parallel extinction. Gedrite is generally distinguished from anthophyllite by its distinct pleochroism. However, the optical properties were less useful for gedrite and anthophyllite than quantitative electron-microprobe analyses. Three anthophyllite analyses are given in Table 2a (Appendix II) with Mg/(Mg + Fe) from 0.59 to 0.62, and showing no significant variation. Anthophyllite from the study area is also characterized the low CaO and MnO contents. The chemical composition of gedrite (Appendix II: Table 2a) is characterized by higher Mg/(Mg + Fe), Al₂O₃, and Na₂O values but low SiO₂ compared to anthophyllite.

Deer et al. (1963) presented an end-member formula for gedrite of $\text{Mg}_3\text{Al}_2\text{AlSi}_3\text{O}_{11}(\text{OH})_2$, but Robinson et al. (1971) emphasized the importance of Na

as actinolite (or actinolitic hornblende) is transformed into hornblende. This transformation involves a large increase in Al and a smaller increase in (Na + K) as well as a decrease in Mg, due to the tschermakitic substitution, according to the following generalized equations (cf. Grapes & Graham, 1978):

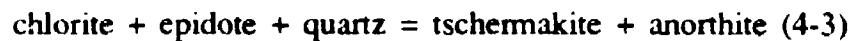
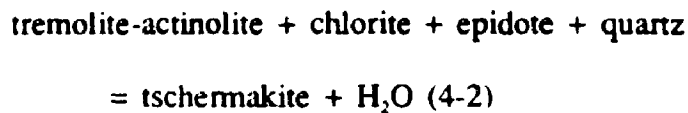


Figure 4.1 depicts the variation in chemical composition of calcic amphibole in a plot of ${}^{\text{IV}}\text{Al}$ versus $(\text{Al}^{\text{VI}} + \text{Fe}^{3+} + \text{Ti})$ (Laird & Albee, 1981). Calcic amphibole from low to medium pressure terrains, such as the Haast River (Cooper, 1972) and the Sudbury Igneous Complex (Fleet et al., 1987) is considerably lower in $({}^{\text{VI}}\text{Al} + \text{Fe}^{3+} + \text{Ti})$ content than that from the Dalradian (Graham, 1974) but higher in these cations than calcic amphibole from the low-pressure Abukuma terrain (Shido, 1958; Shido & Miyashiro, 1959). On this diagram, calcic amphibole from the study area shows a well-defined positive trend regardless of host rock composition towards the ideal composition of $\text{Na}_{0.5}\text{Ca}_2(\text{Mg},\text{Fe})_{1.5}\text{Al}_{1.5}\text{Al}_2\text{Si}_6\text{O}_{22}(\text{OH})_2$. This indicates the coupled substitution of $(\text{Mg}_{1.5} + \text{Si}_2 = \text{Na}_{0.5} + {}^{\text{VI}}\text{Al} + {}^{\text{IV}}\text{Al})$ with evolution of chemical composition during prograde metamorphism of low to medium pressure facies series, rather than a simple pargasitic (Graham, 1974) or tschermakitic (Laird, 1980) substitution.

Compositions of calcic amphibole are also reported on a plot of $(\text{Fe}^{2+} + \text{Fe}^{3+})$ versus ${}^{\text{IV}}\text{Al}$ (Fleet et al., 1987) (Figs. 4.2 and 4.3). This plot along with the ${}^{\text{IV}}\text{Al}$ versus $({}^{\text{VI}}\text{Al} + \text{Fe}^{3+} + \text{Ti})$ plot of Laird and Albee (1981) permits comparison of

Cummingtonite with calcic amphibole (mainly hornblende) is probably the most common two-phase amphibole assemblage in metamorphic rocks because it is stable over a wide range of bulk composition. At the White River property, the cummingtonite-calcic amphibole assemblage is exclusively cummingtonite-hornblende, which occurs in BIF and Fe-rich pillow margins and offers a wide variety of textural features. Commonly, the two amphiboles are relatively coarse-grained and occur in sharp contact with each other. In many cases, neither mineral shows evidence for chemical and optical inhomogeneity, but occasionally, complex intergrowths do occur. Very fine (10 μm) to coarse (1 mm) lamellar cummingtonite may occur within a hornblende host or vice versa, and, in the same thin section, large single grains of each mineral occur in mutual contact. A hornblende rim to cummingtonite grains and patches of hornblende within cummingtonite are also observed.

In chemical composition, cummingtonite from the study area is characterized by higher SiO_2 and lower Al_2O_3 contents than other amphiboles with which it coexists. Other constituents, such as Ca, Mn, and Na are generally low in abundance and show no significant variation. In contrast to orthoamphiboles, cummingtonite shows a wide range of variation in chemical composition, particularly a $\text{Mg}/(\text{Mg} + \text{Fe})$ ratio from 0.472 to 0.628. This ratio in cummingtonite directly correlates with the $\text{Mg}/(\text{Mg} + \text{Fe})$ ratio of its host rock, in which it commonly is the major (Mg, Fe)-bearing mineral (Appendix II: Table 2a).

4.3-3 Calcic Amphibole

Calcic amphiboles are one of most common mineral phases in the study area

(Fig. 2.3). It is the predominant phase in mafic to ultramafic metavolcanic rocks and BIF. It is subordinate to felsic minerals in intermediate to felsic metavolcanic rocks but it is of high abundance in some clastic metasedimentary rocks. Electron-microprobe analyses for calcic amphiboles were calculated on the basis of 23 oxygens and the ferric/ferrous iron ratio was estimated by using the "mid point" in the method of Papike et al. (1974). All analyses in Tables 2b, 2c and 2d of Appendix II satisfy Leake's (1978) criteria for calcic amphibole, having $(Ca + Na)$ in M(4) site > 1.34 and Na in M(4) < 0.67 .

4.3-3a Calcic amphibole in ultramafic metavolcanic rocks

Calcic amphibole in ultramafic metavolcanic rocks of unit 2 of the Playter Harbour Group is tremolite. The tremolite coexists with talc, chlorite, and, locally phlogopite, and is characterized by low contents of Al and alkalis and a $Mg/(Mg + Fe)$ ratio > 0.88 .

Calcic amphibole in ultramafic metavolcanic rocks of unit 4 of the Heron Bay Group is actinolitic hornblende and coexists with the three-phase feldspar assemblage (noted above, and locally quartz + phlogopite + chlorite as well). Actinolitic hornblende is characterized by a narrow range of variation in chemical composition particularly a $Mg/(Mg + Fe)$ ratio from 0.66 to 0.75.

4.3-3b Calcic amphibole in mafic metavolcanic rocks

Calcic amphibole in high-iron tholeiitic basalts (metamorphosed to coarse-grained amphibolites of units 1 and 4) is mainly tschermakitic/pargasitic hornblende. It is generally homogeneous in chemical composition. However, tremolite [$Mg/(Mg$

+ Fe) > 0.86] is also present as thin rims of coarse-grained tschermakitic hornblende or as fibrous crystals associated with epidote in vesicles or veins in the lowest unit (unit 1) of the Playter Harbour Group, and appears to represent a later crystallization. In the amphibolites of unit 4, actinolite is also locally present (mainly adjacent to the Hemlo Shear Zone) and is mostly observed as a lamellar intergrowth with tschermakitic/pargasitic hornblende. In general, this type of texture for actinolite and hornblende would be interpreted as representing equilibrium crystallization, and hence evidence in favour of a miscibility gap (Graham, 1974). Both calcic amphiboles from two-phase calcic amphibole assemblages are conspicuously enriched in total iron content compared to their counterparts in single-phase calcic amphibole assemblages from the same lithologic unit.

Calcic amphibole from mafic metavolcanic layers of lithologic units 2 and 9 are generally medium- to coarse-grained and, locally, display a distinct core and margin; the core comprising a colourless to pale-green actinolite or actinolitic hornblende and the margin consisting of blue-green to brown-green hornblende (Plate IIc). Electron-microprobe spot analyses reveal that each individual grain of zoned calcic amphibole becomes progressively more tschermakitic outwards, both within the core and the margin. This compositional relation is interrupted by an abrupt change in all major components at the optical boundary between the core and the margin. Graham (1974) suggested that the progressive increase in tschermakite content of both the core and the margin may represent a prograde growth zoning. I shall return to this observation in an attempt to constrain metamorphic history of these calcic amphibole-bearing rocks in Chapter 5.

Many authors have discussed the stability of calcic amphibole in prograde metamorphism of mafic metamorphic rocks (metabasites). Wiseman (1934) showed that in diabasic intrusions (epidiorites) of the Grampian Highlands of Scotland, actinolite is stable in the chlorite and biotite zones, whereas hornblende is stable in the garnet zone and in higher-grade zones. Eskola (1939) suggested that the Al_2O_3 contents in calcic amphiboles are related to metamorphic grade. The most extensive studies on the stability of calcic amphiboles in mafic metamorphic rocks were made by Graham (1974) and Laird and Albee (1981), who dealt with the mineralogy of the Dalradian and Vermont metamorphic terrains, respectively. They demonstrated that the change in colour of calcic amphibole from light green in greenschist facies to dark blue-green to brown-green in epidote amphibolite facies and amphibolite facies respectively is due to an increase in atomic substitution of ^{IV}Al , ^{VI}Al , Ti, Fe, Na, K and the ratio of Fe/Mg, with a concomitant decrease in Si, Mg and Ca. These observations from world-wide localities were further supported by the hydrothermal experiments of Liou et al. (1974), Moody et al. (1983), and Spear (1981).

Chemical compositions of calcic amphiboles in mafic to ultramafic metavolcanic rocks from the study area are given in Table 2b (Appendix II). Notable variations are the increase of ^{IV}Al with increase in ^{VI}Al , Fe and (Na + K), and decrease of Mg with decrease in ^{IV}Al and ^{VI}Al . These variations are consistent with the two common substitutions:



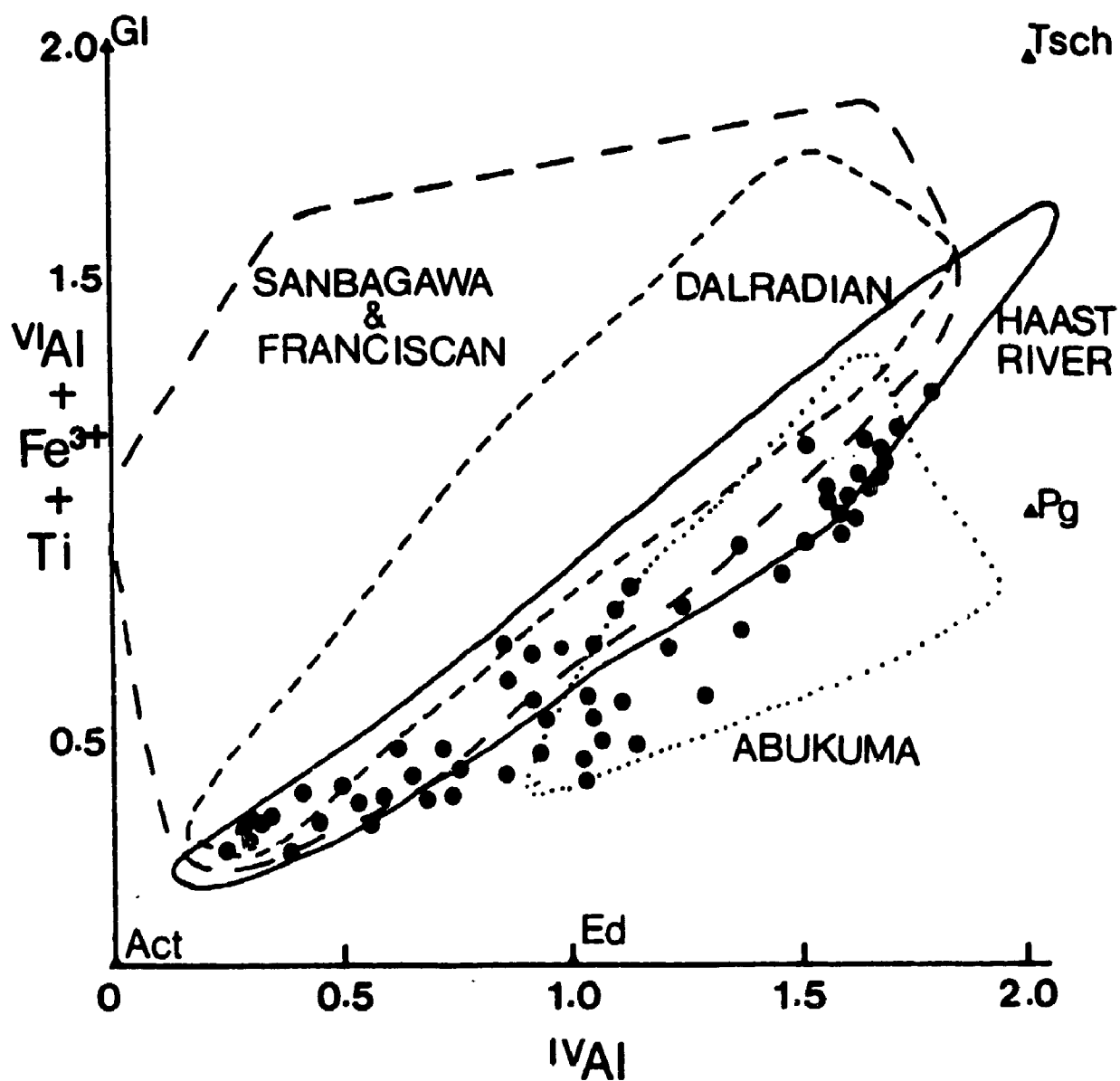


Fig. 4.1. Comparisons of $(VIAl + Fe^{3+} + Ti)$ versus $IVAl$ in calcic amphiboles of mafic and ultramafic metavolcanic rocks of the White River property, with data for reference metamorphic terrains of Laird & Albee (1981).

as actinolite (or actinolitic hornblende) is transformed into hornblende. This transformation involves a large increase in Al and a smaller increase in (Na + K) as well as a decrease in Mg, due to the tschermakitic substitution, according to the following generalized equations (cf. Grapes & Graham, 1978):

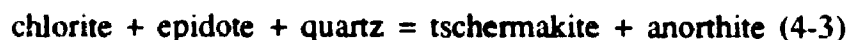
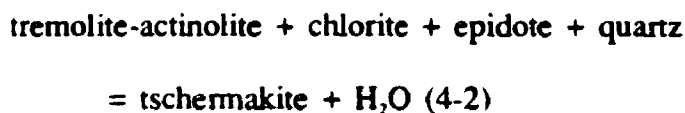


Figure 4.1 depicts the variation in chemical composition of calcic amphibole in a plot of ${}^{\text{IV}}\text{Al}$ versus $(\text{Al}^{\text{VI}} + \text{Fe}^{3+} + \text{Ti})$ (Laird & Albee, 1981). Calcic amphibole from low to medium pressure terrains, such as the Haast River (Cooper, 1972) and the Sudbury Igneous Complex (Fleet et al., 1987) is considerably lower in $({}^{\text{VI}}\text{Al} + \text{Fe}^{3+} + \text{Ti})$ content than that from the Dalradian (Graham, 1974) but higher in these cations than calcic amphibole from the low-pressure Abukuma terrain (Shido, 1958; Shido & Miyashiro, 1959). On this diagram, calcic amphibole from the study area shows a well-defined positive trend regardless of host rock composition towards the ideal composition of $\text{Na}_{0.5}\text{Ca}_2(\text{Mg},\text{Fe})_{1.5}\text{Al}_{1.5}\text{Al}_2\text{Si}_8\text{O}_{22}(\text{OH})_2$. This indicates the coupled substitution of $(\text{Mg}_{1.5} + \text{Si}_2 = \text{Na}_{0.5} + {}^{\text{VI}}\text{Al} + {}^{\text{IV}}\text{Al})$ with evolution of chemical composition during prograde metamorphism of low to medium pressure facies series, rather than a simple pargasitic (Graham, 1974) or tschermakitic (Laird, 1980) substitution.

Compositions of calcic amphibole are also reported on a plot of $(\text{Fe}^{2+} + \text{Fe}^{3+})$ versus ${}^{\text{IV}}\text{Al}$ (Fleet et al., 1987) (Figs. 4.2 and 4.3). This plot along with the ${}^{\text{IV}}\text{Al}$ versus $({}^{\text{VI}}\text{Al} + \text{Fe}^{3+} + \text{Ti})$ plot of Laird and Albee (1981) permits comparison of

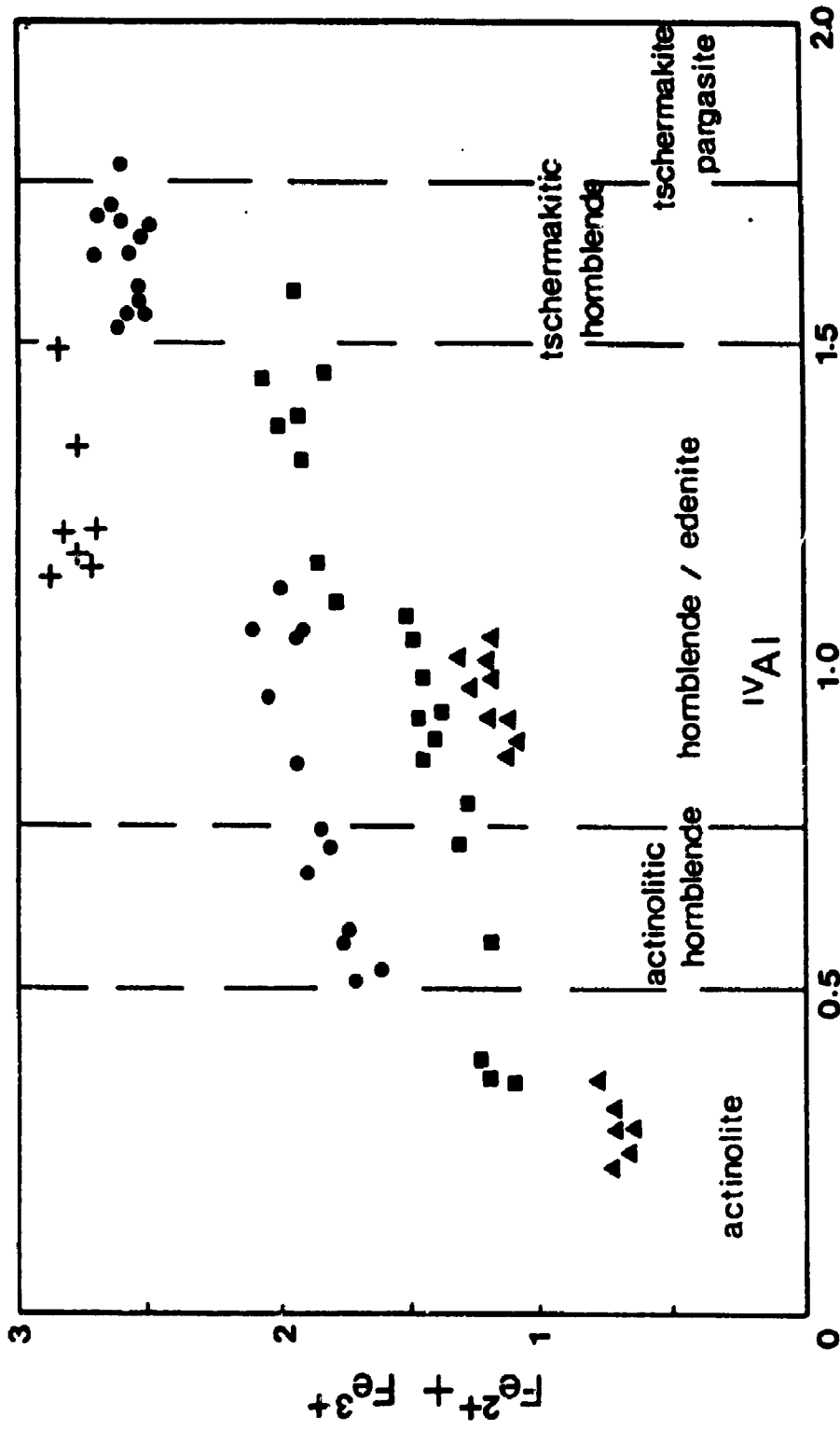


Fig. 4.2. Variation of total Fe cations with $IVAl$ in calcic amphiboles of mafic and

ultramafic metavolcanic rocks of the White River property; triangles represent

komatiite; squares represent komatiitic basalts; circles represent high-iron tholeiitic

basalts; crosses represent Fe-rich calc-silicates of unit 4 (cf. Fleet et al., 1987)

octahedral (M) site ($M = \text{Mg}, \text{Fe}^{2+}, \text{}^{\text{IV}}\text{Al}, \text{Fe}^{3+}$ and Ti) and tetrahedral (T) site ($T = \text{Si}$ and Al) substitutions (Fleet et al., 1987) and gives direct insight into the chemical variation in calcic amphiboles with metamorphic grade and host rock composition.

On Figure 4.2, a number of important features in calcic amphibole composition can be recognized immediately: (1) an increase in both ($\text{Fe}^{2+} + \text{Fe}^{3+}$) and $\text{}^{\text{IV}}\text{Al}$ with metamorphic grade, (2) discrimination in both ($\text{Fe}^{2+} + \text{Fe}^{3+}$) and $\text{}^{\text{IV}}\text{Al}$ with bulk chemistry and (3), most interestingly, parallel trends defined by calcic amphiboles from rock-types with limited variation in bulk chemistry as indicated by constant distribution coefficients (K_D). The first one is obvious and well-studied by many authors (Wiseman, 1934; Graham, 1974; Laird & Albee, 1981) and no further consideration needs to be given to it. However, the latter two features are newly resolved features of amphibole chemistry (Fleet et al., 1987) and will be discussed in detail in the following sections.

Studies on the evolution in chemistry and associated mineral assemblage of calcic amphibole in mafic volcanic rocks of metamorphic terrains are generally restricted to rocks of a limited range of bulk rock composition. Spear (1982) demonstrated systematic variation in calcic amphibole corresponding to carbonate-bearing and carbonate-free assemblages in Vermont. Amphibolites from the study area can be classified into three precursor types: (1) komatiite (2) komatiitic basalt and (3) tholeiitic basalt based on a Jenson Cation Plot (Fig 7.2 of Chapter 7; cf. Jenson, 1976).

On Figure 4.2, it is apparent that three well-defined trends exist corresponding to the three rock types of limited whole-rock chemistry. Moreover,

calcic amphibole from komatiite is depleted in both Fe and ${}^{\text{IV}}\text{Al}$ compared to that of komatiitic basalt, which, in turn, is depleted in these cations relative to high-iron tholeiitic basalt.

Calcic amphibole in metabasites from the Sudbury Igneous Complex exhibits similar features in this type of plot (Fleet et al., 1987), where the low or low-medium pressure regional metamorphism varies from greenschist-amphibolite transitional facies to middle amphibolite facies. Calcic amphibole from different localities of the Sudbury Igneous Complex (with different whole-rock compositions) shows well-defined trends (both core to margin and grain to grain) on this plot, and again the trends are invariably parallel or subparallel to one another.

The complex variation of ${}^{\text{IV}}\text{Al}$ and Fe^{2+}/Mg in calcic amphiboles with metamorphic grade and whole-rock chemistry have been discussed above. Czamanske and Wones (1973) postulated that high ${}^{\text{IV}}\text{Al}$ contents balance high iron contents in amphibole to maintain a good fit between the tetrahedral and octahedral structural units. Thus, spatial accommodation of ${}^{\text{IV}}\text{Al}$ and Fe may explain the good linear correlation between Fe and ${}^{\text{IV}}\text{Al}$ in calcic amphiboles from the study area and other metamorphic terrains.

4.3-3c Calcic amphibole in other lithologies

Calcic amphibole is one of the major constituents in intermediate to felsic metavolcanic rocks of units 3 and 7 of the Heron Bay Group. Chemically, calcic amphibole is, with few exceptions, actinolite or actinolitic hornblende. No detailed study of these calcic amphiboles was carried out due to the lack of sensitivity of their chemical compositions towards change in metamorphic grade.

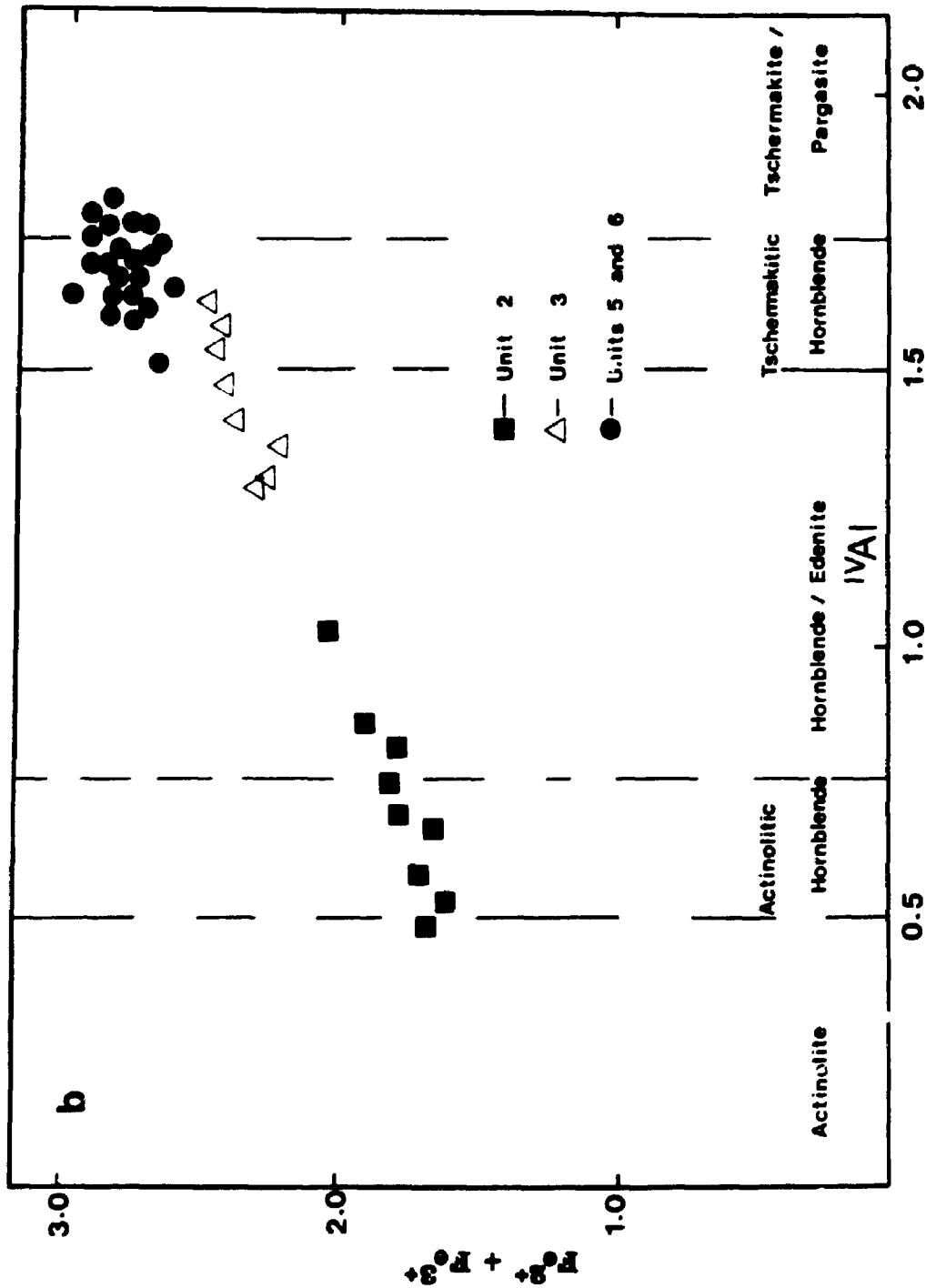


Fig. 4.3. Variation of total Fe cations with ^{IV}Al in calcic amphiboles of

metasedimentary rocks (circles, unit 2; and crosses, triangles, unit 3; squares banded iron formations of units 5 and 6); cf. Fleet et al., 1987).

Calcic amphibole is characteristically present in clastic metasediments of the lithological unit 2 of the Playter Harbour Group. In the Heron Bay Group, however, calcic amphibole is one of the major constituents of the chemical sediments (BIF) but it is typically absent in clastic metasediments. Similarly to its occurrences in metabasites, calcic amphibole of unit 2 is also locally zoned with an Al- and Fe-poor core and an Al- and Fe-rich margin and is essentially actinolite or actinolitic hornblende. In the banded iron formation (BIF), calcic amphibole has abundant magnetite inclusions but is, however, generally homogeneous in chemical composition, and is characterized by a high Al content (up to 14.5 wt. % Al_2O_3) and a low $\text{Mg}/(\text{Mg} + \text{Fe})$ value (less than 0.42). It is apparent that, for similar $(\text{Mg}/(\text{Mg} + \text{Fe}))$ values, the Al content of a given calcic amphibole from clastic metasediments of unit 2 is considerably higher than that of calcic amphibole from metabasites of unit 2. This is probably attributable to the relatively higher Al concentration in the clastic metasediments. On a plot of $(\text{Fe}^{2+} + \text{Fe}^{3+})$ versus $^{\text{IV}}\text{Al}$ (Fig. 4.3), a well-defined trend is also evident for calcic amphiboles from metasediments (both clastic and chemical), but, this trend is not parallel to those of calcic amphiboles from the above metabasites. One possible explanation for this is the diversity in mineral assemblages between metabasites and metasediments. Also calcic amphibole does not play a leading role in controlling the chemical composition of the coexisting phases with change of metamorphic grade of metasediments.

Calcic amphibole is abundant in late calc-silicate veins, particularly in those from metabasites. Calcic amphibole in veins is commonly fibrous and its composition is generally within the actinolite-tremolite series. Although the tremolite

variety is most common, the atomic $Mg/(Mg + Fe)$ ratio is as high as 0.67 in a few cases.

4.4 Garnet Group Minerals

4.4-1 Introduction

Garnet group minerals are commonly subdivided into two subgroups (ugrandite and pyralspite). At the study area, almandine-rich garnet (pyralspite) is the most common garnet mineral. Ugrandite subgroup minerals with a number of diverse species are restricted to the Cr- and Fe-rich calc-silicate rocks associated with mafic and ultramafic metavolcanic rocks. Chemical compositions for garnet group minerals are given in the Table 3 of the Appendix II.

4.4-2 Pyralspite

Almandine garnet is locally present in intercalated metasedimentary rocks in the lowest mafic metavolcanic rocks of unit 1. It generally occurs as large porphyroblasts (up to 2 mm in diameter) with well-developed crystal forms. It is characteristically homogeneous in chemical composition and is distinguished from almandine garnet from the Heron Bay Group by the absence of mineral inclusions. Chemically, the garnet is characterized by a $Mg/(Mg + Fe + Mn)$ ratio of 0.22 to 0.25 and high Ca and Mn contents (up to 5.21 and 4.61 wt. % in CaO and MnO, respectively).

In the lowest metasedimentary sequence of the Playter Harbour Group, garnet is locally present as a minor phase in a few high-aluminum samples, and is generally altered partly to fine-grained sericite along grain fractures and grain

margins. This garnet is characterized by high Ca and Mn contents (up to 4.33 and 4.65 wt. % CaO and MnO, respectively).

In the middle mafic metavolcanic rocks of unit 4, almandine garnet in association with hornblende, biotite, cummingtonite, quartz and plagioclase is restricted to samples from the Fe-rich margins of pillows. This garnet is generally homogeneous in chemical composition but contains abundant mineral inclusions (principally magnetite, quartz, and plagioclase). It is characterized by a low $Mg/(Mg + Fe + Mn)$ ratio (< 0.141).

Almandine garnet is one of the most abundant mineral phases in the middle metasedimentary rocks of units 5 and 6. Large almandine garnet porphyroblasts (up to 4 mm in diameter) are of distinct reddish colour in field exposure.

Microscopically, the garnet is idioblastic and contains a distinct zonation with an inclusion-rich core and an inclusion-free margin, separated by a boundary with very abundant mineral inclusions (Plate II d). Occasionally, zoned garnet porphyroblasts are broken into two or more pieces and cross-cut by the schistosity as defined by matrix minerals, such as muscovite, biotite, amphibole and quartz (Fig. 4.4); the significance of this type of texture in garnet will be discussed further in Chapter 5. Bell-shaped profiles in Mn content within both the core and the margin are similar to those for many other medium grade almandine garnets (e.g. Hollister, 1969; Woodsworth, 1977). Iron increases from core to margin to offset the decrease in Mn. Magnesium increases slightly from core to margin, but occasionally shows no significant variation and rarely a reversed trend. Zoning in Ca content is generally weak in these garnets; frequently, only slight fluctuations in Ca are present.

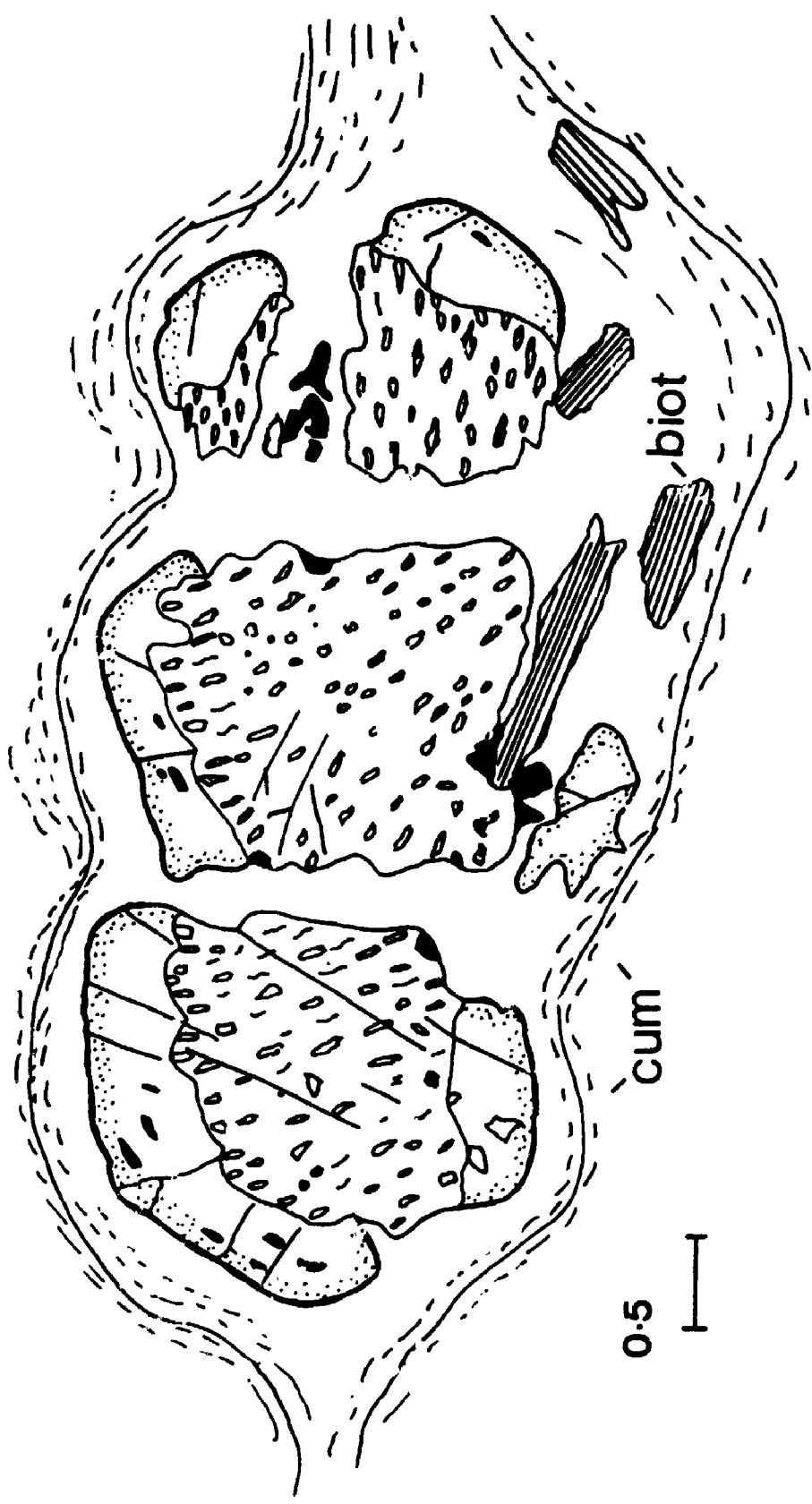


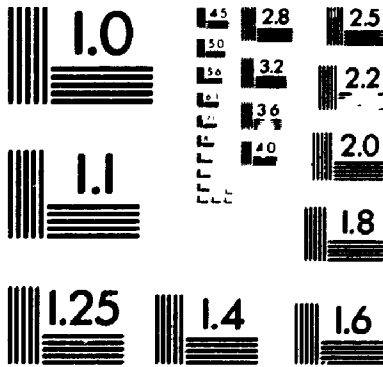
Fig. 4.4. Sketch of a broken garnet porphyroblast in metasedimentary rocks of unit 5 from the White River property.

Almandine garnet from the upper metasedimentary sequence of units 8 and 9, is similar to its counterpart in the lower metasedimentary sequence. It is of limited occurrence in high-aluminum samples and is characterized by extensive alteration. With rare exceptions, almost all garnet grains studied from these two units are extensively replaced by very fine-grained chlorite and sericite along grain fractures or around grain margins. Detailed profiles for chemical zonation are not possible due to their extensive alteration. However, electron microprobe analyses on a few unaltered spots reveal that these garnet grains are characterized by a high Mn content (up to 9.5 wt. % MnO; equivalent to 21 mol. % spessartine) and low Mg/(Mg + Fe) ratio (<0.65, Appendix II: Table 3a). In contrast to its counterpart from the lowest metasedimentary sequence, Ca is typically low (no more than 1.8 wt. %) in this manganesian garnet.

4.4-3 Ugrandite

In field exposures, one of the most distinct features of the calc-silicate rocks in the Cadi Fracture Zone of the Playter Harbour Group is the presence of large idiomorphic grains of green Cr-bearing grossular garnet and brown Cr-poor grossular garnet. Uvarovite is also observed in thin section and in most cases is a minor phase. Idiomorphic, medium to coarse-grained (up to 0.8 mm in diameter) crystals of green Cr-bearing grossular garnet and brown Cr-poor grossular garnet are mainly present in thin garnet-rich feldspar bands or as fine-grained granular grains in close association with clinopyroxene, epidote, calcic amphibole and plagioclase (Plate Ib). Anomalous birefringence together with prominent dodecahedral twinning are observed for both Cr-bearing and Cr-poor garnets (Plate If). Single crystal and

2



composite twinned grain fragments were removed from polished thin sections for X-ray precession study. Some composite, compositionally-zoned crystals did exhibit a small rotation of reciprocal lattice rows, but careful study of the single and twinned crystals failed to detect evidence of either a lower symmetry or lattice strain (cf. Allen & Buseck, 1988).

The brown Cr-poor garnet, which is largely grandite (grossular-andradite series), is the most frequent garnet species in the Cadi Fracture Zone. Electron microprobe analyses reveal that this garnet is characterized by a low Cr content (< 0.80 wt. % Cr_2O_3) and variable amounts of MgO (up to 1.89 wt. % MgO) and Ti (up to 1.66 wt. % TiO_2) and ranges from $\text{Gr}_{54}\text{And}_{33}$ to $\text{Gr}_{84}\text{And}_{11}$. Although slight compositional changes are found in the different rocks analyzed, no significant compositional zoning has yet been detected.

Green Cr-bearing garnet is also a major mineral phase in some rocks in the Cadi Fracture Zone, where the brown garnet is absent. It is generally zoned in both colour and chemical composition with a green core of a higher Cr content and a yellowish green margin of a lower Cr content (Appendix II: Table 3b). The morphology of the zoning is similar to grossular garnet from hydrothermal and skarn deposits (cf. Allen & Buseck, 1988). However, these Cr-bearing grains never contain a high enough Cr content to be uvarovite. Although these large grandite garnet crystals vary in both colour and the Cr content in different samples, it should be pointed out here that the subdivision into brown and green garnets is rather artificial, for the convenience of description. A definite composition gap does not exist (Fig. 4.5).

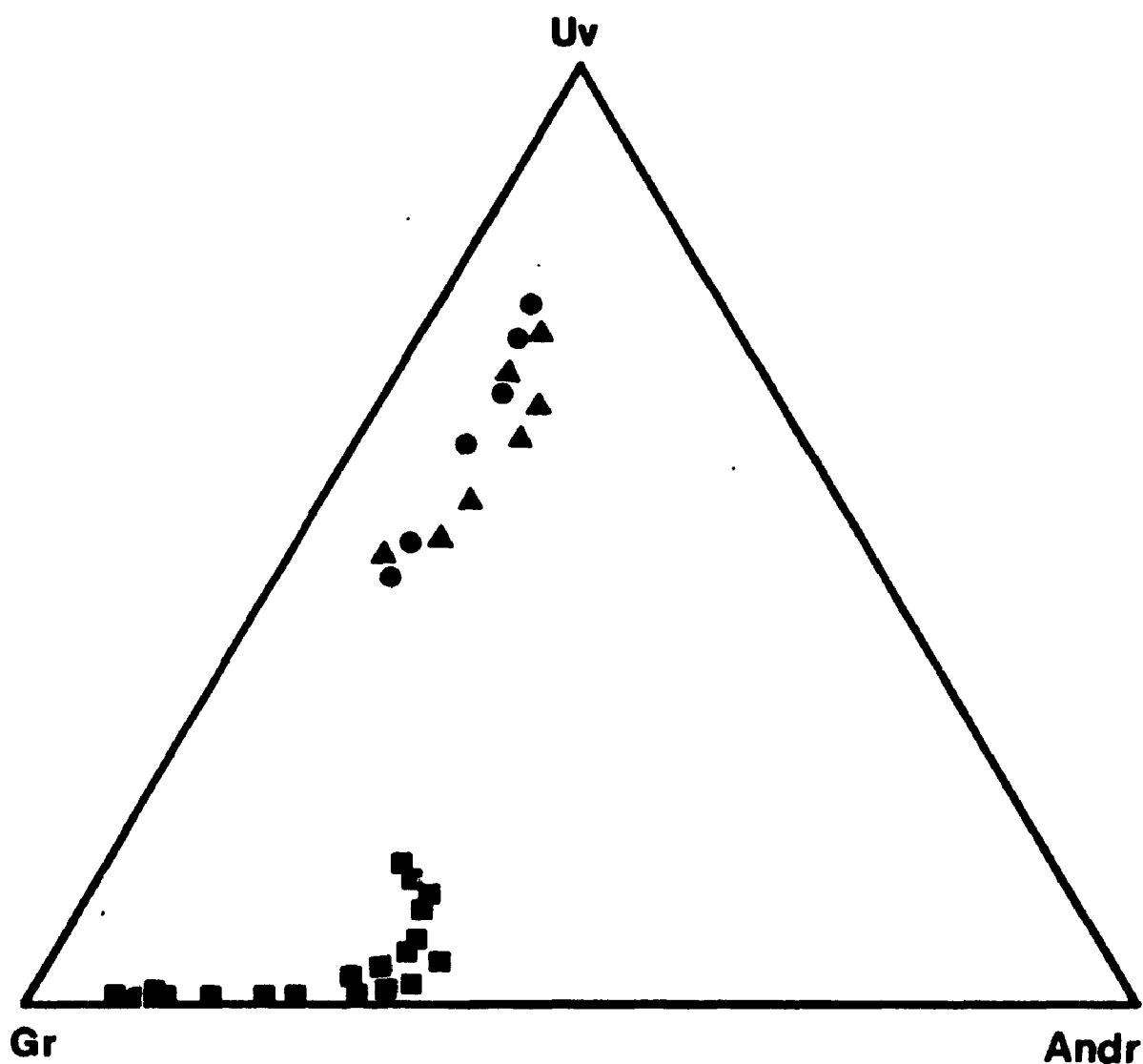


Fig. 4.5. Garnet compositions from the Cr-rich calc-silicate rocks on the uvarovite(Uv)-grossular(Gr)-andradite(Andr) compositional plane. Solid triangles represent uvarovite; solid squares represent grandite; solid circles represent those compositions from sample K72/80.

Uvarovite is present as a minor phase and occurs as deep green fibrous aggregates generally with a rounded relict core of chromite (Plate IIe). X-ray precession study of grains removed from polished thin sections indicated that the uvarovite granules are randomly-oriented; they do not exhibit a preferred crystallographic orientation with the single-crystal chromite core. Electron-microprobe analysis reveals that the uvarovite content decreases systematically with distance away from the chromite core. The decrease in uvarovite content of sample I72/80 is from 65 to 40 mole per cent [Appendix II: Table 3b and Fig. 4.5 (solid circles)], but the andradite content remains fairly constant at about 12 ± 2 mol. % both within grains and from grain to grain.

Although both grandite garnet and uvarovite occur together in almost all examined samples, they are texturally and compositionally distinct with a well-defined compositional gap between them ($Gr_{54}And_{25}Uv_{16}$ to $Gr_{17}And_{11}Uv_{40}$). Grandite and uvarovite do occur in mutual contact with each other but they appear to represent different generations of garnet crystallization. In comparison, uvarovite and Cr-poor grandite have been reported from a Cr-rich granoblastic xenolith of calc-silicate gneiss in a small granodiorite body near the Kiplapint layered intrusion, Labrador (Kalamawrides & Berg, 1988). These authors reported that grandite garnet is in abrupt contact with uvarovite at the margins of grandite garnet and suggested that they coexisted at 2 kbar and 500°C. However, these garnets from Labrador are conspicuously more andradite rich than the garnets from the Cadi Fracture Zone (Fig. 4.6). It is also notable that the uvarovite compositions from the Cadi Fracture Zone are relatively rich in Fe_2O_3 , and poor in Cr_2O_3 , compared to the uvarovite from the Outokumpu skarn formation, Finland (Von Knorring et al., 1986); consistent

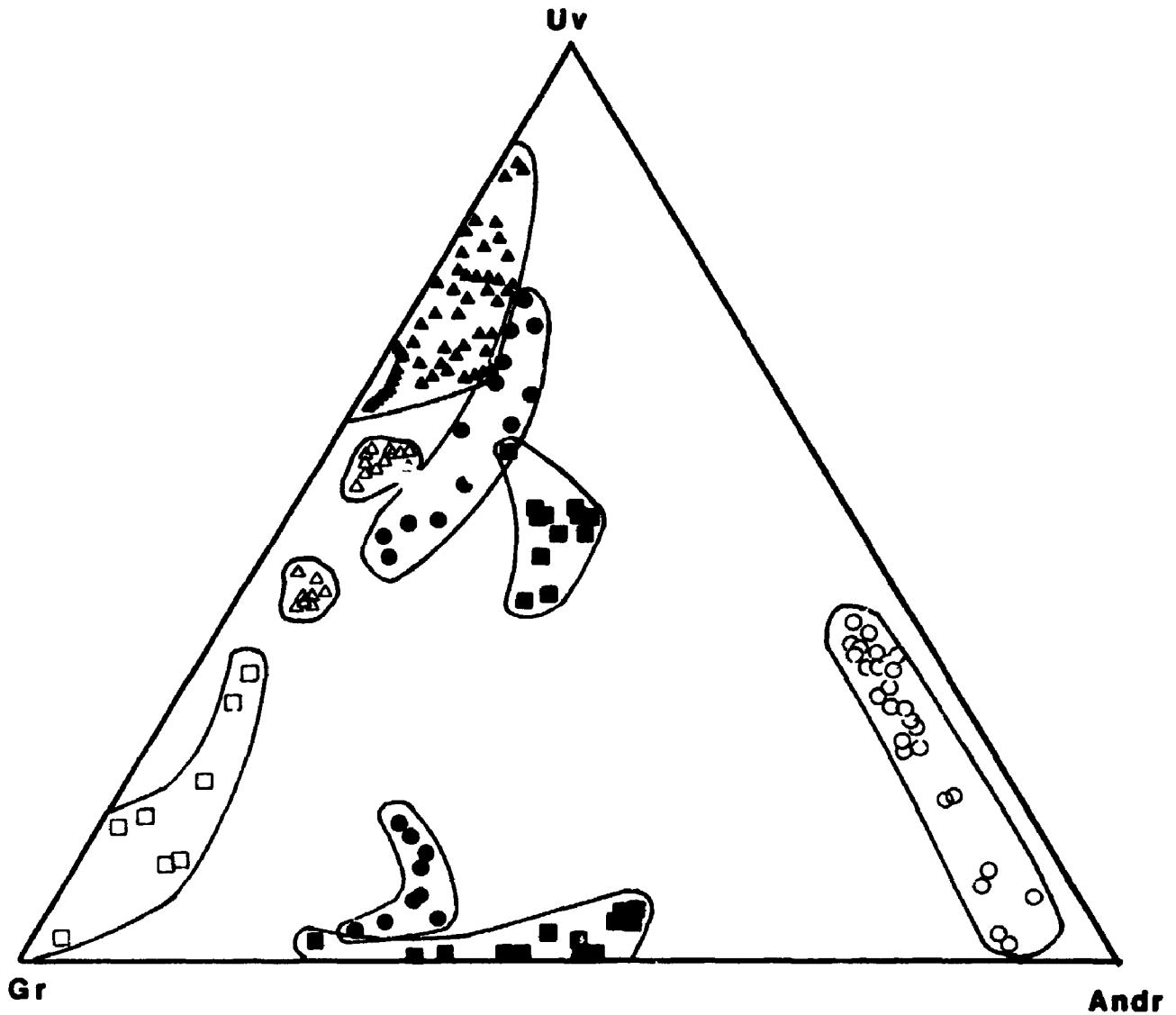


Fig. 4.6. Comparison of Cr-garnet compositions on the uvarovite (Uv)-

grossular(Gr)-andradite(Andr) compositional plane. Solid circles represent Cr-garnet in Cr-rich calc-silicates from the White River property; solid squares represent garnet from Labrador (Kalamarides & Berg, 1988); solid triangles represent garnet from Labrador (Kalamarides & Berg, 1988); solid triangles represent garnet from Outokumpu (von Knorring et al., 1986); open triangles represent garnet from Luikonlahti (von Knorring et al., 1986); open circles represent garnet from Reaume Township (Duke & Bonardi, 1982); and open squares represent garnet from some Canadian localities (Dunn, 1978).

with differences in the composition of chromite (Fig. 4.6) from the two localities.

Calcium-rich garnet is also locally present in the Fe-rich calc-silicate rocks within the middle mafic metavolcanic sequence of unit 4 of the Heron Bay Group. Medium to coarse-grained garnet grains are commonly replaced by calcic amphibole and chlorite along grain fractures and grain margins. Microprobe analyses show that this garnet is characterized by high Mn and Fe²⁺ contents [up to 8.4 wt. % and 5.2 wt. % in MnO and Fe₂O,* (as inferred from the charge-balance calculation), respectively], with Cr, Ti, Co and V (which are present as minor constituents in grandite of the Cadi Fracture Zone) being below the limits of detection.

4.5 Mica Group Minerals

4.5-1 Introduction

In the study area, mica group minerals (including biotite, phlogopite, muscovite and margarite) are abundant in metasedimentary rocks, being subordinate in amounts in mafic to ultramafic metavolcanic rocks and typically absent in intermediate to felsic metavolcanic rocks. They will be described in the two petrographically-distinguishable subgroups: dioctahedral (white) mica and trioctahedral (dark) mica.

4.5-1 Dioctahedral Mica

This group include muscovite and margarite. Paragonite has been observed in kyanite-bearing assemblages at the Hemlo deposit area (Barnett, 1989, pers. comm.) but has not been identified in the study area.

4.5-1a Muscovite

Muscovite is one of the most common minerals in metapelitic rocks of the Heron Bay Group (units 5, 6 and 8), but is minor or absent in metagreywackes of units 1 and 9. Detailed electron-microprobe analyses (Appendix II: Table 4a) indicate that a wide range of variation occurs in the chemical composition of muscovite from the study area. The chemical variation of muscovite in metapelites with metamorphic grade has been discussed in a number of studies (Guidotti, 1978; Guidotti & Sassi, 1976). These authors demonstrated that systematic changes in muscovite do occur with metamorphic grade in many metamorphic terrains. In this thesis study, emphasis is focused on muscovite in metapelites of units 5, 6 and 8, in which muscovite is one of the major phases. X-ray powder diffraction study reveals that muscovite from the study area is invariably of $2M_1$ structure. Therefore, the following variation and comparison are made on one polytype of muscovite only.

Guidotti & Sassi (1976) and Guidotti (1978) discussed the difficulties of comparing muscovite compositions from specimens with non-equivalent assemblages. In this study, metapelites from the study area are subdivided into two types based on both mineral assemblages and bulk rock composition (see Chapter 3): (1) high-Al assemblages and (2) low-Al assemblages. The high-Al assemblages (> 17 wt. % in Al_2O_3) contain Al_2SiO_5 -mineral(s) (sillimanite, andalusite or kyanite), garnet and/or staurolite and are (or are close to being) aluminum saturated. In contrast, the low-Al assemblages do not contain any of above Al-rich phases and generally have Al_2O_3 contents less than 17 wt. %.

In general, in low aluminum assemblages, the contents of ^{IV}Al , ^{VI}Al , Ti and the ratio of $Na/(K + Na)$ increase, whereas the Si content decreases from units 5

and 6 to unit 8. These variations are similar to those observed in muscovite from the upper garnet zone to staurolite zone in metapelites of northwestern Maine by Guidotti (1978). The $Mg/(Mg + Fe)$ ratio of muscovite from the study area, however, displays a wide range of variation and appears to roughly correlate with its whole-rock composition (Appendix II: Table 4a).

Similar trends are observed in muscovite of high-aluminum rocks from units 5 and 6 to unit 8. However, muscovite in high-aluminum rocks, particularly those containing Al_2SiO_5 -mineral(s), has a considerably higher Al content than that in low-aluminum rocks from the same stratigraphic unit (which corresponding to metamorphic grade as discussed later in Chapter 5). For example, the ^{IV}Al content of muscovite in the andalusite-bearing assemblage from unit 8 is higher than that of its counterpart in low-aluminum assemblages from units 5 and 6 (Appendix II: Table 4a).

Green vanadian muscovite (containing up to 8.5 wt. % V_2O_5 , and with 2M structure) has been reported in close association with gold mineralization at the Hemlo gold deposit area (Harris, 1986; 1989). Dark-green Ba- and Cr-bearing muscovite ($2M_1$ structure) also occurs at lithologic boundaries between metasedimentary rocks and mafic metavolcanic rocks of the Heron Bay Group at the Black River area (30 km to the west). V and Cr are typically at or below detection limits in all muscovites from the study area.

4.5-2b Margarite

Margarite is confined to the Local Shear Zone (LSZ) at or near the lithological boundary between units 7 and 8. It occurs as fine-grained aggregates

along fractures in porphyroblastic andalusite (Plate IIg). In a few cases, margarite has completely replaced andalusite with only the latter's pseudomorph remaining. Therefore, margarite from the study area is a variety of "a mineral forming pseudomorphs after other minerals" and apparently differs from a "normal prograde rock-forming mineral interspersed and intergrown with other minerals" (Bucher-Nurminen et al., 1983). In chemical composition, margarite from the study area is characterized by the presence of a minor Na content (up to 1.25 wt. % in Na₂O corresponding to 16 mol. % paragonite component), whereas the contents of other cations, such as Fe, Mg, Mn, Ba and K, are generally very low.

4.5-3 Trioctahedral Mica

4.5-3a Phlogopite

Phlogopite is only present in two parageneses at the study area. It occurs as one of the major phases together with actinolite and chlorite in ultramafic metavolcanic rocks of unit 4 and as a minor phase in the Local Shear Zone at or near the lithologic boundary between units 7 and 8. In the former, phlogopite is, locally, a major phase in close association with other major phases, such as actinolitic hornblende and chlorite, and is characterized by a low Mg/(Mg + Fe) ratio (less than 0.775). In the Local Shear Zone, however, phlogopite is invariably a minor or a trace phase and is characterized by a high Mg/(Mg + Fe) ratio (up to 0.87).

4.5-3b Biotite

Biotite is very common in all rock-types at the study area. It is one of the

major phases in all clastic metasedimentary rocks (both pelites and greywackes), being subordinate in mafic metavolcanic rocks and minor to absent in intermediate to felsic metavolcanic rocks. X-ray powder diffraction study indicates that biotite in all supracrustal rocks from the study area is exclusively of $2M_1$ structure, similar to that of muscovite.

Biotite occurs as a major mineral phase in all clastic metasedimentary rocks. A number of textural varieties are observed: (1) small inclusions in the inclusion-rich core of garnet, (2) large porphyroblasts along the main foliation plane, and (3) most abundantly in the rock matrix. Electron microprobe analyses (Appendix II: Table 4b) reveal that the latter two textural varieties of biotite are indistinguishable in chemical composition, whereas the biotite included in the core of garnet is considerably higher in $Mg/(Mg + Fe)$ ratio, within a single thin section.

Biotite is present as a minor phase in mafic metavolcanic rocks (metabasites), with the exception of the upper layer of komatiitic basalt in unit 9, in which biotite is a major phase next only to calcic amphibole in abundance. Biotite is commonly in lamellar intergrowth with other phases, mainly chlorite and prehnite. Biotite and chlorite are also present as coarse-grained plates surrounding almandine garnet porphyroblasts in the Fe-rich margins of pillows in unit 4. This biotite is also commonly in lamellar intergrowth with prehnite (Plate IIh). The geologic significance of these lamellar intergrowth textures will be further discussed later in Chapter 7. Biotite in mafic metavolcanic rocks generally contains minor amounts of Ti and Mn (up to 1.96 and 0.20 wt. % TiO_2 and MnO , respectively). The Ti content in biotite from metabasites is slightly lower than that from intercalated metasedimentary rocks. The $Mg/(Mg + Fe + Mn)$ ratio in biotite from mafic

metavolcanic rocks varies from 0.442 to 0.634 and apparently correlates with the whole-rock value.

Biotite is of green to greenish-brown colour in metabasites of units 2 and 9 and of brown to dark-brown colour of units 1 and 4. Miyashiro (1973) and Laird (1980) correlated this sequence of change in colour of biotite to change in metamorphic grade, from greenschist facies or greenschist-amphibolite transitional facies (epidote-amphibolite facies) to amphibolite facies, respectively. Laird (1980) also suggested that the colour change may be related to increase in the Ti content. However, the corresponding increase in the Ti content of biotite from the study area is not obvious.

4.6 Chlorite

Chlorite is generally present as a minor phase in most rock-types of the study area, except in ultramafic metavolcanic rocks of unit 2, within the Hemlo Fault Zone, and in some metagreywackes of units 2 and 9. Although chlorite occurs as a minor phase in the middle metasedimentary sequence, a number of textural varieties are present: (1) porphyroblasts of millimetre-size in association with biotite and/or muscovite in the rock matrix and along the penetrative foliation; (2) lamellar intergrowth with biotite, and (3) fine-grained aggregates as an alteration product after porphyroblasts of high-Al phases (such as kyanite, staurolite and garnet), along grain fractures or grain margins. In mafic metavolcanic rocks, chlorite is not a major phase and occurs mainly as a lamellae within biotite grains. Chlorite is also locally present in calc-silicate veins. Chemically (Appendix II: Table 5), chlorite

from the study area is clinochlore, pynachlore, and ripidolite, according to the classification scheme of Hey (1954). In contrast to other important phases exhibiting solid solution (e.g. calcic amphibole, biotite, muscovite and garnet), chlorite shows no significant variation in major components with metamorphic grade. Instead its composition correlates with whole-rock compositions, particular in the $Mg/(Mg + Fe + Mn)$ ratio.

4.7 Epidote Group Minerals

4.7-1 Introduction

Epidote group minerals have a general formula of $A_2M_3Si_3O_{12}(OH)$. In the common clinozoisite-epidote series [which may be represented as $(Ca_2(Al,Fe^{3+})_3Si_3O_{12}(OH))$], the A sites generally are fully occupied by Ca and ferric iron (epidote) may substitute for Al (clinozoisite) in the relatively large M(3) site (Dollase, 1971). In allanite [the ideal end-member composition may be represented as $Ca(REE)Fe^{3+}Al_2Si_3O_{12}(OH)$], the ten-fold coordinate A(1) site is always fully occupied by Ca; large cations, such as the REE and possibly Mn^{2+} , which may substitute for Ca, partly occupy the nine-fold coordinated A(2) site; ferrous iron, along with Fe^{3+} , Mn^{3+} , Mn^{2+} , Mg and Ti, is present in the M(3) site.

Epidote group minerals are also very common in the study area, particularly in metasedimentary rocks and intermediate to felsic metavolcanic rocks, being a major phase comprising 5 to 10 vol. % of the lower mafic metavolcanic layer of unit 9 (which is of tholeiitic basaltic composition), but they are typically absent in units 1, 4, 5 and 6, except for cross-cutting veins and cavities and the Fe-rich calc-silicate rocks of unit 4. Epidote is the most common species, while clinozoisite is

generally minor and of restricted paragenesis. Other varieties, including chromian epidote, REE-bearing clinozoisite and halogen-bearing (F, Cl) allanite, are also locally present.

4.7-2 Clinozoisite and Epidote

Clinozoisite and epidote commonly occur together, but are readily distinguished by the presence of anomalous birefringence in clinozoisite, and detailed optical measurements on selected grains (cf., Deer et al., 1986).

Clinozoisite and epidote are a common constituent in both clastic metasedimentary rocks and metavolcanic rocks, and are particularly abundant in intermediate to felsic metavolcanic rocks. However, they are typically absent in rocks of units 1, 4, 5 and 6, with the exception of the Fe-rich calc-silicates of unit 4. The chemical compositions of clinozoisite and epidote are summarized in Appendix II: Table 6. Individual grains of clinozoisite and epidote are generally homogeneous. A few grains have an Fe-rich core and an Al-rich margin. The pistacite content of epidote remains rather constant (at about Ps_{28-34}) regardless of rock-type and lithologic unit, except for epidotes in the Local Shear Zone, which are associated with sulfides and have a composition of Ps_{12-15} .

Epidote is also one of the most phases in the cross-cutting calc-silicate veins in all rock-types and all lithological units (including units 1, 4, 5 and 6) of the study area. In this association, epidote is invariably zoned both optically and chemically. The most common zonal pattern is an Fe-rich core and an Al-rich margin, but other complicated zonal patterns (such as oscillatory) are also not uncommon. The pistacite content does not exhibit a wide variation (Ps_{28-34}) and is

generally similar to that of epidote in the rock matrix, regardless of host rock composition. However, epidote associated with sulfides in veins in the Local Shear Zone is characterized by a low Ps content (Ps_{12-13}).

Chromian epidote is only present in the Cr-rich calc-silicate rocks of the Cadi Fracture Zone. Epidote in the rock matrix of these Cr-rich calc-silicates is generally colourless to yellow and contains a minor amount of Cr (Cr_2O_3 , up to 2.65 wt. %), while very fine-grained dark brown granules of epidote [containing up to 11.77 wt. % Cr_2O_3 , corresponding to 0.86 Cr atoms per formula unit (12.5 oxygen atoms)] are also present in cavities in direct contact with zincian chromite. This is, therefore, close to an end-member Cr-epidote: $Ca_2CrAl_2Si_3O_{12}(OH)$.

4.7-3 Halogen-bearing (F, Cl) Allanite and REE-bearing Clinozoisite

REE-bearing clinozoisite and halogen-bearing (F, Cl) allanite are restricted to the Local Shear Zone at or near the lithologic boundary between units 7 and 8. They generally occur as fine-grained aggregates associated with monazite, apatite, zircon, rutile, clinozoisite, epidote, prehnite and tourmaline (Plate IIi). These aggregates of allanite and other REE-rich minerals occurs either in discordance with the main foliation or as later replacements along the foliation plane (Plate IIj). Large crystals of allanite (2 X 0.5 mm) associated with pyrrhotite or pyrite are locally present (Plate IIk). All large single crystals of allanite are invariably altered (cf. Ghent, 1972). Electron back-scattered images of allanite show two zones separated by a distinct boundary: a Ca- and Al-rich and Fe- and REE-poor core and a Ca- and Al-poor and Fe- and REE-rich margin (Plate III). REE-bearing clinozoisite is locally present as the grain nucleus in some zoned allanite grains and contains up to

PLATE II (cont.)

- I: Electron back-scattered image of a REE-rich mineral aggregate: al is halogen-bearing allanite, ap is apatite; ep is epidote; mz is monazite; and rt is rutile.
- J: Electron back-scattered image of a REE-rich mineral aggregate along the foliation plane: al is halogen-bearing allanite; ap is apatite; and ep is epidote.
- K: Photomicrograph of a large halogen-bearing allanite crystal associated with a pyrrhotite vein; scale bar is 0.5 mm.
- L: Electron back-scattered image of a zonal allanite showing a REE-rich allanite margin (bright); a REE-poor core (grey), and a REE-bearing clinozoisite nucleus (black).



4.0 and 3.1 wt. % REE_2O_3 and Fe_2O_3 , respectively. Locally, clinozoisite with about 1.6 wt. % FeO^* without detectable REE also is present as fine inclusions within the grain nucleus (Plate III). Allanite is characterized by high Cl and F contents, which are evident in the energy dispersion spectrum. Quantitative electron-microprobe analyses confirmed the zonal features and reveal that the allanite is characterized by high contents of F and Cl (up to 0.76 and 0.95 wt. %, respectively). Although allanite occurs in a wide variety of rock types and exhibits a wide variation in chemical composition, varieties with volatile anion species other than $(\text{OH})^-$ are considered to be rare (Deer et al., 1986). Fluorine-bearing allanite has been reported at the contact between calc-granulite and microcline pegmatite from India (Rao et al., 1979) and in quartz veins in granites of the Itulin tin-tungsten deposit from the USSR (Ivanov et al., 1981). Allanite from the study area appears to be a new halogen-bearing variety with both high F and Cl contents. Halogen-bearing allanite also contains minor Mg and Mn (up to 1.3 and 1.2 wt. % in MgO and MnO, respectively; Appendix II: Table 6c).

A significant content of medium-sized divalent cations is required in allanite to charge-balance the high content of REE^{3+} . Therefore, allanite is the only member of the epidote group in which ferrous iron is an essential constituent (Deer et al., 1986). The Halogen-bearing (F, Cl) allanite is characteristically low in total iron content than the summary data listed in Table 7 of Deer et al. (1986); based on the charge-balance calculation, nearly all of the iron is inferred to be in the ferrous state. Allanite compositions reported to date represent a solid solution with the FeAl_2 -epidote end-member species through the coupled substitution: $\text{Ca}_{\text{A}(2)} + \text{Fe}^{2+}_{\text{M}(3)} = \text{REE}_{\text{A}(2)} + \text{Fe}^{2+}_{\text{M}(3)}$. A plot of $(\text{REE} + \text{Fe}^{2+} + \text{Mg})$ versus $(\text{Ca}_{\text{A}(2)} + \text{Mn} + \text{Al}_{\text{M}(3)})$

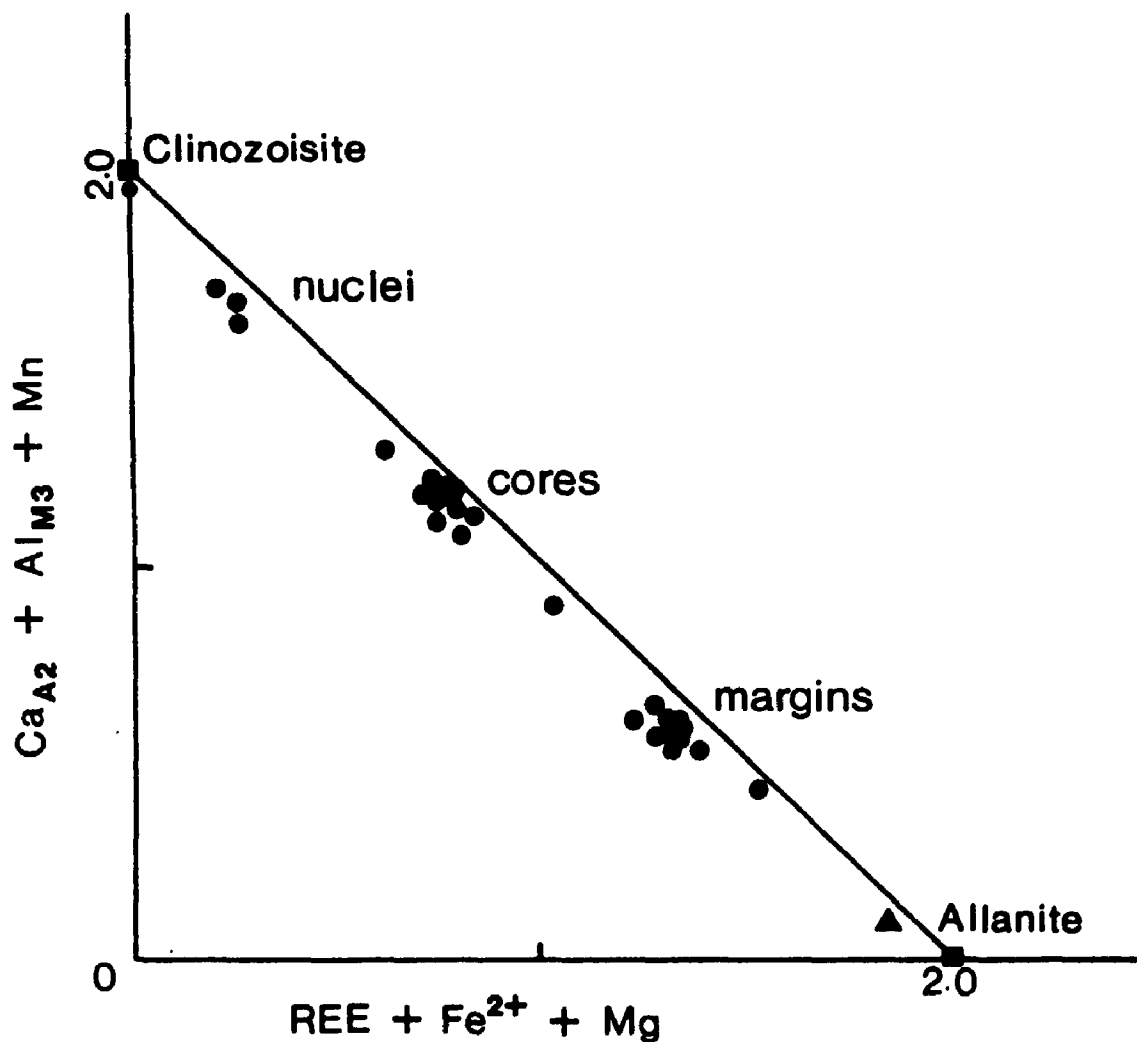


Fig. 4.7. Clinozoisite-allanite compositions: squares are ideal compositions for clinozoisite and allanite end-members; triangle is a Mg-rich allanite from eastern China (Enami & Zang, 1988); circles are analytical data from the White River property.

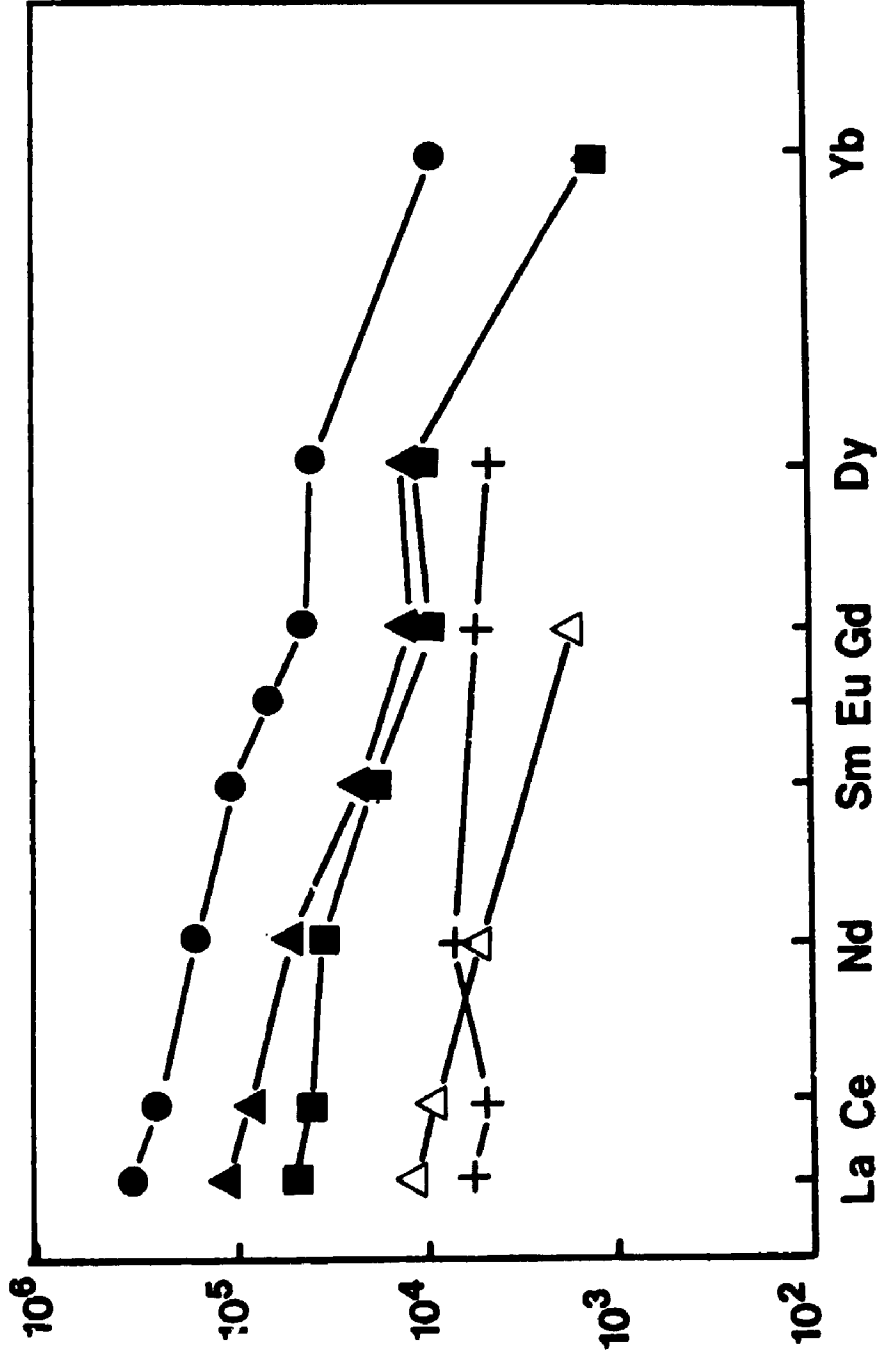


Fig. 4.8. Chondrite-normalized REE-patterns of halogen-bearing allanite, monazite,

apatite and zircon; solid circle is monazite; solid square is REE-poor core of

allanite; solid triangle is REE-rich margin of allanite; open triangle is apatite;

cross is zircon.

shows a well-defined linear relationship from clinozoisite to ideal allanite (Fig. 4.7). Therefore, the concentric zonation in chemical composition from REE-rich allanite grain margin, passing into REE-poor allanite core, REE-bearing clinozoisite grain nucleus, and to REE-free clinozoisite inclusions apparently suggests a complete solid solution between clinozoisite and allanite represented by the substitution: $\text{Ca}_{\text{A}2} + \text{Al}_{\text{M}3} + \text{Mn} = \text{REE}_{\text{A}2} + \text{Fe}_{\text{M}3} + \text{Mg}$, which can be simplified to a coupled substitution: $\text{Ca}_{\text{A}2} + \text{Al}_{\text{M}3} = \text{REE}_{\text{A}2} + \text{Fe}_{\text{M}3}^{2+}$, because Mg and Mn are generally minor and negligible in allanite.

Figure 4.8 shows the REE concentrations of the halogen-bearing allanite from the study area. The chondrite-normalized REE patterns of allanite (both core and margin) are characterized by high fractionation between LREE and HREE, as indicated by moderate to high La_N/Yb_N ratios (average 60 and 95 in the core and the margin, respectively). Moreover, LREE (particularly, La, Ce and Nd) are significantly more abundant in the grain margin ($\text{La}_{\text{margin}}/\text{La}_{\text{core}} = 2.13$, for example), whereas HREE are virtually similar between the grain core and margin.

4.8 Clinopyroxene

Clinopyroxene is a very common constituent in some intrusive rocks, such as diabase dykes and lamprophyre dykes. In the supracrustal rocks of the Hemlo-Heron Bay greenstone belt in the study area, clinopyroxene is confined to calc-silicate occurrences: It occurs as one of the major phases in Cr-rich calc-silicates in the Cadi Fracture Zone and Fe-rich calc-silicates in unit 4. It is also locally present as a minor phase in close association with epidote in some intermediate metavolcanic

rocks within the Local Shear Zone at or near the lithological boundary between units 7 and 8.

The compositions of clinopyroxene in the Cr-rich calc-silicates varies generally within the binary diopside to hedenbergite series ($\text{Di}_{50}\text{Hd}_{46}$ to $\text{Di}_{75}\text{Hd}_{23}$). The contents of Al, Na and Mn are generally low, but minor Cr is characteristically present and is locally up to 0.7 wt. % Cr_2O_3 . Clinopyroxene in the Fe-rich calc-silicates also varies largely within the binary diopside to hedenbergite series from $\text{Di}_{24}\text{Hd}_{68}$ to $\text{Di}_{50}\text{Hd}_{45}$ and is apparently higher in Fe than its counterpart in the Cr-rich calc-silicates. It also contains higher contents of Al and Mn (up to 1.4 and 1.2 wt. % Al_2O_3 and MnO, respectively) than clinopyroxene in the Cr-rich calc-silicates. Clinopyroxene in intermediate to felsic metavolcanic rocks of the Local Shear Zone is characterized by a value of the $\text{Mg}/(\text{Mg} + \text{Fe} + \text{Mn})$ ratio at about 0.725 and low contents of Al, Na and Mn (Appendix II: Table 7).

4.9 Prehnite and Pumpellyite

4.9-1 Prehnite

Prehnite is not uncommon in the study area. Two types of prehnite occurrences have been observed: (1) a major constituents in cross-cutting calc-silicate veins and cavities, and (2) in lamellar intergrowth with biotite (Plate IIh) and, less commonly, with chlorite in mafic metavolcanic rocks.

Prehnite in cross-cutting calc-silicate veins and cavities exhibits characteristic "bow-tie" structure and shows parallel extinction with positive elongation and high birefringence. Prehnite typically has a very restricted variation in chemical composition with minor substitution of Fe^{3+} for Al in octahedral sites. Microprobe

analyses show this type of prehnite is generally close to its ideal chemical formula with a very small amount Fe_2O_3 (< 1.50 wt. %). However, prehnite in association with chromite in cavities of Cr-rich calc-silicate rocks of the Cadi Fracture Zone, is enriched not only in Fe (up to 2.65 wt. % in Fe_2O_3) but also in Cr (up to 1.21 wt. % in Cr_2O_3 ; Appendix II: Table 8).

Prehnite in lamellar intergrowth with biotite and chlorite occurs in all mafic metavolcanic rocks (units 1, 2, 4, and 9). These lamellar prehnites generally contain small amounts of iron (Fe_2O_3 , up to 3.5 wt. %), which strongly correlates with their host rock composition, particularly the ratio of $\text{Fe}_2\text{O}_3^*/\text{Al}_2\text{O}_3$.

4.9-2 Pumpellyite

Pumpellyite is less common than prehnite and occurs in minor amounts with other calc-silicate minerals, such as prehnite, epidote and actinolite (or tremolite), in cross-cutting veins or vesicles associated with metavolcanic rocks of komatiitic affiliation. Pumpellyite of diagnostic "oak leaf" structure is generally colourless with high birefringence. Microprobe analysis reveals that pumpellyite invariably contains considerable amount of Mg (MgO up to 7.0 wt. %) and two chemical analyses of pumpellyite from the Cr-rich calc-silicate rocks of the Cadi Fracture Zone yield high contents of Mg, Cr and Fe (up to 4.10, 2.56, and 2.7 wt. % MgO, Cr_2O_3 , and FeO^* , respectively; Appendix II: Table 8).

4.10 Other Minerals

4.10-1 Al_2SiO_5 Minerals

Sillimanite is generally a major phase in the aluminous metasedimentary

rocks of units 1, 5 and 6 and occurs mostly with muscovite and biotite as fibrous aggregates (fibrolite) along the penetrative foliation. Only small amounts of sillimanite (as fibrolite) occur in direct association with quartz, K-feldspar and plagioclase within rock matrix.

Andalusite is sporadically present as a minor phase and is, locally, concentrated as a major phase, in the aluminous metasedimentary rocks of units 2 and 8. It generally occurs as large porphyroblasts, which are commonly altered extensively to margarite and sericite (Plate IIg), particularly within or near the Local Shear Zone of unit 8.

Kyanite, which is the least common of the three Al_2SiO_5 minerals at the study area, is restricted to the middle metasedimentary sequence (units 5 and 6) of the Heron Bay Group and occurs as a minor to rare phase (mainly as large porphyroblasts) in a very small number of the studied samples. Although kyanite has been reported to be present in intercalated metasedimentary rocks in the lowest mafic metavolcanic unit of the Playter Harbour Group to the west near the Heron Bay area (Muir, 1982a), it has not been identified in samples from this unit at the study area.

4.10-2 Staurolite and Cordierite

Staurolite is only present as a minor phase in the aluminous metasedimentary rocks of units 5 and 6. It generally occurs as large poikiloblasts (up to 3 mm in diameter) in close association with kyanite porphyroblasts. It is generally homogeneous in chemical composition, except along the twin composition planes, where slightly higher contents of Ti and Zn are encountered. The staurolite from the

study area is characterized by the presence of a minor amount of Zn (up to 1.36 wt. % in ZnO) and a small range of variation in the Mg/(Mg + Fe) ratio (from 0.178 to 0.208). Many authors (Ashworth, 1975, Sharma & MacRae, 1981) reported the presence of minor amounts of Zn in staurolite from world-wide localities and have suggested that it actually enlarges its stability field.

Cordierite is present as a major phase in (Mg, Fe)-rich rocks (termed cordierite-anthophyllite rocks) in close association with BIF in the units 5 and 6. It is characterized by a ratio of Mg/(Mg + Fe + Mn) ranging from 0.709 to 0.743 (Appendix II: Table 9).

4.10-3 Carbonate Minerals

Calcite is the only carbonate mineral identified in the study area. It is generally present as a minor phase in both clastic metasedimentary rocks and mafic to ultramafic metavolcanic rocks. Veins consisting mainly of calcite are also locally present, particularly in mafic to ultramafic metavolcanic rocks, and cross-cut the penetrative foliation. Calcite is also locally abundant in late cross-cutting calc-silicate veins, in which calcite generally occurs at the central portion of the veins.

Chemically, the Ca/(Ca + Mg + Fe + Mn) ratio of calcite in the rock matrix generally ranges from 0.90 to 0.95, whereas calcite in veins is characterized by values greater than 0.99.

4.10-4 Tourmaline

Tourmaline is present in all rock types but is generally restricted to the northern part of the Heron Bay Group, with the exception of a local presence in

some sulfide-rich samples in lithologic unit 2 of the Playter Harbour Group near the Dunc Lake Fault to the east of the study area. Tourmaline is locally abundant in the Local Shear Zone and in the two layers of mafic metavolcanic rock within unit 9 metagreywackes. Tourmaline in the Local Shear Zone is conspicuously present in veins associated with quartz and sulfides and is chemically characterized by a high Al content (up to 35.1 wt. % Al_2O_3). Tourmaline in almost all occurrences is optically and compositionally zoned with a Mg-rich core and an Fe-rich margin (Appendix II: Table 9). It is noticeable that the $\text{Mg}/(\text{Mg} + \text{Fe} + \text{Mn})$ ratio in the grain core or margin of tourmaline also strongly correlates with the whole-rock values.

4.10-5 Apatite

Apatite is present as a minor constituent in all rock-types of the study area. It occurs both in the rock matrix in association with major mineral phases and in late cross-cutting veins. Electron-microprobe analyses (Appendix II: Table 9) indicate that these two textural varieties of apatite are indistinguishable in chemical composition. One of the most notable features is the high fluorine content (up to 3.37 wt. % in F). Apatite is, otherwise, close to its ideal chemical formula $[\text{Ca}_5(\text{PO}_4)_3(\text{F},\text{OH})]$ with minor contents (including Si, Al, Cr, Fe, Mg, and Na) all less than 1.0 wt. %. In some cases, apatite is zoned with a turbid core and a clear margin. Chemical analyses of zoned grains show that the turbid core is considerably higher in F content than the clear margin, whereas other major and minor contents remain unchanged.

Apatite is also present in close association with the halogen-bearing (F, Cl) allanite in the Local Shear Zone. The apatite differs distinctly from its counterpart elsewhere from the study area by the presence of minor REE and Cl contents (up to 2.87 and 0.2 wt. % REE_2O_3 and Cl, respectively), in addition to the high F content (Appendix II: Table 9). Its chondrite-normalized REE pattern is plotted on Figure 4.8.

4.10-6 Monazite

Monazite is invariably confined to the Local Shear Zone and occurs as a minor to trace phase in close association with the halogen-bearing allanite and REE-bearing apatite. Monazite is characterized by low concentrations of Th, U, Y, and other minor constituents (such as Si, Al, Mg and Fe) and is generally close to its ideal chemical formula (REEPO_4 ; Appendix II: Table 9). The chondrite-normalized REE pattern of monazite also is plotted on Figure 4.8.

4.10-7 Oxide Minerals

Magnetite is ubiquitous as a minor phase and is the most predominant mineral phase in BIF of the study area, in which it occurs as thin magnetite-rich bands intercalated with thin quartz-rich bands and as inclusions in hornblende porphyroblasts. Magnetite and goethite also are present as laterite-like alteration products of sulfides in most surface samples of the Cr-rich calc-silicates from the Cadi Fracture Zone. They are chemically different from their metamorphic counterparts in other lithologies by high contents of Ni, Co, and Cr, which are apparently inherited from preexisting sulfide and silicate minerals.

Chromite is present as an accessory mineral in almost all calc-silicate rocks from the Cadi Fracture Zone. It occurs either as unaltered euhedral, subhedral, and anhedral grains of millimeter size or as inclusions in uvarovite grains, that are found to be rather optically homogeneous and normally have a very thin porous and slightly brighter margin. Chemical analyses of chromite confirmed this observation and reveal that the brighter porous grain margin has a higher magnetite content and lower Cr/Fe³⁺ ratio, which is similar to chromite from rocks of low amphibolite facies metamorphic grade (cf. Lipin, 1984). The Cadi Fracture Zone chromite has up to 6.59 wt. % ZnO, up to 3.4 wt. % MnO, and minor amounts of V₂O₅ and NiO. In these respects, it is very similar to zincian chromite from the Outokumpu skarn deposits (von Knorring et al., 1986), even though it has less Cr₂O₃ and more Fe₂O₃. In respect to its extremely low Mg content [less than 0.48 wt. % in MgO and Mg/(Mg + Fe) < 0.03], high total iron and significant Al₂O₃ contents, it resembles certain chromite from stratiform deposits associated with ultramafic rocks, which have been attributed to alteration or metasomatic processes (cf. von Knorring et al., 1986; Lipin, 1984). The Cadi Fracture Zone chromite analyses fall on the (Fe, Cr)-rich corner of the base of the spinel prism, with Cr/(Cr + Al) ranging from 0.72 to 0.87 (Appendix II: Table 10).

4.10-3 Sulfide minerals

Minor amounts of Fe-Cu-Zn sulfides (mainly pyrite, pyrrhotite, chalcopyrite and sphalerite) are omnipresent in all rock types and are in substantial quantity in the Local Shear Zone, which is marked in surface exposure by the presence of a rusty pyritic zone.

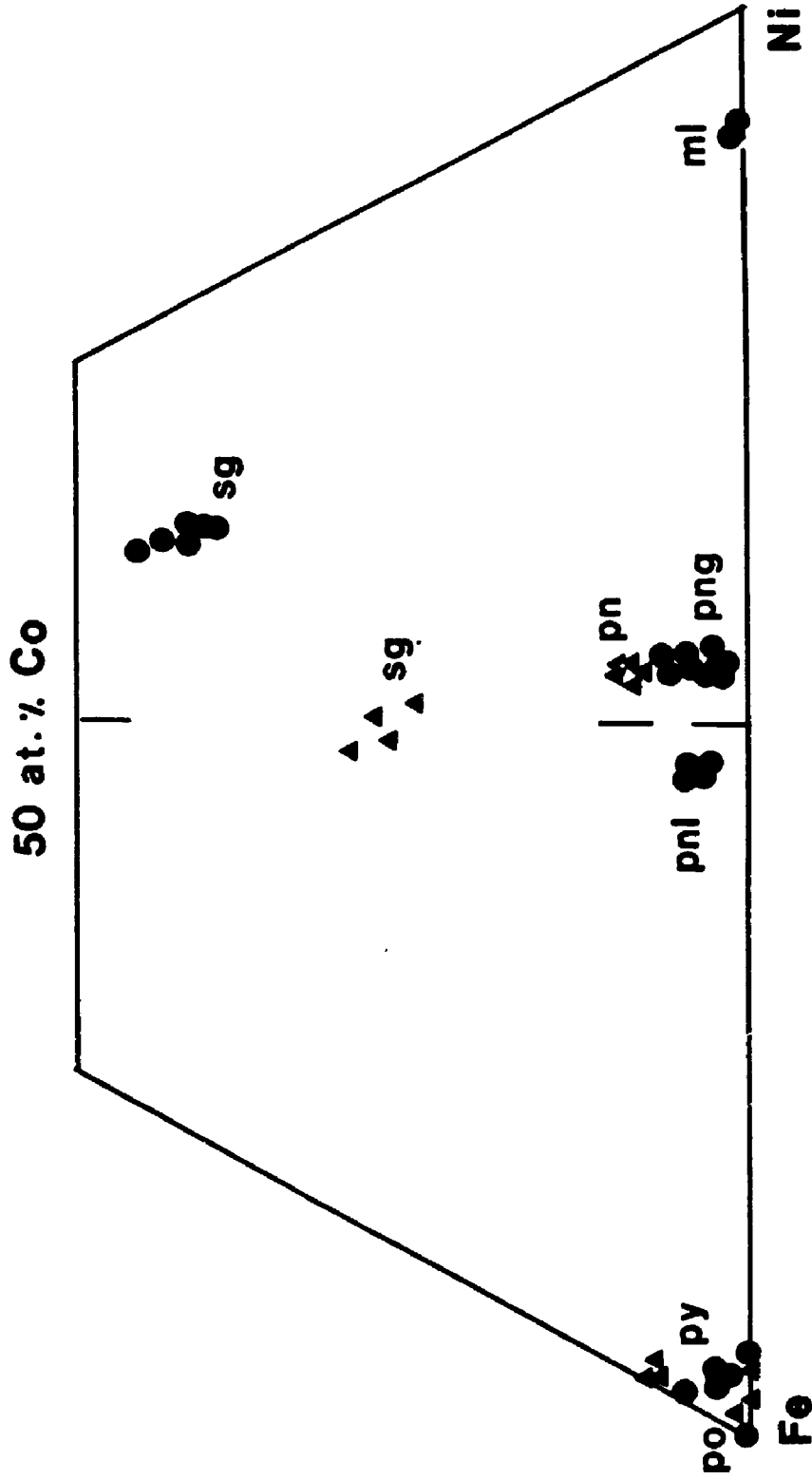


Fig. 4.9. Chemical compositions of sulfide minerals from Cr-rich calc-silicates (circles) and Fe-rich calc-silicates (triangles) on the Fe-Ni-Co system. The diagram shows the distribution of mineral compositions. The labels include: po, py, pn, png, ml, and sg. The 'po' and 'py' points are near the Fe vertex, 'pn' and 'png' are near the Ni vertex, 'ml' is on the Ni-Fe edge, and 'sg' points are in the upper part of the diagram.

Two polymetallic Fe-Ni-Co-Zn-Cu sulfide occurrences within calc-silicate rocks are of particular interest. Firstly, Fe-Ni-Co-Cu-Zn sulfides (consisting of pyrrhotite, pentlandite, chalcopyrite, sphalerite, Fe-rich siegenite and millerite) occur in the Cr-rich calc-silicate rocks associated with mafic and ultramafic metavolcanic rocks in the Cadi Fracture Zone. Secondly, Fe-Cu-Zn-Ni-Co sulfides (pyrite, pyrrhotite, chalcopyrite, sphalerite, pentlandite and Fe-rich siegenite) occur in the Fe-rich calc-silicate rocks associated with high-iron tholeiitic basalt in unit 4. The chemical composition of the Fe-Ni-Co phases are summarized in Appendix II (Table 11) and in Figure 4.9.

Molybdenite is also locally present in albite and microcline veins in the Cr-rich calc-silicate rocks of the Cadi Fracture Zone, and it is also a common constituent in the fractures of the late microcline-quartz pegmatite veins within the Playter Harbour Group. It has not been observed in supracrustal rocks of the Heron Bay Group to the north.

CHAPTER 5 METAMORPHIC PETROLOGY

5.1 Introduction

One of the most unusual features of the Hemlo gold deposit is its geological setting in a medium metamorphic grade (middle amphibolite facies) terrain, whereas most Archean gold deposits in Canada and world wide are generally situated in terrains of low metamorphic grade (i.e., greenschist facies; c.f., Boyle, 1979; Colvine et al., 1984). At the Hemlo gold deposit, particularly in the hanging-wall metasedimentary rocks, mineral assemblages consisting of abundant sillimanite, kyanite, staurolite, cordierite, and garnet clearly indicate a middle amphibolite facies metamorphism. Therefore, documentation of the variation in metamorphic grade within the Hemlo-Heron Bay greenstone belt and reconstruction of the metamorphic history in respect to deformation and gold mineralization are essential for a better understanding of the relative roles of metamorphic processes in either forming or modifying Hemlo-type gold deposits.

5.2 Metamorphic Zones

Metamorphism of the supracrustal rocks of the Hemlo-Heron Bay greenstone belt is regional in distribution and is generally low grade in nature (upper greenschist facies; Muir, 1982a). Over most of the White River property, mineral assemblages are generally characterized by quartz + biotite + oligoclase + muscovite + K-feldspar in clastic metasedimentary rocks and actinolitic hornblende/hornblende + oligoclase + quartz + biotite \pm epidote \pm chlorite in mafic metavolcanic rocks.

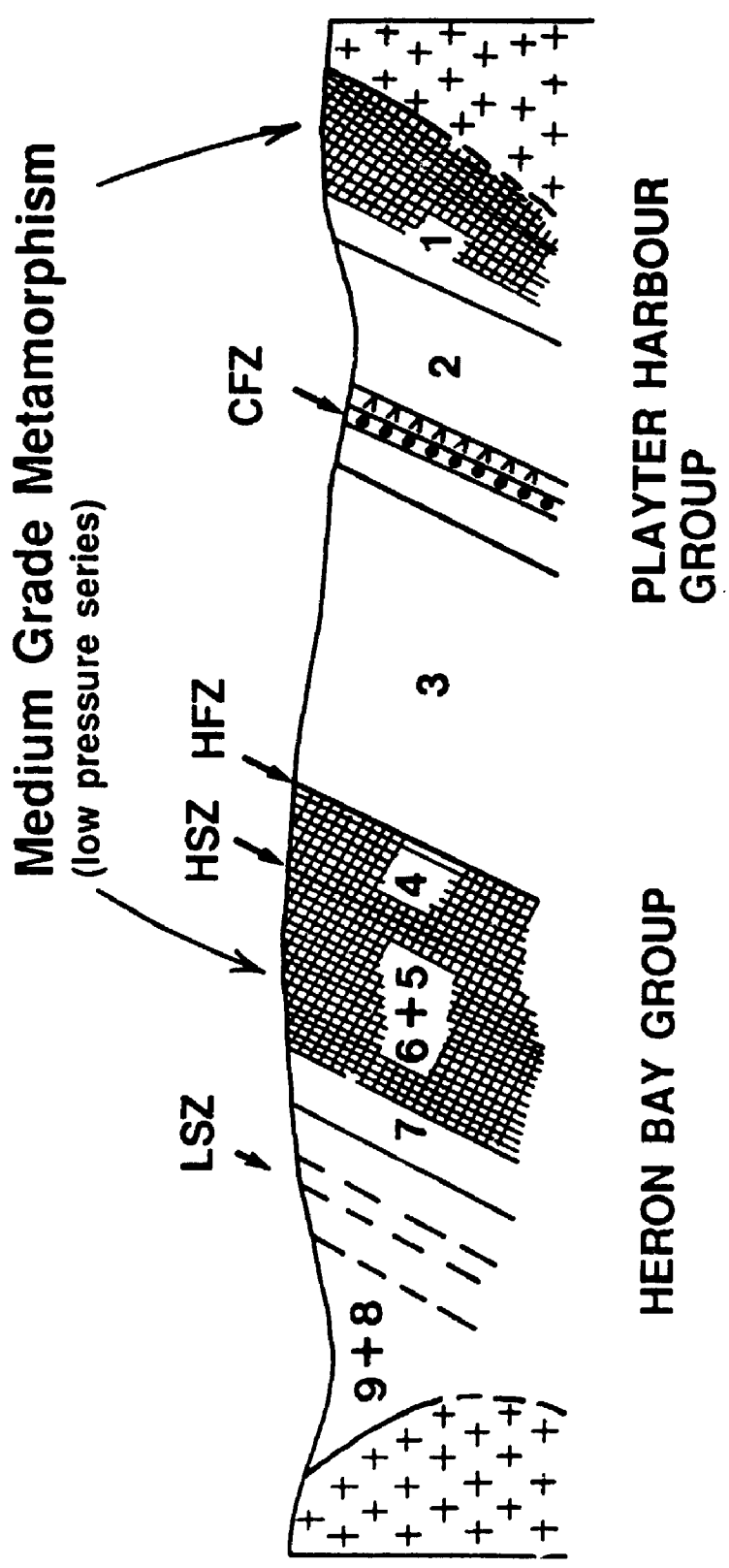


Fig. 5.1. Schematic cross-section illustrating metamorphic zones in supracrustal rocks of the Hemlo-Heron Bay greenstone belt at the White River property: shaded areas represent zones of medium metamorphic grade. For stratigraphic legend see Figure 2.2.

This is equivalent to a metamorphic grade at greenschist-amphibolite transitional facies (Turner, 1981) (or epidote amphibolite facies; Miyashiro, 1973).

Supracrustal rocks in Archean greenstone belts generally have been subjected to different grades of metamorphism due to deformation of various strains (Ramsay & Graham, 1970). At the study area, two stratigraphic zones of higher metamorphic grade are present within the overall low grade (greenschist-amphibolite transitional facies) terrain (Fig. 5.1) : (1) a lower zone within the mafic metavolcanic rocks of the Playter Harbour Group to the south; and (2) an upper zone including lithological units 4, 5 and 6 of the Heron Bay Group in the centre of the study area.

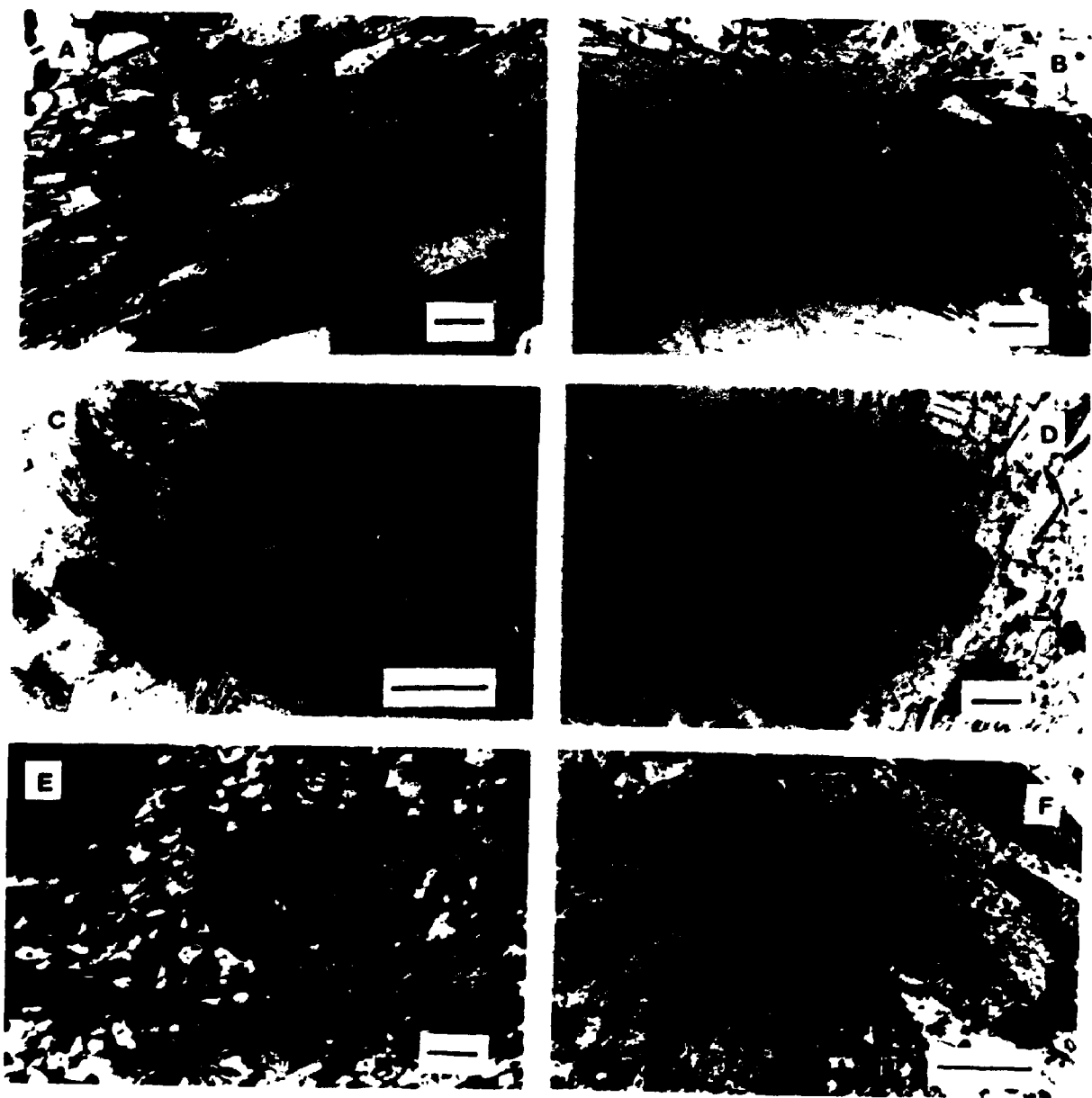
The unit 1 mafic metavolcanic rocks of the Playter Harbour Group (Fig. 5.1) are characterised by coarse-grained textures and mineral assemblages of tschermakitic/pargasitic hornblende + plagioclase (An_{35-38}) + quartz, and minor biotite, chlorite, magnetite, and titanite. In addition, sillimanite- and almandine garnet-bearing assemblages have been observed also in intercalated metasedimentary rocks within the unit 1 mafic metavolcanic rocks of the Playter Harbour Group. The above types of mineral assemblages are apparently comparable to those of metapelites and mafic metavolcanic rocks of middle amphibolite facies from low and low-to-medium pressure metamorphic terrains (Miyashiro, 1973; Laird & Albee, 1981). However, samples of coarse grained mafic metavolcanic rocks were only collected from the lower portion of unit 1 near the contact to the Pukaskwa Gneissic Complex. Therefore, it is not well understood whether the metamorphic grade changes gradationally away from the contact northward or in some other pattern. Nevertheless, the coarse-grained mafic metavolcanic rocks of the Playter Harbour Group have apparently been subjected to a medium grade metamorphism.

In the middle portion of the Hemlo-Heron Bay greenstone belt, all three lithological units (4, 5 and 6) are characterized by coarse-grained textures. In the mafic metavolcanic rocks (unit 4), the most common mineral assemblage is tschermakitic/pargasitic hornblende + andesine + quartz \pm almandine garnet \pm biotite \pm cummingtonite, whereas almandine garnet, biotite and cummingtonite generally occur together in the Fe-rich margins of pillows (Plate 1c). In the middle metasedimentary sequence (units 5 and 6), mineral assemblages are characterized by quartz + biotite + muscovite + andesine + K-feldspar \pm sillimanite \pm almandine garnet \pm kyanite \pm staurolite \pm cordierite \pm orthoamphiboles (anthophyllite and gedrite) \pm cummingtonite. The Al_2SiO_5 -minerals and other aluminous silicate minerals generally occur in thin layers of aluminous schists, whereas cordierite and Mg-Fe-Mn amphiboles are invariably restricted to (Mg,Fe)-rich metasedimentary rocks associated with BIF (Plate IIIa). These two types of mineral assemblages (which are analogous to those in the lower zone of medium metamorphic grade) are, respectively, apparently comparable to that in the kyanite-sillimanite zone metapelites (Miyashiro, 1973) and are equivalent to that in middle amphibolite facies mafic metavolcanic rocks (Laird & Albee, 1981). Therefore, lithological units 4, 5 and 6 apparently represent an upper metamorphic zone of middle amphibolite facies.

The upper metamorphic zone of middle amphibolite facies characteristically encloses the Hemlo Shear Zone, and is apparently bounded to the south by a regional fault zone (i.e., the Hemlo Fault Zone). The northern contact of the upper metamorphic zone of middle amphibolite facies with rocks of greenschist-amphibolite transitional facies is, however, less well-defined, because neither mineral assemblages nor chemical compositions of the major mineral phases of the

PLATE III

- A: Photomicrograph of cordierite-anthophyllite schist; scale bar is 0.5 mm.**
- B: Photomicrograph of a sillimanite (fibrolite) aggregate parallel to the main foliation; scale bar is 0.5 mm.**
- C: Photomicrograph of sillimanite after plagioclase; scale bar is 0.5 mm.**
- D: Photomicrograph of a kyanite porphyroblast; scale bar is 0.5 mm.**
- E: Photomicrograph of a kyanite porphyroblast showing sericitic alteration; scale bar is 0.5 mm.**
- F: Photomicrograph of a staurolite porphyroblast; scale bar is 0.5 mm.**



intermediate to felsic metavolcanic rocks are sensitive to metamorphic grade. The intermediate to felsic metavolcanic rocks of unit 7 are mainly composed of quartz, feldspars, actinolitic hornblende, epidote and titanite. It is assumed here that the lithological boundary between units 6 and 7 is also the northern boundary of the upper metamorphic zone of middle amphibolite facies.

Slight anomalies in terms of both textures and mineral assemblages are present in a very narrow zone (less than a few meters wide) close to the Cedar Lake Pluton. Metagreywackes and small mafic lenses (of local abundances) are conspicuously coarse-grained in textures compared to their counterparts elsewhere in unit 9. In metagreywackes, almandine garnet is locally present as large porphyroblasts but invariably in a minor amount, and the An content of plagioclase is also slightly higher (up to 27). In small mafic lenses, brown-green calcic amphibole, almandine garnet and andesine are typical mineral phases. These characteristic textures and mineral assemblages, confined to a narrow zone close to the Cedar Lake Pluton, apparently indicate a contact effect due to its emplacement. However, the contact effect due to the emplacement of the Cedar Lake Pluton is very limited in scale, and, therefore, has a negligible influence on the peak metamorphic effects of the Hemlo-Heron Bay greenstone belt.

Characteristic mineral assemblages and chemical compositions of major rock-forming minerals in metapelites and mafic metavolcanic rocks have been given above and in Chapter 4, respectively. The variations in mineral assemblages and chemical compositions of major mineral phases in metapelites and mafic metavolcanic rocks in response to prograde metamorphism are clearly systematic and are generally controlled by series of discontinuous and continuous reactions,

respectively. In these respects, they are typical of the response of metapelites and mafic metavolcanic rocks to increase in metamorphic temperature in low to medium pressure metamorphic terrains (Thompson, 1976a; 1976b; Laird & Albee, 1981). Therefore, no further discussion is necessary here.

Experimental studies on the mineral assemblages and mineral chemistry of ultramafic rocks are mainly restricted to in the system $\text{SiO}_2\text{-MgO-H}_2\text{O-CO}_2$. Miyashiro (1973) discussed the significance of additional components, such as Al_2O_3 , FeO and CaO, in MgO- and SiO_2 - dominant systems. Field studies on the systematic variation of mineral association and major mineral chemistry in ultramafic rocks with increase of metamorphic temperature also are generally uncommon in the literature due to their comparatively rare occurrences in prograde, regionally metamorphosed terrains or restricted occurrence within a single metamorphic zone of limited P and T variation in a prograde metamorphic terrain.

At the White River property, ultramafic metavolcanic rocks occur in both low and medium metamorphic grade zones and include: (1) an isolated earlier intrusive body in lithologic unit 2 of the Playter Harbour Group; and (2) a thin layer at the bottom portion of the unit 4 mafic metavolcanic rocks of the Heron Bay Group. The first occurrence within a metamorphic zone of greenschist-amphibolite transitional facies clearly has been subjected to the regional greenschist to amphibolite facies metamorphism (as indicated by a complete recrystallization to tremolite-talc-chlorite-schists with good orientation of all major mineral phases parallel to the main foliation). The second occurrence is interpreted to represent the Hemlo Fault Zone (Muir, 1982b; Patterson, 1984). Inspection of all drill-core intersecting this thin layer of precursor komatiite (MgO ranging from 18 to 24 wt.

%), reveals that only part of it (the lower portion in most cases) has been altered to dark green actinolite-chlorite schists with abundant fault breccia (representing the Hemlo Fault Zone). Most of the ultramafic horizon in unit 4 consists of green actinolitic hornblende schists with a well-developed schistosity defined by the calcic amphibole (preferred orientation along c-axis parallel to the main foliation and lithologic boundaries; Plate IIa). Therefore, the mineral assemblage of the actinolitic hornblende schists appears to represent the peak regional metamorphism in the upper zone of middle amphibolite facies.

Talc is one of the major phases in ultramafic rocks from lithological unit 2 (greenschist-amphibolite transitional facies), but it is typically absent in samples from the second occurrence. Other mineral phases, such as calcic amphibole, chlorite, and plagioclase, are present in both occurrences. However, there is a systematic change in the modal abundance of these mineral phases, reflected in a significant increase in calcic amphibole and plagioclase at the expense of chlorite (and talc, of course). In comparison with experimental studies and other natural occurrences, the noticeable difference in mineral assemblages of the ultramafic rocks from the White River property is the absence of pyroxene and olivine in samples from the upper zone of middle amphibolite facies. These two minerals are generally considered to be stable in ultramafic rocks at medium grade metamorphic conditions. Mineral assemblages in intercalated metasedimentary rocks indicate that the peak regional metamorphism in unit 4 must have reached sillimanite zone conditions. Therefore, the absence of pyroxene and olivine appears to be unusual.

Calcic amphibole is the major phase in ultramafic rocks from the metamorphic zone of greenschist-amphibolite transitional facies and is a predominant

phase in the upper zone of middle amphibolite facies. Compositional characteristics of these two occurrences of calcic amphiboles have been given in Chapter 4. It has been noted that the distribution coefficient between ${}^{\text{IV}}\text{Al}$ and $\Sigma(\text{Fe}^{2+} + \text{Fe}^{3+})$ in calcic amphibole in ultramafic rocks is identical to that in komatiitic basalt and tholeiitic basalt from low metamorphic grade to medium grade (Fig. 4.2). However, it is necessary to point out that the two occurrences of ultramafic rocks of different metamorphic zones cannot be considered as isochemical, because the tremolite-talc-chlorite schist of unit 2 is similar in bulk composition to the actinolite-chlorite schist, and the thin layer of ultramafic rocks in lithological unit 4 progressively decreases in MgO content upwards away from the actinolite-chlorite schists. Therefore, the actinolitic hornblende schists in lithological unit 4 are slightly poorer in MgO than the actinolite-talc-chlorite schists in lithological unit 2.

As in calcic amphibole, systematic variation in plagioclase is also observed with increase of metamorphic temperature. Plagioclase is exclusively albite in ultramafic rocks in the zone of low metamorphic grade (in which plagioclase is oligoclase in metapelites and mafic metavolcanic rocks). Plagioclase is coexisting andesine (An_{38}) + bytownite (An_{66}) in ultramafic rocks from the upper metamorphic zone of medium grade in lithological unit 4 (Plate IIa).

In summary, the response of ultramafic rocks from the White River property to prograde regional metamorphism is characterized by not only continuous reactions (modal and chemical variations in calcic amphibole, plagioclase and chlorite) but also a discontinuous reaction (the absence of talc in the upper metamorphic zone of middle amphibolite facies, unit 4). In addition, the absence of pyroxene and olivine in these ultramafic rocks from the study area also appears to be unusual, and is

probably attributable to high bulk-rock Ca and Al contents (Miyashiro, 1973).

5.3 Textural Relationships and Polymetamorphism

At the White River property, metapelitic rocks, mafic metavolcanic rocks and calc-silicates represent three principal lithologies of the Hemlo-Heron Bay greenstone belt. Their characteristic mineral associations have been outlined in Chapter 2 and in the last section according to the lithological units (stratigraphic position). In this section, the textural relationships of major rock-forming minerals of these three principal lithologies are outlined in order to constrain the metamorphic history of the Hemlo-Heron Bay greenstone belt.

5.3-1 Metapelitic Rocks

Metapelitic rocks present as intercalated thin layers from the lithological unit 1 of the Playter Harbour Group (the lower zone of middle amphibolite facies) mainly consist of sillimanite, almandine garnet, biotite, quartz, plagioclase (An_{60}) and abundant calc-silicate minerals, including epidote, clinozoisite and pumpellyite. Almandine garnet is present as large homogeneous porphyroblasts, and biotite, along with sillimanite, occur in preferred orientation defining a moderately-developed schistosity parallel to the main foliation. This indicates that the main assemblage (consisting of sillimanite, almandine garnet, biotite, bytownite and quartz) represents the peak metamorphism of the region. Calc-silicate minerals, occurring either in discordant veins or along the foliation planes, appear to be late in the paragenetic sequence and most likely represent a late, low- to very-low-grade, calc-silicate

alteration (Chapter 7).

Metapelitic rocks from the middle metasedimentary sequence (units 5 and 6: the upper zone of medium metamorphic grade) are mainly composed of quartz, andesine, biotite, muscovite, K-feldspar, sillimanite, kyanite, staurolite, cordierite, cummingtonite, anthophyllite, gedrite, chlorite, and other minor phases. In general, kyanite, garnet, staurolite, and cordierite are present as porphyroblasts or poikiloblasts, whereas biotite, muscovite, Mg-Fe-Mn amphiboles, and some chlorite occur as large well-oriented plates and define the rock schistosity (Fig. 5.2a). Sillimanite is also a common phase and occurs invariably as fibrous aggregates together with muscovite or biotite showing good preferred orientation defining a well-developed schistosity (Plate IIIb). In detail, however, sillimanite is much more common and abundant than kyanite. Although the presence of these two Al_2SiO_5 -minerals (kyanite and sillimanite) in thin-section scale is locally observed, mutual contacts between kyanite (staurolite) and sillimanite are typically absent, and evidence of sillimanite derived from kyanite or staurolite is not observed either. Instead, the crystallization of sillimanite from plagioclase is locally observed (Plate IIIc). Also, porphyroblasts of kyanite and staurolite exhibit retrogressive alteration to sericite and chlorite (Plates III d,e,f). Plagioclase is also ubiquitous in metapelites, and generally occurs as small granules within the rock matrix, and, occasionally, as large zoned porphyroblasts with a turbid core (partly altered to sericite) rimmed by a clear margin. Almandine garnet is present in nearly all metapelitic samples studied and occurs as idioblasts to hypidioblasts displaying distinct textural unconformity, with an inclusion-rich (quartz, magnetite, biotite, plagioclase) core and an inclusion-free margin. Also the internal inclusion trail in the garnet core is discordant to the

schistosity (Plate II d). Most interestingly, large almandine garnet porphyroblasts are locally broken into several pieces, and the matrix minerals, including the quartz, plagioclase and micas, exhibit a concordant orientation to the rock schistosity (Fig. 4.4). The genetic significance of this type of texture regarding the garnet porphyroblast and its matrix minerals will be discussed later.

All of the textural evidence mentioned above suggest that the peak metamorphism in metapelitic rocks in the upper zone of middle amphibolite facies is characterized by the main assemblage of sillimanite, inclusion-poor garnet margin, biotite, muscovite, K-feldspar, andesine, quartz, Mg-Fe-Mn amphiboles and cordierite. At the same time, the presence of an incompatible (relic) assemblage of kyanite, staurolite, inclusion-rich garnet core, turbid plagioclase core, with included biotite and probably quartz indicates an earlier metamorphic event.

Metapelitic rocks from zones of greenschist-amphibolite transitional facies mainly consist of quartz, oligoclase, biotite, chlorite, muscovite, and, locally, andalusite and Mn-rich almandine garnet. Andalusite occurs as elongated porphyroblasts with the c-axis parallel to the main foliation (Plate II g). This indicates that andalusite, which most likely is an equivalent of sillimanite in zones of middle amphibolite facies, represents the peak metamorphism in zones of low metamorphic grade.

5.3-2 Mafic Metavolcanic Rocks

Mafic metavolcanic rocks from zones of medium metamorphic grade (units 1 and 4) are mainly composed of tschermakitic/pargasitic hornblende, plagioclase, quartz and minor other phases. Biotite, cummingtonite and almandine garnet are also

locally abundant in Fe-rich pillow margins within lithological unit 4. All major phases generally exhibit good preferred orientation, particularly calcic amphibole with c-axis parallel to the main foliation. Moreover, mineral zoning is typically absent in all mineral phases including almandine garnet, except locally coarse-grained tschermakitic/pargasitic hornblende in unit 1 rimmed by tremolite and in samples adjacent to the HSZ of unit 4, both of which appear to be late alteration products.

Calcic amphibole in mafic metavolcanic rocks from zones of low metamorphic grade commonly exhibits gradational zonation in chemical composition and is characterized by a distinct core and margin separated by a sharp boundary: a colourless to pale green grain core and a green to brown-green margin (Plate IIc). The chemical zonation in calcic amphibole has been described and discussed in detail in Chapter 4, and has been attributed to two separate stages of calcic amphibole crystallization (c.f., Graham, 1974).

As in metapelites, mineralogical and textural evidence for retrogression after the peak thermal metamorphism are only locally present. Chlorite is present as aggregates surrounding garnet porphyroblasts, but is typically absent in any other textural relations with the other major mineral phases. Prehnite and epidote are very abundant either in cross-cutting veins or as aggregates replacing calcic amphiboles in mafic metavolcanic rocks. Biotite, chlorite and prehnite also occur in lamellar intergrowth in mafic metavolcanic rocks throughout the study area. It is well known that prehnite is only stable under metamorphic conditions below amphibolite facies. Therefore, the lamellar intergrowth of prehnite with biotite in mafic metavolcanic rocks of lithological unit 4 (Plate IIh) must represent a late crystallization (either

retrogression or late alteration), because the peak metamorphism reached P-T conditions of middle amphibolite facies within this lithologic unit.

5.3-3 Calc-Silicates

Calc-silicate veins are ubiquitous in the supracrustal rocks of the Hemlo-Heron Bay greenstone belt at the White River property, and are particularly abundant in mafic metavolcanic rocks of the Heron Bay Group. In addition to calc-silicate veins, three prominent calc-silicate occurrences also occur in close association with major structural failures: (1) Cr-rich calc-silicates in the Cadi Fracture Zone; (2) Fe-rich calc-silicates closely associated with the Hemlo Shear Zone; and, (3) REE-enriched calc-silicates in a Local Shear Zone. Some aspects of the salient mineralogical characteristics of these three calc-silicate occurrences have been given in Chapter 4. The calc-silicate occurrences are also the main subject of Chapter 7, in which they are associated with a protracted skarn development in the Hemlo-Heron Bay greenstone belt. The evolutionary history inferred from the calc-silicate occurrences in Chapter 7 will be used here to discuss the metamorphic history of the Hemlo-Heron Bay greenstone belt, particularly the late, low- to very-low-grade, calc-silicate alteration after the peak thermal metamorphism.

5.4 Metamorphic Conditions

In this section, internally consistent sets of thermodynamic data, and published calibrations of suitable geothermometers and geobarometers, are used to estimate the P-T conditions of mineral equilibration in major rock types from

different metamorphic zones. Unless otherwise stated, it is assumed that the calculated conditions reflect those operating when the rocks achieved their maximum temperatures (at the peak regional metamorphism).

5.4-1 Stability of Al_2SiO_5 Minerals

The polymorphs of Al_2SiO_5 are important in natural systems because their structures do not relate to atomic substitution and, therefore, their stability depends mainly on the rock-pressure and temperature. In reality, the substitution of a small part of Al^{3+} by Fe^{3+} and (Mn^{2+} , Cr^{3+} , etc.) significantly effects their stability relations (Althaus, 1969). Even worse, the position of the Al_2SiO_5 invariant point in P-T space has been the subject of considerable debate (Winkler, 1979). Two different petrographic grids for the Al_2SiO_5 polymorphs are currently in the literature. Experimental studies by Richardson et al. (1969) place the invariant triple point at a higher pressure and temperature than the grid presented by Holdaway (1971). The major difference in these studies is the position of the andalusite-sillimanite boundary, which can also be significantly affected by the common occurrence of fibrolite instead of sillimanite in natural systems. Calorimetric studies (Helgeson et al., 1978) are consistent with Holdaway's (1971) result. According to Holdaway (1971), the kyanite-sillimanite boundary does not appear to be significantly affected by the presence of fibrolite in place of sillimanite.

At the White River property, all three Al_2SiO_5 minerals are present in the supracrustal rocks of the Hemlo-Heron Bay greenstone belt. The distribution and mineral association of all three Al_2SiO_5 polymorphs have been outlined in Chapters 2 and 4. The extent of equilibration between each individual Al_2SiO_5 polymorphs

and major mineral phases and between themselves has also been discussed in previous sections of this chapter. Although quantitative analysis was not made for the three Al_2SiO_5 phases, a significant Fe^{3+} content (exceeding the range given by Holdaway, 1971) is unlikely as indicated by the common occurrence of magnetite and pyrite rather than haematite (the replacement of Al^{3+} by Fe^{3+} requires an oxidizing environment; cf., Chinner et al., 1969). Therefore, the possible effects of additional components in the Al_2SiO_5 -minerals can be ignored (Holdaway, 1971). The incompatible texture of sillimanite and kyanite has been interpreted as evidence of polymetamorphism in the Archean terrain (relict kyanite representing an earlier Barrovian-type metamorphic event), whereas the occurrence of sillimanite in zones of medium metamorphic grade and andalusite of low metamorphic grade classify the peak regional metamorphism as a low-pressure (andalusite-sillimanite) facies series according to Miyashiro's (1973) scheme.

5.4-2 Garnet-Biotite Geothermometer

The partitioning of Mg/Fe^{2+} between garnet and biotite was calibrated as a geothermometer by Thompson (1976), Goldman & Albee (1977), Holdaway & Lee (1977), Ferry & Spear (1978), Wells & Richardson (1979), Perchuk & Lavrant'eva (1983), Hodges & Spear (1982), Pigage & Greenwood (1982) and Ganguly & Saxena (1984; 1987). All of these studies are based on an assumption that the Mg-Fe solid solution in biotite is nearly ideal (Mueller, 1972). Natural garnet is not a simple Mg-Fe binary solution (Ganguly & Saxena, 1984; 1987). Therefore, the calculated temperatures from the direct application of the experimental calibration of Ferry & Spear (1978) are systematically in error due to the common presence of

Table 5.1 Summary of P and T conditions calculated from geothermometers and geobarometers.

Unit	Sample	Biot. F/M	F/M	Garnet X_{Mn}	X_{Ca}	F&S (°C)	P&G (°C)	G&S (°C)	Hn. F/M	G&P (°C)	Pl. An	G. kbar
1	M131/81	1.008	5.972	0.104	0.147	561	702	581			0.86	4.4
2	L81/16	0.808	6.147	0.107	0.058	478	566	476			0.29	3.2
4	J83/77	1.275	5.898	0.063	0.123	650	756	649	0.52	553	0.55	
4	J91/99	0.956	4.153	0.039	0.090	660	761	601	0.47	567	0.38	
5	I92/245	0.891	5.047	0.137	0.089	576	700	568			0.38	4.5
6	I82/119C	0.779	5.656	0.020	0.109	491	571	500			0.23	6.2
6	I82/119F	1.027	6.125	0.021	0.090	550	625	551			0.47	4.3
6	I82/144C	0.843	5.504	0.009	0.108	530	600	481			0.22	6.5
6	I82/144F	1.017	6.246	0.015	0.129	550	635	563			0.48	6.0
6	I812/313C	0.596	4.514	0.100	0.106	488	594	462			NA	
6	I812/313F	0.954	3.927	0.048	0.080	699	785	604			NA	
6	I812/345C	0.573	3.731	0.057	0.082	531	608	456			NA	
6	I812/345F	0.788	3.558	0.026	0.086	660	731	545			0.38	4.2
6	I813/315C	0.840	8.556	0.148	0.079	415	518	456			NA	
6	I813/315F	1.062	5.637	0.108	0.070	598	706	582			NA	
6	I815/520C	0.915	5.689	0.010	0.108	546	616	520			0.20	6.4
6	I815/520F	1.318	6.834	0.014	0.085	607	666	591			0.52	4.2
8	I87/63	0.804	6.029	0.212	0.052	483	614	503			0.29	3.2

Notes: Biot. is biotite; F&S, P&G, and G&S are the Ferry & Spear (1978), Pigage & Greenwood's (1982), and Ganguly & Saxena's (1984) calibrations of the Mg-Fe partitioning between biotite and garnet, respectively; Hn. is hornblende; G&P is the Mg-Fe partitioning geothermometer of Graham & Powell (1984); Pl. is plagioclase; G. is the geobarometer of Ghent et al. (1979); F/M is the atomic ratio of Fe/Mg; X_{Mn} is Mn/(Mg + Mn + Ca) molar ratio; X_{Ca} is Ca/(Mg + Fe + Mn + Ca) molar ratio; An is anorthite content [Ca/(Ca + Na + K)] in plagioclase; and NA is "not available".

minor amounts of Ca and Mn in natural garnets. In the White River property, Ca and Mn as minor components are typically present in garnets of metapelites from the zone of highest metamorphic grade, and Ca and Mn are characteristically high in garnets of metavolcanic rocks from zones of higher metamorphic grade and metapelites of lower metamorphic grade, respectively. Table 5.1 reports the calculated metamorphic temperatures for coexisting garnet and biotite from the White River property using three calibrations (Ferry & Spear, 1978; Phipps & Greenwood, 1982; and Ganguly & Saxena, 1984; 1987). The systematic error in a direct application of Ferry & Spear's (1978) experimental calibration has been discussed above, the calculated metamorphic temperatures for the peak metamorphism in units 5 and 6 show a wide range of variation, which cannot be related to the analytical error alone. Moreover, the maximum calculated metamorphic temperature is up to 700°C. The calibration of Phipps & Greenwood (1982), which adopted the excess parameters for garnet suggested by Ganguly (1979), corrects the metamorphic temperatures upwards from Ferry & Spear's (1978) calibration, and gives a large number of calculated metamorphic temperature over 700°C. The calibration of Ganguly & Saxena (1984; 1987) is also based on Ferry & Spear's (1978) experimental calibration, but the effects of Ca and Mn in garnet are corrected based on the most recent comprehensive treatment of garnet solid solution. The following discussion of metamorphic temperatures in the White River property is, therefore, mainly based on this latter calibration. Although small amounts of Ti are invariably present in biotite from the study area, an application of the recent work by Indares and Martignole (1985), correcting for the influence of Ti and Al in biotite, doesn't significantly change the calculated temperature conditions from

those in Table 5.1.

Almandine garnet and biotite assemblages are locally present in mafic metavolcanic rocks (e.g., in Fe-rich margins of pillows) of lithological unit 4. Almandine garnet is generally homogeneous in chemical composition. The application of Ganguly & Saxena's (1984; 1987) calibration gives a metamorphic temperature of about 600°C (Table 5.1). However, lamellar intergrowth with prehnite has been observed locally in biotite. It is not clear whether the lamellar intergrowth is a replacement of a metamorphic biotite by prehnite or a late crystallization of prehnite and biotite. If it is the latter, the calculation for metamorphic temperatures by a garnet and biotite geothermometer would not be valid since biotite and garnet did not coexist.

Almandine garnet and biotite assemblages are locally present in metapelitic schists from zones of low metamorphic grade. It is noticeable that the calculated metamorphic temperatures from units 2 and 8 (at 476 and 503°C, respectively; Table 5.1) are similar and are within the range of the greenschist-amphibolite transitional facies.

Almandine garnet porphyroblasts are homogeneous in chemical composition, and occur in close association with biotite and sillimanite in intercalated metasedimentary rocks. The calculated metamorphic temperature at about 580°C confirms petrographic observations on textures and mineral associations that the metamorphism in the lower portion of the lithological unit 1 has reached middle amphibolite facies.

In the middle metasedimentary sequence (lithological units 5 and 6), almandine garnet occurs as porphyroblasts with obvious compositional zonations, and

biotite is also present in a number of textural varieties with different chemical compositions. Therefore, in the estimation of the metamorphic temperatures, the chemical compositions of the grain core and margin of garnet porphyroblasts and defined textural varieties of biotite (e.g., included in porphyroblasts and platy, defining the schistosity), where applicable, were used. As discussed in previous sections, the inclusion-rich core of garnet and included biotite are interpreted to represent an earlier metamorphic event, whereas the margin of garnet and platy biotite characterize the peak thermal metamorphism.

The compositions of margin-garnet and platy biotite give rather consistent metamorphic temperatures, between 552° to 604°C with a mean value of 580°C. These values are also similar to those calculated from garnet and biotite assemblages in lithological units 1 and 4. This clearly indicates that the two zones of medium metamorphic grade were metamorphosed under similar temperature conditions (middle amphibolite facies) during the peak regional metamorphism.

Core-garnet and included biotite gives considerably lower temperatures (from 456° to 520°C with a mean value of 475°C) than those from margin-garnet and platy biotite. This is consistent with the presence of kyanite as the stable Al_2SiO_5 polymorph in the earlier metamorphic event. However, I should emphasize here that this application is somewhat artificial as point analyses across the zoned garnet do not necessarily include the actual core of the garnet.

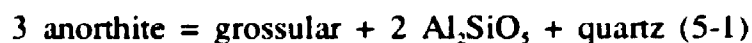
5.4-3 Garnet-Hornblende Geothermometer

Graham & Powell (1984) have calibrated the Mg-Fe exchange equilibrium

between garnet and pargasitic hornblende as a pressure-independent geothermometer. This geothermometer is applicable to rocks with Mn-poor garnet and common hornblende of widely varying chemistry metamorphosed at low oxygen fugacities. Garnet and hornblende assemblages are locally present in the Fe-rich margins of pillows in the mafic unit 4 of the Heron Bay Group. As noted in Chapter 4, garnet and hornblende from mafic metavolcanic rocks are generally homogeneous in chemical composition. Mn is characteristically low in garnet, but a significant amount of Fe³⁺ is present in hornblende as inferred from the "mid point" of Papike et al.'s (1974) method (Appendix II: Table 2b). The temperatures (560-570°C) calculated with total iron as Fe²⁺ in hornblende are consistent with those estimated from the garnet-biotite geothermometer in intercalated metasediments. Unlike the garnet-biotite geothermometer in mafic metavolcanic rocks (above), no significant late alteration effect is possible in the garnet-hornblende geothermometer, because garnet and hornblende, with little doubt, are characteristic phases of the peak metamorphism.

5.4-4 Garnet-Plagioclase-Al₂SiO₅-Quartz Geobarometer

The partitioning of Ca between garnet and plagioclase coexisting with an Al₂SiO₅ and quartz is pressure sensitive (Kretz, 1959; Ghent, 1976; Ghent et al., 1979; Newton & Haselton, 1981; Koziol & Newton, 1988; Koziol, 1989). A number of experimental determinations of the univariant reaction:



have been made, each with slightly different positions in P-T space. In the present study, the calibration of Ghent (1976; as modified by Ghent et al., 1979) will be

employed. The temperatures used in the pressure calibration are those from garnet-biotite Mg-Fe partitioning geothermometer (given in Table 5.1). In the absence of reliable activity coefficients for garnet and plagioclase, Ghent et al. (1979) evaluated a $\log K_r$ (corresponding to the cubed ratio of activity coefficients) for garnet and plagioclase from the known pressure of a kyanite-sillimanite isograd crossed by their metapelites. Newton & Haselton (1981) have confirmed that Ghent et al.'s (1979) empirical K_r is valid based on their structural models for garnet and plagioclase. More recently, however, Ashworth & Evirgen (1985) suggested that the Newton-Haselton's (1981) composition-activity model for plagioclase is invalid in oligoclase close to the peristerite gap, and garnet-plagioclase assemblages are not reliable as geobarometers where plagioclase is more sodic than approximately An_{20} . In the study area, plagioclase in the garnet-plagioclase assemblages is generally more calcic than An_{20} (Table 5.1).

As mentioned in previous sections, kyanite, the inclusion-rich core of garnet, staurolite, and the sodium-rich core of plagioclase (commonly partly altered to sericite) represent the earlier assemblage, whereas sillimanite, the margin of garnet, and the Ca-rich rim of plagioclase represent the main assemblage corresponding to the peak thermal metamorphism. The calculated metamorphic pressures from different equations of Ghent (1976) (involving different Al_2SiO_5 polymorphs) are present in Table 5.1.

In metapelitic rocks from the zones of low metamorphic grade, the Al_2SiO_5 polymorph is andalusite. The calculated metamorphic pressures from the assemblages of garnet + oligoclase + andalusite + quartz are rather consistent at about 3.2 kbar.

In the intercalated metasedimentary rocks of lithological unit 1, sillimanite is the only Al_2SiO_5 polymorph present and occurs in assemblages containing Ca-rich almandine garnet, bytownite, and quartz. This assemblage gives a pressure of about 4.4 kbar.

In the middle metasedimentary sequence (lithological units 5 and 6), the Al_2SiO_5 polymorphs are either sillimanite or kyanite or both. However, as discussed above, petrographic evidence indicates that sillimanite and kyanite do not belong to one coexisting mineral assemblage. The compositions of core-garnet and core-plagioclase give rather consistent pressures from 6.2 to 6.5 kbar with a mean value of 6.4 kbar by using the reaction (5-1) involving kyanite. This indicates that the earlier metamorphic event is more Barrovian-type (medium pressure). The compositions of margin-garnet and margin-plagioclase also yield consistent pressures from 4.2 to 4.5 kbar with a mean value of 4.3 kbar, with the exception of one sample (e.g., 6.0 kbar from I82/144) giving a considerably higher pressure. It is apparent that this higher pressure from sample I82/144 is unreasonable, because sillimanite is the stable phase in I82/144, but a pressure of 6.0 kbar and a temperature of 563°C corresponds to the kyanite stability field (Fig. 5.2). This unreasonable pressure estimation is probably related to either a large analytical error or a very localized domain of disequilibrium.

If the single unreasonable pressure estimation is ignored, all calculated metamorphic pressures, along with the calculated metamorphic temperatures, fall in the appropriate Al_2SiO_5 stability fields (Fig. 5.2). Moreover, the average pressure of the peak metamorphism is considerably lower than that of the earlier metamorphism.

However, the calculated pressure of the peak andalusite-sillimanite series metamorphism is a transition from low to medium, this is supported by the occurrence of almandine garnet in iron-rich pillow margins of mafic metavolcanic rocks (Winker, 1979).

5.4-5 The Orthoamphibole Solvus

The solvus between anthophyllite-gedrite has been discussed by Robinson et al. (1971), Ross et al. (1969) and Stout (1971). Spear (1980) studied coexisting orthoamphiboles (low Na-Al anthophyllite and high Na-Al gedrite) from the Post Pond Volcanics, Vermont and constructed a hypothetical T-X solvus with published orthoamphibole data. According to Spear (1980), the crest of the anthophyllite-gedrite solvus is at about $600 \pm 20^\circ\text{C}$. In the study area, orthoamphibole analyses from the upper zone of medium metamorphic grade completely bridge the solvus. Therefore, the metamorphic temperature of the peak metamorphism in the upper zone of middle amphibolite facies must have reached $600 \pm 20^\circ\text{C}$ or higher. This is consistent with values estimated from published geothermometers (Table 5.1).

5.5 P-T-t Trajectory and Discussion

5.5-1 P-T-t Trajectory.

The physical conditions of metamorphism which have been estimated independently in the principal lithologies of the Hemlo-Heron Bay greenstone belt in the last section and in Chapter 7 (calc-silicates), can be summarized into the following four groups:

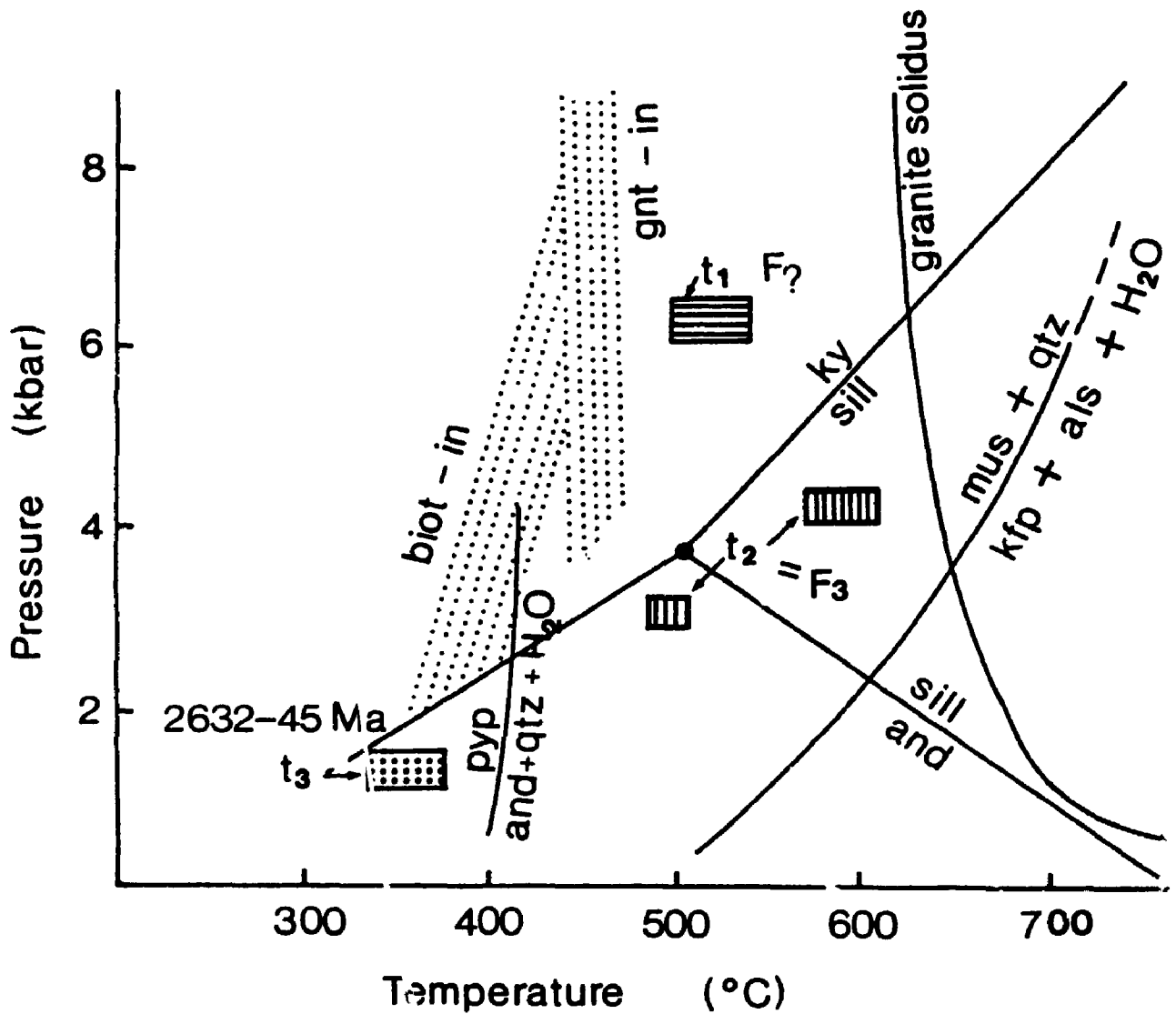


Fig. 5.2. P-T diagram summarizing the calculated temperatures and pressures from principal lithologies of the Hemlo-Heron Bay greenstone belt at the White River property, and possible timing and relationship of individual episodes of metamorphism with deformation: t_1 is the earlier Barrovian-type metamorphism; t_2 is the peak thermal metamorphism (low grade and medium grade); t_3 is the calc-silicate alteration; and F_3 represents the third generation structures of Muir & Elliott (1987).

(1) 6.0-6.5 kbar and 456-520°C for the earlier metamorphism associated with kyanite;

(2) 4.2-4.5 kbar and 580±20°C for the peak metamorphism in zones of medium metamorphic grade (units 1, 4, 5 and 6);

(3) 3.2 kbar and 476-503°C for the peak metamorphism in zones of low metamorphic grade; and

(4) 1.2-1.7 kbar and 360±20°C for the late alteration.

In principle, the P-T estimates from the earlier (relict) assemblages, the main assemblages and late calc-silicate veins can be combined with the geochronologic data of Corfu & Muir (1989a; 1989b) to construct a more or less complete P-T-t path to picture the metamorphic evolution of the Hemlo-Heron Bay greenstone belt. Figure 5.2 summarizes P-T-t relationships calculated from all supracrustal rocks of the Hemlo-Heron Bay greenstone belt.

There is no doubt that all supracrustal rocks of the Hemlo-Heron Bay greenstone belt have been subjected to a peak regional metamorphism, which is characterized by the presence of metamorphic zones of different metamorphic grade (P-T conditions). Petrographic evidence and P-T calculations on the principal lithologies of the White River property also indicate that there was an earlier metamorphic event prior to the peak metamorphism. This is consistent with the study of Burk et al. (1986), who proposed two episodes of metamorphism for Teck-Corona metapelites at the Hemlo gold deposit.

Figure 5.2 also illustrates a low- to very-low grade calc-silicate alteration for all supracrustal rocks, which overprints all metamorphic zones of the peak metamorphism. This is consistent with the observations of Walford et al. (1986) for

the Hemlo gold deposit. The calc-silicate alteration is certainly post-peak metamorphism, and is apparently without direct genetic relationship with the peak metamorphism. This is strongly supported by the geochronological data of Corfu & Muir (1989b), who have shown that the crystallization of rutile and monazite (typical mineral phases of the calc-silicate rocks) was at least 30 Ma later than the peak metamorphism at the Hemlo gold deposit. The timing and cause of the late calc-silicate alteration is one of the major subjects in Chapter 7, and, therefore, will not be discussed further in this chapter.

5.5-2 The Timing and Cause for the Earlier Metamorphism

The discordant occurrences (relative to the main foliation) of kyanite and staurolite porphyroblasts, along with the discordant inclusion-trail in garnet cores, apparently pre-date the main shear deformation (i.e., F_3 of Muir & Elliot, 1986). Unfortunately, it is not possible to deduce the timing of kyanite, staurolite and core-garnet crystallization relative to earlier deformation fabrics, because F_1 and F_2 are not preserved in these crucial samples.

Burk et al. (1986) suggested that the earlier metamorphism is characterized by higher-pressure (up to 7.3 kbars) and moderate temperature. Mineral assemblages and P-T calculations on principal lithologies of the White River property in the present study indicate that the earlier metamorphic event at the White River property is medium in pressure (6.0-6.5 kbar) and low in temperature (typical Barrovian-type).

Burk et al. (1986) also suggested that the earlier metamorphic event probably occurred in response to tectonically-induced crustal-thickening (Archibald et al., 1978; Poulsen et al., 1980; DeWit, 1982). Limited information on the earlier

metamorphism in the study area, particularly the uncertainty regarding its relative timing to the earlier deformation, hampered a more precise elucidation of its cause. However, the tectonically-induced crustal-thickening scenario of Burk et al. (1986) is also considered as a possible candidate for the earlier metamorphic event.

On the other hand, it is noted also that evidence for the earlier metamorphic event prior to the peak metamorphism is mainly from metapelitic rocks in the upper zone of medium metamorphic grade. The earlier relict (kyanite-, staurolite-bearing) assemblages in the upper zone of medium metamorphic grade could also be a recrystallization at low temperatures of a protracted progressive metamorphism, which culminated in the peak metamorphism. However, the lack of textural evidence of sillimanite from kyanite favours two separate metamorphic events rather than one single protracted, progressive metamorphism.

5.5-3 The Timing and Cause for the Peak Metamorphism

Many investigators (Hugon, 1984; 1986; Muir & Elliot, 1987; Muir, 1988) have linked the peak metamorphism of the supracrustal rocks of the Hemlo-Heron Bay greenstone belt to the major ductile shear deformation (i.e. F₁ of Muir & Elliott, 1987). This is clearly indicated by the alignment of major mineral phases [sillimanite (or andalusite in low metamorphic grade), micas, feldspars, quartz, Mg-Fe-Mn amphiboles in metapelites and calcic amphibole mafic metavolcanic rocks] parallel to the regional shear zone (Hemlo Shear Zone). However, the garnet porphyroblasts show a somewhat more complicated story. As discussed earlier, only the inclusion-poor margin-garnet is part of the peak thermal metamorphism. A number of garnet porphyroblasts have been broken into several pieces, and the zonal

pattern (inclusion-rich core and inclusion-poor margin) is well-preserved in individual pieces (Fig. 4.4). The concordant alignment of matrix minerals within the broken garnet porphyroblasts with the rock schistosity clearly indicates that the inclusion-poor garnet margin only crystallized during the earlier stages of the major shear deformation. This deformation continued after fragmentation of the garnet porphyroblasts. The splitting of garnet porphyroblasts probably reflects a sporadic transition to brittle in style (see Chapter 6), although the major shear deformation is predominantly ductile in nature (Hugon, 1984; 1986).

In the Hemlo-Heron Bay greenstone belt, mineral assemblages and P-T calculations indicate that the peak regional metamorphism is an andalusite-sillimanite series thermal metamorphism (Fig. 5.2). The cause of low pressure (andalusite-sillimanite facies series) peak thermal metamorphism in the Hemlo-Heron Bay greenstone belt may be constrained by knowledge of possible mechanism for low pressure metamorphism in more recent settings. Andalusite-sillimanite facies series metamorphism is commonly associated with island arc terrains in modern orogenic belts (Miyashiro, 1973) and the thermal requirement for the low pressure metamorphism in island arc terrains is often taken to be the addition of mantle-derived magma (Oxburgh & Turcotte, 1974) Hence low pressure metamorphism in more recent settings seems to develop in response to intrusion or generation of magma in the lower crust.

In many of the more recent geological settings, a direct relationship between magma and regional metamorphism is obvious (Scottish Highlands, for example). In many others, however, this relationship is less certain. Miyashiro (1973) suggested that the low pressure regional metamorphism, in the Ryoke Belt of Japan, was

likely caused by high heat flow. However, the large scale distribution of regional metamorphic isograds in the Ryoke Belt appears independent of individual granitic plutons; intrusions were mainly late to post-metamorphism and some intrusions have a contact metamorphic aureole. Hence, in many areas, the heat source for the low pressure metamorphism is difficult to ascribe directly to magmatism.

A possible tectonic setting for the Hemlo-Heron Bay greenstone belt in an island arc (either oceanic or continental) basin has been inferred from geochemical characteristics of the clastic metasedimentary rocks. In addition, multiple generations of magmatism in the lower crust and migmatization in the Pukaskwa Gneissic Complex (Corfu & Muir, 1989a; 1989b) have also been recognized. Therefore, the peak metamorphism in the Hemlo-Heron Bay greenstone belt most likely is a typical low pressure type caused by high heat flow in an island arc terrain. This is supported by the lack of extensive retrogression, especially along major structural failures. However, similarly to the Ryoke Belt of Japan (Miyashiro, 1973), the low pressure peak metamorphism in the Hemlo-Heron Bay greenstone belt is characterized by regional scales of metamorphic zones of different metamorphic grades independent of individual granodioritic plutons.

The low pressure series peak metamorphism in the Hemlo-Heron Bay greenstone belt characteristically climaxed in two narrow zones at middle amphibolite facies within a terrain of an overall low metamorphic grade (greenschist-amphibolite transitional facies). It is quite obvious that the upper metamorphic zone of middle amphibolite facies encloses the Hemlo Shear Zone [as at the study area (Fig. 5.1), the Hemlo area (Hugon, 1986; Burk et al., 1986) and to the west near the Black River Bridge on Highway 17 (Patterson, 1984)].

Muir (1982a) reported kyanite-, sillimanite- and staurolite-bearing assemblages in intercalated clastic metasedimentary rocks within the mafic metavolcanic rocks of the Playter Harbour Group to the west near Heron Bay. Muir (1982a) attributed these middle amphibolite facies assemblages to the contact effect of the emplacement of the Heron Bay Pluton in that region. As noted by the present study, sillimanite- and garnet-bearing assemblages also occur in intercalated metasedimentary rocks of the Playter Harbour Group mafic metavolcanic rocks in the White River property remote from the Cedar Lake Pluton (the large granodioritic intrusive equivalent of the Heron Bay Pluton; Muir, 1982a). Moreover, the contact effect due to the emplacement of the Cedar Lake Pluton is considered above to be negligible in terms of metamorphism of the entire Hemlo-Heron Bay greenstone belt. The lower metamorphic zone of middle amphibolite facies appears to be regional in distribution, and therefore, cannot be ascribed to the contact effect of individual granodioritic intrusive bodies. Muir (1988) reported that an 1 km-thick zone of a weak mylonitic fabric generally occurs at the margin of the Pukaskwa Gneissic Complex. This marginal mylonitic zone occurs apparently parallel to the lithologic contact and the main foliation in the Hemlo-Heron Bay greenstone belt.

In terrains that exhibit spatially progressive metamorphism (increasing grade towards some area of the belt) there is frequently disagreement as to the cause of variation in grade. Some authors relate this to a "thermal domain"-that is, to proximity to an augmented heat supply (contact metamorphism for example), while others relate it to increasing burial depth in collision zones (Thompson & England, 1984, and references herein). In the Hemlo-Heron Bay greenstone belt, the peak metamorphism of low-medium pressure apparently excludes a deep burial, which

would have resulted in a high pressure in addition to a high temperature.

Burk et al. (1986) suggested that the peak metamorphism, following the earlier "higher-pressure" metamorphism, resulted from a rapid uplifting and erosion, resulting in a substantial decrease in pressure without a significant change in temperature. P-T calculations of the present study show that the peak metamorphism (in zones of higher metamorphic grade) is considerably higher in temperature (by about 100°C) and lower in pressure (by about 2 kbars) than the earlier metamorphism. Therefore, rapid uplifting and erosion alone probably resulted in a decrease in pressure, but cannot be responsible for higher temperature during the peak metamorphism in the Hemlo-Heron Bay greenstone belt. In other words, additional heat sources are required for the peak metamorphism in zones of medium metamorphic grade. As discussed above, magmatism in the lower crust, and possibly upper mantle as well, likely provide high heat flow for the peak metamorphism. Therefore, the zones of higher metamorphic grade probably represent regional "thermal-domains". This is supported by abundant quartz-feldspar intrusive dikes within the zones of medium metamorphic grade. For the lower metamorphic zone of medium grade, this is also supported by the occurrence of migmatization at the margin of the Pukaskwa Gneissic Complex. Unfortunately, a geochronological study for the quartz-feldspar dikes is not available at the present time. If the "thermal-domain" scenario above is fundamentally correct, the strong correlation between zones of higher metamorphic grade and higher intensity of shear deformation may imply that magmatic activity in the lower crust probably caused both the peak metamorphism and the major shear deformation.

P-T calculations have also shown that the peak metamorphism in zones of different metamorphic grades differ from each other by not only a large discrepancy in temperature (about 100°C) but also a slight difference in pressure (about 1 kbar) (Fig. 5.2). The metamorphic zones of medium grade occur typically in close association with maximum intensity shear deformation (the lower zone with the marginal mylonitic zone of the Pukaskwa Gneissic Complex and the upper zone enclosing the Hemlo Shear Zone; Fig. 5.1). Therefore, an increase in (confining) pressure by 1 kbar may have been achieved by ductile shortening during the major shear deformation, because mylonitic textures have been developed during the major shear event in HSZ and the marginal zone of the Pukaskwa Gneissic Complex indicating exceptional high deformation intensity.

As discussed above, there is little doubt that the peak thermal metamorphism and the major shear deformation in the Hemlo-Heron Bay greenstone belt were broadly contemporaneous, and related to "deep-seated" magmatism in the lower crust. The multiple generations of plutonism (Corfu & Muir, 1989a) likely reflected magmatic activity in the lower crust. Therefore, an age relationship between the peak metamorphism and a phase of plutonism is desirable, and can be achieved by combining the field and petrographic observations with the geochronological data for intrusive rocks of Corfu and Muir (1989a), although no radiometric age determination has been conducted by the present study. Corfu & Muir (1989a) obtained an age of about 2719 Ma for a granodiorite near the marginal zone of the Pukaskwa Gneissic Complex. As discussed earlier, the lower medium metamorphic grade zone of the peak metamorphism correlated with the migmatization in the marginal zone of the Pukaskwa Gneissic Complex. Therefore, the regional peak

metamorphism probably took place at about 2719 Ma. It is notable that this interpretation is not consistent with that of Corfu & Muir (1989b), who, on the basis of U-Pb determinations on titanite, placed the peak thermal metamorphism (amphibolite facies at the Hemlo gold deposit) at about 2678 Ma, which postdates emplacement of the Cedar Lake Pluton. However, detailed petrographic study indicates that at least some titanite at the White River property recrystallized during late localized retrogression and, therefore, its usefulness for dating the timing of the peak thermal metamorphism is suspect. Moreover, the present study has recognized that xenoliths of identical mineral assemblages and textures to the metagreywackes of unit 9 occur within the margin of the Cedar Lake Pluton. Most importantly, rock samples from the Cedar Lake Pluton are strikingly fresh hornblende-biotite granodiorite showing no evidence of metamorphism. These clearly show that the emplacement of the Cedar Lake Pluton was later than the peak regional metamorphism. In addition, the occurrence of small faults and fractures, which radiate from the Cedar Lake Pluton and cross-cut the main foliation in the northern part of the study area (Plate 1h), was probably caused by the emplacement of the Cedar Lake Pluton.

CHAPTER 6 LOCAL SHEAR ZONE AND GOLD MINERALIZATION

6.1 Introduction

Since the discovery of the Hemlo gold deposit in 1982, there has been active exploration for gold in the Hemlo-Heron Bay greenstone belt, both within the Hemlo gold camp itself and in the vicinity of it. The White River property of LAC Minerals Ltd., 5 km eastward from the Hemlo gold deposit, is one of the leading gold prospects in the area. Assays on core samples from a large number of drill-holes indicated several locations with anomalous gold concentrations. Among these locations, a narrow, but laterally-extensive zone with sporadic high values (up to 27 ppm) of gold and occurring at or near the lithological boundary of units 7 and 8, is of most interest. Description and discussion of the gold mineralization in this thesis study are largely focused on this zone of anomalous gold values, which is hereafter referred to as the Anomalous Zone (Fig. 6.1).

6.2 The Anomalous Zone and the Local Shear Zone

6.2-1 Geological Setting

The Anomalous Zone is largely situated within a thin layer of muscovite schist at the lithological boundary between units 7 and 8, and, locally, within the bottom portion of unit 8 in the Heron Bay Group (Fig. 6.1). The thin layer of muscovite schist occurs parallel to subparallel to the strike of the supracrustal rocks in the greenstone belt. It trends 110° and dips 60° north in the western part of the study area, and gradually changes to a strike of 85-90° and a dip of 45° north in the

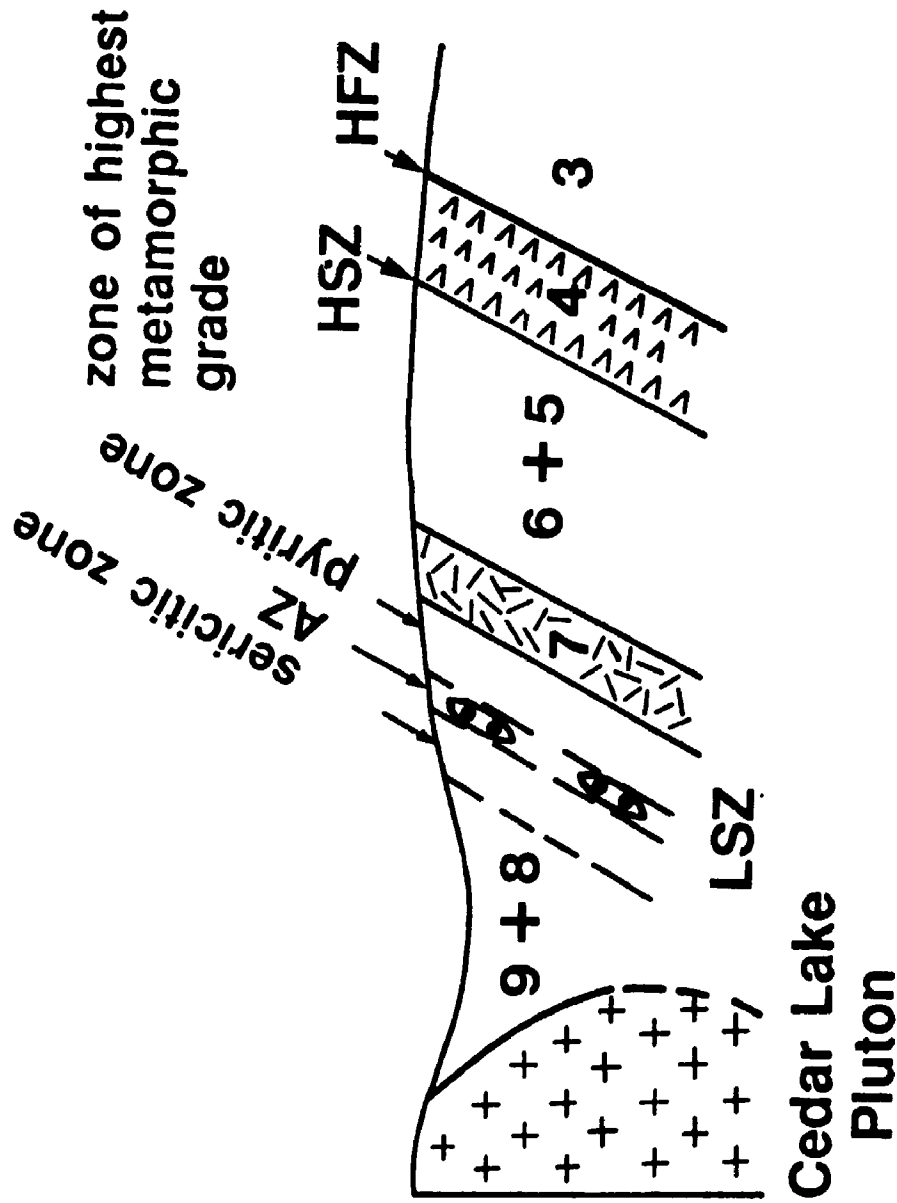


Fig. 6.1. Schematic cross-section of the Heron Bay Group at the White River property (lateral extent of the Local Shear Zone is exaggerated). For stratigraphic legend see Figure 2.2.

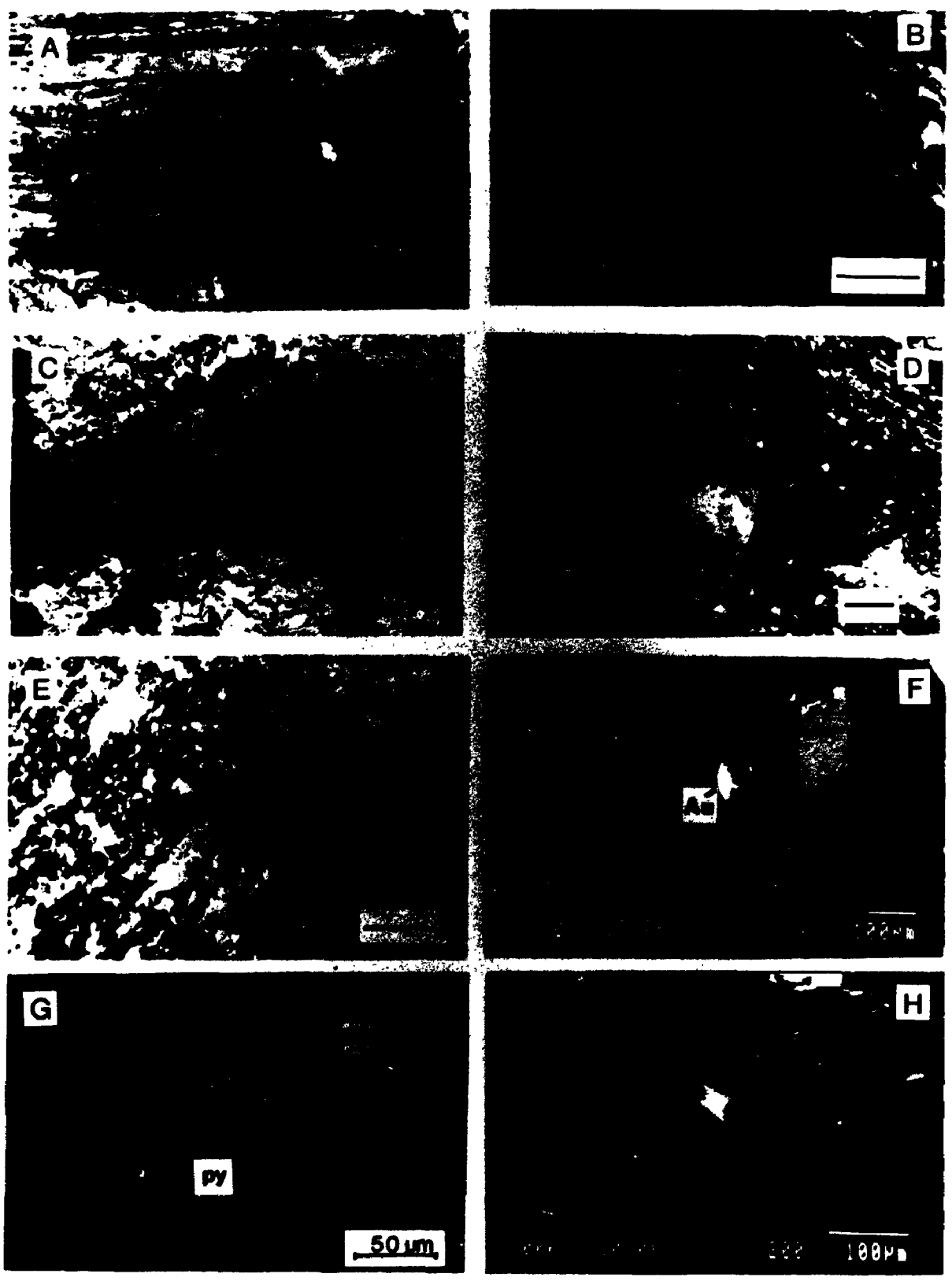
central and eastern parts. In the field, this thin layer of muscovite schist is easily distinguished from the footwall intermediate to felsic metavolcanic rocks and hanging-wall metapelites by its fine-grained and strongly laminated texture and white colour (which is locally rusty due to the weathering of sulfide minerals) (Plate IV-a). The muscovite schist can be traced over a strike length of more than 2 km and attains its greatest thickness (up to 25 m) in the central part of the study area.

6.2-2 Local Brittle-Ductile Shear Zone

Within the lithological units 7 and 8, the strain intensity increases progressively towards the muscovite schist layer, as indicated by the tightness of fold closures and the presence of abundant mafic boudinages (Plate Ig), and close to the muscovite schist, lenses of felsic bodies with well-oriented rock fragments, which have been interpreted as mylonite (Muir, 1988, pers. comm.), are locally present. Therefore, the muscovite schist layer represents a local zone of highest strain and is interpreted as a Local Shear Zone (cf., Ramsay & Graham, 1970; Hugon, 1986). The term "local" is adopted here in order to distinguish it from the Regional Shear Zone (Hemlo Shear Zone) to the south (Fig. 6.1). Mineral lineation is generally absent within the muscovite schist, but can be recognized locally in mafic boudinages in the hanging-wall metapelites and, more rarely, the muscovite schist; it plunges to NW at about 30°. As in the regional shear zone (HSZ), deformation within the Local Shear Zone was predominantly ductile. However, abundant extension veins and breccia veins indicate the sporadic transition to brittle processes. Therefore, the Local Shear Zone is brittle-ductile in nature. The sense of the movement is poorly constrained due to the lack of mineral lineations within the

PLATE IV

- A: Photograph of an outcrop of the Local Shear Zone, Heron Bay Group. Note that the quartz vein is roughly the boundary between the footwall pyritic zone (abundant sulfide in dark layers) and the hanging-wall sericitic zone.
- B: Photomicrograph of elongated pyrite grains in muscovite schists of the Local Shear Zone; scale bar is 0.5 mm.
- C: Photomicrograph of relationship between sulfides (mainly pyrrhotite) and calc-silicate (epidote) veins in the Local Shear Zone; scale bar is 0.5 mm.
- D: Photomicrograph of a prehnite vein from the Local Shear Zone; scale bar is 0.5 mm.
- E: Photomicrograph of massive calcite in a feldspar-rich rock from the Local Shear Zone; scale bar is 0.5 mm.
- F: Electron back-scattered image of native gold along pyrite-grain fractures.
- G: Photomicrograph of a native gold grain along a pyrite grain margin.
- H: Electron back-scattered image of very fine-grained native gold grains showing their association with silicate minerals (epidote, sericite and chlorite).



muscovite schist. However, measurements on a number of rotated porphyroblasts of garnet in oriented samples indicated that the Local Shear Zone is probably dextral, and is, therefore, similar in sense to the regional shear zone (HSZ, cf., Hugon, 1984; 1986) to the south.

The Local Shear Zone is similar in stratigraphic position to the Upper Tectonic Zone (UTZ) in the hanging-wall metasediments of the Hemlo gold deposit (Kuhns et al., 1986). However, a well recrystallized matrix and oriented fabrics (including mylonites; Muir, 1988 pers. comm.) are characteristic of the LSZ, whereas fault breccia is characteristic of the UTZ. Therefore, it is unclear whether the LSZ at the study area is a lateral extension of the UTZ of Kuhns et al.'s (1986). The relative timing of the LSZ and HSZ is not well understood either. It seems unlikely that the LSZ is older than the HSZ. Kuhns et al. (1986) suggested that the UTZ in the hanging wall metasediments is younger than the Lower Tectonic Zone (LTZ; which includes the HSZ) at the Hemlo deposit area. Therefore, the LSZ would be younger than the HSZ if it is a lateral extension of UTZ from the Hemlo area. However, the occurrence of the LSZ parallel to the regional strike and the presence of a well-recrystallized matrix and mylonitic fabrics within it collectively suggest that the development of the LSZ was largely coeval with the HSZ in the study area.

6.2-3 Lithology and Mineralogy

The muscovite schist, which characterizes the Local Shear Zone, is mainly composed of quartz (40-50%), muscovite (15-30%), plagioclase (1-5%), K-feldspar (1-10%), biotite (1-5%), chlorite (1-5%), epidote, prehnite, allanite, biotite, chlorite,

and minor calcite, tourmaline, apatite, monazite, zircon, rutile, titanite and variable amounts of sulfide minerals. Locally, andalusite is present as large elongated porphyroblasts (up to 2mm in length) with 'c-axes parallel to the main foliation (Plate IIg). The porphyroblasts of andalusite are generally altered to sericite or margarite to some degree, and sometimes only the margarite pseudomorphs remain. Poikiloblastic garnet also is sporadically present and is commonly altered to chlorite and sericite. The garnet is characterized by a high Mn content (up to 9.34 wt. %, corresponding to 21.2 % spessartine component), which is similar to the spessartine-rich garnet in the Hemlo gold deposit (Walford et al., 1986).

In the Local Shear Zone, the two major K-bearing phases are muscovite and K-feldspar. Muscovite is generally predominant, and there is an antipathetic relationship in the modal abundance between muscovite and K-feldspar. The alignment of large flakes of muscovite defines the well-developed schistosity within the LSZ (Plate IVb). Small flakes of muscovite (sericite) also are not uncommon in the matrix of the LSZ, and their abundance, which is highlighted by the presence of a sericitic zone in the middle to upper portion. Trioctahedral micas are generally minor in the LSZ. Biotite, which occurs commonly with muscovite, and chlorite, as large flakes, define the schistosity, whereas phlogopite, in a trace amounts, is sporadically present with sericite after plagioclase.

In the field, the Local Shear Zone is partly characterized by its rusty colour, which resulted from the weathering of sulfide minerals. Sulfide minerals are not uncommon in all supracrustal rocks in the greenstone belt and are very abundant in the LSZ. Detailed examination of core materials and petrographic study of thin sections show that sulfide minerals are, locally, major phases in the muscovite schist

of the LSZ. The sulfides are mainly of Fe-Cu-Zn, with pyrite and pyrrhotite being most common and subordinate chalcopyrite and sphalerite. However, sulfate minerals, which are very common in the Hemlo gold deposit (Harris, 1986; 1989), are typically absent in the LSZ. Petrographically, at least two generations of pyrite can be recognized: (1) elongated idiomorphic pyrite with good alignment occurring parallel or subparallel to the main foliation with fine-grained sericite developed in pressure shadows (Plate IVb); and (2) pyrite of variable grain size together with pyrrhotite, chalcopyrite and sphalerite occurring as sulfide veins intersecting the main foliation or as in-filling along the foliation planes (Plate IVc). The sulfide minerals unevenly distributed within the LSZ and are concentrated in a pyritic footwall zone to the Anomalous Zone (Plate IVa; Fig. 6.1).

Large discordant quartz veins are typically absent in the LSZ. However, thin, continuous or discontinuous, monomineralic quartz bands or lenses are very common in the muscovite schist and occur generally parallel to the main foliation. Individual quartz grains of these bands are generally randomly-oriented and are considerably larger in dimension than minerals in the hosting muscovite schists. Although undulose extinction is not uncommon in these quartz grains, the quartz bands are interpreted to be later veins in filling along the foliation planes, on the basis of the coarse-grained texture and lack of preferred orientation.

6.3 Hydrothermal Alterations

6.3-1 Hydrothermal Alterations

The Local Shear Zone is characterized lithologically by a thin layer of muscovite schist and differs from the country rocks by an exceptionally high

abundance in muscovite and, locally, K-feldspar. This clearly indicates that an extensive K-alteration must have occurred in the LSZ. The occurrence of muscovite (as large flakes or plates associated with biotite and chlorite defining the well-developed schistosity; Plate IVb) and K-feldspar (with good triple-point junctions; Plate IVe), however, strongly suggest that the crystallization of the two major K-bearing minerals must be broadly contemporaneous with the peak thermal metamorphism of the region. It is generally believed that the formation of muscovite or K-feldspar in the system $\text{SiO}_2\text{-Al}_2\text{O}_3\text{-K}_2\text{O-H}_2\text{O}$ is mainly controlled by the $a\text{K}^+/a\text{H}^+$ ratio (Helgeson et al., 1978). The predominance of muscovite in the LSZ therefore suggests the K-alteration was associated with a H_2O -rich fluid.

Within the Local Shear Zone, fine-grained sericite (compositionally different from the coarse-grained muscovite; Appendix II: Table 4a) is ubiquitous, and is marked by the presence of a sericitic zone in the middle and upper portion of the LSZ (Plate IVa; Fig. 6.1). Sericite, along with phlogopite, commonly replace plagioclase and porphyroblasts of garnet and andalusite (which were interpreted to represent the peak thermal metamorphism in lower grade zones; Chapter 5), clearly indicating that the sericitization was later than the peak thermal metamorphism of the region.

Calc-silicate alteration is widespread and regional in distribution in the supracrustal rocks at the White River property (see Chapter 7). It is particularly extensive within the Local Shear Zone as indicated by the presence of abundant epidote, prehnite, clinozoisite, allanite and margarite, as either massive aggregates (Plates III,j) or cross-cutting veins (Plates IVc,d).

Sulfidation also is characteristic of the Local Shear Zone, as indicated by abundant Fe-Cu-Zn sulfides (pyrite, pyrrhotite, chalcopyrite and sphalerite), and is particularly marked by the presence of a pyritic zone in the lower portion of the muscovite schist close to the footwall intermediate to felsic metavolcanic rocks (Plate IVa; Fig. 6.1).

Silicification is characterized by the presence of minor amounts of quartz veins or veinlets, which never become significant in abundance in the LSZ. As described earlier, these quartz veins or veinlets (generally parallel to the main foliation) are interpreted as later in-filling (replacement products) along the foliation planes.

Carbonization in the Local Shear Zone, and elsewhere in the greenstone belt at the study area, is only local in significance, and is characterized by the presence of calcite. Calcite is the only carbonate mineral identified in all supracrustal rocks at the study area. Within the Local Shear Zone, calcite (both disseminated and vein varieties) is locally abundant (Plate IVe).

In addition to the alteration styles described above, other notable forms of alteration, such as tourmalinization, are not uncommon, but are of only local significance in the Local Shear Zone. In the case of tourmalinization, Mg-rich tourmaline (dravite) occurs commonly in close association with quartz veins and veinlets.

6.3-2 Genetic Relationships

In this section attention will be focused on the genetic relationships between the numerous hydrothermal alterations in order to bridge a discussion on the

development of the LSZ and gold mineralization within it.

As noted above, at least two K-alteration events must have occurred in rocks of the Local Shear Zone. The earlier K-alteration was no later than the peak thermal metamorphism of the region, because its main products (both muscovite and K-feldspar) are also products of the peak thermal metamorphism as indicated by their fabrics. The late sericitization occurred after the peak thermal metamorphism. As discussed in Chapter 5, retrogression after the peak thermal metamorphism was not extensive in the Hemlo-Heron Bay greenstone belt at the study area. Therefore, a separate K-alteration event must have been superimposed on previous metamorphosed rocks to account for the presence of the abundant fine-grained sericite and, locally, phlogopite.

K-feldspar from the Hemlo gold deposit area yielded generally rather uniform and relative primitive $^{207}\text{Pb}/^{206}\text{Pb}$ ratios (Corfu & Muir, 1989b). These authors suggested that these K-feldspar compositions may indicate that regional magmas and fluids were derived from juvenile crust and/or from the mantle, without significant involvement of the much older (> 2800 Ma) crust. In the Local Shear Zone of the study area, the muscovite schist occurs in spatial association with the footwall intermediate to felsic metavolcanic rocks. Regionally, the earlier K-alteration in the greenstone belt is also generally confined to the northern portion of the belt (the calc-alkaline dominant Heron Bay Group; cf. Muir, 1982a; 1982b), and is invariably in close or direct association with felsic (intermediate) metavolcanic rocks. This may suggest that these felsic (intermediate) metavolcanic rocks were probably the major K sources for the earlier K-alteration event, although other K sources, such as magmatic activity underneath the belt, cannot be excluded. Clearly additional K

must have been transported into the LSZ to produce the exceptionally K-rich lithology (muscovite schist) during the earlier K-alteration.

In contrast to the earlier K-alteration event, two K-sources are possible for the later sericitization in the Local Shear Zone: (1) destruction of earlier major K-bearing phases (muscovite and K-feldspar) and consequently local remobilization of potassium within the LSZ; and (2) additional K introduced from external sources. A discussion on K sources for the later sericitization will be given later, in the section on geochemistry.

Similarly to major K-bearing phases, sulfides in the Local Shear Zone also appear to represent multiple generations. Sulfides in minor amounts are ubiquitous in all supracrustal rocks, particularly metasedimentary rocks, of the Hemlo-Heron Bay greenstone belt at the study area. In the muscovite schist of the LSZ, sulfides occur in a number of textural varieties: (1) as elongated prisms (mainly pyrite) with long axes parallel to the main foliation and, locally, with fine-grained sericite around possible pressure shadows (Plate IVb; similar to pyrite porphyroblasts in metasedimentary rocks and metavolcanic rocks representing the peak thermal metamorphism of the region); (2) in cross-cutting veins (Plate IVc; intersecting the main foliation); and, (3) as massive aggregates also clearly in discordance with the main foliation. The first textural variety is probably the product of the peak thermal metamorphism of the region, whereas the latter two varieties are clearly after than the peak thermal metamorphism and are products of the late sulfidation in the LSZ. In the Local Shear Zone, the pyritic zone, which occurs in the lower portion of the muscovite schist, contains both metamorphic pyrite and later sulfidation products.

In the Local Shear Zone of the study area, other forms of alteration, including calc-silicate alteration, silicification, carbonization and tourmalinization, are mainly in veins or as replacements and apparently post-date the peak thermal metamorphism of the region. Representative mineral phases of individual alteration styles occur commonly in close association with one another, and good correlations in their modal abundances are not uncommon. For example, tourmaline occurs in quartz veins; and abundant secondary sulfide minerals commonly occur in samples with abundant calc-silicate minerals. Therefore, there must be genetic links between these late hydrothermal alterations. Texturally, sulfides and carbonate (calcite) (in central portions of calc-silicate veins (Plate IVc) or as sulfide or calcite veins intersecting calc-silicates) indicate that sulfidation and carbonization were late in the paragenetic sequence related to the formation of calc-silicates (calc-silicate alteration) and probably were a continuation of the calc-silicate alteration at lower temperature.

6.4 Gold Mineralization

Gold assays on 55 drill-core samples reveal the presence of a narrow but laterally continuous zone of anomalous gold values (the Anomalous Zone) within the Local Shear Zone. This Anomalous Zone occurs generally at the central portion of the thin muscovite schist layer and attains a maximum thickness at about 3 m at the central part of the study area. The gold values within the Anomalous Zone vary significantly from 37 ppb to 27 ppm, and the maximum values (3 to 27 ppm) were obtained where the zone of anomalous gold values, the footwall pyritic zone and the hanging-wall sericitic zone coalesce in the centre of the study area (Fig. 6.1).

Native gold is the only major gold-bearing phase identified. A typical sample with microscopic gold is composed of abundant vein or massive varieties of sulfides, sericite and calc-silicate minerals. Native gold grains mainly occur as fine-grained (< 50 μm in diameter) single crystals along fractures or grain boundaries of pyrite and pyrrhotite (Plates IVf,g), and locally as very fine-grained inclusions associated with silicate minerals, including epidote, sericite and chlorite (Plate IVh). Native gold grains are generally irregular in shape without any evidence of alignment and elongation.

Table 6.1 Chemical compositions of native gold from the White River property.

No.	1	2	3	4	5	6
Au	93.55	93.07	93.06	91.62	89.63	86.16
Ag	5.00	4.14	5.51	9.06	9.00	10.84
Hg	1.73	1.02	1.15	1.09	1.10	1.88
S	nd	0.01	0.02	nd	nd	0.05
As	nd	nd	nd	nd	nd	nd
Total	100.3	98.44	99.74	101.8	99.74	98.93

Notes: all analyses are in weight per cent; 1, 2 and 3 are analyses for very fine-grained native gold associated with silicate minerals (Plate IV-f); 4 and 5 are analyses for native gold along pyrite grain fractures (Plate IVd); 6 is an analysis for native gold along pyrite grain margin (Plate IVe); "nd" is "not detectable".

Electron-microprobe analyses (Table 6.1) revealed that native gold from the Anomalous Zone is characterized by high gold/silver ratio with silver content ranging from 8.0 to 16.5 wt. %. Hg also is invariably present (up to 1.88 wt. %) but considerably lower in abundance than in gold from Hemlo (up to 19. wt. %, Harris, 1986). Groen et al. (1989) studied the intermetallic phase equilibria in the ternary system of Au-Ag-Hg at low-temperature (25-300°C) and their preliminary experimental data have demonstrated that Hg does enter into gold-silver alloys by a bulk diffusion process and yields homogeneous and apparently stable ternary phases for the local prevailing conditions.

6.5 Geochemical Characteristics

The geochemistry of gold mineralization in the Local Shear Zone of the White River property was studied systematically by whole-rock analyses of 23 samples from the LSZ (Appendix I: Table 3), and additional samples from the footwall intermediate to felsic metavolcanic rocks and the hanging-wall metapelites. The objectives of this geochemical study were three-fold. Firstly, the major element oxide contents were used to determine the whole-rock chemical variations associated with the observed mineralogy, alteration and gold mineralization of the Anomalous Zone in the Local Shear Zone compared to the hanging-wall metapelites and the footwall intermediate to felsic metavolcanic rocks. Secondly, selective trace element abundances within the zone of anomalous gold values were compared to unmineralized muscovite schists in the LSZ and metapelites in the hanging-wall and intermediate to felsic metavolcanic rocks in the footwall in order to identify

geochemical anomalies associated with the gold mineralization. Thirdly, examination and discussion are made on the behaviour of some elements traditionally considered as either immobile or less immobile, such as rare earth elements (REE), during extensive hydrothermal alteration in a major structural failure.

The major element oxide contents of samples from the LSZ are characterized by a wide range of variation, particularly the contents of SiO_2 (49.7-79.0 wt. %), Fe_2O_3^* (1.94-23.6 wt. %) and CaO (0.35-7.96 wt. %), which, respectively, reflect the presence and uneven distribution of silicification, sulfidation and calc-silicate alteration within the Local Shear Zone. There are apparent correlations between the major element oxide contents and observed mineralogy (which, in turn, partly reflects hydrothermal alteration). For example, sulfide minerals are the main iron-bearing phases due to paucity of mafic silicate minerals (except for epidote) in the muscovite schist of the Local Shear Zone. Therefore, the Fe_2O_3^* content reflects the abundance of sulfide minerals, as does the sulfur content (sulfate minerals being absent in the Local Shear Zone). Similarly, the maximum SiO_2 content (up to 79.0 wt. %) in the Local Shear Zone is higher than that of any samples from the country rocks and is attributable to the high quartz abundance in veins and along the foliation plane (silicification). As noted earlier, plagioclase in the muscovite schist is generally Na-rich in composition (oligoclase and minor albite) and low in modal abundance. The CaO content in the Local Shear Zone also correlates strongly with the modal abundance of calc-silicate minerals (prehnite, epidote, clinozoisite, allanite and margarite), which represent the late, regional, low- to very-low-grade, calc-silicate alteration.

The K_2O content is also characteristically high corresponding to the predominance of muscovite in the LSZ. The K_2O/Na_2O weight ratio, which is typically less than 1 in metapelites (Chapter 3) and in intermediate to felsic metavolcanic rocks, is invariably higher than 1 and is locally up to 11.4. This is attributable to the prominent earlier K-enrichment in the LSZ. However, samples from the sericitic zone do not necessarily have a high K_2O content, but higher values in the K_2O/Na_2O weight ratio are characteristic. This strongly suggests that the later sericitization in the LSZ did not involve additional K. The higher K_2O/Na_2O weight ratio is mainly attributable to depletion of Na as indicated by textural evidence of sericite and phlogopite after plagioclase.

Samples from the Local Shear Zone also are characterized by high L.O.I. (loss on ignition, 1.70-9.10 wt. %) due to the presence of abundant hydrous silicate minerals (muscovite, chlorite, biotite, phlogopite etc.), sulfides and calcite.

The Na_2O content is noticeably lower in all samples from the Local Shear Zone compared to that of country rocks (metapelites and intermediate to felsic metavolcanic rocks), and is significantly depleted in the Anomalous Zone, particularly in samples with high gold values (> 3 ppm) (Appendix I: Table 3). Other minor constituents, such as MgO and MnO (and may be TiO_2 as well), in all samples from the Local Shear Zone are also slightly lower than their counterparts in the country rocks, corresponding to paucity of mafic minerals in the muscovite schist. Therefore, depletion in those minor components probably occurred during the earlier K-alteration. Although some Mg-rich phases, such as phlogopite and Mg-rich calcic amphibole (tremolite), are locally present as late alteration, but are typically low in modal abundances, their formation was likely controlled by the P-T

conditions of the hydrothermal solution rather than significant late enrichment in Mg.

Some trace elements, including Ag⁺ (up to 32 ppm), As (up to 390 ppm), B (20-350 ppm), Ba (470-970 ppm), Cu (15-4600 ppm), Hg (87 ppb), Sr (110-1800 ppm), V (30-100 ppm), W (<3-39 ppm) and Zn (32-130 ppm), in samples from the Local Shear Zone are elevated and show slight anomalies compared to their abundances in country rocks, the footwall intermediate to felsic metavolcanic rocks and the hanging-wall metapelites (Appendix I). Mo is locally abundant, corresponding to the presence of molybdenite, in albite veins in the Cr-rich calc-silicates of the Cadi Fracture Zone and the quartz-microcline pegmatitic veins of the Playter Harbour Group to the south. However, molybdenite is not observed in supracrustal rocks of the Heron Bay Group to the north of the White River property, and Mo is typically at or below its detection limit in the Local Shear Zone of the White River property.

The elevated boron content in the Local Shear Zone directly corresponds to the modal abundance of tourmaline. Tourmaline (mainly in discordant tourmaline-quartz veins) occurs characteristically in all rock types from the northern part of the Heron Bay Group (including lithological units 5, 6, 7, 8 and 9) regardless of the development of gold mineralization (noted in Chapter 3 also).

Barium and strontium in the muscovite schist of the Local Shear Zone are high compared to common sedimentary and volcanic rocks, which is similar to common Archean metasedimentary rocks (Chapter 3), but are significantly lower than their counterparts within the Hemlo orebody and at the Black River area (Harris, 1986; 1989; Patterson, 1984). Their abundances correlate strongly with the

modal abundances of barite, feldspars and muscovite (the main Ba and Sr carriers) with the greenstone belt including the study area, but are not confined to the Local Shear Zone. Similarly, V (and other ferromagnesian trace elements) in the muscovite schist of the Local Shear Zone is higher compared to common sedimentary rocks and volcanic rocks of equivalent MgO content, which is typical for most Archean clastic metasediments (Chapter 3). Green muscovite is typically absent in the Local Shear Zone (and elsewhere in the study area) and V in the white muscovite is generally below detection limit in electron microprobe analyses.

Like the Fe content, Cu and Zn in the Local Shear Zone vary significantly in abundances (8.5-4600 and 32-130 ppm, respectively) and are mainly distributed in chalcopyrite and sphalerite, respectively. Both chalcopyrite and sphalerite are generally products of the late sulfidation in the LSZ.

The Ag, As, Hg and W contents in the Local Shear Zone of the White River property are noticeably high and appear to be anomalous compared to levels in country rocks, the footwall and hanging-wall. High concentrations of these pathfinder elements in the LSZ occur in samples with abundant sulfide minerals, but do not correlate directly with sulfur content (which is a direct measurement of the modal abundance of sulfide minerals). As discussed above, the sulfide minerals from the LSZ appear to represent several generations of mineralization. One sulfide-rich sample from the footwall intermediate to felsic metavolcanic rocks (lithological unit 7) yielded high As, Ag, Hg and W contents. The sulfide minerals (predominantly pyrite) in this sample appear to be metamorphic in origin as indicated a good alignment for all grains (prismatic and granular) parallel to the main foliation (not well-developed in unit 7). Therefore, the high contents of As, Hg and W are

probably not related to the late sulfidation.

Rare earth element (REE) distributions in the LSZ differ from those in country rocks and show evidence of enrichment or depletion in the light REE, without significant variation in the heavy REE, associated with calc-silicate alteration and the formation of REE-rich minerals such as allanite, monazite, rutile and apatite. Most of the samples are similar in REE content to the hanging-wall metapelites; however, samples consisting of REE-rich minerals are generally enriched in the LREE, whereas some samples without REE-rich minerals are depleted in the light REE (Fig. 6.2).

REE behaviour during hydrothermal alteration of basaltic materials has been the subject of several studies but remains quite controversial. Hydrothermal experiments (Menzies et al. 1979; Hajash, 1984) on a glassy tholeiite at temperatures of 150 to 600°C and water/rock ratios of 1 to 125 showed the REE are immobile even when basalt is altered totally to clay. However, other investigators (Staudigel & Hart, 1983; Michard et al., 1983) suggested that removal (but not fractionation) of REE from basalt glass occurs at the basalt-seawater interface where water/rock ratios are extremely high during alteration to palagonite. The present whole-rock data for REE indicate a wide range of variation for samples from the LSZ (Appendix I: Table 3; Fig. 6.2). Most samples are generally similar in both absolute abundances of individual REE and chondrite-normalized pattern to the hanging-wall metapelites. However, other samples exhibit selective depletion or addition of LREE without significant variation in HREE, resulting in change in the fractionation between LREE and HREE. In a few samples, the total REE content is almost doubled, and there is a close correlation between the whole-rock REE

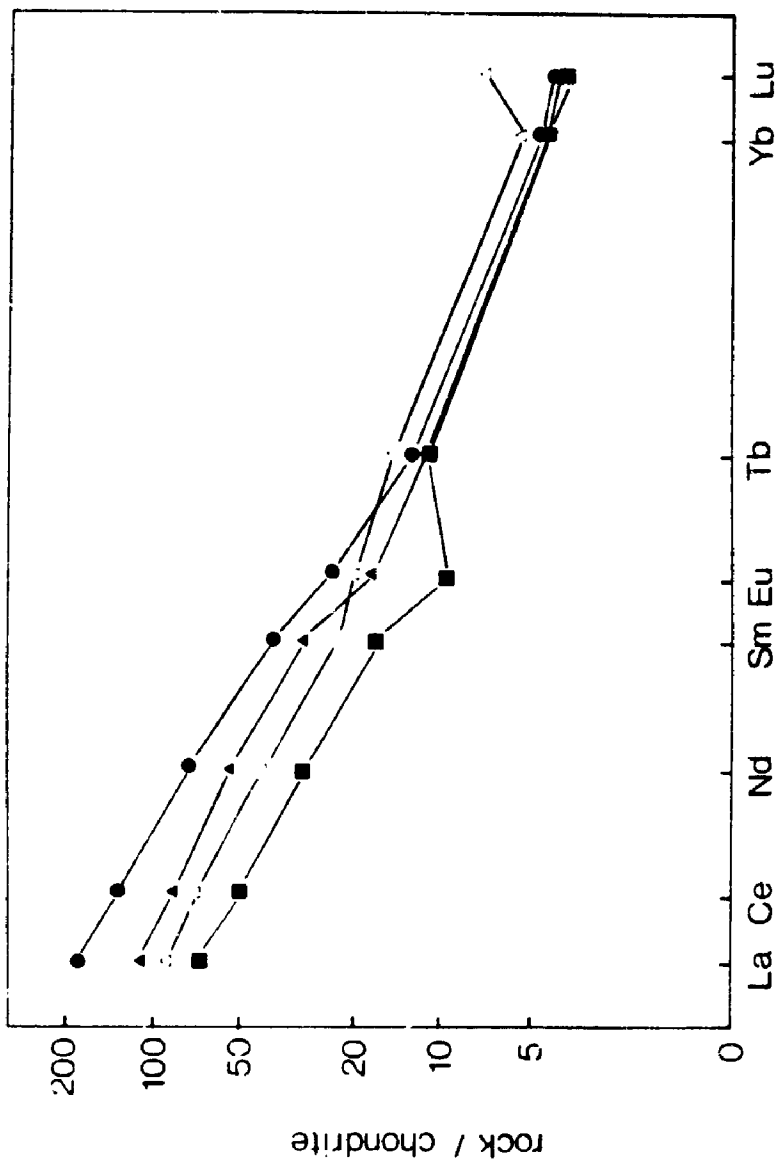


Fig 6 2. Chondrite-normalized REE-patterns of whole-rock samples from the

Local Shear Zone (solid circles represent REE-enriched sample and solid squares represent REE-depleted sample, solid triangles represent the overlying metapelites, and open triangles represent underlying intermediate to felsic metavolcanic rocks)

abundance and modal abundance of allanite and other REE-rich minerals. Moreover, the La_N/Yb_N values in allanite and monazite are considerably higher than those of the whole-rock samples (average value 25, increase to up to 39 in allanite-bearing samples, Fig. 6.2). Therefore, local remobilization of REE must have occurred within the LSZ, and mineral stability, particularly of the REE-bearing minerals, not only affected the REE distribution in terms of total REE contents but also influenced the REE fractionation between LREE and HREE during calc-silicate alteration. The available evidence suggests that a high water/rock ratio prevailed during calc-silicate alteration in the LSZ, and elevated contents of Cl, F, and possibly CO_2 must have been present in the hydrothermal fluid, at least for a period of time during alteration, although the hydrothermal fluid was essentially H_2O -rich during calc-silicate alteration based on a thermodynamic calculation (discussed later in Chapter 7). Such a fluid could promote the mobility of REE and result in their local concentration (Michard et al., 1986; Lottermoser, 1989). However, allanite and other REE-rich minerals have a very local distribution within the LSZ, and are found within host rocks rather than in cross-cutting veins. Therefore, it must be emphasized that the scale of REE mobility was restricted; the LREE seem to have been relatively more mobile than HREE during hydrothermal alteration. This finding is consistent with the study of Exley (1980).

6.6 Summary

Although there is no direct correlation between a single geochemical anomaly (or a single hydrothermal alteration) and high gold concentrations, the emplacement

of gold in the Anomalous Zone of the White River property must relate in some way to the hydrothermal alteration. First of all, high gold concentrations occur in this major structural failure (Local Shear Zone) in which extensive and diverse hydrothermal alteration has been documented. Secondly, maximum gold values are obtained where the zone of anomalous gold values (Anomalous Zone), the footwall pyritic zone and the hanging-wall sericitic zone coalesce. Thirdly, in addition to high abundances of sulfide minerals and sericite, samples with maximum gold values are also characterized by an exceptionally wide range of variation in CaO and REE contents and low Na₂O (Appendix I: Table 3). This clearly indicates the local remobilization of Ca and REE and the depletion of Na were most extensive here as well. Above all, native gold occurs in direct association with secondary minerals either sulfide or silicate minerals or both. Therefore, the gold mineralization in the Local Shear Zone of the study area was associated with the late hydrothermal alterations in general rather than with a single alteration style. As a matter of fact, all of the late hydrothermal alteration styles observed are integral parts of the late, protracted calc-silicate alteration in the Local Shear Zone, which, in turn, is part of the late, low- to very-low-grade calc-silicate alteration at the study area and elsewhere in the Hemlock-Heron Bay greenstone belt.

CHAPTER 7 SKARN DEVELOPMENT

7.1 Introduction

At the White River property, three prominent calc-silicate occurrences are present at or near major structural failures (Fig. 7.1): (1) the Cr-rich calc-silicates in the Cadi Fracture Zone of the Playter Harbour Group; (2) the Fe-rich calc-silicates at or near the Hemlo Shear Zone; and, (3) the REE-enriched calc-silicates in the Local Shear Zone of the Heron Bay Group. Several aspects of their salient mineralogical characteristics in individual occurrences have been given in previous sections. In this chapter, attention will be focused on their genetic relationships and, particularly, the evolutionary history of all the three calc-silicate occurrences in a protracted skarn development within this Archean terrain. In addition, high gold concentration occurs in association with the REE-enriched calc-silicates in the Local Shear Zone (as discussed in Chapter 6). Therefore, an understanding of the development of the (skarn-like) calc-silicates must include their genetic relationship with the gold mineralization within the study area and within the entire Hemlo-Heron Bay greenstone belt.

7.2 Calc-silicate Occurrences

Calc-silicate alteration is widespread in the study area and is particularly pervasive at or near major structural failures. Three calc-silicate occurrences with salient mineralogical and geochemical characteristics are of particular interest: (1)

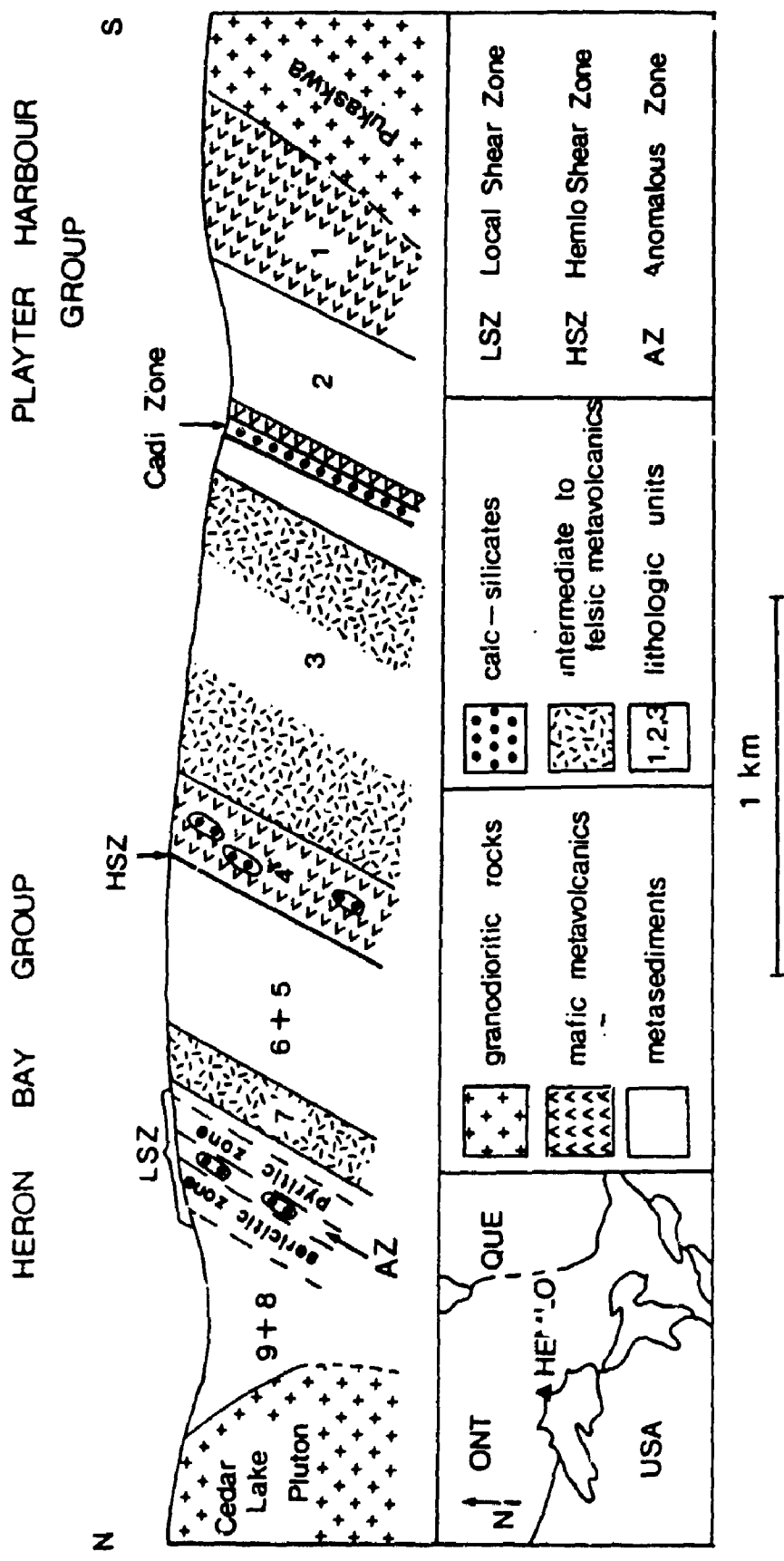


Fig. 7.1. Schematic cross-section of the Hemlo-Heron Bay greenstone belt at the White

River property illustrating calc-silicate occurrences. Note that lateral extents of all

three calc-silicate occurrences are exaggerated.

Cr-rich calc-silicates in the Cadi Fracture Zone of the Playter Harbour Group to the south; (2) Fe-rich calc-silicates at or near the Hemlo Shear Zone; and, (3) REE-enriched calc-silicates in the LSZ of the Heron Bay Group in the central and northern parts of the study area, respectively (Fig. 7.1).

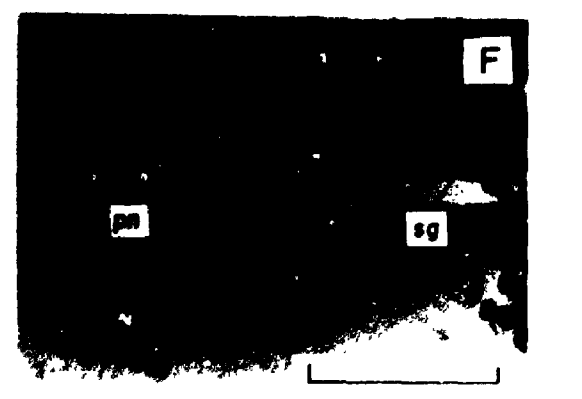
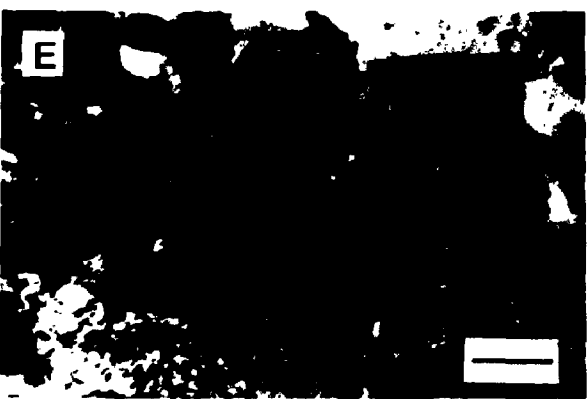
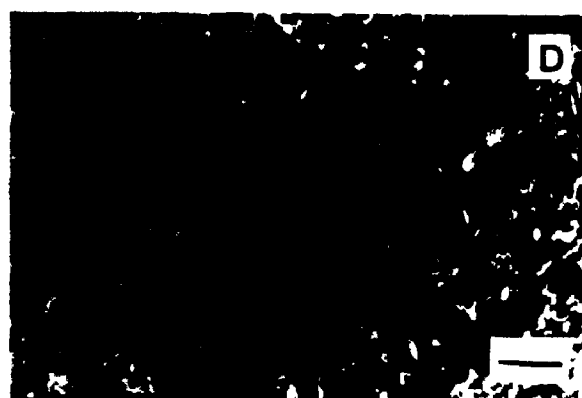
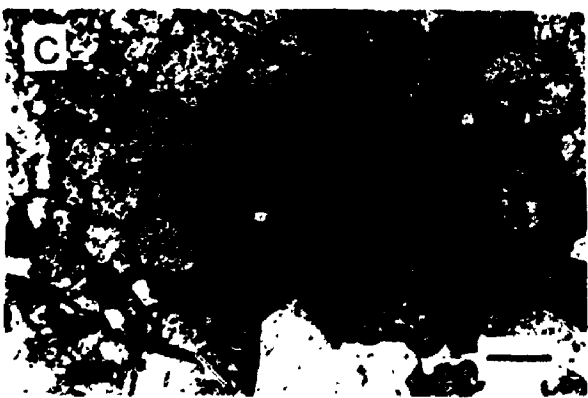
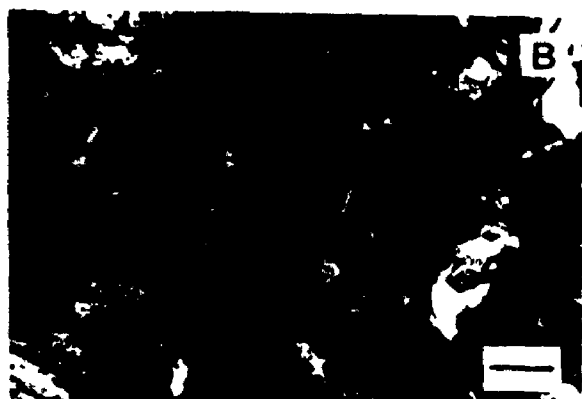
7.2-1 Cr-rich Calc-silicates

The Cr-rich calc-silicates of the Playter Harbour Group are situated at or near lithologic boundaries between overlying clastic metasedimentary rocks (calcic amphibole-bearing) and underlying komatiitic basalt flows (amphibolite) (Fig. 7.1). They occur as elongated lenses or layers (up to 10 m thick) with moderate to well-developed compositional banding parallel to the main foliation of the study area (Fig. 2.2). Fragments of komatiitic basalt (Plate Ib) and komatiite with well-preserved microspinifex-texture (tremolite-talc-chlorite after olivine) are locally abundant within individual calc-silicate lenses.

Mineralogically, the Cr-rich calc-silicates are characterized by a main assemblage of clinopyroxene, epidote, grandite garnet, actinolite, zincian chromite, plagioclase, titanite, magnetite and minor sulfides (pentlandite, pyrrhotite, Fe-rich siegenite, mullerite, sphalerite, pyrite and chalcopyrite) (Plate Va). All major silicate phases generally are chemically homogeneous within individual grains, although a wide range of variation is common among all samples analyzed. For example, clinopyroxene varies generally within binary diopside to hedenbergite series ($Di_{40}Hd_{60}$ to $Di_{75}Hd_{25}$), and epidote group minerals include clinozoisite ($Ps < 10$) and epidote (Ps_{20-29}). Brownish grandite (Cr-poor) is a common phase and generally occurs as large porphyroblasts. Locally, green grandite (Cr-bearing) is also present in some

PLATE V

- A: Photomicrograph of Cr-rich calc-silicates from the Cadi Fracture Zone; scale bar is 0.5 mm.
- B: Photomicrograph illustrating calcic amphibole after clinopyroxene along fractures in Fe-rich calc-silicates from unit 4; scale bar is 0.5 mm.
- C: Photomicrograph illustrating pyrite in-filling along garnet fractures in Fe-rich calc-silicates from unit 4; scale bar is 0.5 mm.
- D: Photomicrograph illustrating pervasive prehnite alteration in mafic metavolcanic rocks of unit 4; calcite is present in the central portion of the prehnite vein in the right of the field of view; scale bar is 0.5 mm.
- E: Photomicrograph of epidote after pyrite within the Local Shear Zone; scale bar is 0.5 mm.
- F: Photomicrograph illustrating Fe-rich siegenite and cobaltian pentlandite as exsolution lamellae in pyrrhotite in Cr-rich calc-silicates from the Cadi Fracture Zone; a gradational colour change from pentlandite (grey) to siegenite (bright) probably indicates that the latter is an alteration product of the former (for explanation see text); scale bar is 0.5 mm.



Cr-rich samples (Plate II f). Anomalously Cr-rich minerals (including chromian epidote, and Cr-bearing chlorite, prehnite, and pumpellyite), and other minerals (albite, microcline, calcite and molybdenite) are only present in cross-cutting veins and vesicles, whereas uvarovite (and Cr-rich garnet) is locally present as fibrous aggregates surrounding zincian chromite grains (Plate II e).

7.2-2 Fe-rich Calc-silicates

The Fe-rich calc-silicates are locally present within unit 4 of metamorphosed high-iron tholeiitic basalt and are particularly abundant at the upper portion near the Hemlo Shear Zone (Fig. 7.1). They occur as small lenses or thin bands of brown colour with sharp boundaries with their dark green to black amphibolite host, and have been recovered only from diamond-drill core. Despite their close association with a major regional structure, Fe-rich calc-silicates are generally massive in nature with local weakly-developed foliation parallel to the main foliation.

Mineralogically, the Fe-rich calc-silicates are characterized by coarse-grained Fe-rich phases such as clinopyroxene, epidote, garnet and calcic amphiboles. Although there is a wide range of variation in chemical composition among samples analyzed, all major phases (except garnet) are generally homogeneous. Clinopyroxene varies from $Di_{24}Hd_{68}$ to $Di_{50}Hd_{45}$, but most analyses are close to $Di_{24}Hd_{68}$. Minor amounts of Al and Mn (up to 1.4 and 1.2 wt. % in Al_2O_3 and MnO, respectively) are present in clinopyroxene. Garnet, on the other hand, generally shows a slight iron-enrichment towards margin, and is characterized by high Mn content (ranging from 4.8 to 8.4 wt. % MnO). The high total iron content in garnet analyses is in both ferric and ferrous states as inferred by charge-balance

calculations. Calcic amphiboles in the Fe-rich calc-silicates are brownish in colour and generally occur as short prismatic crystals rimming or along grain fractures of anhydrous minerals (mainly clinopyroxene, Plate Vb). The composition of the brownish calcic amphibole (with high Al content, 10.0 ± 1.5 wt. % Al_2O_3 , and low $\text{Mg}/(\text{Mg} + \text{Fe} + \text{Mn})$ ratio, less than 0.2) is similar to tschermakitic/pargasitic hornblende in the host amphibolite. Bimineralic aggregates of brownish tschermakitic/pargasitic hornblende and colourless to yellowish green actinolite are also common within the Fe-rich calc-silicates. Actinolite as a minor phase is present generally as lamellae in tschermakitic/pargasitic hornblende hosts.

Tschermakitic/pargasitic hornblende from these aggregates is similar in composition to its replacement counterparts in anhydrous minerals. Actinolite is characterized by a similar $\text{Mg}/(\text{Mg} + \text{Fe} + \text{Mn})$ ratio to its host but is low in Al (< 4.0 wt. % Al_2O_3). Epidote is typically absent in metasedimentary rocks and mafic metavolcanic rocks of middle amphibolite facies at the study area, but is present as a minor phase in the Fe-rich calc-silicates. In contrast to other Fe-rich phases, epidote shows no Fe-enrichment, with a Ps content ranging from 28 to 30. Plagioclase is only locally present and is characterized by an An content at about 91 % in the Fe-rich calc-silicates. Magnetite is present only locally as a minor phase. Sulfides include pyrite, pyrrhotite, pentlandite, sphalerite, chalcopyrite and Fe-rich siegenite occurring as infilling in anhydrous mineral grain fractures (Plate Vc).

7.2-3 REE-enriched Calc-silicates

The REE-enriched calc-silicates occur in the Local Shear Zone at or near contacts between metapelites and intermediate to felsic metavolcanic rocks of the

Heron Bay Group (Fig. 7.1). They are characterized by massive epidote-clinozoisite-prehnite aggregates in addition to abundant epidote-prehnite veins in muscovite schists (Plates IVc,d). Textural varieties of epidote (massive and vein) are of similar composition (Ps_{12-15}) and exhibit similar zonal patterns to disseminated epidote associated with pyrite (Plate Ve), with an Fe-rich core and an Al-rich margin; whereas the other two calc-silicate minerals (prehnite and clinozoisite) are generally close to their ideal stoichiometries with minor iron (< 1.0 wt. % FeO* in both phases). Fine aggregates consisting of halogen-bearing (F and Cl) allanite, monazite and REE-bearing apatite and rutile also are locally present in close association with massive calc-silicate aggregates and are commonly enveloped by epidote (Plates III, j). The REE-rich mineral aggregates occur either discordant to the main foliation or as in-filling (later replacement) along the main foliation planes (Plate IIj). Single crystals of halogen-bearing allanite also are present in close association with the secondary sulfide (pyrite, pyrrhotite, sphalerite and chalcopyrite) veins (Plate IIIk).

7.2-4 Other Calc-silicates

In addition to the three major calc-silicate occurrences, calc-silicate veins are very common at the study area, particularly pervasive in mafic metavolcanic rocks (Plate Vd) and lithological boundaries. Most of the calc-silicates veins transect the main foliation. Others, still in large quantity, occur as in-filling along the foliation planes or in small-scale fold noses. These calc-silicate veins are clearly late in the structural history of the study area because they are not themselves penetratively deformed. They are normally less than 5 cm (a few up to 20 cm) wide and can rarely be traced laterally for more than a few metres. Mineralogically, the calc-

silicate veins are composed of any combination of the following minerals: epidote, prehnite, clinozoisite, actinolite, chlorite, pumpellyite, albite, microcline, quartz, calcite, titanite and minor sulfides (mainly pyrite). Although all of these mineral phases are observed in the calc-silicate veins, most veins are generally mono- or bi-mineralic in nature. Locally, veins consisting of more than two mineral phases are generally zoned (Plates IVc and Vd). A zoned vein could contain a dark-coloured zone of calc-silicate minerals, passing into a light-coloured (commonly pinkish) zone of microcline, albite and quartz and centred by another light-coloured zone of calcite with sulfides. However, veins consisting of all three zones are rare, and most zoned veins generally contain just a dark-coloured zone and one light-coloured zone. Moreover, the mineralogy (both mineral assemblage and chemical composition) of the individual zones also varies from vein to vein but strongly correlates with their host lithologies. For example, pumpellyite, which is characterized by a minor amount of Mg content (and minor Cr content as well in Cr-rich calc-silicates), is restricted to veins or vesicles associated with komatiitic basalt or komatiite.

7.3 Geochemistry of Calc-silicates

Geochemical characteristics of the REE-enriched calc-silicates associated with gold mineralization in the Local Shear Zone have been discussed in detail in Chapter 5. In this section, the description and discussion on geochemistry is restricted to the Cr-rich calc-silicates from the Cadi Fracture Zone and the Fe-rich calc-silicates associated with the Hemlo Shear Zone.

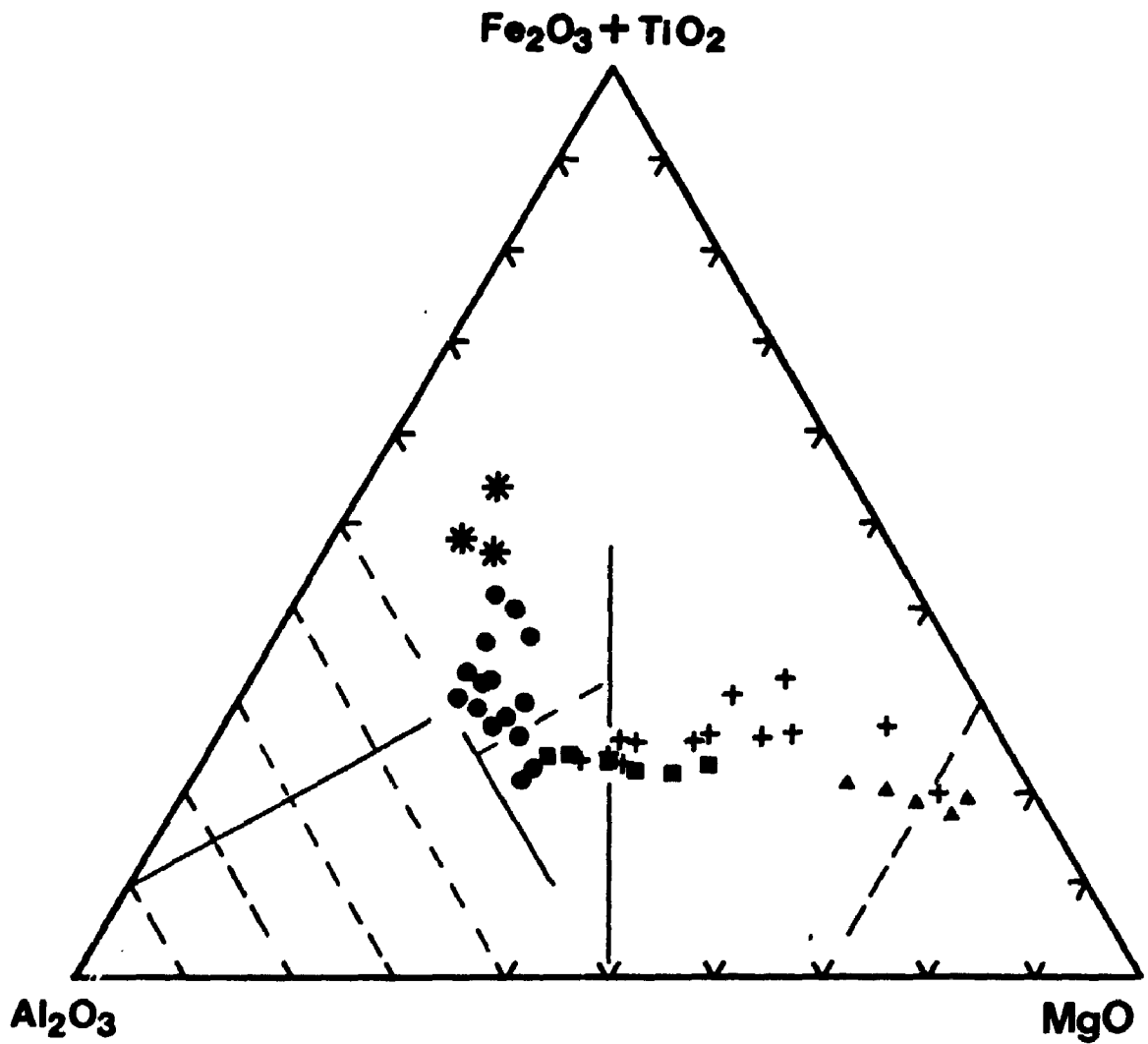


Fig. 7.2. A Jenson Cation Plot for Cr-rich calc-silicates (crosses), Fe-rich calc-silicates (stars), unit 2 amphibolites (komatiitic basalt, squares); unit 4 amphibolites (tholeiitic basalt, circles), and ultramafic metavolcanic rocks of unit 2 and 4 (triangles) from the White River property (cf. Jenson, 1976).

On a Jenson cation plot (Fig. 7.2), most points of the Cr-rich calc-silicates are in the komatiitic basalt field and a few points fall into the komatiite field. This supports the textural evidence that the Cr-rich calc-silicates are the alteration product of the Cadi Fracture Zone. However, the compositional field of the Cr-rich calc-silicates above the trend (defined by unaltered komatiitic basalt and komatiite from the study area) indicates a significant Fe-enrichment. This is supported by the presence of Fe-rich sulfides (pyrrhotite, pentlandite and chalcopyrite). In addition, plots of Cr-rich calc-silicates also are more scattered relative to those for unaltered komatiitic basalt and komatiite. This may be explained by the addition of Ca and Si and the depletion of Mg. On an AFM diagram (Irvine & Baragar, 1971; not presented here), the plots of Cr-rich calc-silicates fall on the calc-alkaline trend, which is explained by the additional enrichment of Ca, Na and K as calcite, albite and microcline in later veins.

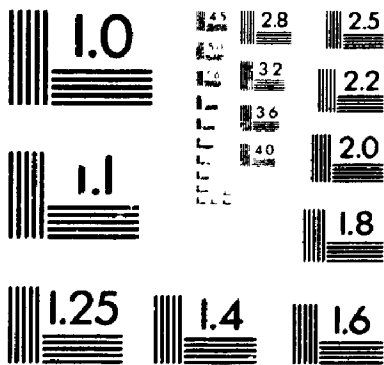
Inspection of Figure 7.2 suggests that the Fe-rich calc-silicates are of a tholeiitic affinity, and all analyses of the Fe-rich calc-silicates fall onto the trend for tholeiitic basalt. In comparison with its host rocks of unit 4 (high-iron tholeiitic basalt), the Fe-rich calc-silicates show a marked iron enrichment. If some iron is combined with sulfur to allow for the abundance of pyrite, the plots of the Fe-rich calc-silicates on Figure 7.2 are still above the field defined by the unit 4 high-iron tholeiitic basalt. This strongly indicates that hydrothermal metasomatism was characterized by the addition of Fe, S and Ca and depletion of Mg and Al.

Trace element (particularly transition-metal) geochemistries of the Cr- and Fe-rich calc-silicates are also characterized by strong correlations with their host lithologies: particularly, the high Cr, Ni and Co concentrations in Cr-rich calc-

3

OF/DE

3



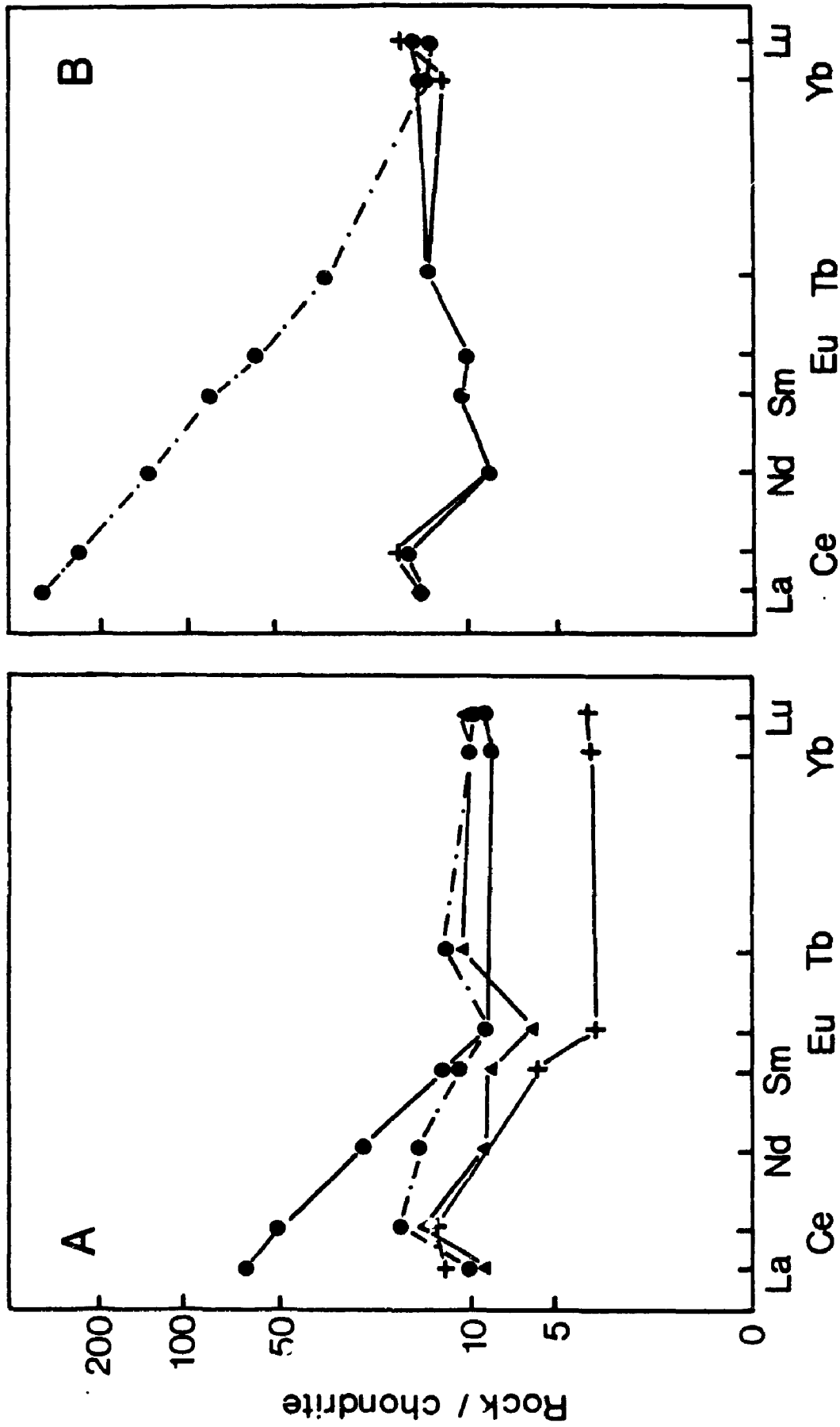


Fig. 7.3. Representative chondrite-normalized REE-patterns of (A): Cr-rich calc-silicates (circles) and unit 2 komatiitic basalt (triangles) and komatiite (crosses); (B) Fe-rich calc-silicates (circles) and unit 4 high-iron tholeiitic basalt (crosses).

silicates and Cu, Zn and Co concentrations in the Fe-rich calc-silicates (Appendix I: Table 4). However, the chromium content in the Cr-rich calc-silicates (up to 5100 ppm) is higher than that of any mafic or ultramafic (meta-)volcanic rock in the study area. Therefore, secondary enrichment in Cr must have occurred as well.

As discussed in Chapter 5, extreme caution must be taken on the interpretation of the rare earth element (REE) geochemistry of the calc-silicates associated with major structural failures, because local remobilization of these elements must have occurred during hydrothermal alteration with extremely high water/rock ratios. Similarities in both absolute abundance and chondrite-normalized REE patterns between most samples of the calc-silicates and their host lithologies are obvious (Fig. 7.3). This strongly supports textural and other geochemical evidence that the Cr- and Fe-rich calc-silicate were derived from their respective host mafic (meta-)volcanic rocks. However, a few samples (both Cr- and Fe-rich calc-silicates) do show a considerable increase in REE abundance accompanied by an increase in La_N/Yb_N ratio indicating higher fractionation between light REE (LREE) and heavy REE (HREE) (Fig. 7.3). In contrast to the REE-enriched calc-silicates associated with gold mineralization, no REE-rich mineral, such as allanite and monazite, is observed in the Cr- and Fe-rich calc-silicates, which may be explained by the restricted stability of these REE-rich minerals.

7.4 Skarns

7.4-1 Terminology and Classification

Skarn is recently defined as rocks consisting of a coarse-grained, generally iron-rich, mixture of Ca-Fe-Mg-Mn silicates (Meinert, 1990; person. commun.).

Previous criteria for skarn (i.e. as a type of sulfide mineral deposit and formed by processes at relatively high temperatures; cf. Einaudi et al., 1981; Einaudi & Burt, 1982) are now considered unnecessary. In the study area, the two types of calc-silicates associated with mafic and minor ultramafic rocks (Cr-rich in the Cadi Fracture Zone of the Playter Harbour Group and Fe-rich within the high-iron tholeiitic pillow basalt unit of the Heron Bay Group) would be regarded as varieties of skarn in the sense of Meinert (1990; person. commun.). However, carbonate rocks are typically absent in the study area and its vicinity, and calcite is only sporadically abundant (mainly in late veins). Furthermore, these two calc-silicate occurrences are situated at or near major structural failures and contain abundant fragments of volcanic rocks, and their salient mineralogical and geochemical characteristics strongly correlate with their host lithologies. Therefore, these two calc-silicates, which differ from classic "reaction skarn" at contacts between carbonate strata and their associated plutonic bodies, were most likely formed by metasomatic processes which replaced volcanic or metavolcanic rocks at or near major structural failures and should be classified as "replacement skarns" in the sense of Einaudi et al. (1981) and as "stratiform skarns" of Stanton (1987).

In contrast to the Cr- and Fe-rich calc-silicates, REE-enriched calc-silicates in the Local Shear Zone are often volumetrically predominant only on a small scale (centimetre or millimetre), but are volumetrically minor on the scale of the entire alteration zone. The term "skarn" is adopted here for rocks of abundant calc-silicate minerals, as in the gold-silver skarns in the Southern Cross greenstone belt of Western Australia (Mueller, 1988) and the Cantung tungsten skarn of Northwest Territories, Canada (Mathieson & Clark, 1984).

Skarn deposits generally exhibit a systematic evolution parallel to the emplacement and cooling history of the associated plutons and three distinct stages in development are commonly recognized: (1) contact metamorphism; (2) metasomatism (skarn formation); and (3) retrograde alteration (Einaudi et al., 1981). In the following section, attention will be focused on the development of the three skarn occurrences and the pervasive calc-silicate alteration of the study area, in order to identify genetic relationships with and any systematic evolution relative to deformation, metamorphism, and later plutonic activity in this Archean terrain.

7.4-2 Regional Metamorphism

The Cr- and Fe-rich skarns occur as conformable layers or lenses in the supracrustal rocks, and are characterized by compositional banding and locally-developed foliation parallel or subparallel to the main foliation (representing the peak metamorphism of the study area; for discussion see Chapter 5). Therefore, the formation of these two skarns must have commenced during the peak metamorphism. However, the peak metamorphism in the Hemlo-Heron Bay greenstone belt is characterized by heterogeneous shear deformation and is regional in nature (distinguishing it from contact metamorphism of common skarn deposits).

The REE-enriched skarn is restricted to the Local Shear Zone and is generally of local significance (Fig. 7.1). The characteristic mineral assemblages of the REE-enriched skarn are comparable to that of low to very-low-grade metamorphic rocks. Therefore, it is possible that the formation of REE-enriched skarn also commenced during the peak metamorphism, because the Local Shear Zone itself is located in a metamorphic zone of greenschist-amphibolite transitional

facies. However, the characteristic calc-silicate minerals occur either as veins discordant to the foliation or as in-filling aggregates along the foliation planes. In addition, the elevated halogen contents (F and Cl) in allanite and REE-bearing clinzoisite appear to suggest that the REE-enriched skarn was formed during the late, low- to very-low grade alteration rather than the peak metamorphism, because halogens are typically absent in metamorphic minerals, but are characteristically present as minor constituents in a number of typical alteration mineral phases (i.e. sericite and phlogopite).

7.4-3 Retrograde Alteration

Retrogression after the peak metamorphism is generally absent or poorly-developed in the Hemlo-Heron Bay greenstone belt at the study area. In the Cr-rich skarn of the Playter Harbour Group, all major mineral phases, including clinopyroxene, garnet, epidote, calcic amphibole, plagioclase, quartz, and, probably, some calcite, appear to have attained equilibrium with their ambient fluid.

In the Fe-rich skarn, however, hydrous minerals such as calcic amphiboles and, locally, chlorite as well, occur along grain fractures of earlier anhydrous minerals such as clinopyroxene and garnet (Plate Vb). This is similar to the "normal" internal replacement sequence in most skarn deposits (Einaudi et al., 1981).

Sulfides in the two earlier skarns exhibit a rather complicated crystallization history: disseminated pentlandite and pyrrhotite in Cr-rich calc-silicates are the main sulfide phases showing textural equilibrium with major silicate phases. Pyrite, the most abundant sulfide mineral in Fe-rich calc-silicates, generally occurs as in-filling

along anhydrous mineral grain fractures (Plate Vc). Cobaltian pentlandite is also present as lamellae in pyrrhotite grains in both Cr and Fe-rich calc-silicates, and appears to be an exsolution product of the earlier pyrrhotite. The lamellar cobaltian pentlandite was further altered to Fe-rich siegenite (Plate Vf). This apparently is attributable to retrograde alteration in these earlier skarns.

7.4-4 Late Calc-silicate Alteration

Calc-silicate alteration is characterized by epidote-prehnite-clinzoisite veins intersecting earlier structures (Plates IIj, IVd and Vd), which indicate its late position in the paragenetic sequence. This type of calc-silicate alteration is regional in distribution, being pervasive in mafic metavolcanic rocks, and overprints all supracrustal rocks in the Hemlo-Heron Bay greenstone belt.

The late calc-silicate alteration event also apparently overprinted on the earlier skarns, which are associated with major structural failures. In the Cr-rich skarns from the Cadi Fracture Zone of the Playter Harbour Group, the late calc-silicate alteration is characterized by the presence of veins and vesicles of anomalous Cr-rich minerals such as uvarovite, chromian epidote, chromian chlorite and Cr-bearing prehnite, actinolite, and pumpellyite. In the Fe-rich skarn of the Heron Bay Group, the cross-cutting veins consist mainly of epidote, actinolite, prehnite and chlorite and are similar to other calc-silicate veins in metabasites. However, the chemical composition of mineral phases in veins from the Fe-rich skarn is distinct from those in metabasites by their high Fe contents, with the exception of epidote. For example, the molar ratio of $Mg/(Mg + Fe + Mn)$ of vein actinolite from the Fe-rich skarn is considerably lower than that in vein actinolite

elsewhere, although the latter is apparently enriched in Mg relative to its lamellar counterparts in tschermakitic/pargasitic hornblende hosts.

The third skarn occurrence (REE-enriched) has been suggested in a previous section to be part of the late, low- to very-low-grade, calc-silicate alteration. Its formation may reflect an exceptional pervasiveness of the calc-silicate alteration along the Local Shear Zone during its dilatation. Interestingly, the REE-enriched skarn itself also exhibits a rather complicated paragenesis. It began with crystallization of epidote, clinozoisite and allanite at apparently higher temperatures, continued with the formation of prehnite, quartzite and feldspars, and concluded with carbonization, sulfidation and gold deposition. This type of paragenetic sequence is locally observed in well-developed individual calc-silicate veins within the mafic metavolcanic rocks, and, therefore, most likely reflects a general crystallization sequence of the late, low- to very-low-grade calc-silicate alteration in a regional scale.

7.4-5 Discussion

As discussed above, the earlier (Cr- and Fe-rich) skarns are not classic "reaction skarns" at contacts between carbonate strata and proximal plutonic bodies but are "replacement skarns" associated with mafic (or minor ultramafic) metavolcanic rocks in major structural failures. In addition, these types of skarns are situated in a regionally metamorphosed terrain rather than contact metamorphic aureoles. The whole-rock composition and calc-silicate mineralogy of these earlier skarns point to a prominent calcium metasomatism. If the host mafic volcanic rocks for Cr-rich and Fe-rich skarns are "normal" komatiitic or tholeiitic basalt,

respectively, the high Ca content of the calc-silicate assemblages required a significant introduction of calcium, although a pyroxenitic precursor for the Cr-rich skarn in the Cadi Fracture Zone cannot be excluded. It is well known that a metamorphogenic fluid, generated by a progressive metamorphism, should not be enriched in calcium, as calcium-bearing minerals are progressively stable in common lithologies with increasing metamorphic grade. However, the close association and strong correlation of the earlier skarns with ultramafic and mafic metavolcanic rocks probably suggest that calcium was derived locally from host lithologies through a "reactive" fluid, which liberated calcium from the ultramafic and mafic metavolcanic rocks and concentrated it in the calc-silicate bodies.

As discussed in Chapter 5, the peak regional metamorphism was a rather protracted event and was most likely related to deep-seated magmatism. Multi-generation of magmatism in the Hemlo-Heron Bay greenstone belt has been confirmed by the geochronological studies of Corfu & Muir (1989a; 1989b). Therefore, a magmatic fluid would be a good candidate for such a "reactive" fluid and would be readily concentrated into the dilatant major structural failures (Cadi Fracture Zone and Hemlo Shear Zone) during the peak thermal metamorphism. The reaction products of the "reactive" fluid and host lithologies would be further metamorphosed while the peak thermal metamorphism prevailed.

The timing of the pervasive, late calc-silicate (epidote-prehnite) alteration is well-defined by textural evidence and geochronological data. In the study area, this type of calc-silicate alteration overprinted all supracrustal rocks, and was particularly pervasive in mafic metavolcanic rocks and along major structural failures, and reached its maximum development with the formation of a REE-enriched skarn

within the Local Shear Zone. It certainly post-dated the regional, peak thermal metamorphism and occurred at about 2632-2645 Ma, based on U-Pb age determinations on monazite and rutile (Corfu & Muir, 1989b), which are stable phases in the REE-enriched skarn of the Local Shear Zone of the study area. In detail, the late calc-silicate alteration was initiated with a pervasive epidote-prehnite alteration and terminated by carbonization, sulfidation and gold mineralization.

7.5 Conditions of Skarn Formation

7.5-1 The Earlier Skarns

As discussed above, the formation of the earlier (Cr- and Fe-rich skarns) began broadly contemporaneously with the peak thermal metamorphism. The Fe-rich skarn occurs within the lithological unit 4 where the regional metamorphism was at middle amphibolite facies, and the Cr-rich skarn occurs in the lithological unit 2 where the metamorphic grade was greenschist-amphibolite transitional facies (Chapter 5). The P and T conditions for the peak regional metamorphism, therefore, could provide valuable information for the formation of the earlier skarns, even though there is a lack of well-studied geothermometers and geobarometers in the calc-silicate assemblages themselves. A temperature of $580 \pm 20^\circ\text{C}$ and a pressure of 4.2 to 4.5 kbar for the middle amphibolite facies, and a temperature of $476\text{-}502^\circ\text{C}$ and a pressure of 3.2 kbar for the greenschist-amphibolite transitional facies have been estimated by using various available geothermometers and geobarometers in metapelites and metabasites (Chapter 5).

7.5-1a Geothermometers and Geobarometers

The association of a high abundance of calcic amphibole (mainly actinolite),

epidote, sodium-rich plagioclase (oligoclase), microcline, and minor calcite in the Cr-rich skarn is similar to that in common metabasites of greenschist facies or lower amphibolite facies metamorphic grade. The presence of oligoclase and microcline in the Cr-rich skarn yields temperatures ranging from 350° to 400°C, using Whitney & Stormer's (1977) two-feldspar geothermometers, which are consistent with greenschist facies, metamorphic conditions. The two-feldspar geothermometer of Whitney & Stormer (1977) has been considered to be less successful for low-temperature assemblages (Nesbitt & Essene, 1982). However, an overall temperature of about $400\pm 50^\circ\text{C}$ is favoured for the formation of the Cr-rich skarns, and is consistent with the formation temperatures on similar calc-silicate mineral assemblages in present active geothermal fields (Bird et al., 1984).

Sphalerite is present in both the Cr-rich skarn of the Cadi Fracture Zone and the Fe-rich skarn of lithological unit 4 and appears to coexist with both pyrrhotite and pyrite. The iron content of sphalerite in assemblages with pyrrhotite and pyrite has long been used as a geobarometer (Scott & Barnes, 1971; Hutchinson & Scott, 1981). The FeS content of the Cadi Fracture Zone sphalerite (10 to 14 mol. %; Appendix II: Table 11) corresponds to a pressure of 5 to 7 kbar, which is considerably higher than pressures estimated from overlying metapelitic rocks. The unit 4 sphalerite with 12 to 15 mol. % FeS corresponds to 5 to 6 kbar, which is in reasonable agreement with pressure estimated from intercalated metapelites.

7.5-1b P-T-X calculations

Temperatures and fluid compositions for the formation of the White River calc-silicate rocks (skarns) may also be calculated in the system of $\text{SiO}_2\text{-Al}_2\text{O}_3\text{-MgO-}$

CaO-CO₂-H₂O using the PTX program of Berman et al. (1986), and assuming ideal mixing of H₂O and CO₂. Activities were calculated from the analytical mineral compositions according to the following schemes (cf. Skippen & Carmichael, 1977):

$$a_{\text{crs}} = (\text{Ca}/2)^2 \cdot [1 - (\text{Fe} + \text{Mn} + \text{Cr})] \cdot (\text{Si}/3)^3$$

$$a_{\text{Ab}} = \gamma \cdot X_{\text{Ab}} \text{ where } \gamma = 1.276 \text{ (Orville, 1972)}$$

$$a_{\text{Di}} = (\text{Ca}) \cdot (\text{Mg}) \cdot (\text{Si}/2)^2$$

$$a_{\text{Gr}} = (\text{Ca}/3)^3 \cdot (\text{Al}/2)^2 \cdot (\text{Si}/3)^3$$

$$a_{\text{Cc}} = (\text{Ca}) = \text{Ca}/(\text{Ca} + \text{Fe} + \text{Mg} + \text{Mn})$$

$$a_{\text{Tr}} = [1 - (\text{Na} + \text{K})] \cdot (\text{Ca}/2)^2 \cdot (\text{Mg}/5)^2 \cdot (\text{Si}/8)^4 \cdot (\text{OH}/2)^2$$

As discussed in previous sections, in the Cr-rich skarn from the Cadi Fracture Zone of the Playter Harbour Group, the crystallization of uvarovite, chromian epidote and chromium-bearing chlorite, pumpellyite and prehnite, albite, and some calcite was later than the formation of the main assemblages. Therefore, the metamorphic conditions were constrained based on the assemblages of clinopyroxene, epidote, garnet, calcic amphibole, chromite, microcline and calcite. Chromite is a characteristic mineral phase and appears to coexist with other major silicate phases. Unfortunately, Cr₂O₃ is not included in Berman et al.'s (1986) system, and chromite is not well studied either in low-temperature metamorphism. As a first approximation, spinel was included in the PTX calculation with activities calculated from the analytical data of chromite following the scheme $a_{\text{sp}} = (\text{Mg}) \cdot (\text{Al}/2)^2$ (cf. Stroh, 1976). The temperature calculated for the assemblage corresponding to the intersection of equilibria (1), (2), (5) and (6) (the invariant point I₁, Fig. 7.4) range from 390 to 440°C, whereas for those assemblages corresponding to the intersection of equilibria (3), (4), (6) and (7) (the invariant

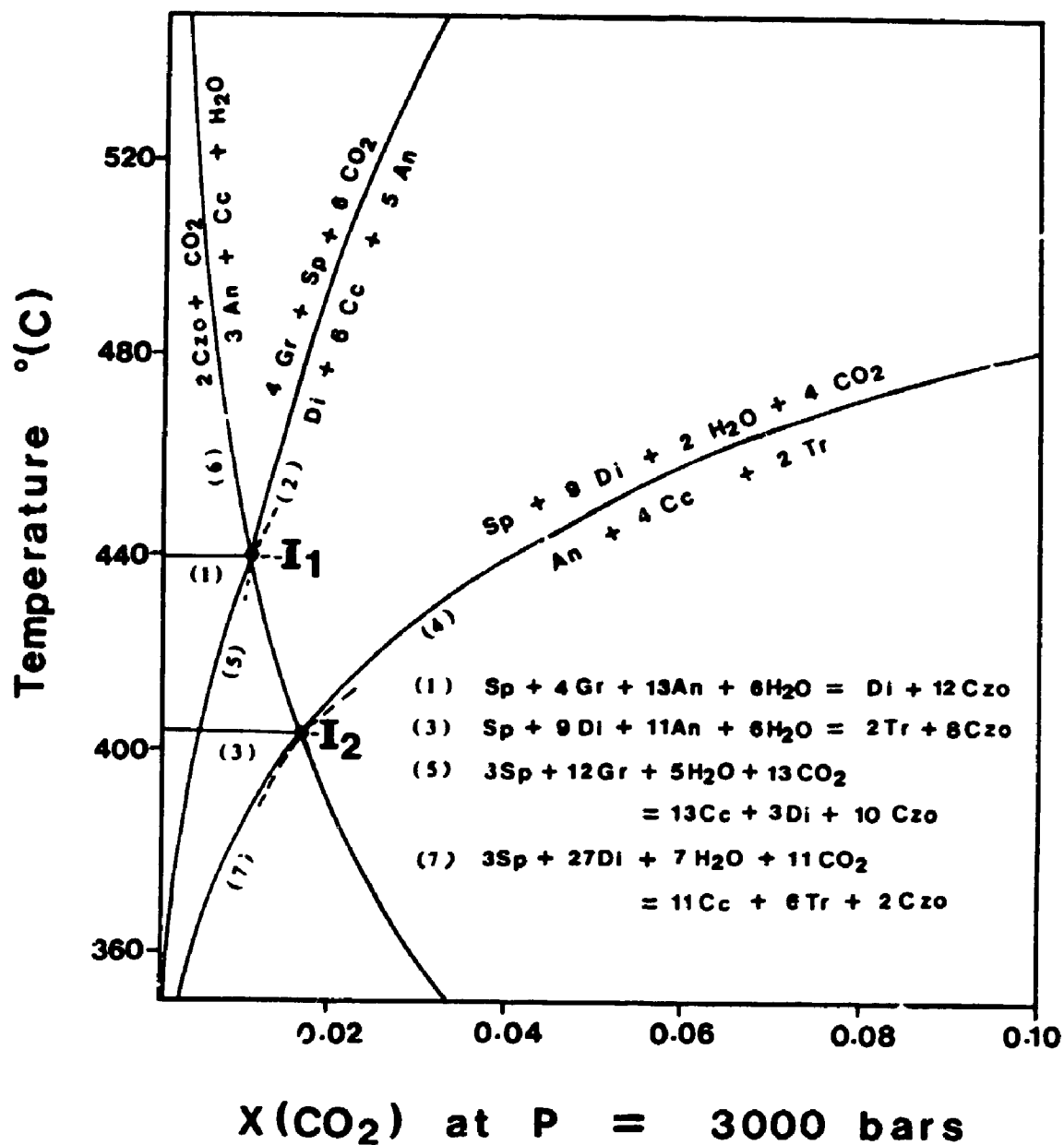


Fig. 7.4. Calculated T-X(CO₂) phase diagram section in the system of SiO₂-Al₂O₃-MgO-CaO-CO₂-H₂O for Cr-rich calc-silicates of the Cadi Fracture Zone at a pressure of 3 kbar; with mineral activities from analytical data (Appendix II). Note that the precise positions of the invariant points I₁ and I₂ vary from sample to sample, but X(CO₂) does not exceed 0.03. Solid lines are stable phase-boundaries; broken lines are metastable extensions.

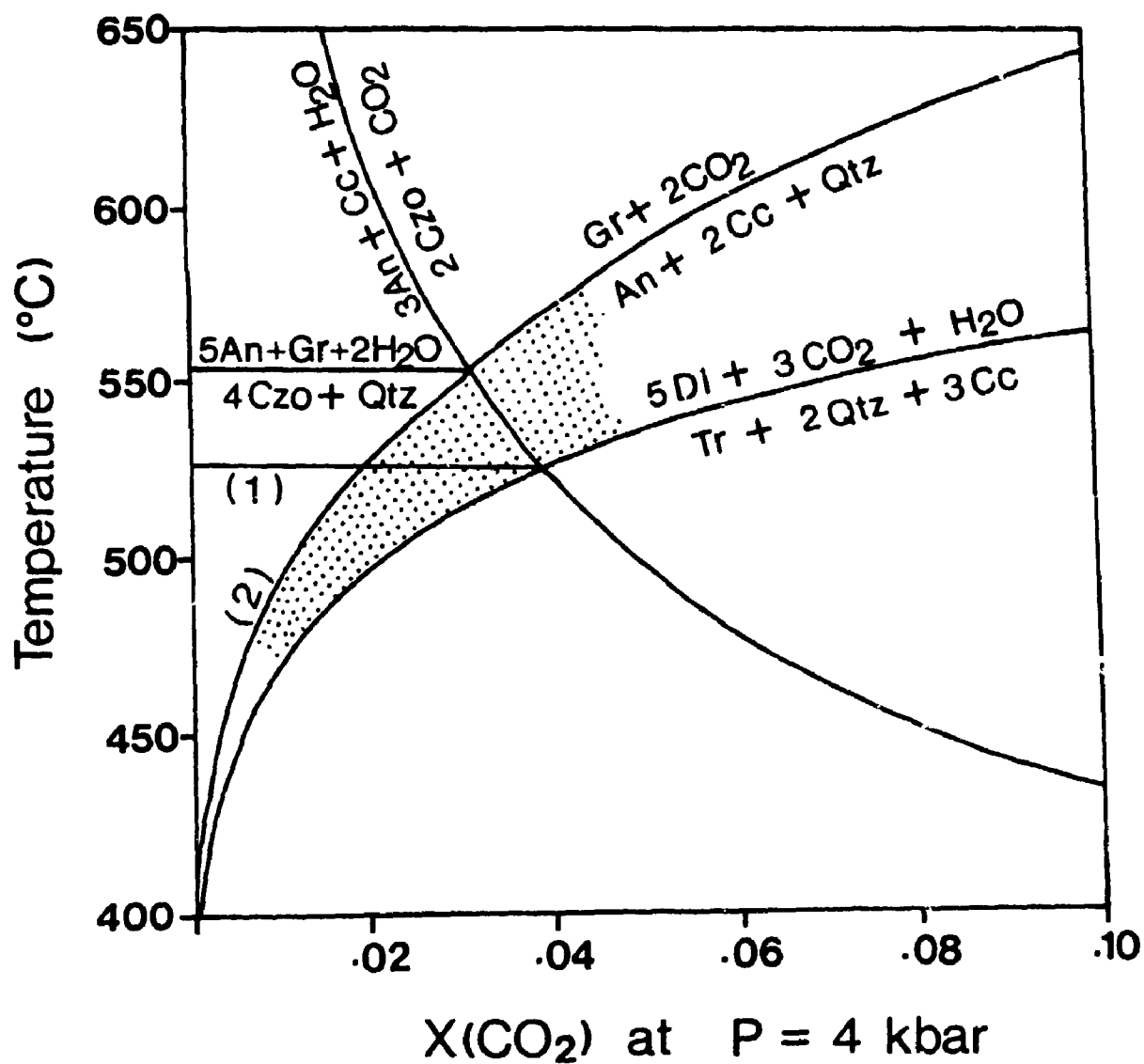


Fig. 7.5. Calculated T-X(CO₂) phase diagram section in the system of SiO₂-Al₂O₃-MgO-CaO-CO₂-H₂O for Fe-rich calc-silicates of unit 4 at a pressure of 4 kbar; with mineral activities from analytical data (Appendix II). The shaded area represents stable conditions for the main assemblages of Fe-rich calc-silicates.

point I_2) range from 360 to 410°C. These values are similar to or slightly higher than the temperatures estimated by using the two-feldspar geothermometer of Whitney & Stormer (1977). However, the analytical data for plagioclase have been used for both sets of calculations. An independent check using the garnet/biotite geothermometer of Ganguly & Saxena (1984; 1987) for the overlying clastic metasediments (Table 5.1) gives temperatures of about 476-502°C and agrees reasonably well with those calculated from the calc-silicate assemblages. The positions of the invariant points I_1 and I_2 do not exceed $X(\text{CO}_2) = 0.03$ (Fig. 7.4), and indicate very low CO_2 fugacities during the formation of the Cr-rich skarn.

In the Fe-rich skarn, hydrous minerals after anhydrous minerals exhibit a "normal" replacement sequence. Therefore, the maximum temperatures for the formation of the Fe-rich skarn can be constrained by the main assemblage of clinopyroxene, garnet, epidote, quartz, plagioclase and calcite. P-T-X calculation for the Fe-rich skarn has also been performed in the system of $\text{SiO}_2\text{-Al}_2\text{O}_3\text{-MgO-CaO-CO}_2\text{-H}_2\text{O}$ at a pressure of 4 kbar (Fig. 7.5). In Figure 7.5, "required" temperatures at a given $X(\text{CO}_2)$ value for the main assemblages of the Fe-rich skarn is apparently higher than that for the Cr-rich skarn (Fig. 7.4), and the temperature of 500-560°C at a $X(\text{CO}_2)$ of 0.01 to 0.03 (values in Cr-rich skarn) appear to be in good agreement with those estimated from host amphibolites by using the garnet/hornblende geothermometer (Graham & Powell, 1984).

7.5-2 Late Calc-silicate Alteration

7.5-2a P-T-X grids

Mineral assemblages of the calc-silicate veins are similar to those in:

metabasites from low to very-low grade (prehnite-pumpellyite facies and prehnite-pumpellyite to greenschist transitional facies) metamorphic terrains. Mineral stability from hydrothermal experimental data for the major phases (Liou, 1971; 1973; Holdaway, 1972; Liou et al., 1983) should be an excellent tool for the reconstruction of the P-T conditions and fluid composition in the late calc-silicate alteration. However, the scale over which equilibrium assemblages were developed during the alteration of metabasites in low to very-low grade metamorphic terrains has been controversial. Many authors (Zen, 1974; Nakajima et al., 1977; Liou et al., 1985; 1988; Cho & Liou, 1987) stress the extremely small scale (single thin section, minerals in direct contact, and in an area of 1 mm² in any thin section) over which equilibrium assemblages were developed. Despite the small size and limited magnitude of most individual calc-silicate veins, their regional distribution and local pervasiveness, and their diversity and correlation of mineralogy with host rock compositions (prehnite with proximity to mafic metavolcanic rocks and pumpellyite to komatiitic basaltic rocks, for example). All suggest that some degree of thermal and chemical equilibrium existed between the host rocks, alteration assemblages and their ambient fluids. Liou et al. (1985) argued that only assemblages of low variance are useful for P-T estimation. However, calc-silicate veins from the study area are generally mono- or bi-mineralic and exhibit zonation in mineral association. In a few cases, a low variance assemblage of epidote + prehnite + actinolite + pumpellyite + chlorite is observed in small veins or vesicles in komatiitic basaltic rocks, with common mutual contacts between minerals and rather consistent chemical compositions of individual minerals. This may indicate an approach towards equilibrium and, therefore, satisfies the conditions for a P-T-X grid of Liou

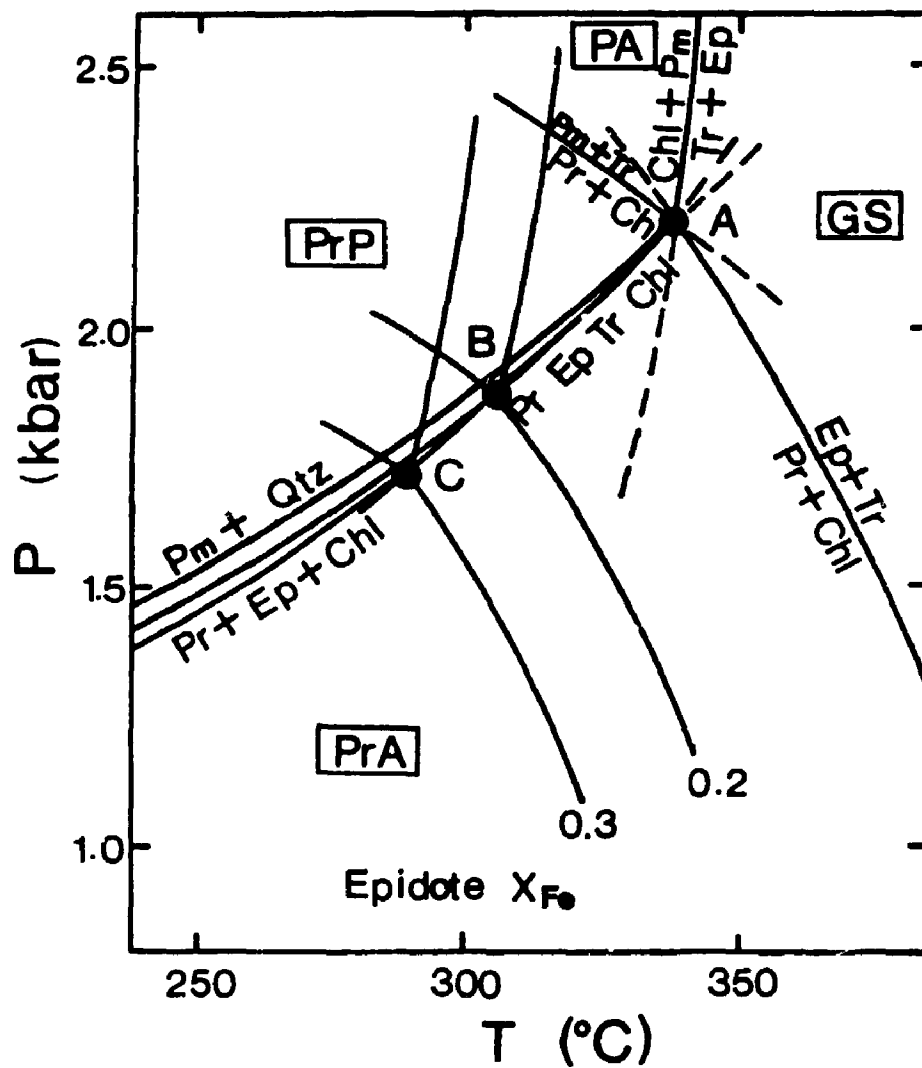


Fig. 7.6. P-T diagram in the model basaltic system at low and very-low grade metamorphism [$X(\text{CO}_2)$ is very low and constant]: GS is greenschist facies; PA is pumpellyite actinolite facies; PrA is prehnite actinolite facies; PrP is prehnite-pumpellyite facies: the migration of the invariant point from A to B, to C occur with increasing Fe^{3+} content in the model system (after Liou et al., 1985).

et al. (1985). On Figure 7.6, ambient metamorphic conditions for the calc-silicate veins, involving a temperature of 320°C and a pressure of 1.7 kbar, have been indicated by a mean epidote composition of Ps_{30} intersecting the univariant curve at point C. This is consistent with the upper pressure limit of 2 kbar defined by the presence of a margarite + quartz assemblage ($T < 500^{\circ}\text{C}$, cf., Chatterjee, 1976).

7.5-2b Fluid inclusion study

Quartz grains from the calc-silicate veins contain two types of fluid inclusions: the majority are irregular shapes and occur in long trails along resealed grain fractures, and contain both liquid and gas phases. These are apparently secondary inclusions. Primary inclusions are typically few in number relative to secondary inclusions, are isolated ellipsoidal in shape, and generally contain a single liquid phase. Occasionally a gas phase and, rarely, a cubic daughter crystal (NaCl ?) are also present in primary inclusions.

Freezing points of 30 primary inclusions range from -2.3 to -3.1°C indicating a dilute- to moderate-salinity with 4.5 wt. % NaCl equivalent (Potter et al., 1978). Homogenization temperatures of 35 primary inclusions range from 340 to 368°C , showing a very small range of variation. This yields a pressure of about 1.2 kbar, according to the calibration of Potter & Brown (1977), which is in reasonable agreement with that estimated from consideration of calc-silicate mineral stabilities.

Homogenization temperatures of 25 secondary inclusions range from 225 to 278°C showing a wide range of variation reflecting their secondary nature. Most importantly, the range of homogenization temperatures is considerably lower than that of primary inclusions. This may indicate that a significant decrease in

temperature occurred when the calc-silicate alteration prevailed, if the secondary inclusions were trapped during the late stages of the protracted calc-silicate alteration.

7.6 A Genetic Model for Gold Mineralization in the Local Shear Zone

7.6-1 An Auriferous Skarn Deposit

A protracted skarn development in this Archean greenstone belt has been outlined in previous sections of this chapter and can be best summarized in terms of the following genetic sequence: skarn development began during the peak thermal metamorphism with the formation of earlier (Cr- and Fe-rich) skarn occurrences in direct association with mafic to ultramafic metavolcanic rocks. This was followed by a discordant, late, regional, low to very-low grade calc-silicate alteration, which was particularly pervasive within the LSZ and resulted in the formation of a REE-rich skarn. Within the Local Shear Zone, the late, regional calc-silicate alteration began with the crystallization of calc-silicate minerals at high temperatures and terminated with sulfidation and carbonization at lower temperatures.

In Chapter 6, a good correlation between the late calc-silicate alteration and gold mineralization in the Local Shear Zone of the White River property has also been established. Therefore, the gold mineralization in the Local Shear Zone of the White River property is skarn-type. Greenstone-hosted "Au-Ag" skarn deposits in an Archean terrain have been described recently in the Southern Cross greenstone belt, Yilgarn block, Western Australia (Mueller, 1988).

Gold mineralization in the Anomalous Zone of the White River property is associated with REE-enriched skarn and is situated in a brittle-ductile Local Shear

Zone. As discussed above, the REE-enriched skarn resulted from an exceptionally pervasive late calc-silicate alteration in the Local Shear Zone (a major structural failure of the study area). Therefore, the dilatant Local Shear Zone probably acted as a fluid conduit during the formation of this auriferous REE-enriched skarn.

Structural data and petrographic observation indicate that the formation of REE-enriched skarn certainly post-dated the major shear deformation and the peak thermal metamorphism. This is supported by the geochronologic data of Corfu and Muir (1989b), who obtained an age of 2632-45 Ma from U-Pb dating on rutile and monazite at the Hemlo gold deposit area (which are typical mineral phases of the REE-enriched skarn of the study area). Although all major magmatic phases in the Hemlo area are older than this late calc-silicate alteration (Corfu & Muir, 1989a), late magmatism is not uncommon and is indicated by quartz-feldspar porphyritic dikes and quartz-microcline pegmatitic veins within supracrustal rocks of the Hemlo-Heron Bay greenstone belt. The quartz-microcline pegmatitic veins are particularly interesting, because they commonly contain various amounts of molybdenite, which is characteristically present in late albite veins (product of the late calc-silicate alteration) in the Cr-rich skarn of the Cadi Fracture Zone. The presence of these quartz-microcline pegmatitic veins and quartz-feldspar porphyritic veins probably reflects magmatism in the lower crust, and the genetic link between calc-silicate alteration and quartz-microcline pegmatitic veins is probably an indication that the late calc-silicate alteration resulted from late magmatism in the lower crust.

7.6-2 Sources, Transportation and Deposition of Gold

For most hydrothermal gold deposits, there is no single favourable rock type

for the source of the gold, and gold generally occurs in a readily mobilized state (cf. Romberger, 1986). Therefore, the nature and physicochemical conditions of the fluid solutions involved are more important for the extraction, transportation and deposition of this metal in hydrothermal systems. In the White River property, the petrographic and mineral-chemical data and thermodynamic calculations on the observed mineral assemblages discussed in previous sections and chapters may be used here to place limits on the physicochemical conditions of the fluids that controlled the transport and deposition of gold in the Local Shear Zone.

A large amount of geochemical evidence, particularly in the form of oxygen and hydrogen isotope data, suggest that hydrothermal gold deposits were formed mainly from solutions dominated by meteoric or metamorphically-derived water (Taylor, 1979; Radtke et al., 1980; Fyfe & Kerrich, 1984; Groves et al., 1984). In the White River property, there is little doubt that dehydration and decarbonation reactions can release H₂O and CO₂ since the peak thermal metamorphism climaxed at middle amphibolites facies. It is commonly argued that the metamorphically-derived fluids would be concentrated into arborescent channels rather than distributed uniformly through the overlying rock column (Fyfe et al., 1978). However, the geochronologic study by Corfu & Muir (1989b) has demonstrated that the peak thermal metamorphism of the Hemlo-Heron Bay greenstone belt was at least 30 Ma before the late calc-silicate alteration, and the present petrographic observations have excluded the existence of a prominent retrogression after the peak thermal metamorphism. Therefore, a metamorphically-derived fluid was not likely the dominant source for the calc-silicate alteration at the study area. Moreover, a fluid generated by prograde metamorphism should not be enriched in calcium as

calcium-bearing minerals are progressively stable with increasing metamorphic temperature (Mueller, 1988). As noted above, magmatic activity after the peak thermal metamorphism was not uncommon in the greenstone belt, as indicated by the presence of abundant quartz-feldspar porphyritic dykes and quartz-microcline pegmatitic veins. Magmatic activity could provide both the heat and fluid for the metasomatic alteration. The presence of halogen-bearing (F, Cl) minerals, such as allanite, apatite, phlogopite and sericite also favours a magmatic source for at least part of the fluid.

The mechanism of gold transport and deposition in hydrothermal systems have been the subject of many studies (Romberger, 1986 and references herein). Although many aqueous gold complexes are known, under the physicochemical conditions appropriate for the formation of epithermal deposits sufficient data exist only for aurous chloride and sulfide complexes. Henley (1973) suggested that gold was transported as an uncharged gold chloride complex at high temperatures and ionic or sulfide complexes may be dominant at lower temperatures. In contrast, the transport of gold as various aqueous sulfide complexes has been supported by Seward (1973; 1984; 1988) and Grigoryeva & Sukneva (1981). As discussed above, elevated Cl must have been present in the fluid during the earlier stage of the late calc-silicate alteration in the Local Shear Zone. Fluid inclusion data also indicate that the hydrothermal fluid responsible for the calc-silicate alteration was elevated in temperature ($360 \pm 20^\circ\text{C}$) with a moderate salinity (4.5 wt. % NaCl equivalent), in the AuCl_2^- dominant field (Fig. 7.7; cf, Large et al., 1988). However, native gold generally occurs in direct association with pyrite in the Anomalous Zone, and the maximum values of gold occur where the Anomalous Zone, the footwall pyritic

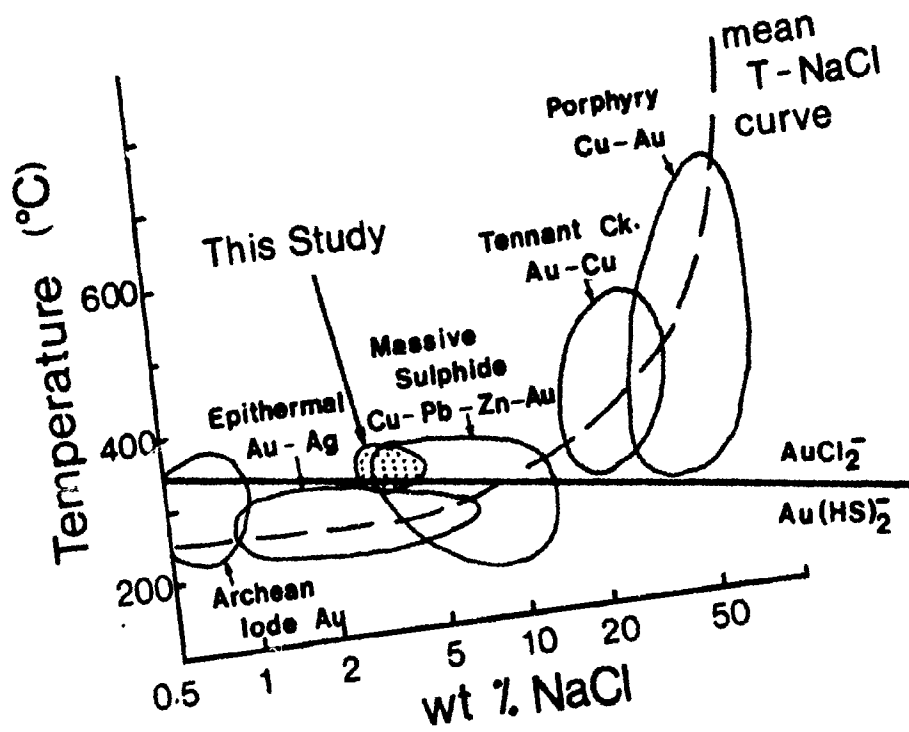


Fig. 7.7. Fields of temperature-salinity for a range of common gold-bearing ores showing the split into AuCl_2^- -transport and $\text{Au}(\text{HS})_2^-$ -transport fields (after Large et al., 1988).

zone and the hanging-wall sericitic zone coalesce. Therefore, bisulfide complexes may have been important also for the transportation of gold in the White River property.

Cooling (decrease in temperature) seems the most obvious mechanism for the deposition of gold since the solubilities of most minerals, including ore minerals, decrease at lower temperatures (Fournier, 1985). A decrease in temperature with progression of the alteration is obvious and is supported by temperatures from fluid inclusions in the Local Shear Zone and by the deposition of both sulfide and gold during the final stage of metasomatic/hydrothermal alteration. However, temperature also affects other parameters, such as oxygen and sulfur fugacities, which may have had great influence on the solubility of gold, so that the effects of a single parameter in a complex natural system are difficult to evaluate (Romberger, 1986).

The experimental study of Grigoryeva & Sukneva (1981) suggested that gold may be transported as a thioarsenide complex, based on solubility measurements for this metal in arsenic-containing solutions. Also, Seward (1988) suggested that gold could be scavenged from the hydrothermal fluid by arsenides and thioarsenides. Romberger (1986) discussed the important variables involved in the transport and deposition of gold as a thioarsenide species. However, insufficient data exist to calculate quantitatively the solubility of gold-arsenic complexes in hydrothermal systems. The transport of gold as a thioarsenide complex is certainly consistent with the common association of gold and arsenic in many different types of hydrothermal systems from epithermal to metamorphogenic deposits hosted by greenstone belts. Therefore, the possibility of the transport and deposition of gold as a thioarsenide complex can not be excluded here as As is elevated in abundance in the Local

Shear Zone.

The gold anomalous zone, in the Local Shear Zone of the White River property, is marked by a footwall pyritic zone, which appears on textural evidence to have recrystallized prior to the formation of the REE-enriched skarn. Although the pyritic zone is generally a few meters below the gold anomalous zone, maximum gold values were obtained where the anomalous zone coalesces with its footwall pyritic zone and hanging-wall sericitic zone.

The skarns of the White River property exhibit a local decrease in the iron content of calc-silicates where abundant sulfide minerals occur. In particular, for calc-silicates associated with the gold mineralization in the Local Shear Zone, the composition of epidote decreases to a pistacite content (Ps) of 12-15 mol. % in the pyritic footwall zone, from Ps28-34 elsewhere in the greenstone belt. In addition, the halogen-bearing (F, Cl) allanite is extremely low in ferric iron content showing a complete solid-solution to clinozoisite rather than epidote. This appears to indicate that pre-existing pyrite controlled the composition of coexisting calc-silicates according to sulfur-buffer reactions of the type: $\text{Fe}^{3+}\text{-silicate} + \frac{1}{2}\text{S}_2 + \text{Al}^{3+} + \frac{3}{2}\text{H}_2\text{O} = \text{Al}^{3+}\text{-silicate} + \text{FeS} + 3\text{H}^+ + \frac{3}{4}\text{O}_2$. This type of sulfur-buffer reaction is also supported by the fact that pyrrhotite is the dominant sulfide mineral during the late calc-silicate alteration within the Local Shear Zone. Most importantly, the crystallization of pyrrhotite (via this type of sulfur-buffer reactions) would also reduce the sulfur fugacity of the hydrothermal fluid, which, in turn, is one of the leading factors controlling the gold deposition. Therefore, the dilatant Local Shear Zone probably acted as a fluid conduit during the REE-enriched skarn formation, but the precise localization of gold deposition was controlled by the pre-existing

pyritic zone.

7.6-3 Comparison with Other Auriferous Skarns.

Auriferous skarn deposits have been recorded on a world-wide basis, including British Columbia (Boyle, 1979; Meinert, 1984; Ettliger & Ray, 1989), Yukon, Canada (Bostock, 1952; Brown & Nesbitt, 1987), Australia (Ewers & Sun, 1989); Japan (Kitamura, 1975; Shimazaki, 1980), Mexico (Buseck, 1966), Nicaragua (Bevan, 1973), Thailand (Sitthithaworn, 1989), U.S.A. (Theodore & Blake, 1978; Meinert, 1989), U.S.S.R. (Ettliger & Meinert, 1990). The most important features of many of these auriferous skarn deposits are their concentration in much younger (Phanerozoic) terrains and their common association with carbonate strata and granitic-granodioritic intrusive bodies. In many of these Phanerozoic skarn deposits, the common association with cogenetic albitization and potassium-silicate alteration in the adjacent plutons also indicates a magmatic fluid component, and gold (or other metallic) mineralization is generally associated with late alteration rather than the earlier contact (thermal) metamorphism/metasomatism (Einuadi et al., 1981; Meinert, 1989). In this latter respect, the Archean auriferous skarn deposit from the study area is similar to Phanerozoic skarn deposits; but its structural setting in a (brittle-) ductile shear zone and its carbonate-free host rocks distinguish it from its younger counterparts (Mueller, 1988).

The hydrothermal fluid responsible for the formation of the auriferous REE-enriched skarn of the White River property was largely aqueous (with very low X_{CO_2}) based on thermodynamic calculations on the calc-silicate mineral assemblages. However, concentrations of other anions, such as F, Cl and HS⁻, must

have been elevated as well, as indicated by the crystallization of F-,Cl-bearing calc-silicate minerals (allanite for example) and sulfide minerals. This is also supported by fluid inclusions of a moderate salinity (about 4.5 wt. % NaCl equivalent). In this respect, the auriferous skarn of the White River property is similar to some of its Phanerozoic counterparts (Meinert, 1984), but is clearly differentiated from typical Archean lode gold deposits, which generally involve H₂O-CO₂ predominant fluids with very low salinities (Fig. 7.7).

7.7 Genetic Significance to the Hemlo Gold Deposit and Metallogensis in the Hemlo-Heron Bay Greenstone Belt

The various genetic models proposed for the gold mineralization in the Hemlo gold deposit have been summarized in Chapter 1. The controversial nature of the ore genesis resulted mainly from its geological setting within a regional structure (the Hemlo Shear Zone, Hugon, 1984; 1986) in a medium grade metamorphosed terrain, the association with anomalies of incompatible elements (As-Hg-Mo) and, particularly, uncertainty among investigators regarding the relative timing of the gold emplacement related to deformation, metamorphism and hydrothermal alteration.

The White River property is located 5 km eastward along strike from the Hemlo gold deposit. The overall stratigraphy, representation of characteristic rock units, and nature and complexity of deformation and metamorphism are very similar to those at the Hemlo area. The gold mineralization in the Anomalous Zone of the White River property, however, is situated in a Local Shear Zone within a metamorphic zone of low grade (greenschist-amphibolite transitional facies), and is

stratigraphically above the Hemlo Shear Zone and the metamorphic zone of medium grade (middle amphibolite facies). Above all, gold mineralization of the anomalous zone in the Local Shear Zone is associated with a late calc-silicate (skarn) alteration, which certainly post-dated the peak regional metamorphism. The occurrence of gold mineralization in the Local Shear Zone is probably due to the concentration of hydrothermal fluid in the shear zone during a phase of dilatation.

The prominent As-Ag-Sb-V-Ba-W-Mo anomalies spatially associated with the ore zones of the Hemlo gold deposit have been emphasized by many investigators (Harris, 1986; Kuhns, 1986 and others), particularly the troublesome incompatibility of As-Sb-Hg mineralization (Harris, 1986) with amphibolite facies metamorphic conditions. At the gold anomalous zone of the White River property, V and Mo anomalies are typically absent corresponding to the lack of vanadian muscovite and molybdenite in the Local Shear Zone, but the As-Ag-Ba-Hg-Sb-W anomalies (all in smaller magnitude compared to their counterparts in the Hemlo gold deposit) are present in spatial association with high gold concentrations. As discussed earlier in Chapter 6, however, the As-Ag-Hg-Sb-W anomalies are directly associated with the footwall pyritic zone, and there is no direct correlation between high gold concentration and these types of geochemical anomaly in the study area. It is possible that the formation of the prominent geochemical anomalies and gold mineralization were associated with separate events.

Although U-Pb radiometric age determination on rutile and monazite from the Hemlo gold deposit yielded an extensive alteration event of much younger age (2632-2645 Ma), which was interpreted to reflect low-grade hydrothermal activity probably accompanied by episodic deformation and dynamic recrystallization, Corfu

& Muir (1989b) suggested that gold mineralization in the Hemlo gold deposit was contemporaneous with the peak metamorphism of the region. Rutile and monazite commonly occur together in the halogen-bearing allanite aggregates and have been interpreted to be part of the late calc-silicate (skarn) alteration in the Local Shear Zone of the White River property. Unpublished electron microprobe analyses (of the author) have revealed that monazite in microcline-rich rocks (ores) from the Hemlo gold deposit is similar in REE composition (both total REE abundance and chondrite-normalized REE pattern) to its counterpart in the LSZ of the study area. Moreover, epidote and clinozoisite are not uncommon in the Hemlo gold deposit and occur mainly in cross-cutting veins (although prehnite and pumpellyite have not been reported, probably due to paucity of mafic to ultramafic volcanic rocks in the Hemlo deposit area). Calc-silicate alteration (as indicated by Mn-rich garnet, tremolite, microcline, titanite and scapolite) has also been documented within the Hemlo deposit and its country rocks by Walford et al. (1986), particularly in the hanging-wall. Therefore, the Hemlo gold deposit must have undergone a late low- to very-low-grade calc-silicate alteration, similar to that of the White River property. The reported irregularity and strain-free nature of native gold grains (the main gold-bearing phase) in the Hemlo gold deposit may also support the association of gold mineralization with the late calc-silicate (skarn) alteration.

The present study suggests that the gold mineralization in the Local Shear Zone of the White River property is skarn-type. As discussed above, the late calc-silicate alteration also occurred at the Hemlo area, where it was probably more extensively developed (Walford et al., 1986). The present study also emphasizes that the precise localization of gold deposition was controlled by the pre-existing pyrite,

although the major structural failure (i.e. LSZ at the White River property) probably provided an excellent fluid conduit during a phase of dilatation. According to Hugon (1984; 1986), the Hemlo gold deposit is situated within the Hemlo Shear Zone. High abundance of sulfide minerals is also one of the many features of the Hemlo gold deposit (Harris, 1986). Petrographic observations in the present study have revealed that some pyrite prisms in the ore zones of the Hemlo gold deposit show a good alignment parallel to the main foliation and, locally, contain shearing strain on crystal surfaces. This may suggest that pre-existing pyrite also occurred in the Hemlo gold deposit. If this is the case, the gold mineralization in the Hemlo gold deposit may be similar to that in the Local Shear Zone of the White River property; resulting from the late calc-silicate alteration and being localized by pre-existing pyrite. However, it is necessary to point out that, at the Hemlo area, the most spectacular calc-silicate occurrences are generally present in the hanging-wall metasedimentary rocks, and are less important within the ore zones (which are characterized mainly by potassium alteration; cf., Walford et al., 1986). It has been demonstrated that the late calc-silicate alteration (and the entire protracted skarn development as well) at the White River property varies significantly in mineralogical, geochemical and metallogenic characteristics with host lithologies. It is possible that the calc-silicate assemblages did not develop extensively within the ore zones of the Hemlo gold deposit because its country rocks are mainly felsic metavolcanic rocks and metasedimentary rocks.

CHAPTER 8 CONCLUSIONS

The White River exploration property of LAC Minerals Ltd. is situated in the Hemlo-Heron Bay greenstone belt of the Superior Province of the Canadian Shield, and is about 5 km east along strike from the Hemlo gold deposit. The supracrustal rocks, which are bounded by a earlier crystalline basement (Pukaskwa Gneissic Complex) to the south and a late granodioritic intrusion (Cedar Lake Pluton) to the north, are divided into two sequences: (1) the Playter Harbour Group (consisting mainly of metamorphosed high-iron tholeiitic basalt flows and intercalated clastic sedimentary rocks) to the south, and (2) the Heron Bay Group (consisting mainly of metamorphosed sedimentary rocks, intermediate to felsic calc-alkalic pyroclastic rocks, and high-iron tholeiitic basalt flows) to the north.

The clastic metasedimentary rocks are characteristically low in indices of chemical maturity (CIA and Al_2O_3/Na_2O values) and have high concentrations of ferromagnesian minor and trace elements (up to 770 and 500 ppm Cr and Ni, respectively). The Ni-MgO distribution coefficient of the metasedimentary rocks, however, clearly distinguishes them from the metavolcanic rocks (i.e. the former showing a more rapid increase in Ni with increase in MgO). The clastic metasedimentary rocks were mainly derived from intermediate volcanic sources, admixed with minor mafic or ultramafic volcanic materials and continental weathering products, and deposited as turbidites in a large volcanoclastic-sedimentary basin.

All supracrustal rocks of the study area have been subjected to multi-phase deformation and metamorphism. The major brittle-ductile shear deformation resulted

in a number of profound structural failures at or near lithologic boundaries in the study area: (1) a marginal mylonitic zone of the Pukaskwa Gneissic Complex underlying the lower metamorphic zone of medium grade; (2) the Cadi Fracture Zone between mafic metavolcanic rocks and clastic metasedimentary rocks of the Playter Harbour Group; (3) the Hemlo Shear Zone between mafic metavolcanic rocks and metasedimentary rocks enclosed by the upper medium grade metamorphic zone, which is bounded by (4) the Hemlo Fault Zone to the south; and (5) the Local Shear Zone, proximal to the Cedar Lake Pluton, between intermediate to felsic metavolcanic rocks and metapelites of the Heron Bay Group.

The earlier Barrovian-type metamorphism (6.0-6.5 kbar and 455-520°C) occurred probably in response to tectonically-induced crustal thickening. The present geometry of this Archean terrain, however, largely resulted from a progressive dextral shear deformation broadly contemporaneous with the peak metamorphism. The peak andalusite-sillimanite facies series metamorphism is generally low in grade at greenschist-amphibolite transitional facies (3.2 kbar and 475-500°C) and climaxed at middle amphibolite facies (4.2-4.5 kbar and 580±20°C) in two narrow zones associated with the maximum intensity of shear deformation. The peak metamorphism was probably associated with heat from magmatism in the lower crust, and the zones of medium metamorphic grade and maximum intensity of shear deformation were related to "thermal domains". The supracrustal rocks have been affected also by a pervasive low- to very-low-grade (1.2-1.7 kbar and 360±20°C) calc-silicate alteration at about 2632-2645 Ma.

The occurrences and chemical compositions of major rock-forming minerals strongly correlate with their host lithologies and metamorphic grades. Plagioclase is

andesine in zones of medium metamorphic grade and oligoclase in zones of low metamorphic grade. Al_2SiO_5 -minerals are restricted to aluminous schists: kyanite represents the earlier Barrovian-type metamorphism, whereas andalusite and sillimanite represent the peak thermal regional metamorphism, and occur in metamorphic zones of low grade and medium grade, respectively. Calcic-amphiboles show consistent partitioning between $(\text{Fe}^{2+} + \text{Fe}^{3+})$ and $^{\text{IV}}\text{Al}$ from greenschist-amphibolite transitional facies to middle amphibolite facies in komatiites, komatiitic basalts and tholeiitic basalts, considered separately.

Three distinct ore mineral-calc-silicate occurrences (Cr-rich, Fe-rich and REE-enriched) are located within major structural failures and their salient mineralogical and geochemical characteristics and metallogenic associations strongly correlate with host lithologies. All three calc-silicate occurrences belong to a protracted phase of skarn development, which commenced during the peak metamorphism, continued with a pervasive epidote-prehnite alteration, and concluded with sulfidation, carbonization and gold mineralization.

A Cr-rich skarn occurs in the Cadi Fracture Zone of the Playter Harbour Group and appears to have developed by metasomatic processes from pre-existing komatiitic basalt or komatiite. Cr-rich epidote with up to 11.77 wt. % Cr_2O_3 and approaching end-member $\text{Ca}_2\text{CrAl}_2\text{Si}_3\text{O}_{12}(\text{OH})$ is associated with zincian chromite (up to 6.59 wt. % ZnO). Other chromium-rich minerals include uvarovite, Cr-bearing grandite and Cr-bearing prehnite, pumpellyite and chlorite. The association of zincian chromite, Cr-rich silicates and Fe-Ni-Co-Zn-Cu(-Mo) sulfides in the Cr-rich skarn is a typical assemblage of Outokumpu-type skarn deposits.

An Fe-rich skarn occurs at or near the Hemlo Shear Zone of the Heron Bay Group and appears to have developed by metasomatic processes from high-iron tholeiitic basalt. The association of Fe-rich calc-silicates and Fe-Cu-Zn-Ni-Co sulfides is a common assemblage of calcic iron skarn deposits.

The REE-enriched skarn occurs within the Local Shear Zone of the Heron Bay Group. Local remobilization of REE, particularly light REE, occurred during the calc-silicate alteration within the Local Shear Zone, and the REE-mineral stability appears to have greatly influenced the behaviour of REE.

Halogen-bearing allanite from the REE-enriched skarn is characterized by high contents of both F and Cl (up to 0.76 wt. % and 0.95 wt. %, respectively) and exhibits a complete solid solution towards clinozoisite rather than epidote, through a coupled substitution: $Ca_{A2} + Al_{M3} = \underline{REE}_{A2} + Fe^{2+}_{M3}$.

The laterally extensive horizon of anomalous gold values in the Local Shear Zone of the Heron Bay Group is associated with REE-enriched skarn, and is marked by a footwall pyritic zone and a hanging-wall sericitic zone. Although the dilatant Local Shear Zone acted as a fluid conduit during the calc-silicate alteration, the precise localization of gold deposition was controlled by a pre-existing pyritic zone. This auriferous skarn is similar to Archean greenstone-hosted "Au-Ag" skarn deposits. It is clearly differentiated from typical Archean lode gold deposits by fluid inclusions of moderate salinity (about 4.5 wt. % NaCl equivalent), and from Phanerozoic counterparts by its structural setting in a brittle-ductile shear zone and carbonate-free host rocks.

Although there are some discrepancies, the auriferous skarn of the study area and the Hemlo gold deposit in the Hemlo-Heron Bay greenstone belt share many

remarkable similarities. It is possible that gold mineralization of the Hemio gold deposit is similar to that of the auriferous skarn from the study area and was related to the calc-silicate alteration after the peak metamorphism.

APPENDIX I
WHOLE-ROCK COMPOSITIONS

Table 1. Analytical results for metasedimentary rocks from the White River property.

Unit	Unit 2						1		Unit 3		
Sample	K72/ 109	K72/ 142	L81/ 16	L81/ 54	L81/ 68	L81/ 72	L81/ 105	I72/ 268	J85/ 31	J85/ 152	J91/ 21
SiO ₂	61.20	61.90	66.20	61.80	60.10	59.40	63.30	62.00	62.30	61.50	62.50
TiO ₂	0.59	0.49	0.48	0.46	0.56	0.55	0.47	0.65	0.49	0.56	0.72
Al ₂ O ₃	15.80	15.70	15.30	15.40	15.30	15.00	15.70	16.40	15.70	15.60	17.30
Fe ₂ O ₃ ^a	5.38	5.39	3.42	6.42	6.00	6.62	4.79	6.17	5.39	7.08	6.92
MgO	3.41	3.40	2.10	2.65	3.49	3.65	2.64	3.22	3.40	3.06	3.13
MnO	0.08	0.08	0.06	0.08	0.10	0.11	0.08	0.08	0.08	0.10	0.08
CaO	4.40	5.30	4.00	5.25	5.53	5.32	4.93	2.73	5.30	3.83	2.14
Na ₂ O	5.59	4.63	3.81	4.24	4.44	4.45	4.62	4.23	3.83	3.72	3.49
K ₂ O	1.60	1.51	3.09	2.21	1.65	2.19	1.58	2.50	2.58	2.27	2.70
P ₂ O ₅	0.23	0.16	0.28	0.16	0.18	0.18	0.14	0.18	0.17	0.24	0.20
LOI	0.50	0.50	1.40	1.30	0.80	1.50	0.70	1.10	1.00	1.30	1.20
Total	98.80	99.00	100.1	100.0	98.30	99.0	98.90	99.50	99.20	99.20	100.6
B	20	30	50	30	20	30	40	60	40	40	70
Ba	630	650	990	980	680	740	580	800	590	810	850
Co	19	20	14	17	21	21	18	30	25	28	26
Cr	130	130	130	270	190	130	130	360	410	130	350
Cu	27	30	59	37	44	29	29	47	67	33	50
Ni	51	63	33	71	50	64	55	110	110	61	120
Pb	6	10	12	12	8	6	8	12	10	4	12
Rb	30	40	110	80	40	90	60	70	90	80	110
Sc	11.5	12.9	8.8	10.0	16.1	14.3	10.5	20.9	14.4	14.9	19.1
Sr	1100	830	1000	890	900	920	1000	760	690	950	480
Ta	4	<3	<3	<2	<1	<3	<3	7	<3	<3	<1
Th	3.2	3.7	7.9	2.9	4.6	4.3	3.0	5.6	4.5	6.4	6.2
U	1.0	<1.1	2.5	1.0	1.4	1.2	1.0	2.3	1.4	2.1	1.8
V	120	120	86	98	130	140	94	130	140	110	130
Y	10	10	<10	20	<10	20	<10	20	10	20	10
Zn	120	95	79	87	97	110	98	110	140	100	100
Zr	120	70	130	90	90	80	60	110	100	120	110
La	36.9	33.8	50.3	27.7	32.3	33.7	29.7	37.5	31.4	53.9	35.0
Ce	62	57	82	48	70	53	57	43	53	92	68
Nd	30	27	38	14	37	32	40	<5	31	57	32
Sm	5.4	4.2	5.7	4.4	5.2	4.4	3.9	2.0	4.3	6.3	5.4
Eu	2.5	1.5	2.5	2.4	1.5	2.4	1.3	<0.4	1.8	2.0	1.5
Tb	<0.6	<0.6	<0.5	<0.7	<0.5	<0.7	1.1	<0.5	<0.8	0.7	<0.5
Yb	0.6	1.0	0.8	1.0	1.0	1.0	0.7	0.4	1.1	1.4	1.3
Lu	0.08	0.16	0.13	0.19	0.19	0.19	0.13	0.08	0.20	0.29	0.21
A/N	2.83	3.39	4.02	3.63	3.45	3.37	3.40	3.88	4.10	4.19	4.96
A/T	26.8	32.4	31.9	33.5	27.3	27.3	33.4	25.2	32.0	27.9	24.0
CIA	51.4	52.7	53.6	52.1	50.9	50.8	53.2	57.5	56.9	56.4	62.0
K/N	0.29	0.33	0.81	0.52	0.37	0.49	0.34	0.59	0.67	0.61	0.77
L/Y	41.5	22.8	42.5	10.6	21.8	22.8	28.7	19.5	19.3	26.0	18.2

Notes: Fe₂O₃^a is total iron content; LOI is "loss on ignition"; A/N is the Al₂O₃/Na₂O weight ratio; A/T is the Al₂O₃/TiO₂ weight ratio; CIA is the chemical index of alteration; and K/N is the K₂O/Na₂O weight ratio; L/Y is the REE fractionation index (La_n/Yb_n).

APPENDIX I (cont.)

WHOLE-ROCK COMPOSITIONS

Table 5. Analytical results for (meta-)volcanic rocks from the White River property.

Unit	Unit 1			Unit 2					Unit 4			
	U1-1	U1-2	U1-3	X72/ 78	L81/ 81	TSL	L93/ 55	I72/ 382	I72/ 367	J71/ 52	J87/ 160	J87/ 162
SiO ₂	50.10	48.30	48.60	47.30	47.90	42.70	50.00	48.00	47.60	43.40	46.30	49.70
TiO ₂	0.63	0.73	0.87	0.89	0.19	0.41	0.87	0.31	0.35	0.39	0.65	0.27
Al ₂ O ₃	16.90	15.00	20.40	14.90	3.92	8.71	14.60	7.17	7.42	7.79	9.82	5.30
Fe ₂ O ₃ *	9.26	12.90	10.00	12.80	9.13	11.30	12.80	9.48	9.00	11.00	13.40	9.59
MgO	6.84	7.71	2.81	7.28	17.50	22.50	6.20	19.40	19.00	22.40	16.50	22.40
MnO	0.18	0.20	0.17	0.25	0.21	0.17	0.24	0.19	0.19	0.19	0.22	0.16
CaO	10.40	10.90	12.50	11.00	14.30	5.42	10.60	8.41	9.20	7.23	8.36	7.42
Na ₂ O	3.51	2.82	3.19	2.17	1.05	0.50	3.14	0.55	0.68	0.44	0.63	0.14
K ₂ O	0.68	0.67	0.57	0.81	0.14	0.03	0.54	2.16	0.34	0.05	0.16	0.02
P ₂ O ₅	0.24	0.07	0.08	0.06	0.03	0.03	0.07	0.01	0.03	0.04	0.05	0.04
LOI	0.90	0.50	0.90	0.70	3.60	6.30	0.50	2.70	4.10	5.30	3.70	4.90
Total	99.60	100.0	99.60	98.20	98.00	98.10	99.60	98.70	97.90	98.20	100.1	100.2
B	40	30	20	<10	20	10	<10	10	40	30	<10	<10
Ba	130	90	100	60	<10	80	240	200	70	60	70	10
Co	38	45	35	62	110	63	53	75	81	98	71	68
Cr	200	410	270	460	2000	2900	350	2200	1600	2300	2000	1800
Cu	4.5	43	74	64	26	19	86	<0.5	4.0	44	<0.5	61
Ni	98	120	82	250	2100	680	140	890	860	1000	560	960
Rb	20	20	<10	20	10	10	20	390	30	10	<10	20
Sr	35.4	42.3	35.8	48.9	19.5	24.1	45.9	26.2	28.1	30.7	41.1	20.2
Sc	420	210	220	90	10	20	130	120	50	40	<10	<10
V	180	250	240	260	96	180	220	150	190	160	230	100
Y	20	<10	10	<10	<10	<10	10	<10	10	10	20	20
Zn	120	110	170	130	66	70	100	93	130	64	98	59
Zr	<10	10	40	20	<10	20	30	<10	<10	<10	20	<10
La	10.5	2.1	3.8	3.0	0.5	4.3	3.2	2.0	5.7	1.6	1.9	1.0
Ce	32	5	12	10	<3	12	13	12	14	6	4	4
Nd	18	10	<5	5	<5	<5	6	<5	6	<5	<5	<5
Sm	3.8	1.4	2.1	1.9	0.4	1.3	1.9	1.0	1.4	0.8	1.4	0.6
Eu	<1.1	<1.0	0.8	0.6	<0.3	0.3	0.5	0.7	0.6	0.6	0.6	<0.2
Tb	0.9	<0.6	0.6	0.5	<0.5	<0.5	0.6	<0.5	<0.5	<0.5	0.5	<0.5
Yb	1.8	1.7	2.1	2.3	0.5	0.9	2.3	0.9	1.0	1.2	1.7	0.9
Lu	0.28	0.32	0.31	0.33	0.08	0.13	0.35	0.13	0.22	0.16	0.26	0.14

Notes: U1-1, U1-2 and U1-3 are surface samples from the mafic metavolcanic rocks of unit 1; TSL is a surface sample from the ultramafic intrusive body within unit 2; Fe₂O₃* is total iron content; and LOI is "loss on ignition".

APPENDIX I (cont.)

WHOLE-ROCK COMPOSITIONS

Table 2. Analytical results for CAR and BIF from the White River property.

Lithology	Cordierite-anthophyllite rocks					Banded iron formation			
	Sample I815/ 510	I812/ 345	I813/ 368	I91/ 131	I92/ 110	I72/ 245	I815/ 520	J82/ 151	J83/ 12
SiO ₂	57.40	55.90	63.00	58.30	57.00	60.60	53.80	59.80	63.10
TiO ₂	0.90	0.80	0.62	0.71	0.80	0.24	0.50	0.21	0.33
Al ₂ O ₃	19.10	17.90	13.40	16.50	15.40	7.13	11.80	5.79	9.90
Fe ₂ O ₃ *	10.20	9.20	8.67	8.41	9.32	21.70	23.50	26.30	16.90
MgO	7.46	6.16	6.51	5.59	6.35	3.04	5.20	2.08	2.82
MnO	0.16	0.14	0.12	0.04	0.19	0.08	0.24	0.12	0.13
CaO	1.38	3.15	2.51	3.33	3.13	4.23	3.50	4.00	3.50
Na ₂ O	1.04	2.60	2.30	3.16	3.65	1.41	1.13	1.09	0.61
K ₂ O	0.83	2.37	1.57	1.78	1.47	0.95	0.59	0.44	0.68
P ₂ O ₅	0.12	0.12	0.08	0.11	0.11	0.51	0.15	0.31	0.15
LOI	1.10	1.30	1.50	2.00	1.80	<0.5	<0.5	<0.5	0.50
Total	99.90	99.60	100.5	99.90	99.20	100.1	100.4	100.2	98.80
B	120	100	20	30	40	10	20	10	10
Ba	220	530	410	430	330	910	220	320	250
Co	54	62	49	60	53	12	21	10	14
Cr	670	480	770	550	680	180	230	380	270
Cu	140	66	64	180	68	59	79	21	93
Ni	500	370	370	300	300	32	95	38	59
Pb	2	4	<2	4	6	<2	<2	<2	<2
Rb	40	90	70	50	50	<10	<10	20	50
Sc	32.1	36.1	29.0	37.7	29.7	8.0	19.6	8.5	12.0
Sr	50	200	160	280	300	290	190	180	260
Ta	<1	<1	1	<3	<1	1	1	1	1
Th	2.2	3.5	1.8	2.9	2.2	1.7	4.4	2.3	3.5
U	0.8	<1.3	0.7	1.4	0.6	2.0	1.4	0.8	0.9
V	210	210	180	220	200	60	86	46	90
Y	20	20	10	20	20	<10	<10	<10	<10
Zn	120	100	100	100	130	47	82	36	59
Zr	90	90	60	70	90	30	120	<10	40
La	15.4	23.7	11.5	19.0	18.9	15.2	31.1	14.7	21.6
Ce	35	46	28	25	35	35	61	31	49
Nd	18	17	<5	9	21	<5	30	<5	25
Sm	3.6	4.0	2.4	2.7	2.9	2.6	4.7	2.6	3.7
Eu	0.4	2.2	0.6	<1.1	1.3	1.0	1.4	0.9	0.8
Tb	<0.5	<0.5	<0.5	2.0	<0.5	<0.5	<0.5	<0.5	0.5
Yb	3.1	2.2	1.3	1.7	1.6	1.0	1.8	1.2	1.2
Lu	0.51	0.46	0.22	0.22	0.30	0.09	0.30	0.21	0.21
A/N	2.12	6.88	5.83	5.22	4.22	5.06	10.44	5.31	16.23
A/T	18.4	22.4	21.6	23.2	19.3	29.7	23.6	27.6	30.0
CIA	83.2	64.8	63.3	61.9	59.6	49.8	67.5	49.5	66.8
K/N	0.80	0.91	0.68	0.56	0.40	0.67	0.51	0.40	1.11
L/Y	5.5	7.3	6.0	7.6	8.0	10.3	11.7	8.3	12.2

Notes: CAR is cordierite-anthophyllite rocks; BIF is banded iron formation; Fe₂O₃* is total iron content; LOI is "loss on ignition"; A/N is the Al₂O₃/Na₂O weight ratio; A/T is the Al₂O₃/TiO₂ weight ratio; CIA is the chemical indices of alteration (Nesbitt & Young, 1982); K/N is the K₂O/Na₂O weight ratio; and L/Y is the REE fractionation index (La_n/Yb_n).

APPENDIX I (cont.)

WHOLE-ROCK COMPOSITIONS

Table 3. Analytical results for the Local Shear Zone from the White River property.

Sample	I85/ 63	I85/ 65	I87/ 130	I87/ 134	I810/ 302	I810/ 335	I810/ 338	I810/ 340	I815/ 435	I815/ 437	I815/ 439
SiO ₂	59.30	49.70	69.90	63.50	66.60	64.00	65.00	61.70	79.00	71.50	54.20
TiO ₂	0.54	0.41	0.44	0.68	0.42	0.63	0.54	0.54	0.29	0.50	0.27
Al ₂ O ₃	19.20	13.10	15.30	17.70	15.30	16.70	16.90	13.80	10.70	16.60	12.60
Fe ₂ O ₃ *	4.96	23.60	2.56	4.63	4.84	4.96	3.92	10.20	2.30	2.05	16.70
MgO	2.81	0.83	0.41	1.00	0.49	0.97	1.25	0.82	<0.01	0.10	0.93
MnO	0.08	0.05	<0.02	0.03	0.02	0.02	0.04	0.03	<0.02	0.02	0.04
CaO	4.05	1.51	1.34	1.71	2.32	0.87	2.23	1.16	0.35	0.50	6.35
Na ₂ O	1.10	0.59	4.41	4.11	1.16	1.67	2.22	1.93	0.39	0.63	0.21
K ₂ O	4.42	3.45	2.22	2.66	4.76	4.23	4.13	2.97	2.73	3.84	2.40
P ₂ O ₅	0.22	0.15	0.13	0.18	0.09	0.16	0.14	0.13	0.14	0.22	0.14
LOI	1.80	5.40	2.00	2.70	2.80	3.80	2.40	6.00	2.20	2.80	4.30
Total	98.70	98.90	98.90	99.20	99.10	98.30	99.00	99.50	98.30	98.90	98.30
S	na	10.5	1.27	2.37	na	2.76	na	5.88	1.03	1.02	8.31
Ag	<0.5	<0.5	<0.5	<0.5	<0.5	<0.5	<0.5	<0.5	<0.5	<0.5	8.5
As	320	3	43	83	90	110	62	200	120	110	38
Au	37	530	13	12	na	5	<0.1	7	4300	1700	11000
Hg	11	<5	16	36	190	24	170	24	<5	<5	20
W	11	14	33	7	11	20	13	8	8	14	7
B	110	80	80	120	270	240	170	180	20	30	80
Ba	810	680	810	1000	360	1400	700	910	460	580	470
Co	20	19	10	19	14	20	16	18	10	11	29
Cr	290	290	230	210	390	310	200	270	250	300	390
Cu	35	120	27	44	21	41	43	25	15	8.5	4600
Mo	<5	<5	<5	<5	<5	<5	<5	<5	<5	<5	<5
Ni	64	270	33	58	43	59	45	53	44	48	190
Pb	8	<2	<2	<2	10	6	12	<2	4	<2	<2
Rb	110	90	70	70	40	120	60	80	90	110	60
Sc	14.3	7.9	4.9	14.9	7.9	15.4	12.3	11.8	4.8	6.2	5.8
Sr	470	170	790	950	840	460	780	370	170	320	110
Ta	1	<1	<1	<1	2	<1	<1	<1	<1	<1	<1
Th	4.2	3.1	4.7	4.3	2.4	4.8	3.9	3.6	3.1	6.6	3.1
U	0.5	0.9	1.6	1.2	0.7	1.5	1.1	0.8	1.7	1.9	1.4
V	100	58	38	80	72	100	98	74	48	80	58
Y	<10	<10	<10	<10	<10	10	10	<10	<10	<10	<10
Zn	100	130	61	100	290	110	240	120	61	32	56
Zr	110	80	80	130	80	110	100	100	50	110	40
La	35.7	25.6	38.8	39.1	14.9	33.0	26.8	26.6	23.3	59.1	29.4
Ce	76	55	71	74	30	67	56	50	44	116	55
Nd	44	23	32	34	<5	29	19	23	18	45	24
Sm	5.8	3.8	5.5	5.3	2.4	4.7	4.4	3.9	3.1	7.3	3.2
Eu	1.2	0.5	1.2	0.8	0.7	1.3	1.3	0.6	0.7	1.7	0.9
Tb	<0.5	<0.5	<0.5	<0.5	0.7	<0.5	<0.5	<0.5	<0.5	<0.5	<0.5
Yb	0.8	0.7	0.6	1.1	0.6	1.2	1.1	1.0	0.7	0.6	0.5
Lu	0.13	0.11	0.11	0.16	0.15	0.20	0.13	0.15	0.09	0.15	0.09
L/Y	30.2	24.7	43.7	24.0	16.8	18.6	16.5	18.0	22.5	66.6	39.7

Notes: Fe₂O₃* is total iron content; LOI is "loss on ignition"; na is "not analyzed"; and L/Y is the REE fractionation index (La_n/Yb_n).

APPENDIX I (cont.)

WHOLE-ROCK COMPOSITIONS

Table 3 (cont.)

Sample	I72/ 163	I81/ 83	I811/ 70	I811/ 74	I812/ 240	I814/ 514	I816/ 470	I816/ 472	I816/ 474	I94/ 214	I94/ 215	I815/ 493
SiO ₂	60.10	62.70	70.50	58.60	60.30	62.70	69.50	70.40	63.50	67.40	58.20	50.90
TiO ₂	0.39	0.44	0.31	0.57	0.47	0.41	0.44	0.34	0.40	0.48	0.56	0.44
Al ₂ O ₃	1290	16.60	15.30	17.20	16.40	16.50	15.40	13.20	10.20	13.10	15.30	11.80
Fe ₂ O ₃ *	3.51	3.75	1.94	9.39	4.54	4.06	3.44	2.45	9.21	4.08	6.80	18.00
MgO	2.03	2.62	1.01	1.48	3.44	3.00	0.25	0.75	1.44	2.04	1.57	0.48
MnO	0.12	0.05	0.04	0.07	0.09	0.07	<0.02	0.03	0.07	3.94	0.05	<0.02
CaO	8.67	2.76	1.82	2.58	6.78	5.36	0.54	1.80	7.96	0.05	5.23	2.58
Na ₂ O	2.32	6.55	1.21	0.87	3.11	2.65	0.51	1.87	2.77	7.63	7.63	1.68
K ₂ O	4.63	2.62	3.98	3.93	3.18	3.18	5.38	5.01	0.41	0.12	0.61	4.48
P ₂ O ₅	0.24	0.18	0.12	0.15	0.19	0.18	0.21	0.16	0.21	0.20	0.22	0.12
LOI	2.50	<0.5	1.70	3.80	0.80	1.50	3.10	1.80	2.90	0.80	1.60	9.10
Total	97.50	98.90	98.10	98.90	99.50	99.90	99.00	98.00	99.40	100.0	98.10	99.90
S	na	na	0.36	3.45	na	na	1.48	0.78	4.48	na	2.09	10.40
Ag	<0.5	<0.5	<0.5	<0.5	<0.5	<0.5	<0.5	<0.5	<0.5	<0.5	<0.5	<0.5
As	3	<2	11	69	4	11	67	63	50	2	2	390
Au	42	<0.1	40	27000	<0.1	<0.1	4200	1400	88	610	200	8
Hg	27	6	8	8	<5	8	20	8	87	8	<5	31
W	12	<3	9	17	14	20	13	11	<3	8	<3	39
B	20	<10	200	350	40	50	40	140	20	10	10	150
Ba	80	1600	730	630	940	840	970	670	70	140	560	1200
Co	13	<1	11	43	18	14	14	10	88	16	35	16
Cr	170	<2	240	340	220	300	200	240	440	220	320	220
Cu	19	29	15	68	36	25	23	23	53	57	65	32
Mo	<5	<5	<5	<5	<5	<5	<5	<5	<5	<5	<5	<5
Ni	29	32	38	94	63	65	42	48	84	66	98	47
Pb	12	12	4	<2	12	10	10	10	10	4	10	16
Rb	20	70	110	120	80	70	110	100	80	20	40	130
Sc	8.9	<0.1	8.5	15.2	14.3	10.3	9.9	7.5	7.7	11.0	14.0	8.0
Sr	190	1500	240	310	1000	1100	330	450	1800	800	1700	420
Ta	11	1	<1	<1	1	1	<1	<1	<1	1	<1	<1
Th	7.7	<0.5	2.5	3.5	5.0	4.2	5.2	5.5	3.6	5.1	5.5	3.8
U	2.8	<0.5	1.0	1.0	0.8	1.2	1.3	1.5	1.9	1.7	1.1	1.2
V	80	78	48	100	98	84	88	76	70	96	98	74
Y	10	10	<10	<10	<10	20	<10	<10	<10	<10	<10	<10
Zn	76	91	74	100	92	97	97	40	84	100	100	70
Zr	90	110	80	110	70	90	90	60	20	100	80	100
La	81.8	<0.5	18.8	33.8	35.6	33.2	38.3	34.0	30.6	31.6	36.8	33.7
Ce	97	<3	34	65	74	71	73	67	57	61	86	64
Nd	<5	<5	14	33	28	23	31	25	27	30	30	26
Sm	9.4	<0.1	2.6	4.9	5.4	5.1	5.3	4.3	4.7	4.6	5.9	3.9
Eu	3.0	<0.2	0.7	1.3	1.4	1.1	1.2	0.8	1.9	1.6	1.4	1.1
Tb	<0.6	<0.5	<0.5	<0.5	<0.5	<0.5	<0.5	<0.5	<0.5	<0.5	<0.5	<0.5
Yb	1.2	<0.2	0.5	0.9	1.1	0.6	1.2	0.8	0.9	0.8	1.0	0.6
Lu	0.16	<0.05	0.09	0.13	0.17	0.09	0.17	0.12	0.13	0.23	0.20	0.09
L/Y	46.2		25.4	25.4	21.9	37.4	21.6	28.7	23.0	26.7	24.9	38.0

Notes. I815/493 is a pyrite-rich sample from the intermediate to felsic metavolcanic unit 7; Fe₂O₃* is total iron content, LOI is "loss on ignition"; na is "not analysed"; and L/Y is the REE differentiation index (La_n/Yb_n).

APPENDIX I (cont.)

WHOLE-ROCK COMPOSITIONS

Table 4. Analytical results for calc-silicates from the White River property.

Sample	No. 2	No. 3	No. 5	No. 6	No. 7	No. 7*	No. 8	K71/ 76	K72/ 43	K72/ 80
SiO ₂	51.10	47.90	46.40	50.70	50.30	46.40	46.30	50.70	44.00	48.60
TiO ₂	0.40	0.43	0.34	0.82	0.36	0.51	0.32	0.52	0.25	0.49
Al ₂ O ₃	2.38	3.44	8.74	4.86	2.20	9.16	9.00	7.73	8.45	15.20
Fe ₂ O ₃ *	9.62	10.70	8.57	9.54	7.61	13.60	7.84	8.57	9.34	7.33
MgO	11.40	8.11	6.90	7.66	14.00	12.30	6.09	7.02	7.07	5.33
MnO	0.31	0.44	0.40	0.41	0.29	0.29	0.42	0.39	0.55	0.40
CaO	22.10	25.40	24.70	21.60	22.00	11.00	26.40	21.30	26.90	19.00
Na ₂ O	0.57	0.47	0.74	1.22	0.35	0.93	0.77	1.16	0.13	2.28
K ₂ O	0.27	0.19	0.32	0.91	0.15	0.59	0.36	1.38	0.18	0.83
P ₂ O ₅	0.02	0.02	0.13	0.03	0.02	0.06	0.05	0.33	0.04	0.15
LOI	<0.5	<0.5	0.80	<0.5	0.60	3.80	<0.5	0.60	1.20	1.10
Total	99.10	98.00	98.40	98.10	98.10	99.10	98.10	100.0	98.50	99.30
S	na	na	na	na	na	na	na	0.08	0.52	na
Ag	<0.5	<0.5	<0.5	<0.5	<0.5	<0.5	<0.5	<0.5	<0.5	<0.5
As	<2	<2	<2	<2	<2	<2	<2	<2	<2	<2
Au	5	8.9	1.1	1.6	0.6	0.9	5	0.8	0.6	na
B	10	20	<10	<10	10	<10	<10	<10	10	30
Ba	80	10	60	140	30	180	910	910	60	90
Co	130	90	87	84	78	58	85	57	110	53
Cr	4200	5100	2700	1700	1500	3300	2600	1300	2700	1300
Cu	0.5	12	4.0	12	22	29	2.5	2.5	38	15
Hg	20	21	28	8	<1	12	8	8	20	8
Mo	<5	45	17	<5	<5	32	<5	<5	<5	79
Ni	920	790	980	560	1000	440	1100	600	1300	560
Pb	<2	<2	<2	<2	<2	<2	<2	4	<2	14
Rb	30	20	20	80	20	40	20	60	30	70
Sr	70	40	30	140	40	120	90	250	80	540
Th	0.8	2.0	<0.5	<0.5	<0.5	<0.5	<0.5	5.1	<0.5	1.5
U	0.5	<0.5	0.5	0.7	<0.5	<0.5	<0.5	1.1	<0.5	1.7
V	90	92	140	140	80	170	110	160	130	140
W	<3	<3	<3	<3	<3	<3	<3	<3	<3	<3
Zn	210	260	200	200	110	160	180	180	270	190
Zr	20	10	<10	<10	<10	<10	<10	50	<10	20
La	11.7	21.1	5.8	3.4	0.9	6.2	3.4	43.3	2.4	12.6
Ce	30	42	11	16	7	18	3	89	6	30
Nd	10	15	6	14	<5	5	5	40	<5	12
Sm	1.8	2.6	1.0	2.6	0.9	1.1	0.8	8.1	0.8	2.1
Eu	0.5	0.7	0.4	0.7	0.4	0.4	<0.2	2.3	0.5	0.6
Tb	<0.5	<0.5	<0.5	0.7	<0.5	<0.5	<0.5	0.7	<0.5	<0.5
Yb	1.1	2.0	0.9	2.4	1.1	1.2	0.9	1.4	1.1	0.9
Lu	0.14	0.34	0.15	0.37	0.15	0.21	0.15	0.22	0.16	0.16

Notes: No. 2, No. 3, No. 5, No. 6, No. 7, No. 7* and No. 8 are surface samples of Cr-rich calc-silicate rocks; Fe₂O₃* is the total iron content; LOI is "loss on ignition"; and na is "not analyzed".

APPENDIX I (cont.)

WHOLE-ROCK COMPOSITIONS

Table 4 (cont.)

Sample	L81/ 19	L81/ 28	L81/ 81	L93/ 53	J83/ 91	J87/ 150	K91/ 12
SiO ₂	50.20	53.10	47.90	46.60	41.80	40.80	46.10
TiO ₂	0.32	0.09	0.19	0.25	0.79	0.58	1.22
Al ₂ O ₃	4.88	8.86	3.92	4.53	12.20	9.85	9.54
Fe ₂ O ₃ *	9.73	8.74	9.13	7.78	21.80	24.70	22.70
MgO	10.60	7.38	17.50	8.10	2.98	5.72	3.03
MnO	0.29	0.39	0.21	0.48	0.80	1.00	0.46
CaO	21.20	16.90	14.30	27.60	18.20	14.50	13.60
Na ₂ O	1.10	1.99	1.05	0.15	0.18	0.70	0.30
K ₂ O	0.12	1.74	0.14	0.09	0.27	0.32	0.25
P ₂ O ₅	0.03	0.21	0.03	0.03	0.11	0.19	0.25
LOI	<0.5	0.70	3.60	2.90	0.80	1.10	1.00
Total	99.00	100.3	98.00	98.80	100.0	99.50	98.50
S	na	na	na	0.06	1.35	2.48	3.71
Ag	<0.5	<0.5	<0.5	<0.5	<0.5	<0.5	<0.5
As	<2	<2	<2	<2	<2	<2	<2
Au	na	na	na	34	25	62	<0.1
B	20	20	20	<10	<10	<10	20
Ba	<10	560	<10	20	30	60	90
Co	96	99	110	120	39	45	100
Cr	2600	1100	2000	2300	150	150	360
Cu	74	5.5	26	1.5	510	350	670
Hg	<5	<5	<5	8	<5	<5	21
Mo	13	<5	<5	<5	<5	<5	<5
Ni	1200	970	2100	1600	85	67	310
Pb	6	4	2	<2	<2	<2	6
Rb	10	140	10	<10	<10	30	<10
Sr	210	190	10	30	60	<10	30
Th	<0.5	<0.5	<0.5	<0.5	<0.5	<0.5	5.3
U	1.1	0.7	<0.5	<0.5	<0.5	<0.5	1.9
V	150	110	96	78	240	200	300
W	<3	<3	<3	<3	<3	<3	3
Zn	120	220	66	69	110	200	2100
Zr	<10	<10	<10	<10	30	10	60
La	2.3	0.5	0.5	1.0	5.3	3.0	114
Ce	5	<3	<3	<3	15	9	222
Nd	<5	<5	<5	<5	6	<5	94
Sm	0.8	0.2	0.4	0.4	2.4	1.4	18.5
Eu	0.7	0.2	<0.3	<0.2	0.9	0.4	4.7
Tb	<0.5	<0.5	<0.5	<0.5	0.8	0.7	1.8
Yb	0.8	0.2	0.5	0.4	3.5	2.5	3.4
Lu	0.21	<0.05	0.08	0.07	0.58	0.38	0.5

Notes: Samples L81/19, L81/28, L81/81 and L93/53 are Cr-rich calc-silicates of the Playter Harbour Group; samples J83/91, J87/150 and K91/12 are Fe-rich calc-silicates of the Heron Bay Group; Fe₂O₃* is total iron content; LOI is "loss on ignition"; and "na" is "not analyzed".

APPENDIX 1 (cont.)

WHOLE-ROCK COMPOSITIONS

Table 5. Analytical results for (meta-)volcanic rocks from the White River property.

Unit Sample	Unit 1			Unit 2			Unit 4					
	U1-1	U1-2	U1-3	X72/ 78	L81/ 81	TSL	L93/ 55	I72/ 382	I72/ 367	J71/ 52	J87/ 160	J87/ 162
SiO ₂	50.10	48.30	48.60	47.30	47.90	42.70	50.00	48.00	47.60	43.40	46.30	49.70
TiO ₂	0.63	0.73	0.87	0.89	0.19	0.41	0.87	0.31	0.35	0.39	0.65	0.27
Al ₂ O ₃	16.90	15.00	20.40	14.90	3.92	8.71	14.60	7.17	7.42	7.79	9.82	5.30
Fe ₂ O ₃ *	9.26	12.90	10.00	12.80	9.13	11.30	12.80	9.48	9.00	11.00	13.40	9.58
MgO	6.84	7.71	2.81	7.28	17.50	22.50	6.20	19.40	19.00	22.40	16.50	22.40
MnO	0.18	0.20	0.17	0.25	0.21	0.17	0.24	0.19	0.19	0.19	0.22	0.16
CaO	10.40	10.90	12.50	11.00	14.30	5.42	10.60	8.41	9.20	7.23	8.36	7.42
Na ₂ O	3.51	2.82	3.19	2.17	1.05	0.50	3.14	0.55	0.68	0.44	0.63	0.14
K ₂ O	0.68	0.67	0.57	0.81	0.14	0.03	0.54	2.16	0.34	0.05	0.16	0.02
F ₂ O ₃	0.24	0.07	0.08	0.06	0.03	0.03	0.07	0.01	0.03	0.04	0.05	0.04
LOI	0.90	0.90	0.90	0.70	3.60	6.30	0.50	2.70	4.10	5.30	3.70	4.90
Total	99.60	100.0	99.60	98.20	98.00	98.10	99.60	98.70	97.90	98.20	100.1	100.2
B	40	30	20	<10	20	10	<10	10	40	30	<10	<10
Ba	130	90	100	60	<10	80	240	200	70	60	70	10
Co	38	45	35	62	110	63	53	75	81	98	77	68
Cr	200	410	270	460	2000	2900	350	2200	1600	2300	2000	1800
Cu	4.5	43	74	64	26	19	86	<0.5	4.0	44	<0.5	61
Ni	98	120	82	250	2100	680	140	890	860	1000	560	960
Rb	20	20	<10	20	10	10	20	390	30	10	<10	20
Sc	35.4	42.3	35.8	48.9	19.5	24.1	45.9	26.2	28.1	30.7	41.1	20.2
Sr	420	210	220	90	10	20	130	120	50	40	<10	<10
V	180	250	240	260	96	180	220	150	150	160	230	100
Y	20	<10	10	<10	<10	<10	10	<10	10	10	20	20
Zn	120	110	170	130	66	70	100	93	130	64	98	59
Zr	<10	10	40	20	<10	20	30	<10	<10	<10	20	<10
La	10.5	2.1	3.8	3.0	0.5	4.3	3.2	2.0	5.7	1.6	1.9	1.0
Ce	32	5	12	10	<3	12	13	12	14	6	4	4
Nd	18	10	<5	5	<5	<5	6	<5	6	<5	<5	<5
Sm	3.8	1.4	2.1	1.9	0.4	1.3	1.9	1.0	1.4	0.8	1.4	0.6
Ku	<1.1	<1.0	0.8	0.6	<0.3	0.3	0.5	0.7	0.6	0.6	0.6	<0.2
Tb	0.9	<0.6	0.6	0.5	<0.5	<0.5	0.6	<0.5	<0.5	<0.5	0.5	<0.5
Yb	1.8	1.7	2.1	2.3	0.5	0.9	2.3	0.9	1.0	1.2	1.7	0.9
Lu	0.28	0.32	0.31	0.33	0.08	0.13	0.35	0.13	0.22	0.16	0.26	0.14

Notes: U1-1, U1-2 and U1-3 are surface samples from the mafic metavolcanic rocks of unit 1; TSL is a surface sample from the ultramafic intrusive body within unit 2; Fe₂O₃* is total iron content; and LOI is "loss on ignition".

APPENDIX I (cont.)
WHOLE-ROCK COMPOSITIONS

Table 5 (cont.)

Unit Sample	Unit 4											
	J85/ 202	J91/ 57	K91/ 98	I72/ 370	I72/ 371	J71/ 5	J83/ 77	J83/ 132	J83/ 126	J85/ 165	J91/ 99	K91/ 20
SiO ₂	45.00	47.60	45.40	47.70	46.70	49.90	50.00	48.00	47.10	49.80	45.30	49.90
TiO ₂	0.34	0.37	0.46	1.39	1.13	1.06	1.42	0.67	0.93	1.21	1.58	1.18
Al ₂ O ₃	6.68	7.43	6.98	14.10	12.80	13.80	15.10	10.60	13.20	13.50	14.30	14.20
Fe ₂ O ₃ *	10.80	10.20	11.80	17.60	19.90	14.20	15.60	13.80	20.60	12.00	20.10	14.30
MgO	23.00	20.70	21.70	5.25	5.60	5.15	5.24	12.00	5.42	4.96	7.02	6.99
MnO	0.17	0.19	0.19	0.33	0.35	0.27	0.27	0.23	0.85	0.24	0.36	0.22
CaO	7.03	9.27	7.99	8.88	9.77	10.20	8.07	12.50	8.89	14.30	8.42	8.42
Na ₂ O	0.12	0.44	0.16	2.08	1.50	3.28	3.16	0.86	1.57	1.22	1.67	3.14
K ₂ O	0.03	0.04	0.02	0.73	0.55	0.78	0.63	0.31	0.18	0.52	0.55	0.67
P ₂ O ₅	0.03	0.05	0.07	0.10	0.13	0.10	0.11	0.03	0.05	0.11	0.10	0.10
LOI	6.20	3.80	5.10	1.10	1.00	0.80	<0.50	0.70	1.40	2.10	1.00	0.80
Total	99.80	100.5	100.1	99.40	99.50	99.50	100.1	99.90	100.2	98.70	100.5	99.90
B	<10	<10	<10	<10	<10	40	20	20	10	20	70	20
Ba	<10	10	30	180	200	120	100	60	120	60	230	290
Co	79	80	73	46	42	69	51	66	43	50	61	54
Cr	2500	2300	1600	270	220	68	280	1100	230	180	330	200
Cu	51	6.0	79	150	280	130	140	1.0	260	86	360	95
Ni	1200	940	400	85	70	66	90	120	64	81	99	84
Rb	20	10	<10	60	20	40	50	30	30	10	80	40
Sc	28.1	27.4	36.3	58.0	52.2	30.7	52.5	64.2	51.2	48.3	58.5	50.6
Sr	50	60	<10	90	150	40	70	170	30	110	60	250
V	120	120	170	340	330	160	360	300	310	230	370	280
Y	<10	<10	20	20	20	10	10	<10	20	<10	<10	20
Zn	67	72	72	130	140	64	150	98	220	180	140	120
Zr	<10	<10	10	40	30	<10	50	20	20	50	60	50
La	1.3	1.7	2.0	4.9	4.4	1.6	4.2	2.4	5.3	5.5	4.8	4.3
Ce	4	6	7	17	16	6	19	12	16	18	14	13
Nd	<5	<5	<5	9	<5	<5	<5	<5	6	9	8	<5
Sm	0.7	0.9	1.8	3.1	2.4	0.8	2.8	1.6	2.4	2.7	2.8	2.0
Eu	0.2	0.4	0.4	1.2	0.8	0.6	0.9	0.3	0.9	1.4	0.3	<1.0
Tb	<0.5	<0.5	0.6	0.9	0.7	<0.5	0.6	<0.5	0.8	0.6	0.9	<0.6
Yb	0.9	1.1	2.1	3.1	3.5	1.2	3.1	1.8	3.1	3.3	3.1	2.2
Lu	0.16	0.17	0.31	0.53	0.55	0.16	0.52	0.29	0.63	0.61	0.51	0.37

Notes: Fe₂O₃* is the total iron content; and LOI is "loss on ignition".

APPENDIX I (cont.)

WHOLE-ROCK COMPOSITIONS

Table 5 (cont.)

Unit Sample	Unit 4		Unit 5				Unit 7					
	K91/ 40	I72/ 327	J85/ 121	J85/ 136	J83/ 50	I72/ 163	I813/ 294	I92/ 29	I94/ 250	J82/ 33	J82/ 41	I92/ 69
SiO ₂	50.20	71.50	71.10	68.80	68.40	60.10	64.20	61.20	60.50	62.50	64.80	64.20
TiO ₂	1.00	0.35	0.34	0.36	0.25	0.39	0.45	0.43	0.52	0.44	0.44	0.40
Al ₂ O ₃	14.30	14.50	15.10	15.50	15.20	12.90	13.60	17.10	15.80	15.80	16.80	15.40
Fe ₂ O ₃ *	13.00	2.18	2.17	2.61	2.05	3.51	3.96	3.87	5.50	3.77	2.50	2.52
MgO	4.62	0.54	0.48	1.01	0.81	2.03	2.65	2.59	4.01	2.17	0.97	0.89
MnO	0.33	0.07	0.06	0.04	0.03	0.12	0.10	0.07	0.10	0.10	0.05	0.03
CaO	12.50	3.45	3.26	2.64	2.29	8.67	6.11	3.53	6.82	4.49	4.90	8.56
Na ₂ O	2.47	5.11	4.42	5.13	6.52	4.63	4.92	5.93	3.20	6.21	5.11	2.75
K ₂ O	0.69	1.29	1.68	2.12	2.00	2.32	2.35	3.29	2.02	2.48	3.18	2.32
P ₂ O ₅	0.11	0.08	0.09	0.14	0.10	0.24	0.18	0.18	0.20	0.18	0.14	0.11
LOI	1.00	1.00	0.60	1.00	1.00	2.50	0.90	<0.5	0.60	0.90	1.10	1.40
Total	100.4	100.2	99.30	99.10	99.00	97.50	99.80	98.80	99.50	99.50	100.4	98.80
B	20	30	40	40	20	20	20	30	40	20	30	<10
Ba	520	280	350	1500	940	80	920	940	740	1500	1200	1100
Co	59	7	6	5	4	13	16	13	18	4	12	11
Cr	150	310	200	200	230	170	340	180	240	54	280	230
Cu	63	6.5	9.0	20	8.5	19	33	15	32	27	21	69
Ni	72	22	26	18	11	29	37	35	59	30	30	28
Rb	40	50	30	90	60	20	70	110	60	60	100	70
Sc	59.9	6.6	6.4	4.3	3.6	8.9	10.0	8.1	14.3	2.0	8.7	4.9
Sr	330	550	340	1300	1500	190	1800	1400	970	1500	1100	720
V	370	46	46	36	44	80	94	80	100	76	76	50
Y	20	10	<10	<10	<10	10	20	<10	<10	10	<10	20
Zn	150	30	68	80	76	76	100	95	96	87	61	40
Zr	180	80	100	130	30	90	70	80	70	90	70	70
La	6.0	15.3	13.8	43.8	14.3	81.8	45.6	57.7	29.9	11.0	42.9	36.2
Ce	21	28	21	71	29	97	105	125	62	15	84	71
Nd	<5	<5	11	21	25	<5	49	61	33	<5	36	15
Sm	2.6	2.0	1.5	4.6	2.4	9.4	7.2	9.1	4.9	1.5	6.5	5.0
Eu	0.8	<0.4	1.0	3.1	0.8	3.0	2.6	2.3	1.3	0.5	1.2	1.1
Tb	<0.5	<0.5	<0.5	<0.5	<0.5	<0.6	0.7	0.7	<0.5	<0.5	<0.5	<0.5
Yb	2.8	0.4	0.4	0.5	0.2	1.2	0.9	0.8	1.0	0.2	0.7	0.6
Lu	0.47	0.08	0.09	0.12	0.06	0.16	0.15	0.18	0.15	<0.05	0.12	0.13

Notes: Fe₂O₃* is total iron content; and LOI is "loss on ignition".

APPENDIX I (cont.)

WHOLE-ROCK COMPOSITIONS

Table 5 (cont.)

Unit Sample	Unit 9					Miscellaneous						
	I72/ 87	I813/ 122	I813/ 223	I814/ 367	I814/ 454	PGC	CLP	PGMT	K72/ 20	L81/ 10	DIKE	I810/ 330
SiO ₂	49.50	48.70	54.60	48.40	48.10	70.70	63.00	74.70	69.10	67.90	49.20	25.40
TiO ₂	0.87	0.89	0.65	0.85	0.73	0.26	0.56	0.07	0.34	0.35	0.71	3.84
Al ₂ O ₃	13.70	13.40	15.40	11.60	9.89	14.80	17.10	13.90	15.40	15.00	14.40	5.15
Fe ₂ O ₃ *	11.30	11.70	8.09	12.00	12.40	1.93	3.57	0.50	2.03	2.23	10.80	15.50
MgO	8.25	8.98	5.00	12.70	13.40	0.71	1.23	0.07	0.85	1.10	8.74	9.26
MnO	0.21	0.19	0.15	0.22	0.21	0.04	0.04	nd	0.03	0.03	0.18	0.27
CaO	9.95	8.60	8.97	8.61	10.90	2.03	3.52	0.85	2.56	2.28	12.40	20.00
Na ₂ O	3.33	2.64	3.90	1.64	1.29	5.43	5.80	5.13	5.77	5.57	1.68	0.87
K ₂ O	1.07	2.29	2.08	2.68	1.32	2.61	2.72	4.04	2.80	2.83	0.72	2.40
P ₂ O ₅	0.23	0.22	0.27	0.20	0.21	0.08	0.23	0.02	0.15	0.15	0.07	1.50
LOI	1.50	1.10	0.80	1.10	1.50	<0.5	<0.5	<0.5	<0.5	1.50	1.10	14.70
Total	100.1	99.00	100.2	100.2	100.1	99.20	98.40	99.50	99.50	98.90	100.0	99.20
B	860	200	40	40	10	<10	10	10	40	10	30	<10
Ba	60	730	690	660	280	1100	1200	260	1200	1200	100	900
Co	47	51	34	55	62	5	13	2	9	7	59	60
Cr	640	750	470	840	900	240	230	240	68	130	410	380
Cu	130	90	130	86	58	3.5	15	3.0	9.0	1	98	140
Ni	82	110	90	140	140	11	16	7	18	7	110	240
Rb	10	80	60	70	30	70	80	150	90	0	50	90
Sc	39.1	45.9	25.9	46.7	53.4	3.4	4.5	0.4	3.2	3	53.3	23.9
Sr	150	770	870	300	460	930	1500	410	1400	800	190	850
V	28	300	200	270	270	26	68	8	34	38	250	290
Y	20	20	20	10	10	<10	<10	<10	<10	<10	10	20
Zn	110	120	100	110	100	72	110	20	80	59	77	210
Zr	40	20	60	20	10	40	150	10	100	120	10	440
La	20.0	10.3	27.3	10.7	12.1	13.0	54.0	5.5	32.7	31.2	6.5	145
Ce	28	31	60	29	33	28	62	9	49	53	11	256
Nd	<5	<5	23	<5	17	<5	<5	<5	26	20	<5	113
Sm	3.9	3.3	4.7	3.1	3.7	1.7	6.6	0.7	4.0	3.8	1.7	20.5
Eu	1.5	0.9	1.2	1.0	0.9	0.5	2.8	<0.3	<1.3	<1.3	1.0	6.4
Tb	<0.5	<0.5	0.5	<0.5	0.5	<0.5	<0.5	<0.5	<0.6	<0.7	<0.5	2.0
Yb	1.8	2.2	1.7	1.7	1.7	0.2	0.6	<0.2	0.6	0.3	1.7	2.7
Lu	0.34	0.53	0.28	0.31	0.28	0.05	0.08	<0.05	<0.05	0.08	0.23	0.41

Notes: PGC is a surface sample from the Pukaskwa Gneissic Complex, CLP is a sample from the Cedar Lake Pluton; PGMT is a surface sample of a quartz-microcline pegmatitic vein, K72/20 and L81/10 are quartz-feldspar porphyres; DIKE is biabase dike, I810/330 is lamprophyre dike, Fe₂O₃* is total iron content; and LOI is "loss on ignition"

APPENDIX II

TABLE 1 FELDSPAR COMPOSITIONS

Table 1a. Plagioclase from the White River property, Hemlo area.

Unit	1		2		3		4		5		
Sample	U1-1		M131/ 81	K72/ 43	L81/ 16	L81/ 28	I72/ 370	I83/132		I92/245	
	core	rim					clear	dark	core	rim	
SiO ₂	61.54	55.30	46.14	68.80	60.74	67.96	56.78	57.15	46.57	59.90	59.76
Al ₂ O ₃	24.80	28.94	35.73	18.65	24.44	18.45	27.64	26.90	35.10	24.76	25.50
CaO	4.98	10.33	17.11	0.03	6.49	0.00	9.26	8.40	17.03	5.49	8.32
Na ₂ O	8.84	5.42	1.62	13.02	8.87	11.44	6.28	7.59	1.50	9.67	7.56
K ₂ O	0.04	0.04	0.00	0.04	0.14	0.12	0.12	0.11	0.00	0.04	0.06
Total	100.2	100.1	100.6	100.5	100.7	98.32	100.1	99.70	100.2	99.86	101.2
Si	2.722	2.484	2.105	3.003	2.694	3.015	2.543	2.573	2.130	2.626	2.643
Al	1.295	1.532	1.919	0.959	1.278	0.983	1.459	1.418	1.892	1.305	1.329
Ca	0.239	0.498	0.838	0.001	0.308	0.000	0.446	0.404	0.835	0.263	0.394
Na	0.758	0.472	0.143	1.102	0.763	0.984	0.546	0.655	0.133	0.839	0.648
K	0.002	0.002	0.000	0.002	0.008	0.008	0.007	0.006	0.000	0.002	0.004
An	23.9	51.2	85.5	0.1	28.5	0.0	44.6	38.0	86.3	23.9	37.7

Table 1a. (cont.)

Unit	6										
Sample	I82/119		I82/144		I812/ 345	I815/520		I92/ 110	I92/ 202	J82/92	
	core	rim	core	rim		core	rim			core	rim
SiO ₂	60.92	56.80	60.67	58.47	57.46	61.20	57.93	60.77	60.80	60.00	58.85
Al ₂ O ₃	25.02	27.34	24.96	26.81	26.92	23.84	26.45	24.78	23.84	24.55	25.26
CaO	5.13	9.91	4.86	9.64	8.41	4.48	10.54	6.71	5.88	4.68	8.88
Na ₂ O	9.44	6.18	9.53	5.90	7.56	9.93	5.40	8.16	8.23	9.08	6.60
K ₂ O	0.04	0.02	0.07	0.05	0.01	0.03	0.00	0.07	0.03	0.02	0.07
Total	100.6	100.3	100.1	100.9	99.64	99.88	100.3	100.5	98.78	100.2	99.66
Si	2.697	2.544	2.697	2.593	2.571	2.725	2.587	2.694	2.732	2.709	2.640
Al	1.305	1.443	1.307	1.401	1.419	1.258	1.393	1.294	1.262	1.306	1.335
Ca	0.243	0.476	0.232	0.459	0.404	0.210	0.505	0.419	0.383	0.227	0.428
Na	0.810	0.537	0.821	0.507	0.655	0.863	0.467	0.701	0.717	0.795	0.574
K	0.002	0.001	0.004	0.003	0.001	0.002	0.000	0.004	0.002	0.001	0.004
An	23.0	46.9	21.9	47.4	38.1	19.5	51.9	31.2	28.9	22.1	42.5

Notes: U1-1 is a surface sample from unit 1 of the Playter Harbour Group; and An is the anorthite content.

Table 2d. Calcic amphiboles in other rock-types from the White River property, Hemlo area.

Lithology	Cr-rich calc-silicates				Fe-rich calc-silicates					veins		
	sample	K72/ 43	K72/ 80	L81/ 19	L81/ 28	I07/150 *	I07/150 **	J83/ 91	K91/12 *	K91/12 **	U1-1	I72/ 370
SiO ₂	52.14	55.36	52.13	54.14	40.81	51.50	39.09	40.75	48.23	57.11	53.10	56.56
TiO ₂	0.00	0.00	0.06	0.00	0.71	0.11	0.72	0.56	0.16	0.04	0.15	0.00
Al ₂ O ₃	3.38	1.27	2.52	0.63	11.35	2.34	12.05	11.30	4.13	0.13	2.74	1.56
Cr ₂ O ₃	0.09	0.07	0.45	0.70	nd	nd	nd	nd	nd	nd	nd	0.02
Fe ₂ O ₃	0.58	0.08	1.14	0.78	4.67	0.58	6.04	5.47	3.59	0.00	----	----
FeO	11.74	10.14	12.37	12.21	19.88	18.51	22.39	21.57	21.61	5.89	14.89	6.94
MgO	15.47	17.38	14.39	15.52	5.58	10.78	3.51	4.35	7.42	20.91	14.52	19.04
MnO	0.28	0.20	0.42	0.57	0.73	0.63	0.57	0.48	0.56	0.32	0.00	0.00
CaO	12.70	12.93	13.04	13.30	12.13	12.50	11.99	12.18	12.11	13.77	12.29	13.57
Na ₂ O	0.66	0.47	0.21	0.04	1.51	0.28	1.11	1.18	0.46	0.05	0.26	0.12
K ₂ O	0.22	0.18	0.27	0.06	0.58	0.02	1.47	0.75	0.14	0.02	0.00	0.00
Total	97.53	96.83	97.01	97.95	97.97	97.25	98.94	98.59	98.41	98.24	98.20	98.00
Si	7.582	7.866	7.657	7.860	6.324	7.706	6.129	6.328	7.338	7.928	7.685	7.896
"Al	0.419	0.134	0.343	0.110	1.676	0.294	1.871	1.472	0.662	0.022	0.315	0.104
"Al	0.160	0.079	0.093	0.000	0.397	0.119	0.357	0.397	0.079	0.000	0.154	0.153
Ti	0.000	0.006	0.007	0.000	0.083	0.012	0.085	0.065	0.018	0.004	0.017	0.000
Cr	0.012	0.010	0.053	0.082	-----	-----	-----	-----	-----	-----	-----	0.006
Fe ⁺	0.063	0.008	0.127	0.086	0.546	0.066	0.713	0.640	0.411	0.000	-----	-----
Fe ⁺⁺	1.421	1.210	1.519	1.482	2.576	2.316	2.935	2.801	2.749	0.684	1.804	0.896
Mg	3.336	3.680	3.150	3.358	1.289	2.404	0.820	1.007	1.682	4.326	3.139	3.964
Mn	0.034	0.024	0.052	0.070	0.096	0.080	0.076	0.063	0.072	0.038	0.000	0.000
Ca	1.969	1.970	2.052	2.069	2.014	2.004	2.014	2.027	1.974	2.048	1.913	2.032
Na	0.180	0.077	0.060	0.011	0.454	0.081	0.338	0.355	0.137	0.014	0.073	0.032
K	0.041	0.054	0.051	0.011	0.115	0.004	0.294	0.149	0.027	0.004	0.000	0.000
M/MF	0.701	0.753	0.675	0.694	0.350	0.517	0.234	0.276	0.390	0.865	0.635	0.816

Notes: * and ** in samples of the Fe-rich calc-silicates are brownish green hornblende and colourless actinolite, respectively; nd is "not detectable"; and M/MF is the atomic ratio of Mg/(Mg + Fe + Mn).

APPENDIX II (cont.)

TABLE 2 AMPHIBOLE COMPOSITIONS

Table 2a. Mg-Fe-Mn amphiboles from the White River property, Hemlo area.

Sample	I84/ 113c	I813/368 ay-ged	I92/110 ay-ged	J83/ 77c	J91/ 99c	I815/510 ay-ged				
SiO ₂	53.70	54.51	49.70	46.27	53.11	50.47	52.63	52.67	53.30	44.40
TiO ₂	0.04	0.09	0.10	0.15	0.03	0.14	0.05	0.05	0.05	0.15
Al ₂ O ₃	0.60	1.16	7.04	11.38	1.64	6.33	0.42	0.54	2.67	15.15
Fe ₂ O ₃	0.74	0.49	3.24	5.83	1.67	3.10	0.38	0.51	0.00	0.19
FeO	20.76	23.29	21.34	18.31	20.79	19.91	28.56	26.96	22.06	22.26
MgO	19.32	18.29	15.40	13.65	18.55	16.52	13.62	14.94	18.34	13.23
MnO	0.54	0.84	0.91	0.97	0.89	0.96	1.29	0.64	0.10	0.16
CaO	0.59	0.27	0.41	0.62	0.38	0.52	0.74	0.63	0.26	0.40
Na ₂ O	0.04	0.85	0.85	1.73	0.10	0.85	0.09	0.03	0.29	1.58
K ₂ O	0.01	0.23	0.02	0.05	0.00	0.00	0.01	0.00	0.00	0.00
Total	96.38	100.0	99.00	98.96	97.17	98.80	97.79	96.97	97.38	97.83
Si	7.886	7.813	7.212	6.722	7.763	7.287	7.929	7.917	7.395	6.560
^{IV} Al	0.104	0.187	0.788	1.278	0.237	0.713	0.071	0.083	0.435	1.440
^{VI} Al	0.000	0.009	0.417	0.671	0.046	0.364	0.004	0.013	0.000	1.214
Ti	0.004	0.010	0.011	0.016	0.003	0.015	0.006	0.006	0.004	0.017
Fe ³⁺	0.082	0.053	0.354	0.637	0.184	0.337	0.043	0.058	0.000	0.000
Fe ²⁺	2.548	2.791	2.589	2.226	2.542	2.404	3.599	3.389	2.674	2.772
Mg	4.225	3.907	3.330	2.955	4.041	3.555	3.058	3.347	3.794	2.936
Mn	0.082	0.102	0.112	0.119	0.110	0.117	0.165	0.082	0.012	0.020
Ca	0.093	0.042	0.064	0.097	0.060	0.080	0.120	0.102	0.038	0.070
Na	0.011	0.150	0.239	0.487	0.028	0.239	0.026	0.009	0.039	0.457
K	0.002	0.042	0.004	0.009	0.000	0.000	0.002	0.000	0.000	0.000
M/MF	0.628	0.590	0.571	0.580	0.620	0.604	0.472	0.503	0.589	0.540

Notes: c. is cummingtonite; ay-ged is anthophyllite and gedrite; and M/MF is atomic ratio of Mg/(Mg + Fe + Mn).

Table 2b. Calcic amphiboles in (ultra-)mafic metavolcanics from the White River property

Unit	1			2			4				
Sample	U1-1	U1-2	U1-3	L81/6 core	rim	K72/ 78	I72/ 371	J83/ 77	J91/ 99	K91/ 40	I85/ 166
SiO ₂	44.44	44.02	42.46	51.42	48.67	50.87	41.42	41.38	40.99	43.65	42.98
TiO ₂	0.80	0.51	0.64	0.30	0.59	0.27	0.57	0.65	0.31	0.64	0.79
Al ₂ O ₃	11.15	10.91	12.08	4.40	6.26	4.50	13.11	13.27	15.70	10.18	11.99
Fe ₂ O ₃	3.17	2.85	3.2	1.19	1.11	1.34	3.23	5.25	4.16	2.10	3.15
FeO	12.04	14.08	17.07	13.06	14.74	15.96	18.20	15.82	13.60	20.34	17.31
MgO	11.79	10.73	8.04	13.89	12.59	11.92	6.84	8.00	8.55	6.54	7.99
MnO	0.38	0.29	0.46	0.16	0.15	0.41	0.41	0.43	0.15	0.61	0.47
CaO	12.21	12.21	11.85	12.01	12.59	11.76	11.85	11.18	11.12	12.04	11.71
Na ₂ O	1.35	1.29	1.18	0.64	0.92	0.78	1.56	1.98	1.80	1.21	1.46
K ₂ O	0.74	1.14	1.24	0.33	0.64	0.40	0.62	0.42	0.25	0.38	0.63
Total	98.04	98.04	98.23	97.39	98.26	98.21	97.83	98.39	96.63	97.69	98.49
Si	6.545	6.558	6.418	7.491	7.150	7.467	6.312	6.228	6.163	6.683	6.459
^{IV} Al	1.455	1.442	1.582	0.509	0.849	0.533	1.688	1.772	1.837	1.317	1.541
^{VI} Al	0.480	0.474	0.571	0.247	0.234	0.246	0.668	0.582	0.946	0.520	0.583
Ti	0.083	0.057	0.073	0.033	0.065	0.030	0.065	0.074	0.035	0.074	0.089
Fe ³⁺	0.352	0.320	0.366	0.130	0.122	0.148	0.371	0.595	0.471	0.242	0.357
Fe ²⁺	1.479	1.755	2.158	1.591	1.811	1.960	2.320	1.992	1.710	2.604	2.176
Mg	2.588	2.382	1.811	3.015	2.757	2.608	1.554	1.794	1.916	1.492	1.789
Mn	0.047	0.037	0.059	0.020	0.019	0.051	0.053	0.055	0.019	0.079	0.060
Ca	1.927	1.949	1.919	1.874	1.982	1.850	1.935	1.803	1.792	1.975	1.886
Na	0.385	0.372	0.345	0.181	0.261	0.222	0.467	0.577	0.525	0.359	0.425
K	0.139	0.217	0.239	0.061	0.120	0.075	0.121	0.081	0.048	0.074	0.121
M/MF	0.641	0.580	0.464	0.656	0.605	0.576	0.409	0.409	0.531	0.376	0.459

Table 2b. (cont.)

Unit	9								2*	4*	
Sample	I72/ 87	I813/ 122	I813/223		I814/367		I814/454		TSL	J83/ 132	J83/ 160
			rim	core	rim	core	rim	core			
SiO ₂	46.71	47.07	47.22	50.52	48.64	50.27	47.29	51.67	59.34	48.57	48.96
TiO ₂	0.48	0.46	0.48	0.10	0.39	0.21	0.44	0.11	0.08	0.39	0.39
Al ₂ O ₃	7.41	8.66	6.81	3.78	6.80	5.79	8.22	3.75	2.17	8.16	8.49
Fe ₂ O ₃	3.50	1.01	3.70	2.03	1.73	1.04	3.06	2.99	1.38	0.64	0.46
FeO	13.08	14.36	13.78	12.54	9.92	9.88	9.73	7.26	5.02	12.13	9.01
MgO	12.68	12.59	12.45	14.11	15.29	15.74	14.55	17.34	19.84	13.27	15.48
MnO	0.20	0.30	0.25	0.26	0.12	0.16	0.23	0.18	0.14	0.00	0.00
CaO	12.31	12.82	12.06	12.80	12.84	12.82	13.07	12.95	12.21	12.53	13.26
Na ₂ O	1.33	1.54	1.33	0.59	1.10	0.88	1.14	0.50	0.63	0.80	0.79
K ₂ O	0.75	0.99	0.73	0.40	0.59	0.40	0.86	0.19	0.05	0.10	0.30
Total	98.45	99.80	98.81	97.12	97.41	97.19	98.59	96.94	96.86	96.58	97.14
Si	6.880	6.844	6.946	7.428	7.071	7.271	6.845	7.425	7.770	7.113	7.045
"Al	1.120	1.	1.054	0.572	0.929	0.729	1.155	0.575	0.230	0.887	0.953
"Al	0.166	0.3	0.127	0.083	0.236	0.259	0.248	0.060	0.130	0.521	0.484
Ti	0.053	0.050	0.053	0.011	0.043	0.223	0.048	0.012	0.008	0.043	0.042
Fe ³⁺	0.388	0.111	0.410	0.224	0.189	0.113	0.333	0.324	0.146	0.070	0.050
Fe ²⁺	1.611	1.746	1.696	1.541	1.206	1.194	1.178	0.872	0.589	1.485	1.084
Mg	2.783	2.728	2.730	3.092	3.312	3.395	3.139	3.713	4.152	2.896	3.321
Mn	0.025	0.037	0.031	0.032	0.015	0.020	0.028	0.022	0.017	0.000	0.000
Ca	1.943	1.997	1.901	2.016	1.999	1.989	2.027	1.994	1.837	1.996	2.048
Na	0.349	0.433	0.379	0.168	0.310	0.247	0.320	0.139	0.171	0.227	0.220
K	0.141	0.184	0.137	0.075	0.109	0.075	0.159	0.035	0.009	0.019	0.055
M/MF	0.635	0.613	0.619	0.670	0.735	0.741	0.729	0.811	0.876	0.661	0.754

Notes: U1-1, U1-2 and U1-3 are surface samples of unit 1; TSL is a surface sample of the ultramafic intrusive body in unit 2; and M/MF is the atomic ratio of Mg/(Mg + Fe)

Table 2c. Calcic amphiboles in metasedimentary rocks from the White River property, Hemlo area.

Unit	2								5 + 6			
Sample	K72/ 14	K72/ 101	K72/ 117	L81/54		L81/ 81	L81/ 96	L81/ 105	I72/ 245	I72/ 250	J83/ 12	J82/ 151
				core	rim							
SiO ₂	46.17	50.71	44.53	51.09	44.16	50.79	46.09	46.78	42.16	41.46	41.71	41.13
TiO ₂	0.56	0.27	0.46	0.18	0.58	0.22	0.46	0.55	0.34	0.15	0.41	0.30
Al ₂ O ₃	9.30	4.36	9.43	4.67	9.37	5.15	8.58	8.10	11.09	12.41	14.34	12.44
Fe ₂ O ₃	2.04	0.52	1.21	0.59	2.28	0.00	1.56	1.11	6.60	9.27	5.56	6.00
FeO	15.54	14.53	18.27	13.27	15.62	14.71	15.67	15.13	16.84	14.90	17.05	16.40
MgO	10.90	13.04	8.86	13.72	9.96	12.21	10.72	10.93	8.05	7.33	6.88	7.83
MnO	0.15	0.37	0.51	0.29	0.44	0.33	0.42	0.39	0.31	0.16	0.00	0.00
CaO	12.22	12.67	12.05	13.29	12.60	13.01	12.03	13.00	11.79	10.32	11.52	12.09
Na ₂ O	1.19	0.52	1.32	0.67	1.30	0.64	1.21	0.92	1.41	1.30	1.42	1.31
K ₂ O	0.88	0.29	1.11	0.30	1.00	0.35	0.79	0.74	1.22	0.39	0.38	1.10
Total	98.95	97.28	97.75	98.07	97.32	97.41	97.53	97.65	99.81	97.69	99.27	98.57
Si	6.802	7.463	6.755	7.426	6.681	7.461	6.892	6.963	6.337	6.288	6.224	6.233
"Al	1.198	0.537	1.245	0.574	1.319	0.539	1.108	1.037	1.663	1.712	1.776	1.767
"Al	0.418	0.219	0.442	0.226	0.352	0.352	0.405	0.384	0.302	0.508	0.746	0.456
Ti	0.062	0.030	0.053	0.020	0.066	0.024	0.052	0.062	0.038	0.017	0.046	0.034
Fe ³⁺	0.227	0.058	0.139	0.065	0.260	0.000	0.175	0.124	0.747	1.058	0.624	0.685
Fe ²⁺	1.915	1.788	2.318	1.612	1.977	1.807	1.960	1.883	2.117	1.891	2.128	2.075
MgO	2.393	2.860	2.003	2.972	2.246	2.672	2.389	2.424	1.803	1.657	1.530	1.748
Mn	0.019	0.046	0.066	0.036	0.056	0.041	0.053	0.049	0.040	0.021	0.000	0.000
Ca	1.929	1.998	1.959	2.070	2.042	2.047	1.928	2.073	1.899	1.677	1.842	1.963
Na	0.339	0.148	0.388	0.189	0.381	0.182	0.350	0.266	0.411	0.382	0.410	0.370
K	0.165	0.054	0.215	0.056	0.193	0.066	0.151	0.141	0.234	0.076	0.072	0.213
M/MF	0.557	0.619	0.472	0.651	0.538	0.600	0.555	0.568	0.465	0.470	0.418	0.460

Notes: M/MF is the atomic ratio of Mg/(Mg + Fe + Mn).

Table 2d. Calcic amphiboles in other rock-types from the White River property, Hemlo area.

Lithology	Cr-rich calc-silicates				Fe-rich calc-silicates					veins		
	Sample	K72/ 43	K72/ 80	L81/ 19	L81/ 28	I87/150 *	I87/150 **	J83/ 91	K91/12 *	K91/12 **	U1-1	I72/ 370
SiO ₂	52.14	55.36	52.13	54.14	40.81	51.50	39.09	40.75	48.23	57.11	53.10	56.56
TiO ₂	0.00	0.00	0.06	0.00	0.71	0.11	0.72	0.56	0.16	0.04	0.15	0.00
Al ₂ O ₃	3.38	1.27	2.52	0.63	11.35	2.34	12.05	11.30	4.13	0.13	2.74	1.56
Cr ₂ O ₃	0.09	0.07	0.45	0.70	nd	nd	nd	nd	nd	nd	nd	0.02
Fe ₂ O ₃	0.58	0.08	1.14	0.78	4.67	0.58	6.04	5.47	3.59	0.00	----	----
FeO	11.74	10.14	12.37	12.21	19.88	18.51	22.39	21.57	21.61	5.89	14.89	6.94
MgO	15.47	17.38	14.39	15.52	5.58	10.78	3.51	4.35	7.42	20.91	14.52	19.04
MnO	0.28	0.20	0.42	0.57	0.73	0.63	0.57	0.48	0.56	0.32	0.00	0.00
CaO	12.70	12.93	13.04	13.30	12.13	12.50	11.99	12.18	12.11	13.77	12.29	13.57
Na ₂ O	0.66	0.47	0.21	0.04	1.51	0.28	1.11	1.18	0.46	0.05	0.26	0.12
K ₂ O	0.22	0.18	0.27	0.06	0.58	0.02	1.47	0.75	0.14	0.02	0.00	0.00
Total	97.53	96.83	97.01	97.95	97.97	97.25	98.94	98.59	98.41	98.24	98.20	98.00
Si	7.582	7.866	7.657	7.860	6.324	7.706	6.129	6.328	7.338	7.928	7.685	7.896
"Al	0.419	0.134	0.343	0.110	1.676	0.294	1.871	1.672	0.662	0.022	0.315	0.104
"Al	0.160	0.079	0.093	0.000	0.397	0.119	0.357	0.397	0.079	0.000	0.154	0.153
Ti	0.000	0.006	0.007	0.000	0.083	0.012	0.085	0.065	0.018	0.004	0.017	0.000
Cr	0.012	0.010	0.053	0.082	-----	-----	-----	-----	-----	-----	-----	0.006
Fe ⁺	0.063	0.008	0.127	0.086	0.546	0.066	0.713	0.640	0.411	0.000	-----	-----
Fe ⁺⁺	1.421	1.210	1.519	1.482	2.576	2.316	2.935	2.801	2.749	0.684	1.804	0.896
Mg	3.336	3.680	3.150	3.358	1.289	2.404	0.820	1.007	1.682	4.326	3.139	3.964
Mn	0.034	0.024	0.052	0.070	0.096	0.080	0.076	0.063	0.072	0.038	0.000	0.000
Ca	1.969	1.970	2.052	2.069	2.014	2.004	2.014	2.027	1.974	2.048	1.913	2.032
Na	0.180	0.077	0.060	0.011	0.454	0.081	0.338	0.355	0.137	0.014	0.073	0.032
K	0.041	0.054	0.051	0.011	0.115	0.004	0.294	0.149	0.027	0.004	0.000	0.000
M/MF	0.701	0.753	0.675	0.694	0.350	0.517	0.234	0.276	0.390	0.865	0.635	0.816

Notes: * and ** in samples of the Fe-rich calc-silicates are brownish green hornblende and colourless actinolite, respectively; nd is "not detectable"; and M/MF is the atomic ratio of Mg/(Mg + Fe + Mn).

APPENDIX II (cont.)

TABLE 3 GARNET COMPOSITIONS

Table 3a. Pyrospite from the White River property, Hemlo area.

Unit	1		2	4		5					
Sample	M131/ 81	M131/ 95	L81/ 16	J83/ 77	J91/ 99	I92/245 core rim		I82/119 core rim		I82/144 core rim	
SiO ₂	38.02	37.30	37.64	36.62	37.13	36.52	36.13	36.45	37.14	36.70	36.79
Al ₂ O ₃	19.97	20.97	21.79	21.45	21.18	21.62	21.13	21.64	21.11	21.75	21.64
FeO*	29.79	29.58	31.55	31.63	31.87	29.76	29.60	33.53	33.36	34.48	34.41
MgO	2.71	2.47	2.84	3.00	4.27	3.03	3.30	3.32	3.06	3.56	3.09
MnO	4.61	3.95	4.65	2.83	1.80	7.13	6.18	0.87	0.93	0.39	0.68
CaO	5.14	5.21	1.99	4.34	3.18	2.68	3.17	3.86	4.42	3.91	4.73
Total	100.3	99.53	99.86	99.87	99.42	100.7	99.51	99.67	100.0	100.8	101.3
Si	3.045	2.997	3.002	2.947	2.977	2.929	2.931	2.935	2.980	2.926	2.926
^{IV} Al	0.000	0.003	0.000	0.053	0.023	0.071	0.069	0.065	0.020	0.074	0.074
^{VI} Al	1.886	1.984	2.047	1.986	1.981	1.974	1.951	1.988	1.980	1.964	1.955
Mg	0.324	0.269	0.338	0.360	0.511	0.363	0.399	0.399	0.366	0.423	0.367
Ca	0.441	0.449	0.170	0.374	0.275	0.231	0.276	0.333	0.380	0.334	0.403
Mn	0.313	0.296	0.314	0.193	0.134	0.485	0.425	0.059	0.063	0.027	0.046
Fe	1.996	1.988	2.103	2.229	2.134	1.997	2.008	2.258	2.238	2.299	2.289
pyp	10.8	9.0	11.6	11.8	16.9	11.8	12.8	13.1	12.0	13.7	11.8
gr	14.7	15.0	5.8	12.3	9.0	7.5	8.9	10.9	12.5	10.8	12.9
sps	10.4	9.9	10.7	6.3	3.9	15.8	13.7	2.0	2.1	0.9	1.5
alm	64.5	66.1	71.3	69.6	70.2	65.0	64.6	74.1	73.5	75.4	73.7
M/MF	0.247	0.222	0.346	0.141	0.232	0.298	0.291	0.148	0.166	0.164	0.164

Table 3a. (cont.)

Unit	6		7		8						8
Sample	I812/313 core rim		I812/345 core rim		I813/315 core rim		I815/520 core rim		J82/92 core rim		I87/ 67
SiO ₂	37.38	37.37	37.67	37.53	36.53	36.94	37.29	37.17	36.99	36.60	37.38
Al ₂ O ₃	21.59	22.25	22.14	22.12	21.52	22.02	21.34	21.26	21.45	21.48	21.88
FeO*	29.08	31.21	30.74	31.92	30.51	31.46	33.90	34.86	30.96	31.25	28.25
MgO	3.61	4.46	4.61	5.04	2.00	3.12	3.32	2.87	4.08	4.75	2.63
MnO	4.41	2.13	2.55	1.17	6.43	4.80	0.44	0.59	3.86	1.89	9.34
CaO	3.71	2.79	2.91	3.07	2.71	2.46	3.76	2.93	3.03	2.99	1.83
Total	99.78	100.2	100.6	100.8	99.70	100.8	100.1	99.68	100.4	98.96	101.3
Si	2.984	2.958	2.967	2.950	2.963	2.946	2.975	2.994	2.952	2.975	2.974
^{IV} Al	0.016	0.042	0.033	0.050	0.037	0.054	0.025	0.006	0.048	0.056	0.026
^{VI} Al	2.014	2.032	2.022	1.999	2.019	2.015	1.998	2.011	1.968	1.980	2.024
Mg	0.429	0.526	0.541	0.591	0.242	0.371	0.396	0.345	0.485	0.570	0.312
Ca	0.318	0.237	0.246	0.259	0.236	0.210	0.288	0.253	0.259	0.258	0.156
Mn	0.298	0.143	0.170	0.128	0.442	0.324	0.030	0.040	0.261	0.129	0.630
Fe	1.941	2.066	2.025	2.099	2.069	2.098	2.296	2.348	2.066	2.102	1.779
pyp	14.4	17.7	18.2	19.5	8.1	12.4	1.32	11.5	15.8	18.6	10.5
gr	10.6	8.0	8.2	8.6	7.9	7.0	10.8	8.5	8.4	8.4	5.2
sps	10.0	4.8	5.7	2.6	14.8	10.8	1.0	1.4	8.5	4.2	21.2
alm	65.0	69.5	67.9	69.4	69.3	69.9	75.1	78.6	67.3	68.1	63.3
M/MF	0.272	0.245	0.260	0.255	0.248	0.249	0.157	0.141	0.265	0.250	0.346

Notes: FeO* is total iron content; pyp is pyrope; gr is grossular; sps is spessartine; alm is almandine; and M/MF is the atomic ratio of Mg/(Mg + Fe + Mn).

TABLE 3 GARNET COMPOSITIONS (cont.)

Table 3b. Ugrandite from the White River property, Hemlo area.

Lithology	Cr-rich calc-silicates						Fe-rich calc-silicates					
	K72/80		L81/28		K72/80	K72/43		L81/19	I87/150	J83/91B		
Sample	core	rim	core	rim	80	core	rim	19	150	rim	core	
SiO ₂	36.50	37.37	35.87	35.83	39.23	37.40	37.41	37.80	37.06	36.96	36.45	
TiO ₂	0.60	0.44	0.22	0.16	0.38	1.41	1.42	0.54	0.40	0.07	0.07	
Al ₂ O ₃	4.00	10.05	5.40	6.39	19.75	11.93	12.19	14.98	18.37	17.54	16.56	
Cr ₂ O ₃	20.05	12.67	20.12	18.48	0.27	5.15	3.88	0.96	nd	nd	nd	
Fe ₂ O ₃ *	4.84	3.62	3.28	4.57	3.84	8.53	9.83	8.90	22.67	22.44	19.72	
FeO	0.58	2.96	1.44	1.66	1.88	0.00	0.00	0.63				
MnO	1.00	1.56	0.80	0.72	0.59	0.50	0.50	1.00	8.40	4.17	5.27	
MgO	0.16	0.12	0.03	0.02	0.13	0.07	0.07	0.05	0.56	0.46	0.30	
CaO	33.00	31.01	32.39	32.43	34.68	35.28	35.66	35.01	11.93	16.38	18.38	
Total	99.70	99.80	99.60	100.2	100.7	100.3	100.9	99.90	99.41	98.06	96.78	
Si	2.978	3.002	2.957	2.920	2.980	2.951	2.931	2.984	3.064	3.065	3.066	
Al	0.384	0.952	0.524	0.613	1.767	1.110	1.125	1.394	1.787	1.714	1.642	
Ti	0.036	0.027	0.011	0.010	0.022	0.083	0.083	0.041	0.025	0.004	0.004	
Cr	1.293	0.806	1.312	1.191	0.016	0.322	0.240	0.062	0.000	0.000	0.000	
Fe ³⁺	0.296	0.218	0.198	0.280	0.219	0.506	0.579	0.528	0.211	0.146	0.321	
Fe ²⁺	0.040	0.199	0.099	0.113	0.120	0.000	0.000	0.042	1.200	1.254	0.938	
Mn	0.069	0.106	0.056	0.050	0.038	0.033	0.033	0.067	0.588	0.293	0.376	
Mg	0.019	0.014	0.003	0.002	0.015	0.008	0.008	0.006	0.069	0.057	0.037	
Ca	2.883	2.671	2.860	2.830	2.822	2.983	3.010	2.968	1.057	1.458	1.659	
gr	14.9	37.0	18.9	21.2	8.26	54.1	54.9	65.4	27.5	39.2	38.9	
andr	1.48	10.9	9.9	14.0	11.0	25.3	28.9	26.4	10.6	7.3	16.1	
uv	64.7	40.3	65.6	59.6	0.8	16.1	12.0	3.1	0.0	0.0	0.0	
alm	1.3	6.6	3.3	3.8	4.0	0.0	0.0	1.4	40.0	41.8	31.3	
spa	2.3	3.5	1.9	1.7	1.3	1.1	1.1	2.2	19.6	9.8	12.5	
pyp	0.6	0.5	0.1	0.1	0.5	0.3	0.3	0.2	2.3	1.9	1.2	
F/FA	0.435	0.186	0.274	0.313	0.110	0.313	0.339	0.275	0.106	0.078	0.164	

Notes: Fe₂O₃ is total iron content; gr is grossular; andr is andradite; uv is uvarovite; alm is almandine; spa is spessartine; pyp is pyrope; and F/FA is the Fe³⁺/(Fe³⁺ + Al) atomic ratio.

APPENDIX II (cont.)

TABLE 4 MICA COMPOSITIONS

Table 4a. Dioctahedral micas from the White River property, Keokuk area

Unit	Local Shear Zone											
Sample	I72/ 179	I84/ 75	I813/ 315	I85/ 63	I85/ 67	I87/ 134	plt	I815/435 vein	marg	I72/ 150	I92/ 95	I91/ 49
SiO ₂	46.89	45.07	46.95	48.77	48.16	46.36	44.02	48.03	30.02	46.33	45.48	47.76
TiO ₂	0.61	0.46	0.66	0.63	0.00	0.89	0.69	0.04	0.09	0.51	0.67	0.58
Al ₂ O ₃	36.08	36.57	35.73	32.70	33.75	36.59	38	38.16	50.81	35.89	34.13	34.13
FeO*	1.02	0.67	0.72	1.75	1.16	0.29	1.15	0.66	0.42	0.72	2.80	1.17
MnO	0.01	0.04	0.00	0.06	0.00	0.09	0.00	0.00	0.00	0.17	0.00	0.00
MgO	0.55	0.42	0.62	1.19	1.27	1.51	0.92	0.19	0.18	0.68	0.92	0.48
CaO	0.00	0.02	0.00	0.00	0.00	0.01	0.01	0.01	11.63	0.00	0.01	0.00
BaO	0.00	0.75	0.00	0.31	0.00	0.60	0.20	0.04	0.04	0.28	0.00	0.29
Na ₂ O	1.45	1.80	1.17	0.25	0.02	0.46	0.78	0.19	1.25	1.21	0.90	0.81
K ₂ O	9.30	8.54	10.17	9.58	11.56	9.22	10.05	8.39	0.18	9.74	10.35	8.80
Total	95.87	94.38	96.02	95.28	95.92	96.11	93.28	95.56	94.63	95.51	95.25	94.02
Si	6.160	6.036	6.177	6.459	6.373	6.071	6.003	6.222	4.017	6.123	6.119	6.370
Al	1.840	1.964	1.823	1.541	1.627	1.929	1.997	1.778	3.983	1.877	1.881	1.630
Al	3.746	3.807	3.716	3.562	3.625	3.717	3.689	4.046	4.028	3.745	3.531	3.734
Ti	0.061	0.046	0.065	0.063	0.000	0.088	0.071	0.001	0.001	0.048	0.067	0.058
Fe	0.097	0.075	0.079	0.194	0.128	0.032	0.131	0.071	0.047	0.074	0.315	0.131
Mn	0.001	0.005	0.000	0.007	0.000	0.010	0.000	0.000	0.000	0.038	0.000	0.000
Mg	0.108	0.084	0.122	0.235	0.250	0.295	0.187	0.037	0.036	0.122	0.185	0.095
Ca	0.000	0.003	0.000	0.000	0.000	0.001	0.001	0.001	1.667	0.000	0.001	0.000
Ba	0.000	0.039	0.000	0.016	0.000	0.031	0.011	0.002	0.002	0.013	0.000	0.015
Na	0.369	0.467	0.298	0.064	0.005	0.117	0.206	0.013	0.324	0.301	0.235	0.209
K	1.572	1.459	1.707	1.618	1.951	1.540	1.748	1.386	0.031	1.648	1.776	1.497
M/MF	0.523	0.513	0.605	0.539	0.661	0.867	0.588	0.339	0.433	0.576	0.369	0.420

Notes: plt, vein and marg in sample I815/435 are platy muscovite; vein sericite and margarite, respectively; FeO* is total iron conte; and M/MF is the atomic ratio of Mg/(Mg + Fe + Mn).

Table 4b. Trioctahedral micas from the White River property, Keokuk area.

Unit	Local Shear Zone											
Sample	U1-1	M131/ 81	K72/ 14	K72/ 101	K72/ 142	L81/ 16	L81/ 54	L81/ 96	L81/ 105	L81/ 145	J83/ 77	J91/ 91
SiO ₂	36.27	36.66	37.66	37.66	37.93	35.78	37.47	38.86	37.24	35.28	35.75	35.23
TiO ₂	1.96	2.44	2.18	2.20	2.06	1.73	1.68	1.49	2.22	2.45	1.90	1.69
Al ₂ O ₃	17.75	17.44	15.41	15.86	15.28	18.21	15.70	16.61	15.83	16.73	16.37	17.12
FeO*	17.37	18.93	19.32	20.19	20.80	17.49	18.10	18.70	18.98	22.04	21.80	19.64
MgO	0.12	0.16	0.32	0.12	0.08	0.20	0.26	0.29	0.30	0.25	0.20	0.17
MnO	12.53	10.54	12.02	10.71	10.74	12.13	12.80	11.11	10.03	8.33	9.59	11.52
CaO	0.13	0.06	0.04	0.03	0.02	0.06	0.16	0.03	0.00	0.02	0.00	0.00
Na ₂ O	0.03	0.06	0.00	0.10	0.09	0.25	0.06	0.01	0.04	0.04	0.06	0.00
K ₂ O	8.92	9.29	9.63	9.47	9.84	8.83	8.97	9.75	9.46	8.84	9.41	8.22
Total	95.52	96.23	96.58	96.79	96.84	95.01	95.48	97.68	94.30	94.30	95.02	93.68
Si	5.455	5.536	5.660	5.674	5.722	5.451	5.655	5.761	5.728	5.516	5.553	5.445
Al	2.545	2.464	2.340	2.326	2.278	2.549	2.345	2.239	2.272	2.484	2.467	2.555
Al	0.600	0.640	0.389	0.489	0.438	0.703	0.447	0.676	0.597	0.598	0.518	0.563
Ti	0.222	0.277	0.246	0.249	0.234	0.143	0.191	0.167	0.257	0.288	0.221	0.196
Fe	2.185	2.391	2.528	2.544	2.624	2.227	2.284	2.329	2.441	2.882	2.821	2.538
Mn	0.015	0.021	0.041	0.015	0.010	0.026	0.033	0.037	0.039	0.033	0.026	0.022
Mg	2.809	2.372	2.693	2.405	2.415	2.755	2.879	2.466	2.299	1.941	2.212	2.654
Ca	0.021	0.010	0.006	0.005	0.003	0.000	0.006	0.005	0.000	0.003	0.000	0.000
Na	0.009	0.019	0.000	0.029	0.026	0.074	0.108	0.003	0.012	0.012	0.000	0.027
K	1.722	1.789	1.846	1.820	1.893	1.719	1.727	1.852	1.856	1.763	1.857	1.620
M/MF	0.564	0.500	0.530	0.488	0.480	0.555	0.560	0.518	0.489	0.407	0.442	0.513

TABLE 4 MICAL COMPOSITIONS (cont.)

Table 4b. (cont.)

Unit	4*		5		6						
Sample	I72/ 382	I72/ 268	I92/ 245	I82/119 core rim		I82/144 core rim		I812/313 core rim		I812/345 core rim	
SiO ₂	39.02	36.50	36.48	37.06	37.38	37.43	38.55	36.48	36.56	37.44	37.32
TiO ₂	0.48	2.10	1.39	1.04	1.44	1.00	1.73	1.39	1.00	1.38	0.97
Al ₂ O ₃	14.74	18.17	17.18	17.48	16.68	18.04	17.09	17.18	17.75	17.39	17.43
FeO*	10.73	18.48	15.98	17.97	20.24	18.12	19.73	15.58	17.37	14.92	16.75
MnO	0.08	0.31	0.30	0.11	0.00	0.11	0.00	0.30	0.49	0.09	0.12
MgO	20.68	11.19	14.65	12.93	110.5	12.04	10.85	14.65	12.87	14.58	12.72
CaO	0.09	0.00	0.00	0.02	0.00	0.08	0.03	0.00	0.00	0.00	0.00
Na ₂ O	0.12	0.30	0.19	0.22	0.18	0.16	0.03	0.19	0.02	0.46	0.04
K ₂ O	8.36	8.43	8.76	9.01	8.80	8.88	9.12	9.08	9.38	9.56	9.08
Total	94.42	96.10	95.02	95.84	95.72	95.86	96.74	94.85	95.44	94.82	94.39
Si	5.715	5.474	5.564	5.548	5.625	5.589	5.774	5.502	5.535	5.584	5.649
²⁷ Al	2.285	2.526	2.436	2.452	2.375	2.411	2.226	2.498	2.465	2.416	2.351
²⁹ Al	0.256	0.685	0.614	0.631	0.583	0.763	0.783	0.555	0.702	0.640	0.758
Ti	0.053	0.237	0.181	0.117	0.163	0.112	0.150	0.158	0.114	0.155	0.110
Fe	1.313	2.318	2.347	2.248	2.547	2.261	2.471	1.964	2.188	1.859	2.180
Mn	0.010	0.039	0.024	0.014	0.000	0.013	0.000	0.037	0.061	0.011	0.015
Mg	4.511	2.501	2.633	2.885	2.479	2.681	2.429	3.293	2.293	3.242	2.766
Ca	0.014	0.000	0.002	0.004	0.000	0.013	0.005	0.000	0.000	0.000	0.000
Na	0.034	0.087	0.020	0.063	0.053	0.047	0.009	0.056	0.006	0.138	0.012
K	1.560	1.613	1.681	1.725	1.689	1.696	1.742	1.747	1.811	1.628	1.745
M/MF	0.775	0.523	0.531	0.563	0.493	0.544	0.495	0.629	0.518	0.636	0.439

Table 4b. (cont.)

Unit	6		LSZ		8		9					
Sample	I813/315 core rim		I815/520 core rim		I85/ 63	I810/ 338	I72/ 130	I87/ 67	I72/ 50	I813/ 122	I814/ 454	I817/ 100
SiO ₂	38.04	36.14	35.62	35.35	36.67	40.90	38.33	37.27	37.41	36.38	38.26	36.78
TiO ₂	1.40	1.77	1.53	1.00	1.87	0.91	0.79	1.91	2.43	1.79	0.90	1.71
Al ₂ O ₃	18.39	18.39	16.87	17.03	17.90	18.38	17.30	15.67	16.01	16.53	17.86	15.37
FeO*	17.92	18.66	19.42	22.31	15.94	5.51	14.79	17.27	17.02	17.90	14.63	17.15
MnO	0.20	0.05	0.04	0.42	0.40	0.33	0.24	0.32	0.39	0.22	0.21	0.20
MgO	12.74	9.86	11.89	9.52	11.81	19.81	13.86	12.02	11.65	12.66	14.07	13.16
CaO	0.08	0.00	0.02	0.01	0.08	0.00	0.06	0.02	0.00	0.02	0.02	0.04
Na ₂ O	0.25	0.09	0.34	0.00	0.13	0.09	0.09	0.08	0.03	0.09	0.05	0.06
K ₂ O	8.83	9.48	8.75	9.48	9.25	10.81	9.52	10.00	9.80	9.79	9.81	9.97
Total	95.21	94.79	94.98	95.20	94.26	96.96	95.46	94.59	95.40	95.49	96.01	94.54
Si	5.649	5.517	5.517	5.516	5.551	5.722	5.688	5.685	5.661	5.514	5.636	5.618
²⁷ Al	2.351	2.483	2.483	2.484	2.449	2.278	2.312	2.315	2.339	2.486	2.364	2.382
²⁹ Al	0.644	0.825	0.595	0.647	0.744	0.732	0.714	0.502	0.516	0.467	0.737	0.385
Ti	0.156	0.203	0.178	0.117	0.213	0.096	0.086	0.219	0.277	0.204	0.100	0.196
Fe	2.228	2.382	2.513	2.919	2.018	0.645	1.836	2.197	2.154	2.269	1.802	2.191
Mn	0.000	0.022	0.005	0.056	0.051	0.063	0.030	0.041	0.050	0.028	0.026	0.026
Mg	2.644	2.243	2.745	2.214	2.665	4.131	3.066	2.733	2.628	2.860	3.089	2.996
Ca	0.013	0.000	0.006	0.003	0.013	0.000	0.010	0.000	0.000	0.003	0.003	0.007
Na	0.075	0.021	0.102	0.000	0.087	0.024	0.026	0.024	0.009	0.026	0.014	0.018
K	1.603	1.846	1.728	1.887	1.786	1.933	1.802	1.946	1.892	1.893	1.843	1.943
M/MF	0.543	0.487	0.523	0.442	0.574	0.867	0.628	0.558	0.554	0.560	0.634	0.580

Notes: U1-1 is a surface sample of unit 1 mafic met-volcanic rocks; 4* is actinolite-chlorite schist in unit 4 (representing the Hemle Fault Zone); LSZ is the Local Shear Zone; FeO* is total iron content; and M/MF is the atomic ratio of Mg/(Mg + Fe + Mn).

TABLE 5 CHLORITE COMPOSITIONS

Unit	1	2	CFZ			4			5	6	LSZ	
Sample	U1-1	L81/ 96	K72/ 80	No.2	No.7*	J83/ 91	J71/ 51	J71/ 52	I72/ 268	J82/ 92	I812/ 313	I816/ 439
SiO ₂	27.06	27.47	28.05	27.03	28.06	24.36	31.25	29.66	30.46	25.53	25.61	22.61
TiO ₂	0.02	0.01	0.00	0.00	0.00	0.06	0.00	0.00	0.59	0.15	0.09	0.02
Al ₂ O ₃	18.75	18.33	18.00	18.89	17.32	17.89	13.36	17.85	18.74	22.06	22.13	28.75
Cr ₂ O ₃	0.00	0.00	1.01	3.50	1.24	0.00	0.67	0.79	0.11	0.00	0.00	0.01
FeO*	24.02	25.54	19.04	17.13	16.99	39.54	8.34	11.02	22.53	18.57	19.09	16.74
MgO	17.84	16.13	20.02	19.74	20.31	4.98	30.06	27.97	15.28	19.34	19.21	16.95
MnO	0.29	0.35	0.30	0.36	0.34	0.94	0.10	0.11	0.39	0.20	0.11	0.58
CaO	0.01	0.05	0.02	0.02	0.02	0.17	0.00	0.02	0.09	0.00	0.00	0.19
Na ₂ O	0.00	0.00	0.00	0.00	0.00	0.00	0.00	0.01	0.28	0.00	0.00	0.16
K ₂ O	0.00	0.00	0.00	0.05	0.00	0.04	0.00	0.00	1.95	0.04	0.00	0.00
Total	85.99	87.88	86.89	86.72	84.54	87.98	83.78	87.43	90.42	85.89	86.24	86.02
Si	5.772	5.778	5.873	5.648	5.907	5.594	6.305	5.814	6.152	5.301	5.305	4.666
Al	2.228	2.222	2.127	2.352	2.093	2.406	1.695	2.186	1.848	2.699	2.695	3.334
Al	2.486	2.321	2.146	2.298	2.204	2.435	1.481	1.937	2.612	2.699	2.706	3.659
Ti	0.003	0.002	0.000	0.000	0.000	0.010	0.000	0.000	0.090	0.023	0.014	0.002
Cr	0.000	0.000	0.163	0.578	0.206	0.000	0.107	0.122	0.018	0.000	0.000	0.001
Fe	4.285	4.493	3.128	3.449	2.991	7.593	1.407	1.806	3.805	3.225	3.307	2.887
Mg	5.036	5.057	6.148	5.335	6.373	1.704	9.040	8.172	4.600	5.986	5.931	5.217
Mn	0.052	0.062	0.005	0.064	0.061	0.183	0.017	0.018	0.067	0.035	0.019	0.100
Ca	0.002	0.011	0.005	0.004	0.005	0.042	0.000	0.004	0.019	0.000	0.000	0.041
Na	0.000	0.000	0.000	0.000	0.000	0.000	0.000	0.004	0.110	0.000	0.000	0.063
K	0.000	0.000	0.000	0.013	0.000	0.012	0.000	0.000	0.502	0.011	0.000	0.000
M/MF	0.537	0.526	0.652	0.603	0.681	0.180	0.864	0.777	0.543	0.647	0.641	0.648

Notes: CFZ is Cadi Fracture Zone; LSZ is Local Shear Zone; U1-1 is a surface sample from unit 1, No.2 and No.7* are surface samples from Cadi Fracture Zone; FeO* is total iron content; nd is "not detected"; and M/MF is the atomic ratio of Mg/(Mg + Fe + Mn).

APPENDIX II (cont.)

TABLE 6 EPIDOTE-GROUP MINERAL COMPOSITIONS

Table 6a. Epidote-group minerals in calc-silicates from the White River property, Hemlo area.

Lithology	Cr-rich calc-silicates						Fe-rich calc-silicates				
	Sample	K72/43	No.2	No.7	L81/19	K72/80	No.7*	J83/91	I87/150	K91/12	
SiO ₂	35.82	37.30	38.41	38.15	39.03	38.11	40.98	39.80	37.18	36.94	37.20
TiO ₂	0.03	0.04	0.09	0.10	0.05	0.10	0.02	0.10	0.15	0.16	0.19
Al ₂ O ₃	16.04	19.70	23.01	23.84	22.20	23.61	29.74	24.65	22.45	22.35	22.72
Cr ₂ O ₃	11.77	6.56	1.57	0.53	2.63	0.30	0.07	0.05	nd	nd	nd
Fe ₂ O ₃ *	9.29	8.62	10.77	10.68	10.18	11.70	3.97	3.59	11.96	13.28	12.03
MnO	0.23	0.36	0.01	0.16	0.07	0.18	0.19	0.28	0.06	0.20	0.00
MgO	0.06	0.07	0.05	0.04	0.18	0.02	0.00	0.00	0.00	0.00	0.00
CaO	22.52	22.50	23.10	23.84	23.15	23.38	24.70	24.51	24.21	23.94	24.11
Na ₂ O	0.00	0.00	0.00	0.00	0.00	0.00	0.00	0.03	0.00	0.00	0.00
K ₂ O	0.00	0.00	0.00	0.00	0.02	0.02	0.00	0.00	0.00	0.00	0.00
Total	95.76	95.15	97.10	97.34	97.51	97.42	99.67	97.85	95.99	96.90	96.03
Si	2.940	3.004	3.003	2.975	3.038	2.979	2.988	2.939	3.093	3.066	3.083
Al	1.552	1.870	2.128	2.191	2.036	2.175	2.554	2.567	2.201	2.186	2.219
Ti	0.002	0.002	0.005	0.006	0.003	0.006	0.001	0.006	0.010	0.010	0.012
Cr	0.764	0.418	0.097	0.032	0.162	0.019	0.004	0.003	-----	-----	-----
Fe	0.638	0.581	0.704	0.696	0.663	0.765	0.242	0.200	0.831	0.920	0.833
Mn	0.016	0.025	0.001	0.011	0.005	0.012	0.012	0.004	0.004	0.014	0.000
Mg	0.007	0.008	0.006	0.004	0.021	0.002	0.000	0.000	0.000	0.000	0.000
Ca	1.981	1.942	1.935	1.991	1.931	1.958	1.929	1.972	2.161	2.131	2.145
Na	0.000	0.000	0.000	0.000	0.000	0.000	0.000	0.004	0.000	0.000	0.000
K	0.000	0.000	0.000	0.000	0.002	0.002	0.000	0.000	0.000	0.000	0.000
Ps			24.9	19.6	24.5	26.2	8.7	7.2	27.4	29.5	27.5

Table 6b. Epidote-group minerals from the White River property, Hemlo area.

Unit	1	2	3	4	7	9					
Sample	U1-1 vein	K71/117	L81/54	J83/39	K91/126	K91/40	J91/86	I72/370	I815/493	I72/87	I812/197
SiO ₂	37.30	37.88	37.12	37.88	37.55	38.67	38.19	37.67	37.89	37.56	38.34
TiO ₂	0.05	0.16	0.03	0.06	nd	0.04	0.00	0.00	0.00	0.00	0.04
Al ₂ O ₃	24.65	23.98	20.97	23.68	21.36	21.81	21.45	21.26	22.91	21.12	23.95
Cr ₂ O ₃	nd	0.13	nd	0.03	nd	nd	0.00	0.00	0.00	0.00	0.00
Fe ₂ O ₃ *	10.98	11.39	11.87	11.95	14.96	13.13	14.12	14.75	13.34	14.81	12.63
MnO	0.26	0.20	0.18	0.35	0.11	0.00	0.00	0.00	0.30	0.00	0.00
MgO	0.00	0.05	0.00	0.05	0.00	0.02	0.00	0.00	0.00	0.00	0.00
CaO	24.74	22.88	25.00	23.28	22.10	24.23	23.96	23.08	23.41	22.75	22.48
Na ₂ O	0.05	0.12	0.09	0.05	0.00	0.00	0.00	0.05	0.00	0.09	0.05
K ₂ O	0.00	0.02	0.03	0.05	0.00	0.00	0.00	0.00	0.00	0.00	0.02
Total	97.53	96.81	95.29	97.36	96.08	97.90	97.72	96.81	97.84	96.33	97.52
Si	3.033	2.972	3.003	2.968	3.146	3.096	3.059	3.048	3.099	3.143	3.056
Al	2.362	2.216	1.999	2.187	2.109	2.057	2.024	2.026	2.208	2.083	2.310
Ti	0.003	0.009	0.002	0.004	-----	0.002	0.000	0.000	0.000	0.000	0.002
Cr	-----	0.008	-----	0.002	-----	-----	0.000	0.000	0.000	0.000	0.000
Fe	0.745	0.747	0.803	0.783	1.046	0.795	0.856	0.901	0.912	1.036	0.863
Mn	0.018	0.013	0.012	0.023	0.008	0.000	0.000	0.000	0.021	0.000	0.000
Mg	0.000	0.006	0.000	0.006	0.000	0.002	0.000	0.000	0.000	0.000	0.000
Ca	2.115	1.923	2.167	1.955	1.987	2.081	2.059	2.004	2.055	2.043	1.975
Na	0.008	0.018	0.014	0.008	0.000	0.000	0.000	0.008	0.000	0.015	0.008
K	0.000	0.002	0.003	0.003	0.000	0.000	0.000	0.000	0.000	0.000	0.002
Ps	24.0	25.5	28.7	26.8	33.2	27.9	29.7	30.8	29.2	33.5	27.2

Notes: No.2, No.7 and No.7* are surface samples from the Cadi Fracture Zone; U1-1 is a surface sample of unit 1 mafic metavolcanic rocks; Fe₂O₃* is total iron content; Ps is pistacite content; and "nd" is not detected.

TABLE 6 EPIDOTE-GROUP MINERAL COMPOSITIONS (cont.)

Table 6C Epidote-group minerals in the Local Shear Zone of the White River property

Sample	I815/439							I85/ 63		I816/ 474	
	allanite		core*		clinzoisite			epidote			
Mineral	mrgrn	core	mrgrn*	core*	ncl.	incl.	vein	env.	vein		
SiO ₂	33.37	35.07	32.66	34.07	38.25	40.41	39.89	39.05	38.78	38.44	38.69
TiO ₂	0.15	0.18	0.10	0.05	nd	nd	nd	nd	nd	0.04	0.05
Al ₂ O ₃	20.60	23.81	19.10	21.06	29.52	31.25	30.76	27.90	27.77	26.46	28.29
FeO*	7.93	5.90	6.11	5.15	3.10	1.57	1.66	5.52	5.87	6.95	5.94
HgO	1.20	0.56	1.19	0.61	nd	nd	nd	nd	nd	0.02	nd
MnO	1.29	0.54	1.17	0.55	0.30	nd	0.04	0.03	0.05	0.40	0.12
CaO	13.12	17.56	12.87	15.12	21.07	24.03	24.11	24.08	24.01	23.91	24.31
Na ₂ O	0.12	0.20	0.15	0.10	nd	nd	nd	nd	nd	nd	nd
La ₂ O ₃	4.48	2.10	3.75	1.91	0.99	nd	nd	nd	nd	nd	nd
Ce ₂ O ₃	9.00	4.56	8.64	4.16	2.10	nd	nd	nd	nd	nd	nd
Nd ₂ O ₃	4.15	2.90	3.91	2.68	1.15	nd	nd	nd	nd	nd	nd
Sm ₂ O ₃	0.56	0.48	0.34	0.47	nd	nd	nd	nd	nd	nd	nd
Eu ₂ O ₃	nd	nd	nd	nd	nd	nd	nd	nd	nd	nd	nd
Gd ₂ O ₃	0.51	0.42	0.51	0.47	nd	nd	nd	nd	nd	nd	nd
Dy ₂ O ₃	0.52	0.47	0.50	0.45	nd	nd	nd	nd	nd	nd	nd
Yb ₂ O ₃	0.06	0.05	0.05	0.07	nd	nd	nd	nd	nd	nd	nd
Y ₂ O ₃	0.20	0.50	0.10	0.89	nd	nd	nd	nd	nd	nd	nd
ThO ₂	0.10	0.20	0.20	0.34	nd	nd	nd	nd	nd	nd	nd
U ₂ O ₅	nd	nd	nd	nd	nd	nd	nd	nd	nd	nd	nd
P ₂ O ₅	nd	nd	nd	nd	nd	nd	nd	nd	nd	nd	nd
F	0.50	0.76	0.45	0.60	0.30	nd	nd	nd	nd	nd	nd
Cl	0.86	0.60	0.60	0.36	0.11	nd	nd	nd	nd	nd	nd
Total	98.72	96.86	92.40	89.11	96.81	97.26	96.46	95.58	96.48	96.41	97.21
O-F,Cl	0.41	0.46	0.32	0.33	0.15	0.00	0.00	0.00	0.00	0.00	0.00
Si	3.030	3.026			2.979	3.090	3.088	3.050	3.080	2.962	3.044
Ti	0.010	0.012			-----	-----	-----	-----	-----	-----	0.003
Al	2.204	2.420			2.774	2.826	2.807	2.636	2.600	2.402	2.623
Fe ²⁺	0.536	0.343			0.131	-----	-----	-----	-----	-----	-----
Fe ³⁺	0.066	0.082			0.076	0.100	0.107	0.370	0.390	0.448	0.391
Mg	0.163	0.073			-----	-----	-----	-----	-----	0.002	-----
Mn	0.099	0.039			0.020	-----	0.003	0.002	0.003	0.026	0.008
ΣM	3.078	2.969			3.001	2.916	2.917	3.008	2.993	2.840	3.025
Ca	1.278	1.627			1.805	1.971	2.003	2.068	2.047	1.974	2.049
ΣRE	0.650	0.543			0.123	-----	-----	-----	-----	-----	-----
Th	0.004	0.002			-----	-----	-----	-----	-----	-----	-----
U	-----	-----			-----	-----	-----	-----	-----	-----	-----
ΣA	1.928	1.972			1.928	1.971	2.003	2.068	2.047	1.974	2.049
P	-----	-----			-----	-----	-----	-----	-----	-----	-----
F	0.136	0.207			0.074	-----	-----	-----	-----	-----	-----
Cl	0.126	0.068			0.014	-----	-----	-----	-----	-----	-----
						3.4	3.7	12.3	13.0	15.4	12.9

Notes: mrgrn of grain margin of zoned allanite; core is grain core of zoned allanite, mrgrn* is grain margin of altered allanite; core* is grain core of altered allanite, ncl is small clinzoisite nucleus within zoned allanite; incl is clinzoisite inclusions within allanite; env. is epidote enveloping allanite; nd is "not detectable"; FeO* is total iron content (as ferrous and ferric iron in allanite and epidote, respectively)

APPENDIX II (cont.)

TABLE 7 CLINOPYROXENE COMPOSITIONS

Lithology	Cr-rich calc-silicates						Fe-rich calc-silicates (unit #				
	sample	K72/ 80	No 2	No.3	No.7	L81/ 19	L81/ 28	J83/ 91	J87/ 150	K91/12 A B	
SiO ₂	51.59	52.25	53.47	52.25	52.91	52.53	51.51	49.17	48.84	49.19	52.01
TiO ₂	0.09	0.16	0.07	0.00	0.00	0.07	0.04	0.11	0.13	0.13	nd
Al ₂ O ₃	0.63	1.15	0.54	1.36	0.23	0.91	0.31	1.43	1.33	1.22	nd
Cr ₂ O ₃	0.29	0.40	0.00	0.72	0.14	0.57	nd	nd	nd	nd	nd
FeO*	12.22	8.22	5.60	7.93	9.72	9.76	14.70	18.65	21.44	22.41	8.99
MgO	10.38	12.18	14.05	12.36	12.52	11.13	9.21	6.44	4.98	4.46	14.49
MnO	0.61	0.54	0.35	0.45	0.59	0.62	0.92	0.60	0.36	0.87	0.80
CaO	23.68	24.48	24.92	24.26	24.93	24.03	24.07	23.54	23.49	22.42	23.77
Na ₂ O	0.17	0.34	0.26	0.16	0.29	0.73	0.11	0.37	0.22	0.30	0.11
Total	99.66	99.74	99.28	99.49	100.9	100.4	100.8	100.2	100.7	101.0	99.17
Si	1.986	1.968	1.984	1.967	1.980	1.980	1.970	1.937	1.937	1.952	1.957
Ti	0.014	0.032	0.016	0.033	0.010	0.020	0.014	0.063	0.062	0.048	-----
Al	0.015	0.019	0.018	0.028	0.000	0.020	0.000	0.003	0.000	0.009	-----
Ti	0.003	0.005	0.002	0.000	0.000	0.002	0.001	0.003	0.004	0.004	-----
Cr	0.009	0.012	0.000	0.021	0.004	0.017	-----	-----	-----	-----	-----
Mg	0.595	0.684	0.781	0.694	0.699	0.625	0.525	0.378	0.295	0.264	0.813
Fe	0.394	0.259	0.175	0.250	0.289	0.308	0.470	0.613	0.711	0.743	0.283
Mn	0.020	0.017	0.011	0.014	0.019	0.017	0.030	0.020	0.012	0.029	0.026
Ca	0.977	0.988	0.996	0.979	1.000	0.970	0.988	0.995	1.000	0.956	0.960
Na	0.013	0.025	0.019	0.012	0.021	0.053	0.008	0.028	0.017	0.023	0.008
M/MF	0.626	0.725	0.817	0.724	0.707	0.670	0.513	0.373	0.698	0.717	0.725

Notes: No 2, No.3 and No 7 are surface samples from the Cadi Fracture Zone; A and B are two analyses of sample K91/12; FeO* is total iron content; nd is "not detected"; and M/MF is the atomic ratio of Mg/(Mg + Fe + Mn).

TABLE 8 PREHNITE AND PUMPELLYITE COMPOSITIONS

Mineral	prehnite								pumpellyite			
	Unit	CFZ	2	4	L82	9	CFZ	9	CFZ	9	CFZ	9
Sample	No.7	K72/ 43	L81/ 6	J83/ 77	K91/ 40	J85/ 165	I816/ 439	I85/ 16	No.7	K72/ 43	I812/290 1	2
SiO ₂	42.11	42.95	42.54	42.55	43.37	42.61	43.86	42.10	37.37	38.17	38.10	38.26
TiO ₂	0.00	0.00	0.10	0.10	0.06	0.05	0.00	0.01	0.13	0.00	0.00	0.00
Al ₂ O ₃	22.24	23.13	22.01	22.55	22.98	21.66	23.83	20.30	24.00	23.39	25.10	25.75
Cr ₂ O ₃	1.13	1.21	0.00	0.05	0.09	0.00	0.07	0.00	1.51	1.56	0.00	0.00
FeO*	2.65	1.15	2.65	2.30	0.78	1.43	0.45	3.51	1.61	2.70	0.90	1.57
MgO	0.00	0.00	0.04	0.05	0.06	0.14	0.01	0.14	4.10	3.73	5.27	4.20
MnO	0.00	0.00	0.09	0.09	0.09	0.00	0.01	0.00	0.00	0.14	0.19	0.17
CaO	26.30	26.80	26.91	27.00	27.17	28.40	27.18	28.30	23.68	23.65	22.46	23.12
Na ₂ O	0.00	0.00	0.04	0.02	0.08	0.03	0.00	0.01	0.00	0.00	0.00	0.00
K ₂ O	0.00	0.00	0.04	0.00	0.01	0.05	0.00	0.00	0.00	0.00	0.02	0.00
Total	94.43	95.24	94.42	95.61	94.68	94.47	95.41	94.37	92.56	94.18	92.05	93.07
Si	2.972	2.979	3.010	2.996	3.027	3.014	3.026	3.016	2.998	3.057	3.042	3.027
Al	1.849	1.888	1.836	1.871	1.891	1.806	1.938	1.771	2.267	2.207	2.362	2.402
Ti	0.000	0.000	0.006	0.005	0.003	0.003	0.000	0.001	0.008	0.000	0.000	0.000
Cr	0.063	0.067	0.000	0.003	0.005	0.000	0.004	0.000	0.095	0.099	0.000	0.000
Fe	0.138	0.060	0.157	0.135	0.045	0.085	0.026	0.210	0.097	0.163	0.060	0.104
Mg	0.000	0.000	0.004	0.005	0.006	0.015	0.001	0.015	0.490	0.446	0.628	0.496
Mn	0.000	0.000	0.005	0.005	0.005	0.000	0.001	0.000	0.000	0.011	0.013	0.002
Ca	1.989	1.992	2.043	2.039	2.032	2.151	2.007	2.172	2.035	2.029	1.922	1.960
Na	0.000	0.000	0.003	0.001	0.006	0.004	0.000	0.001	0.000	0.000	0.000	0.000
K	0.000	0.000	0.002	0.000	0.001	0.004	0.000	0.000	0.000	0.000	0.004	0.000

APPENDIX II (cont.)

TABLE 9 MINERAL COMPOSITIONS

Table 9. Chemical compositions of other minerals from the White River property.

Minerals	staurolite			cordierite		talc		tourmaline			sphene	
	Sample I72/179	I84/75	I813/315	I812/345	I815/510	K91/98	J85/202	I72/87	I813/122	I816/439	K91/40	L81/19
SiO ₂	28.67	28.86	29.27	50.05	47.82	60.70	59.31	36.08	35.48	36.66	30.48	30.10
TiO ₂	0.66	0.59	0.59	0.00	0.00	0.00	0.00	0.34	0.21	0.58	33.47	38.31
Al ₂ O ₃	53.51	52.87	53.77	32.40	34.39	0.15	0.19	28.49	28.65	35.07	3.01	1.12
FeO*	12.31	13.08	13.54	6.22	5.88	4.96	3.94	10.42	8.87	3.49	0.91	0.56
MgO	1.46	1.61	1.44	9.38	9.52	27.12	27.14	8.32	8.30	8.67	0.04	0.03
MnO	0.52	0.52	0.36	0.06	0.03	0.00	0.00	0.06	0.06	0.00	0.09	0.14
ZnO	1.28	0.87	1.36	nd	nd	nd	nd	nd	nd	nd	nd	nd
CaO	0.01	nd	nd	0.00	0.00	0.00	0.00	0.71	1.56	1.40	29.53	29.73
Na ₂ O	nd	nd	nd	0.43	0.32	0.00	0.04	2.49	2.15	1.41	0.04	0.03
K ₂ O	0.01	nd	0.01	0.00	0.00	0.00	0.00	0.00	0.00	0.00	0.00	0.01
Total	96.96	96.81	98.89	98.54	97.98	92.97	90.63	86.90	88.28	87.22	98.89	100.2
Si	3.953	3.985	3.998	5.089	6.797	4.016	4.009	7.145	7.107	6.878	4.052	3.940
Ti	0.069	0.062	0.061	0.000	0.000	0.000	0.000	0.051	0.031	0.082	3.346	3.771
Al	8.696	8.602	8.655	3.882	5.762	0.012	0.016	6.647	6.672	7.750	0.472	0.172
Fe	1.419	1.509	1.546	0.583	0.699	0.275	0.223	1.552	1.336	0.493	0.101	0.061
Mg	0.300	0.332	0.293	1.423	2.017	2.675	1.734	2.457	2.480	2.424	0.000	0.006
Mn	0.065	0.065	0.042	0.005	0.004	0.000	0.000	0.009	0.010	0.000	0.010	0.010
Zn	0.133	0.091	0.141	-----	-----	-----	-----	-----	-----	-----	-----	-----
Ca	0.002	0.000	0.000	0.000	0.000	0.000	0.000	0.151	0.336	0.282	4.207	4.169
Na	0.000	0.000	0.000	0.042	0.088	0.000	0.005	0.478	0.835	0.512	0.010	0.008
K	0.002	0.000	0.002	0.000	0.000	0.000	0.000	0.000	0.000	0.000	0.000	0.002

Table 9 (cont.)

Minerals	Apatite											ms.
	Unit	1	2	3	4	6	7	AZ	9	AZ		
Sample	U1-1	L81/6	K82/39	I72/371	K91/40	I72/245 core	I72/245 rim	I92/69	I816/439	I72/87	I813/223	I816/439
SiO ₂	0.00	0.02	0.02	0.00	0.02	0.00	0.00	0.00	9.14	0.01	1.35	0.79
TiO ₂	0.03	0.02	0.03	0.01	0.01	0.00	0.03	0.03	nd	0.00	0.02	nd
Al ₂ O ₃	0.01	0.02	0.06	0.00	0.01	0.02	0.32	0.06	3.37	0.02	0.35	0.56
Cr ₂ O ₃	0.14	0.06	0.00	0.11	0.07	0.94	0.02	0.01	nd	0.13	0.11	nd
Fe ₂ O ₃	nd	nd	nd	nd	nd	nd	nd	nd	2.87	nd	nd	72.48
FeO*	0.12	0.03	0.19	0.13	0.05	0.34	0.06	0.06	0.91	0.36	0.16	0.80
MgO	0.00	0.03	0.09	0.00	0.03	0.12	0.01	0.00	nd	0.00	0.01	0.02
MnO	0.03	0.00	0.04	0.00	0.00	0.00	0.04	0.04	0.07	0.02	0.00	0.24
CaO	55.82	54.79	55.92	59.14	55.68	54.97	57.16	55.49	44.57	55.25	53.78	nd
Na ₂ O	0.00	0.00	0.00	0.00	0.00	0.00	0.00	0.00	0.00	0.00	0.00	0.05
P ₂ O ₅	41.83	43.06	42.97	41.43	43.23	42.15	42.09	42.05	40.01	41.92	42.15	28.01
F	2.44	2.87	2.51	1.79	1.83	3.33	2.17	2.62	nd	2.65	3.37	nd
Cl	0.00	0.00	0.00	0.00	0.00	0.00	0.00	0.00	0.20	0.00	0.00	nd
Total	100.4	100.9	101.8	101.6	100.9	101.4	101.9	100.4	100.3	100.3	101.2	101.6

APPENDIX II (cont.)

TABLE 10 OXIDE COMPOSITIONS

Minerals	Chromite								Ilmenite	
	K72/43		No. 2		No. 7		K72/80		L91/11	K91/98
	core	rim	core	rim	core	rim	core	rim		
SiO ₂	nd	nd	nd	nd	nd	nd	nd	nd	nd	0.06
TiO ₂	0.10	0.13	0.20	0.12	0.27	0.09	0.09	0.02	0.04	51.84
Al ₂ O ₃	10.08	7.40	11.25	8.99	11.78	5.36	10.72	8.19	9.32	0.10
Cr ₂ O ₃	47.80	47.66	50.25	50.04	49.89	52.51	16.41	46.80	50.56	0.00
FeO	8.32	10.87	3.80	6.24	3.75	8.40	8.92	11.20	5.50	45.10
Fe ₂ O ₃	25.04	25.06	26.45	26.61	27.53	26.01	27.00	27.72	26.70	0.20
MgO	0.21	0.13	0.41	0.34	0.48	0.17	0.18	0.16	0.17	1.34
MnO	1.94	2.29	1.80	2.04	2.44	3.09	2.07	1.92	2.53	nd
ZnO	6.59	5.62	5.72	5.28	4.14	3.36	4.22	3.68	3.88	0.06
NiO	0.10	0.00	0.09	0.00	0.00	0.00	0.02	0.00	0.00	nd
CoO	0.18	0.00	0.017	0.21	0.00	0.11	0.10	0.15	0.26	nd
Total	100.2	99.60	100.3	100.0	100.3	99.30	99.90	100.4	100.1	99.98
Si	-----	-----	-----	-----	-----	-----	-----	-----	-----	0.002
Ti	0.003	0.004	0.005	0.003	0.007	0.002	0.002	0.001	0.001	0.992
Al	0.349	0.318	0.470	0.379	0.488	0.232	0.453	0.349	0.397	0.003
Cr	1.359	1.371	1.408	1.433	1.391	1.530	1.317	1.336	1.445	0.000
Fe ⁺⁺	0.224	0.301	0.099	0.167	0.099	0.235	0.224	0.305	0.149	-----
Fe ⁺⁺⁺	0.749	0.776	0.787	0.795	0.812	0.802	0.811	0.837	0.808	0.960
Mg	0.011	0.008	0.022	0.018	0.025	0.009	0.010	0.008	0.009	0.029
Mn	0.059	0.073	0.054	0.062	0.073	0.097	0.063	0.059	0.078	0.008
Zn	0.174	0.157	0.150	0.139	0.108	0.091	0.112	0.098	0.104	0.002
Ni	0.003	0.000	0.003	0.000	0.000	0.000	0.000	0.000	0.000	-----
Co	0.006	0.000	0.006	0.006	0.000	0.002	0.004	0.004	0.008	-----

Notes: No. 2 and No. 7 are surface samples of Cr-rich calc-silicates from the Cadi Fracture Zone, and "nd" is not detected.

APPENDIX II (cont.)

TABLE 11 SULFIDE COMPOSITIONS

Lithology	Cr-rich calc-silicates						Fe-rich calc-silicates					
	S	Fe	Ni	Co	Cu	Zn	S	Fe	Ni	Co	Cu	Zn
pn	47.06	22.56	26.14	4.24	nd	nd	47.26	21.58	24.89	6.26	nd	nd
po	53.53	45.65	0.76	0.06	nd	nd	53.40	46.38	0.21	0.08	nd	nd
sp	50.59	6.56	0.35	0.13	nd	42.37	50.69	6.52	nd	nd	nd	42.76
cp	50.77	25.79	0.06	0.04	23.34	nd	49.58	25.41	nd	0.02	24.91	nd
py	66.93	30.34	1.46	1.27	nd	nd	66.97	30.71	nd	2.32	nd	nd
sg1	57.54	7.19	19.13	16.14	nd	nd	56.58	14.10	19.18	10.14	nd	nd
sg2	56.14	7.04	17.00	19.83	nd	nd	56.36	13.37	14.55	14.68	nd	nd
ml	51.37	4.48	42.80	0.61	0.73	nd						

Notes: pn, pentlandite; po, pyrrhotite; sp, sphalerite; cp, chalcopyrite; py, pyrite; sg1 and sg2, two separate analyses of siegenite; ml, millerite; and "nd", not detectable.

REFERENCES

- ALLEN, F.M. & BUSECK, P.R. (1988): XRD, FTIR, and TEM studies of optically anisotropic grossular garnets. *Am. Mineral.*, **73**, 568-584.
- ALTHAUS, E. (1969): Experimental evidence that reaction of kyanite to form sillimanite is at least bivariant. *Am. J. Sci.*, **267**, 273-277.
- ÅMLI, R. & GRIFFIN, W.L. (1975): Microprobe analysis of REE minerals using empirical correction factors. *Am. Mineral.*, **60**, 599-606.
- ANDREWS-JONES, D.A. (1966): Geology and mineral resources of the northern Kambui schist belt and adjacent granulites. *Geol. Surv. Sierra Leone Bull.*, **6**, 1-100.
- APTED, M.J. & LIOU, J.G. (1983): Phase relations among greenschist, epidote-amphibolite, and amphibolite in a basaltic system. *Am. J. Sci.*, **283A**, 328-354.
- ARGAST, S. & DONNELLY, T.W. (1986): Compositions and sources of metasediments in the upper Dharwar Supergroup, South India. *J. Geol.*, **94**, 215-231.
- ASHWORTH, J.R. (1975): Staurolite at anomalously high grade. *Contrib. Mineral. Petrol.*, **53**, 281-291.
- _____ & EVIRGEN, M.M. (1985): Plagioclase relations in pelites, central Menders Massif, Turkey. II. Perturbation of garnet-plagioclase geobarometers. *J. Metamorph. Geol.*, **3**, 219-229.
- BAILEY, S.W. (1984): Classification and structures of the micas. *MICAS, Reviews in Mineralogy*, **13**, Mineral. Soc. Am., 1-12.
- BARTLEY, M.W., & PAGE, T.W., (1957): A geological report on the Hemlo area, Thunder Bay District, Ontario (unpublished). Dept. Industrial Devel, Can. Pacific Railway, 18p.
- BERMAN, R.G., BROWN, T.H. & GREENWOOD, H.J. (1985): An internally consistent thermodynamic data set for minerals in the system Na₂O-K₂O-CaO-MgO-FeO-Fe₂O₃-Al₂O₃-SiO₂-TiO₂-H₂O-CO₂. Atomic Energy of Canada Ltd. Tech. Rep. 377.
- BHATIA, M.R. (1983): Plate tectonics and geochemical composition of sandstones. *J. Geol.*, **91**, 611-627.
- _____ & CROOK, K.A.W. (1986): Trace element characteristics of greywackes and tectonic setting discrimination of sedimentary basins. *Contrib. Mineral. Petrol.*, **92**, 181-193.

- BIRD, D.K., SCHIFFMAN, P., ELDERS, W.A., WILLIAMS, A.E. & MacDOWELL, S.D. (1984): Calc-silicate mineralization in active geothermal systems. *Econ. Geol.* 79, 671-695.
- BONHAM, H.F., Jr., (1986): Models for volcanic-hosted epithermal precious metal deposits, P.J., eds., *Proc. Symp. 5: Volcanism, Hydrothermal System and Related Mineralization, Intern. Volc. Congr., Auckland, New Zealand: Austr. Inst. Mining Metall. New Zealand Branch*, 13-18.
- BOUMA, A.H. (1962): *Sedimentology of Some Flysch Deposits: Graphic Approach to Facies Interpretation*. Elsevier, Amsterdam, 168p.
- BOYLE, R.W. (1979): The geochemistry of gold and its deposits: *Geol. Surv. Can. Bull.*, 280, 584p.
- BROWN, I.J., & NESBITT, B.E., (1987): Gold-copper-bismuth mineralization in hedenbergitic skarn, Tombstone Mountains, Yukon. *Can. J. Earth Sci.*, 24, 2362-2372.
- BUCHER-NURMINEN, K., FRANK, E. & FREY, M., (1983): A model for the progressive regional metamorphism of margarite-bearing rocks in the Central Alps. *Am. J. Sci.*, 283A, 370-395.
- BURK, R., HODGSON, C.J., & QUARTERMAIN, R.A. (1986): The geological setting of the Teck-Corona Au-Mo-Ba deposit, Hemlo, Ontario, Canada. *Proceeding of Gold'86, Intern. Symp. Geol. Gold: (Toronto) in McDonald, A.J., ed.*, 311-326.
- CAMERON, E.M. & HATTORI, K. (1985): The Hemlo gold deposit, Ontario: A geochemical and isotopic study. *Geochim. Cosmochim. Acta*, 49, 2041-2050.
- CHATTERJEE, N.D. (1976): Margarite stability and compatibility relations in the system $\text{CaO-Al}_2\text{O}_3\text{-SiO}_2\text{-H}_2\text{O}$ as a pressure temperature indicator. *Am. Mineral.*, 61, 699-709.
- CHINNER, G.A. & FOX, J.S. (1974): The origin of cordierite-anthophyllite rocks in the Land's End aureole. *Geol. Magz.*, 111, 397-408.
- _____, SMITH, J.V. & KNOWLES, C.R. (1969): Transition metal contents of Al_2SiO_5 polymorphs. *Am. J. Sci.*, 267, 96-113.
- CHO, M. & LIOU, J.G. (1987): Prehnite-pumpellyite to greenschist transition in the Karmutsen Metabasites, Vancouver Island, B.C., *J. Petrol.*, 28, 417-443.
- COLVINE, A.C., ANDREWS, A.J. CHERRY, M.E., DUROCHER, M.E., FYON, A. J., LAVIGNE, M.J., Jr., MACDONALD, A.J., MARMONT, S., POULSEN, K.H., SPRINGER, J.S., & TROOP, D.G., (1984): An integrated model for the origin of Archean lode gold deposits, *Ont. Geol. Surv., Open File Rep.*, 5524, 99p.

- CONDIE, K.C. (1981): The Archean Greenstone Belts. In Windley, B.F. ed., *Developments in Precambrian Geology*, 3, 434.
- COOPER, A.F. (1972): Progressive metamorphism of metabasic rocks from the Haast schist group of Southern New Zealand. *J. Petrol.*, 13, 457-492.
- COOPER, P., BROWN, P., & MACKIE, B. (1986): The geology and regional stratigraphic setting of Noranda's Golden Giant Joint Venture Deposit No. 1: *Can. Inst. Mining Metall., District 4 Meeting*, 1984, Thunder Bay.
- CORFU, F. & MUIR, T.L. (1989a): The Hemlo-Heron Bay greenstone belt and Hemlo Au-Mo deposit, Superior Province, Ontario, Canada, 1. Sequence of igneous activity determined by zircon U-Pb geochronology. *Chem. Geol.*, 79, 183-200.
- _____ & _____ (1989b): The Hemlo-Heron Bay greenstone belt and Hemlo Au-Mo deposit, Superior Province, Ontario, Canada, 2. Timing of metamorphism, alteration and Au mineralization from titanite, rutile, and monazite U-Pb geochronology. *Chem. Geol.*, 79, 201-223.
- CZAMANSKE, G.K. & WONES, D.R. (1973): Oxidation during magmatic differentiation, Finnmarka Complex, Osla area, Norway: Part 2, the mafic silicates. *J. Petrol.*, 14, 349-380.
- DANCHIN, R.V. (1967): Chromium and nickel in the Fig Tree Shale from South Africa. *Science*, 158, 261-262.
- DEER, W.A., HOWIE, R.A. & ZUSSMAN, J. (1963): *Rock-Forming Minerals*. 2. Chain Silicates. Longmans, London.
- _____, _____ & _____ (1986): *Rock-forming Minerals*. 1B. Disilicates and Ring Silicates. Longmans, London.
- DE ROSEN-SPENCE, A. (1969): Genèse des roches à cordiérite-anthophyllite des gisements cupro-zincifères de la région de Rouyn-Noranda, Québec, Canada. *Can. J. Earth Sci.*, 6, 1339-1345.
- DOLLASE, W.A. (1971): Refinement of the crystal structure of epidote, allanite and hancockite. *Am. Mineral.*, 56, 447-464.
- DRAKE, M.J. & WEILL, D.F., (1972): New rare earth element standards for electron microprobe analysis. *Chem. Geol.*, 10, 179-181.
- DUKE, J.M. & BONARDI, M. (1982): Chromian andradite from Reaume Township, Ontario. *Can. Mineral.*, 20, 49-53.
- DUNN, P.J. (1978): On the composition of some Canadian green garnets. *Can. Mineral.*, 16, 205-206.

- EINAUDI, M.T., MEINERT, L.D., & NEWBERRY, R.J. (1981): Skarn deposits. *Econ. Geol.*, 75th ANNIV. V., 317-391.
- _____ & BURT, D.M. (1982): Introduction - terminology, classification, and composition of skarn deposits. *Econ. Geol.*, 77, 745-754.
- ENAMI, M. & ZANG, Q., (1988): Magnesian staurolite in garnet-corundum rocks and eclogite from the Donghai district, Jiangsu province, east China. *Am. Mineral.*, 73, 48-56.
- ENGEL, A.E.J., ITSON, S.P. ENGEL, C.G., STICKNEY, D.M. & GRAY, E.J., (1974): Crustal evolution and global tectonics: a petrographic view. *Geol. Soc. Am. Bull.*, 85, 843-858.
- ENGLAND, P.C. & THOMPSON, A.B. (1984): Pressure-temperature-time paths of regional metamorphism: I: Heat transfer during the evolution of regions of thickened continental crust. *J. Petrol.*, 25, 894-928.
- ESKOLA, P. (1914): On the petrology of the Orijärvi region in southwestern Finland. *Bull. Comm. Géol. Finl.*, 40, 1-279.
- _____ (1933): On the chrome minerals of Outokumpu. *Bull. Comm. Géol. Finl.*, 103, 26-44.
- _____ (1939): *Die entstehung der Gesteine*. Springer-Verlag, Berlin.
- ETTLINGER, A.D. & RAY, G.E. (1989): Precious metal enriched skarns in British Columbia: An overview and geological study. *B. C. Geol. Surv. Branch, Pap.* 1989-3, 130p.
- _____ & MEINERT, L.D. (1990): Gold in Russian skarns: an example from the Siniukhinskoe District, Siberia, USSR (Abstract). *Gold'90*, Feb. 26 - Mar. 1, 1990, Salt Lake City, Utah.
- EWERS G.R. & SUN, S.-S. (1989): Genesis of the Red Dome gold skarn deposit, Northeast Queensland. *Econ. Geol. Mon.*, 6, 218-232.
- EXLEY, R.A., (1980) Microprobe studies of REE-rich accessory minerals: implications for Skye granite petrogenesis and REE mobility in hydrothermal systems. *Earth Planet. Sci. Lett.*, 48, 97-100.
- FERRY, J.M. & SPEAR, F.S. (1978): Experimental calibration of the partition of Fe and Mg between biotite and garnet. *Contrib. Mineral. Petrol.*, 66, 113-117.
- FLEET, M.E., BARNETT, R.L. & MORRIS, W.A., (1987): Prograde metamorphism of the Sudbury Igneous Complex. *Can. Mineral.*, 25, 499-514.
- FLOYD, P.A. (1965): Metasomatic hornfels of the Land's End aureole at Tater-du, Cornwall. *J. Petrol.*, 6, 223-245.

- FOURNIER, R.O. (1985): Silica minerals as indicators of conditions during gold deposition. in Tooker, E.W., ed., *Geologic characteristics of sediment- and volcanic-hosted disseminated gold deposits - search for an occurrence model*, U.S. Geol. Surv. Bull., 1646, 15-26.
- FOWLER, C.M.R. & NISBET, E.G. (1982): The thermal background to metamorphism: simple two-dimensional conductive models. *Geosci. Can.*, 9, 208-214.
- FROESE, E. (1969): Metamorphic rocks from the Coronation mine and surrounding area. *Geol. Surv. Can. Pap.*, 68-5, 55-77.
- FRYER, B.J. (1977): Rare earth evidence in iron formations for changing Precambrian oxidation states. *Geochem. Cosmochim. Acta*, 41, 361-367.
- FYFE, W.S., PRICE, N.J. & THOMPSON, A.B. (1978): *Fluids in the Earth's Crust*. Elsevier, Amsterdam.
- ____ & KERRICH, R. (1984): Gold-natural concentration processes, in Foster, R.P., ed., *Gold'82: The geology, geochemistry and genesis of gold deposits*: Rotterdam, A.A. Balkema, 99-128.
- GABLE, D.J. & SIMS, P.K. (1969): Geology and regional metamorphism of some high-grade cordierite gneisses, Front Range, Colorado, *Geol. Soc. Am., Special Pap.*, 128, 1-87.
- GANGULY, J. & KENNEDY, G.C. (1974): The energetics of natural garnet solid solution: I. Mixing of the aluminosilicate end-members. *Contrib. Mineral. Petrol.*, 48, 137-148.
- ____ (1979): Garnet-pyroxene solid-solutions, and geothermometry based on Fe-Mg distribution coefficient. *Geochim. Cosmochim. Acta*, 43, 1021-1029.
- ____ & SAXENA, S. (1984): Mixing properties of aluminosilicate garnets: constraints from natural and experimental data, and application to geothermobarometry. *Am. Mineral.*, 69, 88-97.
- ____ & ____ (1987): *Mixtures and Mineral Reactions. Minerals and Rocks*, 19. Springer-Verlag Berlin Heidelberg, 291p.
- GEIST, D.J., BAKER, B.H. & McBIRNEY, A.R. (1985): GPP: A program package for creating and using geochemical data files (version for IBM-PC and compatible microcomputers).
- GHENT, E.D. (1972): Electron microprobe study of allanite from the Mt. Falconer quartz monzonite pluton, Lower Taylor Valley, South Victoria Land, Antarctica. *Can. Mineral.*, 11, 526-530.

- _____ (1976): Plagioclase-garnet- Al_2SiO_5 -quartz: a potential geobarometer-geothermometer. *Am. Mineral.*, **61**, 710-714.
- GHENT, E.D., ROBBINS, D.B., & STOUT, M.Z. (1979): Geothermometry, geobarometry and fluid compositions of metamorphosed calc-silicates and pelites, Mica Creek, British Columbia. *Am. Mineral.*, **64**, 874-885.
- _____ & STOUT, M.Z. (1986): Garnet-hornblende thermometry, $\text{CaMgSi}_2\text{O}_6$ activity, and the minimum pressure limits of metamorphism for garnet amphibolites: *J. Geol.*, **94**, 736-743.
- GOLDIE, R. (1985): The sinters of the Ohaki and Campagne pools, New Zealand: possible modern analogues of the Hemlo gold deposit, Northern Ontario: *Geosci. Can.*, **12**, 60-64.
- GOLDMAN, D.S. & ALBEE, A.L. (1977): Correlation of Mg/Fe partitioning between garnet and biotite with $^{18}\text{O}/^{16}\text{O}$ partitioning between quartz and magnetite. *Am. J. Sci.*, **277**, 750-767.
- GOLDSMITH, J. R. & LEAVES, F. (1954): The microcline-sanidine stability relations. *Geochim. Cosmochim. Acta*, **5**, 1-19.
- GOLDSMITH, J.R. (1982): Plagioclase stability at elevated temperatures and water pressures. *Am. Mineral.*, **67**, 653-675.
- GRAHAM, C.M. (1974): Metabasite amphiboles of the Scottish Dalradian. *Contrib. Mineral. Petrol.*, **47**, 165-185.
- _____ & POWELL, R. (1984): A garnet-hornblende geothermometer: calibration, testing and application to the Pelona Schist, southern California. *J. Metamorphic Geol.*, **2**, 13-22.
- GRANT, J.A. (1968): Partial melting of common rocks as a possible source of cordierite-anthophyllite bearing assemblages. *Am. J. Sci.*, **266**, 908-931.
- GRAPES, R.H. & GRAHAM, C.M. (1978): The actinolite-hornblende series in metabasites and the so-called miscibility gap: a review. *Lithos* **11**, 85-97.
- GRAPES, R.H. (1981): Chromian epidote and zoisite in kyanite amphibolite, Southern Alps, New Zealand. *Am. Mineral.* **66**, 974-975.
- GRIGORYEVA, T.A. & SUKNEVA, L.S. (1981): Effects of sulfur and on antimony and arsenic sulfides on the solubility of gold. *Geochem. Intern.*, **18**, 153-158.
- GROEN, J.C., CRAIG, J.R. & RIMSTIDT, J.D. (1989): Systematics of low-temperature gold-silver-mercury intermetallic phase equilibria (Abstract). *Geol. Assoc. Can. Mineral. Assoc. Can. Joint Annual Meeting, Montreal, 1989*. A95.

- GROVE, T.L., FERRY, J.M., & SPEAR, F.S., (1983): Phase transitions and decomposition relations in calcic plagioclase. *Am. Mineral.*, **68**, 41-59.
- GROVES, D.I., PHILLIPS, N.D., Ho, S.E., HENDERSON, C.A., CLARK, M.E., & WOAD, G.M. (1984): Controls on distribution of Archean hydrothermal gold deposits in Western Australia, in Foster, R.P., ed., *Gold'82: The geology, geochemistry and genesis of gold deposits*; Rotterdam, A.A. Blakema, 689-712.
- GUIDOTTI, C.V. & SASSI, F.P. (1976): Muscovite as a petrographic indicator mineral in pelitic schists. *Neues. Jb. Mineral. Abh.*, **127**, 97-142.
- _____ (1978): Compositional variation of muscovite in medium- to high-grade metapelites of northern Maine. *Am. Mineral.*, **63**, 878-884.
- _____ (1984): Micas in metamorphic rocks. *MICAS, Reviews in Mineralogy*, **13**, Mineral. Soc. Am., 357-468.
- HASHASH, A. Jr. (1984): Rare earth element abundances and distribution patterns in hydrothermal altered basalts: experimental results. *Contrib. Mineral. Petrol.*, **85**, 409-412.
- HALL, B.V. (1982): Geochemistry of the alteration pipe at the Amulet Upper A deposit, Noranda, Quebec. *Can. J. Earth Sci.*, **19**, 2060-2084.
- HARRIS, D.C. (1986): Mineralogy and geochemistry of the main Hemlo gold deposit, Hemlo, Ontario, Canada. *Proceeding of Gold'86, Intern. Symp. Geol. Gold: (Toronto)* in McDonald, A.J. ed., 297-310.
- _____ (1989): The mineralogy and geochemistry of the Hemlo gold deposit, Ontario. *Geol. Surv. Can. Econ. Geol. Rep.* **38**, 88p.
- HEAMAN, L.M. & MACHADO, N. (1987): Isotope geochemistry of the Coldwell Alkaline Complex, I. U-Pb studies on accessory minerals. *Geol. Assoc. Can. Annu. Meet.*, 1987, Univ. Saskatchewan, Saskatoon, Prog. Abstr., **12**, 54.
- HELGESON, H.C., DELANY, J.M., NESBITT, H.W. & BIRD, D.K. (1978): Summary and critique of the thermodynamic properties of rock forming minerals. *Am. J. Sci.*, 278-A.
- HENLEY, R.W. (1973): Solubility of gold in hydrothermal chloride solutions: *Chem. Geol.*, **11**, 73-87.
- HEY, M.H. (1954): A new review of the chlorites. *Mineral. Magz.*, **30**, 277-292.
- HILTUNEN, A. (1982): The Precambrian geology and skarn iron ores of the Rautuvaara area, Northern Finland. *Geol. Sur. Finl. Bull.*, **318**, 133p.

- HODGES, K.V. & SPEAR, F.S. (1982): Geothermometry, geobarometry and the Al_2SiO_5 triple point at Mt. Moosilauke, New Hampshire, *Am. Mineral.*, **67**, 1118-1134.
- _____ & McKENNA, L.W. (1987): Realistic propagation of uncertainties in geologic thermobarometry: *Am. Mineral.*, **72**, 673-682.
- HOLDING, D. A. (1987): The LAC Minerals Ltd. Cadi Zone: a Petrographic-Geochemical Study. B.Sc. thesis, University of Western Ontario, London, Ontario.
- HOLDAWAY, M.J. (1971): Stability of andalusite and the aluminium silicate phase diagram. *Am. J. Sci.*, **271**, 97-131.
- HOLDAWAY, M.J. (1972): Thermal stability of Al-Fe epidote as a function of f_{O_2} and Fe content. *Contrib. Mineral. Petrol.*, **37**, 307-340.
- _____ & LEE, S.M. (1977): Fe-Mg cordierite stability in higher-grade pelitic rocks based on experimental, theoretical and natural observations. *Contrib. Mineral. Petrol.*, **63**, 175-198.
- HOLLAND, R.A.G., BRAY, C.J., & SPOONER, E.T.C. (1978): A method for preparation doubly polished thin sections suitable for microthermometric examination of fluid inclusions: *Mineral. Magz.*, **42**, 407-408.
- HOLLISTER, L.S. (1969): Contact metamorphism in the Kwoiek area of British Columbia - an end member of the metamorphic process: *Geol. Soc. Am. Bull.*, **80**, 2465-2494.
- HUDSON, N.F.C. & HARTE, B. (1985): K_2O -poor aluminous assemblages from the Buchan Dalradian, and the variety of orthoamphibole assemblages in aluminous bulk compositions in the amphibolite facies. *Am. J. Sci.*, **285**, 224-266.
- HUGON, H. (1984): The Hemlo deposits: gold mineralization within a dextral shear zone. *Ont. Geol. Surv. Misc. Pap.* **119**, 212-217.
- _____ (1986): The Hemlo gold deposit, Ontario, Canada: A central portion of a large scale, wide zone of heterogeneous ductile shear. *Proceeding of Gold'86, Intern. Symp. Geol. Gold: (Toronto)* in McDonald, A.J. ed., 379-387.
- HUTCHINSON, M.N. & SCOTT, S.D. (1981): Sphalerite geobarometry in the Cu-Fe-Zn-S system. *Econ. Geol.*, **76**, 145-153.
- INDARES, A. & MARTINGNOLE, J. (1985): Biotite-garnet geothermometry in the granulite facies: the influence of Ti and Al in biotite. *Am. Mineral.*, **70**, 272-278.
- IRVING, A.J. & ASHLEY, P.M. (1976): Amphibole-olivine-spinel, cordierite-anthophyllite and related hornfels associated with metamorphosed serpentinites in the Goobarragandra district, near Tumut, New South Wales, *J. Geol. Soc. Austral.*, **23**, 19-43.

- IVANOV, O.P., VOROB'EV, Yu. K., EFREMENKO, L. Ya. & KNYAZEVA, D.N. (1981): Acicular allanite from the Itulin deposit veins (further study of the existence of lombardite). *Zap. Vses. Mineral. Obshch.* **110**, 361-366 (in Russian).
- JAMES, H.L. (1954): Sedimentary facies of iron formation. *Econ. Geol.*, **49**, 235-293.
- JAMES, R.S., GRIEVE, R.A.F. & PAUK, L. (1978): The petrology of cordierite-anthophyllite gneisses and associated mafic and pelitic gneisses at Manitouwadge, Ontario. *Am. J. Sci.*, **278**, 41-63.
- JENSON, L.S. (1976): A new cation plot for classifying subalkalic volcanic rocks. *Ont. Geol. Surv. Misc. Pap.*, 66.
- KALAMARIDES, R.I. & BERG, J.H. (1988): Coexisting Cr-rich and Cr-poor garnet from a calc-silicate gneiss, Labrador. *Can. Mineral.*, **26**, 335-342.
- KITAMURA, K. (1975): Al-Fe partition between garnet and epidote from the contact metasomatic copper deposits of the Chichibu mine, Japan. *Econ. Geol.*, **70**, 725-738.
- KOZIOL, A.M. & NEWTON, R.C. (1988): Redetermination of the anorthite breakdown reaction and improvement of the plagioclase-garnet-Al₂SiO₅-quartz geobarometer: *Am. Mineral.*, **73**, 216-223.
- _____ (1989): Recalibration of the plagioclase-garnet-Al₂SiO₅-quartz (GASP) geobarometry and applications for natural assemblages. *EOS*, **70**, 493.
- KRETZ, R. (1973): Kinetics of the crystallization of garnet at two localities near Yellowknife: *Can. Mineral.*, **12**, 1-20.
- _____ & JEN, L.S. (1978): Effect of temperature on the distribution of Mg and Fe²⁺ between calcic pyroxene and hornblende. *Can. Mineral.*, **16**, 533-537.
- KUHNS, R.J., KENNEDY, P., COOPER, P., BROWN, P., MACKIE, B., KUSINS, R. & FRIESEN, R. (1986): Geology and mineralization associated with the Golden Giant Deposit, Hemlo Ontario, Canada. *Proceedings of Gold'86, Intern. Symp. Geol. Gold, (Toronto)* in McDonald, A.J. ed., 327-339.
- _____, R.J. (1986): Alteration styles and trace element dispersion associated with the Golden Giant deposit, Hemlo, Ontario, Canada. *Proceedings of Gold'86, Intern. Symp. Gold, (Toronto)* in McDonald, A.J. ed., 346-354.
- KURODA, Y. (1959): Petrological study on the metamorphic rocks of the Hitachi district, northeastern Japan. *Science Reports Tokyo Kyoiku Daigaku Section C*, **7(58)**, 1-70.
- LAIRD, J. (1980): Phase equilibria in mafic schist from Vermont, *J. Petrol.*, **21**, 1-37.

- _____ & ALBEE, A.L. (1981): Pressure, temperature, and time indicators in mafic schist: their application to reconstructing the polymetamorphic history of Vermont. *Am. J. Sci.*, **281**, 127-175.
- LAL, R.K. & MOOREHOUSE, W.W. (1969): Cordierite-anthophyllite rocks and associated gneisses of Fishtail Lake, Harcourt Township, Ontario. *Can. J. Earth Sci.*, **6**, 145-165.
- LARGE, R., HUSTON, D., McGOLDRICK, P., McATHUR, G. & RUXTON, P. (1988): Gold distribution and genesis in Palaeozoic volcanogenic massive sulfide systems, Eastern Australia. In Goode, A.D.T. & Bosma, L.I. eds., *Bicentennial Gold'88, Extended Abstracts (oral program)*, 121-126, Melbourne, 1988.
- LEAKE, B.E. (1978): Nomenclature of amphiboles. *Can. Mineral.*, **16**, 501-520.
- LIU, J.G. (1971): Synthesis and stability of prehnite, $\text{Ca}_2\text{Al}_2\text{Si}_3\text{O}_{10}(\text{OH})_2$. *Am. Mineral.*, **56**, 507-531.
- _____ (1973): Synthesis and stability relations of epidote, $\text{Ca}_2\text{Al}_2\text{FeSi}_3\text{O}_{12}(\text{OH})$: *J. Petrol.*, **14**, 381-413.
- LIU, J.G., KUNYOSHI, S. & ITO, K. (1974): Experimental studies of the phase relations between greenschist and amphibolite in a basaltic system. *Am. J. Sci.*, **274**, 613-632.
- _____, KIM, H.S. & MARUYAMA, S. (1983): Prehnite-pumpellyite equilibria and their petrographic applications. *J. Petrol.*, **24**, 321-342.
- _____, MARUYAMA, S. & CHO, M., (1985): Phase equilibria and mixed parageneses of metabasites in low-grade metamorphism. *Mineral. Magz.*, **49**, 321-333.
- _____, _____ & _____ (1988): Very low metamorphism of volcanic and volcanoclastic rocks - mineral assemblages and mineral facies. In Frey, M., ed., *Very Low-grade Metamorphism*. Blackie and Son Ltd.
- LIPIN, B.R. (1984): Chromite from the Blue Ridge Province of North Carolina. *Am. J. Sci.*, **284**, 507-529.
- MACDONALD, A.J. & SPOONER, E.T.C. (1981): Calibration of a Linkam TH 600 programmable heating-cooling stage for microthermometric examination of fluid inclusions: *Econ. Geol.*, **76**, 1248-1258.
- MATHIESON, G.A. & CLARK, A.H. (1984): The Cantung E Zone scheelite skarn orebody, Tungsten, Northwest Territories: A revised genetic model. *Econ. Geol.*, **79**, 883-901.
- McLENNAN, S.M. & TAYLOR, S.R. (1980): Th and U in sedimentary rocks: crustal evolution and sedimentary recycling. *Nature* **285**, 621-624.

- _____, _____ & ERIKSSON, K.A. (1983): Geochemistry of Archean shales from the Pilbara Supergroup, Western Australia: *Geochim. Cosmochim. Acta*, **47**, 1211-1222.
- _____ & _____ (1984): Archean sedimentary rocks and their relation to the composition of the Archean continental crust. in Kroner et al., eds. *Archean Geochemistry*, Springer-Verlag, Berlin Heidelberg, 1984.
- MEINERT, L.D. (1984): Mineralogy and petrology of iron skarns in western British Columbia, Canada. *Econ. Geol.*, **79**, 869-882.
- _____ (1989): Gold skarn deposits - geology and exploration criteria. *Econ. Geol. Mon.*, **6**, 537-552.
- MENZIES, M., SEYFRIED, W.E. & BLANCHARD, D. (1979): Experimental evidence of rare earth element immobility in greenstones. *Nature*, **282**, 398-399.
- MICHARD, A., ALBAREDE, F. MICHARD, G., MINSTER, J.F. & CHARLOU, J.L. (1983): Rare-earth elements and uranium in high-temperature solutions from East Pacific Rise hydrothermal vein field (13°N). *Nature*, **303**, 795-797.
- MICHARD, A. & ALBAREDE, F. (1986): The REE content of some hydrothermal fluids. *Chem. Geol.*, **55**, 51-60.
- MILNE, V.G., (1968) *Geology of Black River area, District of Thunder Bay: Ont. Geol. Surv. Rep.*, **72**, 68p.
- MIYASHIRO, A. (1973): *Metamorphism and Metamorphic Belt*. George Allen & Unwin Ltd., London.
- MOODY, J.B. & MEYER, D. & JENKINS, J.E. (1983): Experimental characterization of the greenschist/amphibolite boundary in mafic systems. *Am. J. Sci.*, **283**, 48-92.
- MOORE, A.C. (1976): Intergrowth of prehnite and biotite. *Mineral. Magz.*, **40**, 526-529.
- MORTON, R.D. (1972): A discussion. Sulfide mineralization and wall rock alteration at Rødhammeren mine, Sør-Trøndelag, Norway. *Norsk. Geologisk Tidsskrift*, **52**, 313-315.
- MUELLER, R.F. (1961): Analysis of relations among Mg, Fe, and Mn in certain metamorphic minerals. *Geochim. Cosmochim. Acta*, **25**, 119-126.
- MUIR, T.M. (1978): Hemlo area; in *Summary of Field Work*, Milne, V.G. White, O.L., Barlow, R.B., & Robertson, J.A., eds., *Ont. Geol. Surv. Misc. Pap.*, **82**, 90-93.
- _____ (1982a): *Geology of the Heron Bay area, District of Thunder Bay. Ont. Geol. Surv. Rep.*, **218**, p98.

- _____. (1982b): Geology of the Hemlo area, district of Thunder Bay. Ont. Geol. Surv. Rep., 217, p65.
- _____. (1986): Hemlo tectonic-stratigraphic study: in Summary of Filed Work and Other Activities, 1986, Ont. Geol. Surv. Misc. Pap., 132, 95-106.
- _____, & Elliott, C.G. (1987): Hemlo tectonic-stratigraphic study, District of Thunder Bay. in Summary of Field Work and Other Activities, 1987, Ont. Geol. Surv. Misc. Pap., 137, 117-129.
- _____. (1988): Hemlo tectonic-stratigraphic study, District of Thunder Bay. in Summary of Field Work and Other Activities, 1988, Ont. Geol. Surv. Misc. Pap., 141, 226-228.
- NAKAJIMA, T., BANNO, S. & SUZUKI, T. (1977): Reactions leading to the disappearance of pumppellyite in low-grade metamorphic rocks of the Sanbagawa metamorphic belt in Central Shikoku, Japan. *J. Petrol.*, 18, 263-284.
- NANCE, W.B. & TAYLOR, S.R. (1976): Rare earth patterns and crustal evolution: I: Australia Post-Archean sedimentary rocks. *Geochim. Cosmochim. Acta*, 40, 1539-1551.
- NAQVI, S.M., SAWKAR, R.H. RAO, D.V.S., GOVIL, P.K. & RAO, T.G. (1988): Geology, geochemistry and tectonic setting of Archean greywackes fromm Karnataka nucleus, India. *Precamb. Res.*, 39, 193-216.
- NESBITT, B.E. & ESSENE, E.J. (1982): Metamorphic thermometry and barometry of a portion of the Southern Blue Ridge province. *Am. J. Sci.*, 282, 701-729.
- NESBITT, H.W. & YOUNG, G.M. (1982): Early Proterozoic climates and palte motions inferred from major element chemistry of lutites; *Nature*, 299, 715-717.
- NEWTON, R.C. & HASELTON, H.T. (1981): Thermodynamics of the garnet-plagioclase-Al₂SiO₅-quartz geobarometer. In R.C. Newton et al., Eds., *Thermodynamics of Minerals and Melts*, 131-147, Springer-Verlag, New York.
- NILSEN, O. (1971): Sulphide mineralization and wall rock alteration at Rødhammeren mine, Sør-Trøndelag, Norway, *Norsk Geologisk Tidsskrift*, 51, 329-354.
- ORVILLE, P.M. (1972): Plagioclase cation exchange equilibria with aqueous chloride solution: results at 700°C and 2000 bars in the presence of quartz. *Am. J. Sci.* 272, 234-272.
- OXBURGH, E.R. & Turcotte, D.L. (1974): Thermal gradient and regional metamorphism in overthrust terrains, with special reference to the Eastern Alps Schweiz. *Mineral. Petrogr. Mitt.*, 54, 641-662.

- PAPIKE, J.J., CAMERON, K.L. & BALDWIN, K. (1974): Amphiboles and pyroxenes: characterization of other than quadrilateral components and estimates of ferric iron from microprobe data. *Geol. Soc. Am. Abstr. Programs*, 6, 1053-1054.
- PAPUNEN, H. & LINDSJÖ, O. (1972): Apatite, monazite and allanite, three rare-earth minerals from Korsnas, Finland. *Bull. geol. Soc. Finland*, 44, 123-129.
- PATTERSON, G.C. (1983): Exploration history in the Hemlo area, in Colvine, A.C. ed., *The Geology of Gold in Ontario: Ont. Geol. Surv., Misc. Pap.*, 110, 226-229.
- _____ (1984): Field trip Guidebook to the Hemlo area; *Ont. Geol. Surv. Misc. Pap.*, 118, 33p.
- PERKINS, E.H., BROWN, T.H. & BERMAN, R.G. (1986): PTX-SYSTEM: three programs for calculation of pressure-temperature-composition phase diagrams. *Comput. Geosci.* 12, 749-755.
- PHILLIPS, G.N. (1985): Interpretation of Big Bell-Hemlo-type gold deposits: precursors, metamorphism, melting and genetic constraints. *Trans. Geol. Soc. S. Africa*, 88, 159-173.
- PIGAGE, L.C. & GREENWOOD, H.J. (1982): Internally consistent estimates of pressure and temperature: the staurolite problem. *Am. J. Sci.*, 282, 943-969.
- PINSENT, R.H. & Hirst, D.M. (1977): The metamorphism of the Blue River Ultramafic Body, Casiar, British Columbia. *J. Petrol.*, 18, 567-594.
- POLLARD, P.J. (1981): Hydrothermal tin-tungsten mineralization and origin of associated cordierite-anthophyllite rocks at Tommy Burns mine, north Queensland, Australia. *Trans. Inst. Mining Metall.*, B90, 65-69.
- POTTER, R.W. & BROWN, D.L. (1977): The volumetric properties of aqueous sodium chlorides solutions from 0° to 500°C at pressures up to 2000 bars based on a regression of available data in the literature. *Bull. U.S. Geol. Surv.*, 1421-C, 36p.
- PRIDE, R.T. (1940): Cordierite-anthophyllite rocks associated with spinel-hypersthénites from Toodyay, Western Australia. *Geol. Magz.*, 77, 364-382.
- QUARTERMAIN, R. (1985): Road guide to the geology of the Teck-Corona Mine at Hemlo, Ontario, in McMillan, R.H. & Robinson, D.J., eds., *Gold and Copper-Zinc Metallogeny, Hemlo-Manitouwadge-Winston Lake, Ontario, Canada*, *Geol. Assoc. Can. & Can Inst. Mining Metall.*, Toronto, 39-46.
- RAASE, P. (1974): Al and Ti contents of hornblende, indicators of pressure and temperature of regional metamorphism. *Contrib. Mineral. Petrol.*, 45, 231-236.

- RADTKE, A.S. RYE, R.O. & DICKSON, F.W. (1980): Geology and stable isotope studies of the carlin gold deposit, Nevada: *Econ. Geol.*, **75**, 641-672.
- RAMSAY, J.G. & GRAHAM, R.H. (1970): Strain variation in shear belts. *Can. J. Earth Sci.*, **7**, 786-813.
- RAO, A.T., RAO, A., & RAO, P.P. (1979): Fluorian allanite from calc-granulite and pegmatite contacts at Garividi, Andhra Pradesh, India. *Mineral. Magz.*, **43**, 312.
- REINHARDT, J. (1987): Cordierite-anthophyllite rocks from north-west Queensland, Australia: metamorphosed magnesian pelites. *J. Metamorphic Geol.*, **5**, 451-472.
- RICE, J.M. (1977): Progressive metamorphism of impure dolomitic limestone in the Marysville aureole, Montana. *Am. J. Sci.*, **277**, 1-24.
- RICKWOOD, P.C. (1968): On recasting analyses of garnet into end-member molecules. *Contrib. Mineral. Petrol.*, **18**, 175-198.
- RICHARDSON, S.W., GILBERT, M.C. & BELI., P.M. (1969): Experimental determination of kyanite-andalusite and andalusite-sillimanite equilibria; the aluminum silicate triple point. *Am. J. Sci.*, **267**, 259-272.
- ROACH, D., CAMERON, E., & HATTORI, K., (1986): Geology and Geochemistry of baritic bodies west of Hemlo [abstract], in Program with Abstracts: Geol. Assoc. Can. Mineral. Assoc. Can. Geophys. Union Joint Annual Meeting, Carleton University, May 1986, VII, 119.
- ROBINSON, P., ROSS, M. & JAFFE, H. (1971) Composition of the anthophyllite-gedrite series, comparisons of gedrite and hornblende, and the anthophyllite-gedrite solvus. *Am. Mineral.*, **56**, 909-939.
- _____ (1980): The compositional space of terrestrial pyroxenes - internal and external limits. *Mineral. Soc. Am., Rev. In Pyroxenes*, **7**, 419-494.
- ROEDER, P.L. (1985): Electron-microprobe analysis of minerals for rare-earth elements: use of calculated peak-overlap corrections. *Can. Mineral.*, **23**, 263-271.
- ROMBERGER, S. B. (1986): The solution chemistry of gold applied to the origin of hydrothermal deposits. in Clark, L.A., ed., *Gold in the Western Shiled*: Montreal, Can. Inst. Mining Metall. Spec. V., **38**, 168-186.
- SANGSTER, D.F. (1969): The contact metamorphic magnetite deposits of southwestern British Columbia. *Can. Geol. Sur. Bull.*, **172**, 85p.
- SCHERMERHORN, L.J.G. (1978): Epigenetic magnesium metasomatism or syngenetic chloritic metamorphism at Falun and Orijärvi. *Trans. Inst. Mining Metall.*, **B**, 162-167.

- SCHNIEDERS, B.R. & SMYK, M.C. (1988): Schreiber-Hemlo resident geologist's district-1988. Report of Activities 1988, Resident Geologists. Ont. Geol. Surv. Misc. Pap., 142, 133-155.
- SCOTT, S.D. & BARNES, H.L. (1971): Sphalerite geothermometry and barometry. Econ. Geol., 66, 653-669.
- SEWARD, T.M. (1973): Thio complexes of gold and the transport of gold in hydrothermal solutions. Geochim. Cosmochim. Acta, 37, 379-399.
- _____, (1984): The transport and deposition of gold in hydrothermal systems: in Foster, R.P., ed., Gold'82, The Geol. Soc. Zimbabwe Spec. Publ., No. 1, 165-181.
- SEWARD, T.M. (1988): The hydrothermal chemistry of gold and its implications for ore formation. In Goode, A.D. & Bosma, L.I. eds., Bicentennial Gold'88, Extended Abstracts (oral program). 197-198, Melbourne, 1988.
- SHARMA, R.S. & MacRae, N.D. (1981): Paragenetic relations in gedrite-cordierite-staurolite-biotite-sillimanite-kyanite gneisses at Ajitpura, Rajasthan, India. Contrib. Mineral. Petrol., 78, 48-60.
- SHIDO, F. (1958): Plutonic and metamorphic rocks of the Nakoso and Iriton districts in the central Abukuma Plateau. Tokyo Univ. Fac. Sci. J. Sec. II, 11, 131-217.
- _____ & MIYASHIRO, A. (1959): Hornblendes of basic metamorphic rocks. J. Fac. Univ. Tokyo II, 12, 85-102.
- SIRAGUSA, G.M., (1983): White River area, District of Thunder bay, in Wood, J. et al. eds., Summary of Field Work, 1983, Ont. Geol. Surv. Misc. Pap., 116, 41-44.
- SITTHITHAWORN, E. (1989): Gold mineralization at Phu Lon Copper-Iron skarn prospect in northern Thailand (M.Sc. thesis). University of Western Ontario, London, Ontario, Canada.
- SKIPPEN, G.B. & CARMICHAEL, D.M., (1977): Mixed-volatile equilibria. Application of thermodynamics to petrology and ore deposits. in Greenwood, H.J. ed., Mineral. Assoc. Can. Short Course Hand Book 2, 109-124.
- SPEAR, F.S. (1977): Phase equilibria of amphibolites from the Post Pond Volcanics, Vermont. Carnegie Inst. Wash. Yearbook, 76, 613-619.
- _____ (1986): The gedrite-anthophyllite solvus and the composition limits of orthoamphibole from the Post Pond Volcanics, Vermont. Am. Mineral., 65, 1103-1118.

- _____ (1981): An experimental study of hornblende stability and compositional variability in amphibolite. *Am. J. Sci.*, **281**, 697-734.
- _____ (1982): Phase equilibria of amphibolites from the Post Pond Volcanics, Mt. Cube Quadrangle, Vermont. *J. Petrol.*, **23**, 383-426.
- STANTON, R.L. (1987): Constitutional features and some exploration implications of three zinc-bearing stratiform skarns of eastern Australia. *Trans. Inst. Min. Metall. (Sect. Appl. earth sci.)*, **96**, B37-57.
- STAUDIGEL, H. & HART, S.R. (1983): Alteration of basalt glass: Mechanism and significance for the oceanic crust-seawater budget. *Geochim. Cosmochim. Acta*, **47**, 337-350.
- STOUT, J.H. (1971): Four coexisting amphiboles from Telemark, Norway. *Am. Mineral.*, **56**, 212-224.
- STRENS, R.G.J. (1965): Stability and relations of the Al-Fe epidotes. *Mineral. Magz.*, **35**, 464-475.
- STROH, J.M. (1976): Solubility of alumina in orthopyroxene plus spinel as a geobarometer in complex system. Applications to spinel-bearing Alpine-type peridotites. *Contrib. Mineral. Petrol.*, **54**, 173-188.
- SUN, S.-S. & NESBITT, R.W. (1978): Petrogenesis of Archean ultrabasic and basic volcanic rocks: evidences from rare earth elements. *Contrib. Mineral. Petrol.*, **65**, 301-325.
- TAYLOR, S.R. (1977): Island arc models and the composition of the continental crust. *Am. Geophys. Union Maurice Ewing Series I*, 325-335.
- TAYLOR, H.P., Jr. (1979): Oxygen and hydrogen isotope relationships in hydrothermal mineral deposits, in Barnes, H.L., ed., *Geochemistry of hydrothermal ore deposits*: New York, Wiley-Interscience, 236-277.
- THOMPSON, A.B. (1976a): Mineral reactions in pelitic rocks: I. prediction of P-T-X(Fe-Mg) phase relations. *Am. J. Sci.*, **276**, 401-424.
- _____ (1976b): Mineral reactions in pelitic rocks: II. calculation of some P-T-X_(Fe,Mg) phase relations. *Am. J. Sci.*, **276**, 425-454.
- _____ & ENGLAND, P.C. (1984): Pressure-temperature-time paths of regional metamorphism: II. Their inference and interpretation using mineral assemblages in metamorphic rocks. *J. Petrol.*, **25**, 929-955.
- THOMSON, J.E., (1931): Geology of the Heron Bay area, district of Thunder Bay. *Ont. Dept. Mines 40, part 2*, 21-39 Accomp. map 40d, Scale: 1 inch to 1.5 miles.

- TILLEY, C.E. (1935): Metasomatism associated with the greenstone-hornfels of Kenidjack and Botallack, Cornwall. *Mineral. Magz.*, **24**, 181-202.
- _____ (1937): Anthophyllite-cordierite-granulites of the Lizard. *Geol. Magz.*, **74**, 300-309.
- _____ & Flett, J.S. (1929): Hornfels from Kenidjack, Cornwall. Great Britain Geol. Surv., Summary of Progress, 1929, Part. II, 24-41.
- TINTOR, N. (1986): Who really knows?: The Northern Miner Magazine, **1**, 39-43.
- TRACY, R.J., ROBINSON, P. & THOMPSON, A.B. (1976): Garnet composition and zoning in the determination of temperature and pressure of metamorphism, central Massachusetts: *Am. Mineral.*, **81**, 762-775.
- TUOMINEN, H.V. & MIKKOLA, T. (1950): Metamorphic Mg-Fe enrichment in the Orijärvi region as related to folding. *Bull. Comm. Géol. Finl.*, **150**, 67-92.
- TURNER, F.J. (1981): *Metamorphic Petrology: Mineralogy, field and tectonic aspects*. McGraw-Hill, New York.
- VALLANCE, T.G. (1967): Mafic rock alteration and isochemical development of some cordierite-anthophyllite rocks. *J. Petrol.*, **8**, 84-96.
- VALLIANT, R.I. & BRADBROOK, C.J., (1986): Relationship between stratigraphy, faults and gold deposits, Page-Williams Mine, Hemlo, Ontario, Canada. in Macdonald, A.J., ed., *Proc. Gold'86, Intern. Symp. geol. Gold, Toronto, 1986*, 355-361.
- Von KNORRING, O. (1951): A new occurrence of uvarovite from northern Karelia in Finland. *Mineral. Magz.*, **29**, 594-601.
- _____, CONDLIFFE, F. & TONG, Y.L. (1986): Some mineralogical and geological aspects of chromium-bearing skarn minerals from northern Karelia, Finland. *Bull. Geol. Soc. Finl.*, **58**, 277-292.
- WALFORD, P., STEPHENS, J., SKRECKY, G. & BARNETT, R. (1986): The geology of the "A" zone, Page-Williams mine, Hemlo, Ontario, Canada, in Macdonald, A.J., ed., *Proc. Gold'86, Intern. Symp. Geol. Gold: Toronto, 1986*, 362-378.
- WEILL, D.F. (1966): Stability relation in the Al_2O_3 - SiO_2 system calculated from solubilities in the Al_2O_3 - SiO_2 - Na_2AlF_6 system: *Geochim. Cosmochim. Acta*, **30**, 223-237.
- WESTRA, G. & KEITH, S B (1981): Classification and genesis of stockwork molybdenum deposits. *Econ. Geol.*, **76**, 844-873.

- WHITNEY, J.A. & STORMER, J.C. Jr. (1977): The distribution of $\text{NaAlSi}_3\text{O}_8$ between coexisting microcline and plagioclase and its effect on geothermometric calculations. *Am. Mineral.*, **62**, 687-691.
- WINKLER, H.G.F. (1979): *Petrogenesis of Metamorphic Rocks* (5th ed.). Springer-Verlag, New York.
- WISEMAN, J.D.H. (1934): The central and south-west Highland epidiorites: a study in progressive metamorphism. *Quart. J. Geol. Soc. London*, **90**, 354-417.
- WOODSWORTH, G.J. (1977): Homogenization of zoned garnets from pelitic schists: *Can. Mineral.*, **15**, 230-242.
- WRIGHT, T.L. (1968): X-ray and optical study of alkali feldspar. II. an X-ray method for determining the composition and structural state from measurement of 2-theta values for three reflections. *Am. Mineral.*, **53**, 88-104.
- ZEN, E. (1974): Prehnite- and pumpellyite-bearing assemblages, west side of the Appalachian metamorphic belt, Pennsylvania to Newfoundland. *J. Petrol.*, **15**, 197-242.